Synthesis and evaluation of polymer-based nanocarriers for siRNA delivery

PhD Thesis

Cristian Salvador Dittrich

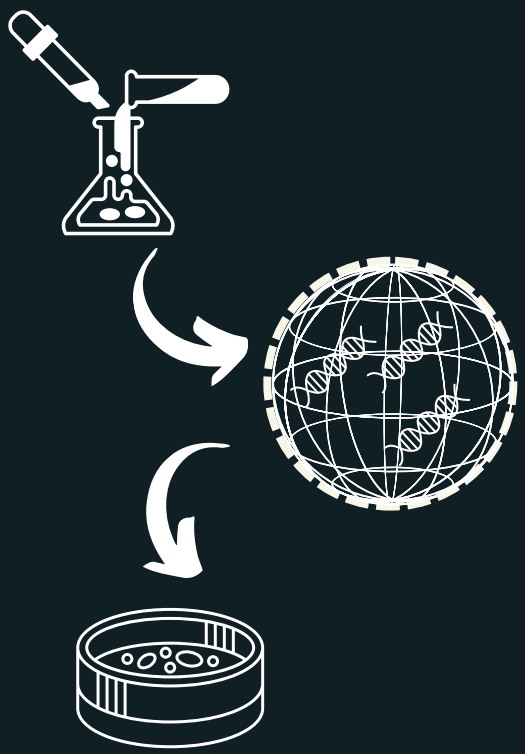

Supervised by Dr. Damien Dupin
and Dr. Sergio Moya

Donostia-San Sebastián 2023

eman ta zabal zazu

Universidad del País Vasco
Euskal Herriko Unibertsitatea

Synthesis and evaluation of polymer-based nanocarriers for siRNA delivery

Dissertation submitted to the University of the Basque Country (UPV/EHU) to obtain the Degree of Doctor of Philosophy in Molecular Biology and Biomedicine

Presented by

Cristian Salvador Dittrich

Under the supervision of

Dr. Sergio E. Moya (Soft Matter Nanotechnology Lab/ CIC BiomaGUNE) and Dr. Damien Dupin (CIDETEC Nanomedicine)

Acknowledgements

Toda etapa tiene su final, echando la vista atrás y viéndola con perspectiva, hace ya 5 años que comencé este camino de la investigación, 5 años que han pasado volando y han dejado cantidad de acontecimientos sucedidos, 2 mundiales, 2 elecciones generales y una pandemia mundial, que conmocionó al mundo entero.

Todavía recuerdo mis inicios y como supusieron un reto personal y profesional. Salir de la comodidad del hogar familiar y de la zona de confort, a una ciudad nueva, a gente nueva y en definitiva a construir una nueva vida. El reto profesional de abordar una tesis doctoral en un campo que había rozado ligeramente en la carrera conllevaba un doble esfuerzo, no solo de aprender lo que ya existe, si no de intentar aportar nuevo conocimiento al mundo. Mi curiosidad innata de entender y aprender nuevas cosas me embarcó en esta aventura académica y como en todos los ámbitos, los comienzos son difíciles. Adaptarse requiere de esfuerzo y es por ello que quería agradecer a las personas que me hicieron este camino más fácil.

En primer lugar, quiero agradecer a mis directores, Damien Dupin y Sergio Moya por haberme dado la oportunidad de realizar la tesis doctoral y de introducirme al mundo de la química de biomateriales. Por haber sacado tiempo para mí cuando la ocasión lo requirió y por haberme dejado libertad a la hora de encontrar ideas.

A mis compañeros de laboratorio, el haber realizado una tesis entre dos centros me ha brindado la oportunidad de conocer gente magnifica.

En primer lugar, a mis compañeros de Cidetec, han sido muchos los que habéis ido yendo y viniendo, así que empezaré desde los más antiguos a los más nuevos. Marco Marradi, Raquel Gracia y Julie Movellan por haberme ensañado a trabajar en el laboratorio y haber compartido vuestro conocimiento conmigo. A Janire Pikabea y Nati por haber tenido paciencia conmigo y haberme acogido en los inicios. A Janire Alkorta por tu disposición y ganas de ayudar, que siempre me han facilitado mucho el trabajo. A Adrián Pérez por los buenos momentos compartidos en laboratorio y por enseñarme el manejo de cultivo celular (Equipo cmRNABone). A Beatriz Palla por tu simpatía y amabilidad (Compi de Residuos). A Cristina Domínguez, por tu alegría y simpatía y ese aceite bueno que traes. Especial mención a Marcos Navascuez, traspasaste el plano profesional, me ayudaste en los comienzos, enseñándome la ciudad y presentándome a los que a día de hoy son amigos. Por las buenas charlas científicas y no tan científicas en el laboratorio (PD: contestación a tu dedicación de tesis, en 4 años no recuerdo que me hayas invitado tu a ninguna copa jajaj). Las nuevas incorporaciones, Diego Cortizo por tus consejos y por tu apoyo científico (Equipo LNPs). A Angela Moncada, por tu cercanía y disposición a ayudar, tu simpatía y confianza en mi.

A Paula, Raquel, José, Janire Martínez, y Claudia por el buen rollo que transmitís, que hacéis que trabajar sea más ameno. Al resto de miembros de Cidetec Nanomedicina, que, aunque no hayamos trabajado de forma tan estrecha habéis contribuido a crear un buen ambiente: Eider, Laura, Juliana, Andrea, Ainhara, Aitziber, June, Xabi, Unai, Aitor, Naiara, Idoia, Natalia, Oliver e Iraida. Gracias

A mis compañeros de CIC BiomaGUNE. También sois muchos los que habéis pasado por el Sergio Moya´s lab. A Martuca por tu buen rollo en el laboratorio y la alegría que transmites. A Edu por tu disposición y simpatía. A la patatina, Elisa tasca por esas risas en la cell room. A María Regato compi de lab y de estancia. Los road trip americanos no serían lo mismo sin ti. Especial mención a Patrizia Andreozzi, la mama del lab, gracias por enseñarme y guiarme en el laboratorio, todos los ensayos biológicos los aprendí de ti. Al resto de integrantes

que hicisteis que los días se hicieran más amenos: Bruno, Raquel, Angi, Angel, Desiré, Tanja, Julia, Paolo, Sofia.

A la Dra Gabriela Romero, por acogerme en tu laboratorio durante mi estancia en San Antonio (Texas), por ser tan amable y cercana. Especial mención al más capo Nico Muzzio tanto durante tu paso por Donosti como por mi estancia en San Antonio, por tu buen humor y por tu disponibilidad.

A la gente con la que no compartí laboratorio, pero influyeron enormemente en mi vida personal. A mis compañeros de piso del Collective Research Association Segundo Izpizua (CRASI): A Stefan por generar buenos planes y amenizar la experiencia del piso, a Mathie Le messie, por tu alegría en la casa y tu buen humor, a Julian Ross, el nómada digital, por tu simpatía y alegría. Al gran Javier Plou, por compartir tu interés científico, por picar mi curiosidad, por tus consejos y por seguirme en mis planes locos.

A la Kuadrilla coooo, Badia, Marcos, Vegan, Edu, Jorge, Imanol, Juan por acogerme como uno más, por esas risas en las sidrerías y en los juegos de mesa. Por las excursiones y los conciertos. Muy buenos planes a los que después se sumaron los integrantes de la maño mansión, Dani, Javi, Guille y de nuevo Marcos. Por esos días post-cuarentena y toques de queda, que daban la vida ante la difícil situación, y por los días de escalada y monte con el buen guía Javi.

A los deportistas David y Dani, por amenizar mis tardes con los buenos partidos de futbol, de pádel, de voleibol y alguna que otra caña.

Al grupo de PhD students y post-docs de Polymat y BiomaGUNE que contribuyeron a la full experience del doctorado, y que me alegraron las tardes y las noches: Donato Mancino, por la energía que transmites y el buen rollo, Damián Pérez, por tu buen humor, por tus buenas charlas, el lol y el buen freestyle; Antonio Dominguez, el pishita, por organizar buenos planes y lo buena persona que eres; Alex Criado, por esos partidos de futbol y las buenas cañas, Cristina Simó, por esas colaboraciones científicas y tu buena disposición. Al resto de personas: Cristina de la Encarnación, Anna, Félix, Joaquín, Jorge, Miguel, Paula, María José, Sergio Fernando. por esas buenas sidrerías y noches de fiesta.

A Daniel y Richard por hacer que mi breve estancia en Texas sea más entretenida.

A mis amigos de toda la vida, que a pesar de que estemos separados nuestros reencuentros siempre siguen siendo como el primer día. No puedo dedicaros unas palabras a cada uno, pues los agradecimientos ocuparían la mitad de la tesis, solo deciros que notado vuestro apoyo y gracias por estar ahí: Pokrym, Varo, Alfa, Duardo, Garci, Lustro, Bixut, Jescol, Java, Tebar, Fabio, Nesthor, Richi, Marco, Leire, Ana, Alicia, Bouzas, huertich, Morio, Rodras.

Por último, agradecerle a mi familia, que me han hecho ser la persona que soy. A mi padre, por sus sabias palabras y consejos “Cristian, hay que buscar el gusto a cada cosa que hagas, hasta las cosas más aburridas y menos importantes, hay que hacerlas bien. El día que le encuentres el gusto, dejará de hacerse tan pesado y disfrutaras del proceso.” A mi madre por todo el cariño y apoyo que me ha dado siempre, por siempre estar ahí en los momentos difíciles e insistirme en hacer lo correcto. A mi hermana, Iris por todos los buenos momentos que hemos pasado juntos. Por hacerme sentir que nuestras bromas inventadas hacen gracia y que algo tiene sentido si dos lo creen. Os quiero mucho.

Table of Contents

List of abbreviations

acronym and abbreviations	meaning
20KDa DXT-cysteamine	a dextran of 20 KDa M_W substituted with cysteamine
6-FAM	6-Carboxyfluorescein
6KDa DXT-cysteamine	a dextran of 6 KDa M_W substituted with cysteamine
AAV	adeno-associated virus
Ago	argonaute
APOC3	apolipoprotein C-III
ApoE	apolipoprotein E
APS	ammonium persulfate
ASO	antisense oligonucleotide
ASPGR	asialoglycoprotein receptor
ATR	attenuated total reflection
ATR-FTIR	attenuated total reflection fourier transformed infrared spectroscopy
AuNP	gold nanoparticle
BACE-1	β amyloid cleaving enzyme 1
BCL2	B-cell lymphoma 2, gene
bp	base pair
BSA	bovine serum albumine
Calcein AM	calcein acetoxymethyl ester
CaP	calcium phosphate
CD47	cluster of Differentiation 47, gene, protein
CDP	cyclodextrin containing polycations
cGMP	current good manufacturing practice
CHNSO	Carbon, Hydrogen, nitrogen, sulfur, oxygen, tipycal elemental analyzer
CLSM	confocal Laser scanning microscpy
cNGQ	cyclic peptide composed of aminoacid, cNGQGEQc
CPA	cyclophilin A, gene, protein
Cq	Cycle quantification
CRISPR	clustered regularly interspaced short palindromic repeats
CT	Cycle Threshold
CytD	cytochalasin D
d	doblet
D_2O	deuterium oxide, deuterated water
Da, KDa	daltons, Kilo daltons
DBT	diffusion barrier technique
DC	degree of crosslinking
diH2O	deionized water
Dlin-MC3-DMA	(6Z,9Z,28Z,31Z)-Heptatriaconta-6,9,28,31-tetraen-19-yl 4-(dimethylamino)butanoate.
DLS	dynamic light scattering
DMAP	4-(N,N-dimethylamino)pyridine
DMEM	Dulbecco's Modified Eagle Medium
DMF	dimethylformamide
DMG-PEG-2000	1,2-dimyristoyl-rac-glycero-3-methoxypolyethylene glycol-2000
DMSO	dimethylsulfoxide
DMTMM	4-(4,6-dimethoxy-1,3,5-triazin-2-yl)-4-methyl-morpholinium chloride
dNTPs	deoxyribonucleotide triphosphate

DODMA	1,2-dioleyloxy-3-dimethylaminopropane
DODT	3,6-dioxa-1,8-octane-dithiol
DOPA	3,4-dihydroxy-l-phenylalanine
DOPC	1,2-dioleoyl-sn-glycero-3-phosphocholine
DOSPA	2,3-dioleyloxy-N-[2-(sperminecarboxamido)ethyl]-N,N-dimethyl-1-propanaminium
DOTAP	1,2-dioleoyl-3-trimethylammonium-propane
DPBS	Dulbecco's phosphate-buffered saline
DPC	Dynamic PolyConjugates
DS	degree of substitution
DSB	double stranded break
DSPC	1,2-distearoyl-sn-glycero-3-phosphocholine
DTT	dithiothreitol
DXT	dextran
DXT-imidazole	dextran substituted with 1-(3-aminopropyl)imidazole
DXT-Imidazole-sper	dextran substituted with 1-(3-aminopropyl)imidazole and spermine
DXT-MA	dextran substituted with methacrylate groups
DXT-NH_2	dextran substituted with cysteamine a
DXT-NH_2-RhB	dextran substituted with cysteamine and Rhodamine B
DXT-piperazine	dextran substituted with 3,3'-(piperazine-1,4-diyl)bis(propan-1-amine)
DXT-SCPN	dextran-based SCPNs
DXT-SCPN-MA	dextran-based SCPNs methacrylated
DXT-sper	dextran substituted with 1-(3-aminopropyl)imidazole
DXT-TAEA	dextran substituted with spermine
EA	elemental analysis
ECL	enhanced chemiluminescence
EDC	1-Ethyl-3-(3-dimethylaminopropyl)carbodiimide
EDTA	ethylenediaminetetraacetic acid
EE	encapsulation efficiency
eGFP	enhanced GFP
EM	electron microscopy
EMEM	Eagle's minimum essential medium
EtBr	ethidium bromide
EtdH-1	ethidium homodimer-1
EtOH	ethanol
Exp5	exportin-5 transporter protein
FBS	fetal bovine serum
Fc	fragment crystallize
FcRn	neonatal Fc receptor
FCS	fluorescence correlation spectroscopy
FDA	Food and Drug Administration
FITC	fluorescein isothiocyanat
FSC	forward scatter
FTIR	Fourier Transformed Infrared Spectroscopy
GalNac	N-acetylgalactosamine
GAPDH	glyceraldehyde-3-phosphate dehydrogenase, gene, protein
GFP	Green Fluorescence Protein
Glc	Glucose
GMA	glycidyl methacrylate
h	hours
HBsAg	Hepatitis B surface antigen
HBV	hepatitis B virus
HCV	hepatitis C virus

HIV-1	immunodeficiency virus type 1
HNSCC	head and neck squamous cell carcinomas
HR	homologous recombination
HRP	horseradish peroxidase
ICAM	intercellular adhesion molecule
ICC	inmunocytochemistry
IF	inmunofluorescence
Ig	inmunoglobulin
IgG1	inmunoglobulin G 1
Imidazole	1-(3-aminopropyl)imidazole
INT	2-(4-iodophenyl)-3-(4-nitrophenyl)-5-phenyl-2H-tetrazolium
IR	infrared spectroscopy
IV	intravenously
KRAS	Kirsten rat sarcoma viral oncogene homolog, gene
LDLR	low density lipoprotein receptor
LHRH	luteinizing Hormone-Releasing Hormone
LNA	locked nucleic acids
LNP	lipid Nanoparticle
LODER™	Local Drug Eluter
m	multiplet
MA	methacrylic acid, methacrylate groups
MeOD	deuterated methanol
MeOH	methanol
miRNA	micro RNA
MLP	membrane lytic peptide
MNA	morphonilo nucleic acid
MNP	magnetic nanoparticle
MRI	magnetic resonance imaging
MSN	mesoporous silica nanoparticles
MTS	3-(4,5-dimethylthiazol-2-yl)-5-(3-carboxymethoxyphenyl)-2-(4-sulfophenyl)-2H-tetrazolium
MTT	3-[4,5-dimethylthiazol-2-yl]-2,5 diphenyl tetrazolium bromide
MVB	multivesicular bodies
M_W	molecular weight
MWCO	molecular weight cut-off
NADH	nicotinamide adenine dinucleotide + hydrogen
NADPH	nicotinamide adenine dinucleotide phosphate + hydrogen
NAION	non-arteritic anterior ischemic optic neuropathy
NHEJ	non-homologous end-joining
NHS	n-hydroxysuccinimide
NMR	nuclear magnetic resonance
NSCLC	non-small cell lung cancer
NT	non-treated
OA	oleic Acid
oligo-dT	oligo deoxyribose thymine
OTEs	off-target effects
P(NIPAM)	poly(N-isopropylacrylamide)
PAGE	polyacrylamide gel electrophoresis
PAH	polyallylamine hydrochloride, Polyallylamine
PAH.OA	polyallylamine modified with oleic acid
PAH.OA.1	polyallylamine-Oleic acid 1% desired degree of substitution
PAH.OA.10	polyallylamine-Oleic acid 10% desired degree of substitution
PAH.OA.2	polyallylamine-Oleic acid 2% desired degree of substitution

PAH.OA.20	polyallylamine-Oleic acid 20% desired degree of substitution
PAH.OA.5	polyallylamine-Oleic acid 5% desired degree of substitution
PAMAM	polyamidoamine
PBAE	poly-beta-amino ester
PBAVE	poly(butyl amino vinyl ether)
PBD	polybutadiene
PBS	phosphate-buffered saline
PBST	phosphate-buffered saline with tween 20 0.1%
PCL	poly(ε-caprolactone)
PCR	polymerase chain reaction
PCS	photon correlation spectroscopy
PDI	polydispersity index
PEG	polyethyleneglicol
PEG-AD	adamantane-PEG
PEI	Polyethyleneimine
PEO	poly(ethyleneoxide)
PFA	paraformaldehyde
piperazine	3,3'-(piperazine-1,4-diyl)bis(propan-1-amine)
PKR	protein kinase R
PLA	polylactic acid
PLGA	poly (lactic-co-glycolic acid)
PLK1	polo like kinase 1, gene
PLL	poly-L-lysine
PMTs	photomultiplier tubes
PNA	peptide nucleic acid
Pol II	RNA polymerase II
Pol III	RNA polymerase III
PPI	poly(propyleneimine)
ppm	parts per million
PS	phosphorotioate group
P/S	penicillin-streptomycin
PTGS	post-transcriptional gene silencing
PVDF	polyvinylidene fluoride
q	quartet
qPCR	quantitative polymerase chain reaction
qu	quintet
RGD	arginine-glycine-aspartic acid motif
RhB	rhodamine B
RIPA	radio inmuno precipitation assay
RISC	RNA-induced silencing complex
RRM2	ribonucleotide reductase subunit 2
RSV	respiratory syncytial virus
RT	room temperature
RT-qPCR	Reverse transcription quantitative polymerase chain reaction
s	singlet
SANS	small-angle neutron scattering
SARS	severe acute respiratory syndrome corona virus
SAXS	small-angle X-ray scattering
SCA1	spinocerebellar ataxia-1
SCPN	single-chain polymer nanoparticle
SCPN-NH_2	DXT-based SCPNs substituted with cysteamine
SCPN-NH_2-RhB	DXT-based SCPNs substituted with cysteamine and Rhodamine B
SDS	sodium dodecyl sulfate

shRNA	short hairpins RNA
siRNA	small interference RNA
SIRPα	signal-regulatory protein α
Sper	spermine
SPION	super paramagnetic iron oxide nanoparticles
SSC	side scatter
t	triplet
TAA	tumor associated antigens
TAE	tris-acetate-EDTA
TAEA	tris (2-aminoethyl)amine
TALEN	transcription activator-like effectors nucleases
TAM	tumor-associated macrophages
TBS	tris buffer saline
TBST	tris buffer saline with tween 20 0.1%
TCD	thermal conductivity detector
TEM	transmission electron microscopy
TEMED	tetramethylethylenediamine
TGA	thermogravimetric analysis
TGS	transcriptional gene silencing
TLC	thin layer chromatography
TLR	toll-like receptor
Tm	melting temperature
TMS	tetramethylsilane
TNFα	tumor necrosis factor-α
TRBP	TAR RNA-binding protein
TriM	targeted RNAi Molecule
TRITC	tetramethylrhodamine
TTR	transthyretin, protein
UNA	unlocked nucleic acids
VEGF	vascular endothelial growth factor,gene
ZFN	zinc finger nucleases

Resumen

El siglo XX marcó un hito en el entendimiento de la genética y en el descubrimiento de las enfermedades de carácter hereditario. Se llevaron a cabo grandes avances científicos que permitieron descubrir el origen de los desórdenes genéticos y la identificación de los genes implicados, gracias a la secuenciación del genoma en el marco del Proyecto Genoma Humano. Emergió así una nueva rama de la medicina, la terapia génica, que se basa en la manipulación directa de los genes en mal estado debido a mutaciones en su código, en vez de utilizar fármacos tradicionales para contrarrestar los efectos. Sin embargo, cualquier daño en el material genético causado por una manipulación errónea podría tener consecuencias catastróficas e irreversibles. Es por ello que a principios del siglo XXI se comenzó a trabajar a nivel postranscripcional con terapias de ARN, evitando cualquier posible daño en el genoma.

Entre estas terapias destacan los fármacos basados en ARN de interferencia (RNAi, por sus siglas en inglés). El ARN de interferencia es un mecanismo que ocurre de manera natural en la mayoría de las células eucariotas y que se encarga de regular la expresión génica a través del silenciamiento del ARN mensajero (mRNA, por sus siglas en inglés). Tras su descubrimiento por Fire y Mello a finales del siglo XX se han logrado importantes avances en la investigación de esta novedosa área, con el objetivo de trasladar a la clínica nuevas terapias basadas en RNAi. El ARN pequeño de interferencia (siRNA, por sus siglas en inglés) es el principio activo de estos nuevos fármacos y está cuidadosamente diseñado para unirse al mRNA del gen diana. En el citoplasma celular, una serie de proteínas interactúan tras la unión del siRNA con el mRNA, provocando la degradación del transcrito y evitando así la producción de la proteína asociada al mRNA a silenciar. De esta forma, una enfermedad provocada por una mutación genética podría verse claramente mitigada sin necesidad de modificar la secuencia de ADN.

No obstante, el potencial de esta nueva terapia se ha visto limitado debido a la naturaleza del siRNA, que dificulta su administración *in vivo* de forma sistémica. El ARN es un material tremendamente sensible a enzimas nucleasas, ubicadas en todo el organismo, las cuales degradan cualquier ARN exógeno. El siRNA (con una longitud entre 20 y 25 pares de bases) posee un tamaño pequeño que se filtra fácilmente en los glomérulos haciendo que su tiempo de circulación sea muy corto. Otra de las barreras que presenta la administración de siRNA es la dificultad para dirigirlo específicamente al tejido diana y su correspondiente internalización celular. El siRNA no es lo suficientemente pequeño para entrar por difusión simple y su carga negativa provoca que sea repelido por componentes de la membrana celular, también de carga negativa. Además, la entrada del siRNA en el citoplasma se realiza por endocitosis y una vez en el interior del endosoma tendrá que liberarse para no terminar siendo degradado en el lisosoma. Todas estas barreras hacen imposible la administración por vía intravenosa del siRNA libre y es necesaria su unión a un vector que lo ayude a llegar al citoplasma celular.

La nanomedicina y el diseño de nanomateriales han avanzado enormemente durante las últimas décadas y hoy en día existen nanomateriales de distinto tipo para el transporte de fármacos. Así

como también se han desarrollado nanomateriales para transportar material genético foráneo de forma sistémica. Los nanovectores proporcionan protección al siRNA frente a las nucleasas, evitan su eliminación por la orina y permiten su acumulación en un tejido especifico. Son capaces de traspasar la membrana plasmática y posibilitan al siRNA escapar del endosoma. Sin la ayuda de estos vectores la aplicación del siRNA no sería posible, salvo en ciertos tejidos y órganos que permiten la captación del siRNA de forma libre tras una administración local. Sin embargo, los nanomateriales tienen que cumplir una serie de características para poder ser utilizados como vectores. Principalmente deben tener la capacidad de interaccionar con el material genético y tener la habilidad de encapsularlo. Se han desarrollado distintos tipos de nanomateriales que pueden actuar como vectores, la mayoría de ellos comparten la característica común de que presentan una carga eléctrica positiva que les permite interaccionar con la carga negativa de los fosfatos en el material genético. Entre las distintas estrategias para el desarrollo de nanovectores encontramos, entre otras, el uso de lípidos y polímeros catiónicos, nanopartículas inorgánicas recubiertas de material catiónico, exosomas y moléculas covalentemente unidas al oligonucleótido. La mayoría de las terapias más avanzadas en ensayos clínicos utilizan vectores basados en lípidos que forman liposomas o nanopartículas lipídicas (LNPs) y siRNAs unidos a un trímero de N-acetilgalactosamina (GalNac). Ambos vectores tienen como diana proteínas de la membrana de los hepatocitos, por lo que su administración se ve limitada al hígado. En 2018 fue aprobado ONPATTRO, el primer medicamento basado en el siRNA para el tratamiento de la amiloidosis hereditaria por transtirretina, que utiliza como vector una nanopartícula lipídica. A este fármaco le siguieron GIVLAARI y OXLUMO que utilizan conjugados GalNac como vector. La mayoría de los ensayos clínicos realizados se han enfocado en enfermedades hepáticas principalmente por las limitaciones de los vectores. Encontrar nuevos transportadores funcionales para explotar el potencial del siRNA es fundamental para el desarrollo de nuevas terapias más allá del hígado. Por ello continúan los esfuerzos en mejorar y desarrollar nuevos vectores. En esta tarea cobran un papel relevante los materiales poliméricos que presentan una gran versatilidad para ser modificados y producidos a gran escala, además de poseer una gran capacidad de encapsulación del material genético.

A lo largo del desarrollo de esta tesis se han investigado dos estrategias orientadas al diseño de un nuevo vector para siRNA. Una de ellas está basada en la funcionalización catiónica del dextrano, un polisacárido de origen natural y la otra basada en la modificación con grupos hidrofóbicos de la polialilamina, un polímero sintético que contiene una amina primaria por unidad repetitiva.

En el **Capítulo 3** se recoge el trabajo realizado con el polímero dextrano, que se utilizó para la formación de nanopartículas de cadena única (del inglés, single-chain polymeric nanoparticles SCPN). El empleo de SCPNs como vectores se consideró como una estrategia prometedora debido al pequeño tamaño de partículas obtenidas y por los buenos resultados previos alcanzados en el transporte de antibióticos con estas nanopartículas. Para poder formar las SCPNs, los anillos de glucosa del dextrano fueron previamente modificados con grupos metacrilato, los cuales se conjugaron posteriormente con una molécula tiolada (3,6-dioxa-1,8-octano-ditiol, DODT) mediante la adición de Michael. El DODT presenta grupos tiol en ambos extremos que reaccionan con los grupos alqueno de una sola cadena de polímero, induciendo su colapso en una nanopartícula. Se introdujo un exceso de grupos metacrilato para la posterior modificación de las SCPNs con grupos

catiónicos, reaccionando nuevamente los grupos metacrilato restantes con la cisteamina, una molécula que presenta un grupo tiol y un grupo amino, a través de la adición de Michael. Así, la nanopartícula adquirió una carga positiva y pasó a denominarse SCPN-NH_2. La modificación del dextrano con estos nuevos grupos fue caracterizada por resonancia magnética nuclear confirmando el éxito de la reacción. La misma estrategia de sustitución con cisteamina se aplicó al dextrano sin entrecruzar con DODT para obtener un sistema de control, que se denominó DXT-NH_2 y de esta forma poder estudiar el efecto del entrecruzamiento en la liberación de siRNA en el interior celular. Se obtuvo un grado de sustitución de cisteamina del 21% en SCPN-NH_2 mientras que con DXT-NH_2 se obtuvo un 42%. Las aminas protonadas permiten el encapsulamiento del material genético debido a las interacciones electrostáticas con grupos aniónicos del siRNA y a la vez favorecen el escape endosomal debido al efecto tampón que producen durante la acidificación del endosoma. El tamaño de las partículas SCPN-NH_2 se analizó por dispersión dinámica de la luz, obteniendo tamaños de 15 nm muy similares a las SCPN sin modificar. El análisis del potencial Z confirmó la carga positiva del SCPN aminado.

Se conoce como poliplejo a la interacción entre un polímero y el material genético. Esta interacción puede variar en función de la cantidad de polímero frente a la cantidad de material genético existente, es lo que se conoce como ratio N/P. El ratio N/P representa los moles de aminas protonables (N) presentes en el polímero dividido entre los moles de grupo fosfato (P) presentes en el material genético. En el caso de la presente tesis se utilizó como material genético siRNA y se formaron poliplejos con los polímeros de dextrano obtenidos. Se estudió dicha interacción mediante la técnica de retraso en gel (del inglés, gel retardation assay) a diferentes ratios N/P, en el que se confirmó la interacción con siRNA de las SCPN-NH_2 y del polímero DXT-NH_2. Además, se observó que a mayores ratios N/P, mayor es la encapsulación obtenida. Por otro lado, se estudió la viabilidad de la línea celular de pulmón A549 en presencia de estos dos materiales y ninguno de los ellos resultó ser citotóxico hasta concentraciones de 50 µg/mL. La internalización del material genético en las células fue evaluada por medio de microscopia confocal de fluorescencia tras marcar los vectores con el fluoróforo Rhodamina B y por otro lado, utilizando un siRNA marcado con carboxifluoresceina. Las imágenes de microscopía confocal se tomaron 24 horas después de la administración de los compuestos en las células A549. Los resultados obtenidos muestran la colocalización de DXT-NH_2 y de siRNA en el interior celular. Sin embargo, las células tratadas con SCPN-NH_2, presentan tan solo las nanoparticulas en el interior, pero no el siRNA.

Posteriormente se realizó el ensayo de eficacia de liberación de siRNA, transfectando con los vectores SCPN-NH_2 y DXT-NH_2. Para este estudio se utilizó la línea celular A549-GFP, que expresa de forma estable la proteína verde fluorescente (GFP, por sus siglas en inglés). Las células fueron transfectadas con los vectores de dextrano acomplejando un siRNA anti-GFP, diseñado para bloquear el mRNA de la proteína GFP. La eficacia del siRNA se evaluó 96 horas después de la transfección, midiendo la fluorescencia media de las células mediante citometría de flujo. Ninguno de los vectores mostró una reducción de la producción de proteína, mientras que el control positivo Lipofectamina RNAimax (vector comercial basado en lípidos) redujo la expresión de GFP hasta un 80%. Se decidió entonces no continuar con el uso de SCPNs como vectores de siRNA debido a su incapacidad de llevar el fármaco al interior celular tras el ensayo de internalización y a la baja eficacia

de transfección obtenida. Sin embargo, continuaron los esfuerzos para modificar la cadena de dextrano debido a los resultados positivos obtenidos en el ensayo de internalización y con el objetivo de mejorar la eficacia de silenciamiento.

El dextrano se modificó con diferentes moléculas aminadas con la idea de proporcionar una mejora en la liberación del siRNA de la cavidad endolisosomal. Se estudiaron las siguientes moléculas aminadas que fueron seleccionadas de acuerdo al número de aminas primarias, secundarias o terciarias presentes en la molécula y a sus pKas, con el objetivo de mejorar la capacidad tampón del polímero en el interior del endosoma: espermina, 1-(3-aminopropil)imidazol, Tris (2-aminoetill)amina y 3,3'-(piperazina-1,4-diil)bis(propan-1-amina). Para la funcionalización del dextrano se utilizó el reactivo de Traut como mediador entre el alqueno del grupo metacrilato y el grupo amino.

De acuerdo con la literatura, también se tuvo en cuenta el peso molecular del dextrano como posible causa de una baja liberación del siRNA del endosoma, ya que pesos moleculares más altos provocan interacciones más fuertes con los oligonucleótidos, impidiendo de esta forma una buena liberación. Para ello, se funcionalizaron con cisteamina dos dextranos de peso molecular 6KDa y 20 KDa.

Todas estas nuevas modificaciones en los polímeros se caracterizaron mediante resonancia magnética nuclear y se formularon con siRNA anti-GFP. Después, los poliplejos obtenidos fueron evaluados como posibles vectores mediante el ensayo de reducción de GFP medido por citometría de flujo. Este ensayo permite de manera rápida, sencilla y cuantitativa discriminar nuevos materiales por su eficacia de silenciamiento. Los resultados obtenidos por citometría de flujo muestran una mejora respecto a las sustituciones con cisteamina, siendo las sustituciones con espermina, Tris (2-aminoetill) amina y 3,3'-(piperazina-1,4-diil)bis(propan-1-amina) los mejores vectores. Sin embargo, ninguno de los polímeros superó una reducción del 50% de proteína, ni se acercaba a los valores del 20% de expresión obtenidos con el control positivo Lipofectamina RNAimax.

Por ello en el **Capítulo 4** se desarrolló otra estrategia que consistió en la modificación de un polímero sintético de alta densidad amínica, en lugar de intentar introducir grupos amino en una cadena polimérica. La polialilamina es un polímero cuya unidad repetitiva presenta una amina primaria, la cual despierta el interés como vector de material genético. Sin embargo, es sabido que una alta densidad amínica puede derivar en citotoxicidad, es por ello que se buscó modificar la polialilamina con ácido oleico para neutralizar parcialmente su carga, buscando un equilibrio entre eficacia y toxicidad.

El ácido oleico se seleccionó debido a la alta eficacia de transfección demostrada en vectores lipídicos. Se estudió el efecto del grado de sustitución unido covalentemente a la polialilamina en su capacidad como vector para el transporte y liberación de siRNA. Se realizaron 5 sustituciones de ácido oleico a equivalentes molares 1:0,01; 1:0,02; 1:0,05; 1:0,1 y 1:0,2 -NH_2: -COOH, las cuales se nombraron PAH.OA.1, PAH.OA.2, PAH.OA.5, PAH.OA.10 y PAH.OA.20, respectivamente. El ácido oleico se unió a la amina del monómero de PAH por medio de la formación de un enlace amida

gracias a la activación del ácido carboxílico mediante carbodiimida e hidroxisuccinimida en una mezcla de disoluciones de dimetilsulfóxido (DMSO) y agua. Los nuevos polímeros fueron caracterizados mediante diferentes técnicas analíticas: Por cromatografía de capa fina se reveló la ausencia de ácido oleico libre en la muestra tras la purificación por diálisis. Por medio de espectroscopia de infrarrojo se demostró la presencia de ácido oleico presente en el polímero mediante unión covalente con el mismo. La determinación del grado de sustitución fue la tarea más compleja de llevar a cabo debido a la poca solubilidad de la polialilamina sustituida con ácido oleico. Se probaron diferentes solventes para disolver la poliamina substituida, de los cuales el agua resultó ser el más eficaz. Sin embargo, la insolubilidad del polímero no permitió una cuantificación exacta del grado de sustitución mediante resonancia magnética nuclear, pero si estimaciones que resultaron ser 1%, 2%, 6%, 14% y >20% para los polímeros PAH.OA.1, PAH.OA.2, PAH.OA.5, PAH.OA.10 y PAH.OA.20. También se emplearon otras técnicas para determinar el grado de sustitución como análisis elemental y análisis por termogravimetría, pero ambas resultaron ser tan solo estimaciones.

La baja solubilidad de la poliamina modificada con oleico se debe a la formación de nanopartículas en agua por medio de autoensamblaje de las cadenas poliméricas, a través de interacciones hidrofóbicas entre las cadenas de oleico. El tamaño de las partículas se determinó por dispersión dinámica de la luz y por microscopia electrónica de transmisión. Se obtuvieron partículas de 10 nm que se agregaban en estructuras más grandes alcanzando tamaños entre los 100 y 300 nm dependiendo de la cantidad de ácido oleico unido. Las partículas formadas presentan una carga superficial positiva, alcanzando valores de Potencial Z de +40 mV aproximadamente en todas las sustituciones.

Se estudió la interacción de siRNA con estas partículas poliméricas, preparando los complejos con distintos ratios N/P 2,5; 5; 10 y 15. Los poliplejos resultantes se caracterizaron por tamaño, carga superficial y eficacia de encapsulación. Se observó que los poliplejos formados por polímeros de mayor cantidad de oleico (PAH.OA.5, PAH.OA.10 y PAH.OA.20) presentan tamaños similares a las partículas formadas solo por polímero, pero los complejos con siRNA presentan una polidispersidad menor. Por otro lado, los polímeros menos sustituidos (PAH.OA.1 y PAH.OA.2) sí que vieron reducido su tamaño. La carga superficial se redujo a +30 mV, debido a la compensación de cargas de las aminas por los fosfatos del siRNA. La eficacia de encapsulación se cuantificó con Quant-IT Ribogreen obteniendo encapsulaciones por encima del 90% en todos las sustituciones y ratios N/P.

La evaluación de la poliamina sustituida con ácido oleico como vector de siRNA se detalla en el **Capítulo 5** donde se llevaron a cabo distintos ensayos de los complejos polímero/siRNA. En primer lugar, se evaluó la viabilidad y el daño de la membrana de las células A549 tras la exposición a los poliplejos formados con las poliaminas substituidas. Se pudo observar que los polímeros con mayor cantidad de ácido oleico resultaron ser menos citotóxicos que los menos sustituidos. Sin embargo, altas cantidades de polímero en ratios N/P 15 resultan citotóxicas en todas las sustituciones. El ratio idóneo resultó ser N/P 5 donde la viabilidad celular se mantiene por encima de un 95%. La internalización de los poliplejos se evaluó por microscopia confocal y citometría de flujo. Para estos experimentos se modificaron covalentemente todos los polímeros con el fluoróforo Atto633 y se

utilizó siRNA-6-FAM, marcado con carboxifluoresceina. Por microscopia confocal se pudo observar la colocalización del polímero y del siRNA en el interior celular para todos los complejos a un N/P 5. La citometría de flujo reveló que de 10.000 células observadas, el 70% presentaron fluorescencia del siRNA en todos las sustituciones de polialilamina con ácido oleico, demostrando que el grado de sustitución no influye particularmente en mejorar la internalización celular. La eficacia de administración de los polímeros se midió por citometría de flujo, utilizando células que expresan GFP y tratándolas con siRNA anti-GFP. En este experimento ya mencionado en el Capítulo 3, las células A549-GFP se expusieron a una transfección de 24 horas con los complejos formados con las distintas sustituciones de polialilamina. A las 96 horas de la transfección se midió la fluorescencia media de las células por citometría de flujo y a diferencia de los experimentos de internalización, se pudo observar que el porcentaje de ácido oleico influye en la liberación de siRNA en el interior celular. Los poliplejos con sustituciones mayores de oleico, PAH.OA.5 y PAH.OA.10, se obtuvieron mejores eficacias de transfección que para los poliplejos con menor grado de sustitución, PAH, PAH.OA.1 y PAH.OA.2. Sin embargo, con los poliplejos formados con PAH.OA.20 no se obtuvo ningún silenciamiento. El sistema más eficiente se obtuvo con PAH.OA.10 con una reducción de proteína de hasta un 70%, niveles muy similares al 80% obtenido con el control positivo Lipofectamina RNAimax.

El punto más destacable de este estudio es que el ácido oleico mejora la eficacia de silenciamiento de la polialilamina, sin embargo, ésta no viene dada por una mayor capacidad de internalización celular, sino por una liberación del endosoma más efectiva. Se llevó a cabo un estudio más detallado de la liberación por parte del siRNA de la cavidad endolisosomal, mediante la colocalización del lisosoma con el siRNA hasta 48 horas de exposición. Las imágenes de microscopia confocal revelan que parte del siRNA consigue liberarse del endosoma, sin embargo hay que puntualizar que una gran cantidad del siRNA también colocaliza con el lisosoma. Aun así, esa pequeña parte de siRNA libre es capaz de inducir el silenciamiento.

Dados estos resultados prometedores, se decidió estudiar la eficacia de estos vectores con un siRNA terapéutico utilizado en el tratamiento de cáncer de pulmón mediante el silenciamiento de la CD47. La CD47 es una proteína de transmembrana que se expresa en la mayoría de las células del organismo, con una especial sobreexpresión en tumores como el de cáncer de pulmón de células no pequeñas. La proteína CD47 tiene un papel en la modulación del sistema inmune, ya que es reconocida por los macrófagos a través del receptor SIRPα, situado en la membrana del mismo. La CD47 actúa como una señal de “no me comas” y evita que las células donde está expresada esta proteína sean fagocitadas por los macrófagos. Por otra parte, ante la ausencia de la CD47, esta unión no puede llevarse a cabo y se inicia el proceso de fagocitosis.

Una estrategia terapéutica interesante consiste en reducir la expresión de la proteína CD47 por medio del silenciamiento génico e inducir la fagocitosis de células tumorales. Se llevaron a cabo varios ensayos para evaluar la reducción de la expresión del gen CD47 en células A549 a nivel de transcrito y a nivel de proteína siguiendo la transfección con siRNA anti-CD47 utilizando los vectores de polialilamina modificada con ácido oleico.

RESUMEN

El contenido de ARN mensajero de CD47 se midió por PCR cuantitativa, observándose una reducción en la expresión de CD47 hasta el 70% con el vector PAH.OA.10, coincidiendo con los porcentajes de transfección medidos por citometría de flujo para el silenciamiento de GFP. El mismo vector con un siRNA negativo no indujo ningún cambio en la expresión, descartando cualquier posible efecto del polímero en los resultados de transfección. Se midió el nivel de proteína en las células con tres técnicas de biología molecular: Western Blot, Inmunofluorescencia y citometría de flujo, demostrando el buen funcionamiento del polímero PAH.OA.10 como vector y anticipando su aplicación futura en el desarrollo de terapias contra el cáncer de pulmón, y a otras nuevas dianas posibles.

Summary

The 20th century a revolution in our understanding of genetics and the discovery of hereditary diseases. Major breakthroughs were made after the discovery of diseases caused by genetic disorders and their possible identification through genome sequencing. A new area of medicine called gene therapy emerged, which is based on genetic manipulation to reverse gene malfunction, aiming at applications in therapy. However, any damage to genetic material could have catastrophic and irreversible consequences, if it is not done carefully. This is the reason why, in the early 21st century, post-transcriptional therapies using RNA were developed, avoiding any possible damage to DNA.

The mechanism of interference RNA occurs naturally in most eukaryotic cells and is responsible for regulating gene expression by silencing messenger RNA (mRNA). After its discovery by Fire and Mello in the late 20th century, there have been significant advances in research in this new area of knowledge to translate new therapies based on interference RNA to the clinic. The active ingredient of these new drugs are small interfering RNAs (siRNAs), which are carefully designed to bind to the target gene's mRNA. A series of proteins are involved in the cell cytoplasm after siRNA binds to mRNA, leading to the transcript degradation and preventing protein production. The potential application of this new therapy has been however hindered by the nature of siRNA, which makes systemic delivery difficult. RNA is easily degraded by nucleases enzymes that are distributed throughout the body, which eliminate all exogenous RNA. On the other hand, siRNA (with a length ranging from 20 to 25 base pairs) exhibits a small size and it is easily filtered through the glomeruli, making its circulation time in the body very short. Another barrier for siRNA administration stems from the difficulties in delivering siRNA to a selected tissue and its corresponding internalization inside cells. SiRNA is not small enough to enter by simple diffusion, and its negative charge is repelled by also negatively charged molecules on the cell surface. The most common cell entry occurs through the formation of an endosome, from which siRNAs must be released to reach the cytoplasm. These barriers prevent the use of intravenous delivery of siRNA alone, requiring the formulation of siRNA within delivery vectors.

Nanomedicine and the design of nanomaterials for drug transport have been explored forthe development of tools for the delivery of foreign genetic material. Nanovectors provide protection to siRNA against nucleases, prolong its residence time in the body, and allow its accumulation to a specific target tissue. Nanovectors are capable of passing through the plasma membrane and escaping from the endosome. Without the help of these vectors, the application of siRNA would not be possible, except for certain tissues and organs that allow siRNA uptake without any vector after local administration. However, nanomaterials must meet certain characteristics to be used as vectors. Mainly, they must have the ability to interact with genetic material and encapsulate it. There are different types of materials that have been used for encapsulation of genetic material, and most of them display a positive electric charge that allows them to interact with the negatively charged phosphates of the genetic material. Among the different materials used for vectorizing nucleic acids, we find cationic lipids and polymers, inorganic nanoparticles coated with cationic

material, exosomes and molecules covalently linked to the oligonucleotides. The most advanced therapies in clinical trials use lipid-based vectors that form liposomes or lipid nanoparticles (LNPs) and siRNAs bound to N-acetylgalactosamine trimer (GalNac). At the end of the second decade of the 21st century, ONPATTRO, the first siRNA-based drug for hereditary transthyretin amyloidosis, was approved, which uses a lipid nanoparticle as a vector. This treatment was followed by the approval of GLIVAARI and OXLUMO, which use GalNac conjugates to siRNA molecule as formulation. Both therapies are targeting the liver and most of the clinical trials in the field have focused primarily on liver-related diseases due to the limitations of vector technologies. However, the exploration of novel functional carriers is essential to unlock the full potential of siRNA for the development of targeted therapeutics for diverse tissues beyond the liver. Accordingly, efforts are underway to improve and develop new delivery vectors. In this effort, polymers play an important role, as they offer remarkable versatility for large-scale modification and production, along with excellent capacity for encapsulation of genetic material.

In the Chapter 3, a new gene delivery strategy based on single-chain polymeric nanoparticles (SCPN) of dextran was studied. The small size of SCPNs offers several advantages in terms of effective delivery. Additionally, the successful outcomes achieved previously for antibiotic delivery make this approach an interesting way to pursuit. In order to form the SCPNs, the glucose rings of a 40KDa dextran were previously modified with methacrylate groups, and some of the alkene groups were used to react with 3,6-dioxa-1,8-octane-dithiol (DODT) via Michael addition in mild alkaline conditions. The DODT presents thiol groups at both ends that react with the alkene groups of a single polymer chain, inducing its collapse into a nanoparticle. The remaining methacrylate groups allowed the subsequent substitution of the SCPNs with cationic molecules, which contain a thiol group and an amino group, again via Michael addition. Thus, the nanoparticle acquired a positive charge and was here after referred to as SCPN-NH_2. The modified dextran was characterized by nuclear magnetic resonance, confirming the success of the reaction. The same cysteamine substitution strategy was applied to the non-crosslinked dextran to obtain a control system, which was named as DXT-NH_2, in order to study the effect of crosslinking on transfection properties. The substitution degree of cysteamine for SCPN-NH_2 was around 21%, while for DXT-NH_2 a substitution degree of 42% was obtained. The presence of amine groups in the polymers allows the genetic material to be encapsulated due to electrostatic interactions. Also, it was expected that the endosomal escape would be promoted due to the buffering capacity of the amine group during the acidification of the endosomal cavity. The size of the nanoparticles SCPN-NH_2 was around 15 nm, as judged by dynamic light scattering, which is similar to the SCPNs before modification. The analysis of the surface charge of the polyplexes confirmed the presence of amine group with a positive charge determined by aqueous electrophoresis.

The interaction between a polymer and genetic material is known as a polyplex. This interaction can vary depending on the amount of polymer relative to the genetic material, which is known as the N/P ratio. The N/P ratio represents the moles of protonable amines (N) present in the polymer versus the moles of phosphate groups (P) present in the genetic material. In the case of this thesis, siRNA was used as the genetic material, and polyplexes were formed with the obtained dextran polymers. This interaction was studied using the gel retardation assay technique at different N/P

ratios, which confirmed the interaction of SCPN-NH_2 and DXT-NH_2 polymer with siRNA. Furthermore, it is noteworthy that the encapsulation increases with the higher N/P ratio. Both systems were classified as good carriers by the different analysis performed. Cell viability tests were carried out, showing no cytotoxic effects in A549 lung cell line up to concentrations of 50 µg/mL. The internalization of the genetic material into the cells was evaluated by means of confocal fluorescence microscopy after labeling the vectors with Rhodamine B fluorophore and, on the other hand, using a carboxyfluorescein-labeled siRNA. Confocal microscopy images were taken 24 hours after adding the compounds to the A549 lung cell line. DXT-NH_2 and siRNA co localize inside the cell, demonstrating that the cationic polymer could bring the genetic material into the cell. However, in the case of polyplexes based on SCPN-NH_2, only the SCPNs could be visualized inside the cell, not siRNA, indicating that the intra-cross-linking did not allow the genetic material to be internalized by the cell.

Subsequently, the efficacy of siRNA for transfection using SCPN-NH_2 and DXT-NH_2 was evaluated. Thus, for this study the A549-GFP cell line was employed, which overexpresses the green fluorescent protein (GFP). Cells were treated with anti-GFP siRNA, designed to block the mRNA of the GFP protein, complexed to the dextran-based vectors. The effect of siRNA was evaluated 96 hours after transfection by flow cytometry. None of the vectors based on either SCPN-NH_2 or DXT-NH_2, showed a significant reduction in protein production, while the positive control based on Lipofectamine RNAimax showed an 80% expression decrease. Therefore, it was decided to focus on the modification of the dextran polymer with different type of amine groups but not with SCPN as these nanoparticles did not show any internalization of siRNAs.

Dextran was modified with different aminated molecules, based on their number of amines and the presence of primary, secondary, or tertiary amines, to improve the release of siRNA from the endolysosomal cavity, by increasing their buffering capacity inside the endosome. Dextran was modified with spermine, 1-(3-aminopropyl)imidazole, Tris(2-aminoethyl)amine, and 3,3'-(piperazin-1,4-diyl)bis(propane-1-amine) using Traut's reagent as a mediator between the alkene of the methacrylate group and the amino group.

Also, dextrans of different molecular weight have been modified to study the effect of the vector molecular weight on the transfection efficacy of the resulting polyplexes. Therefore, dextran with molecular weights of 6 KDa and 20 KDa were substituted with cysteamine using the same conditions as for the 40KDa dextran and characterized by nuclear magnetic resonance. A rapid, simple and quantitative screening of all those candidates as potential siRNA vectors was assessed using GFP reduction assay by flow cytometry. It was shown that polyplexes prepared with dextran substitutions with spermine, Tris(2-aminoethyl)amine, and 3,3'-(piperazin-1,4-diyl)bis(propane-1-amine) could achieve the highest silencing performances. However, the reduction in protein expression only decreased by 50% for the best candidates.

Therefore, in Chapter 4, a different strategy was developed that focused on modifying a synthetic polymer with a high-density of amines, instead of introducing amino groups to a neutral polymeric chain. Polyallylamine (PAH) is a polymer with a one primary amine in each repeating unit with high

potential as a vector for genetic material. However, it is also known that a high amine density can lead to cytotoxicity. Therefore, PAH was substituted with oleic acid (OA) to partially neutralize its charge, aiming at finding a balance between efficacy and toxicity.

Oleic acid was chosen due to the high transfection efficiency demonstrated by lipid-based vectors and the effect of the amount of oleic acid covalently linked to PAH was investigated in terms of their performances as siRNA carrier. Five substitutions of PAH with oleic acid were targeted based on the molar equivalents between the amine group of PAH and carboxyl group of the oleic acid: $-NH_2$: -COOH at 1:0.01; 1:0.02; 1:0.05; 1:0.1 and 1:0.2. The resulting modified PAH were named according to this targeted molar ratio, i.e. PAH.OA.1, PAH.OA.2, PAH.OA.5, PAH.OA.10 and PAH.OA.20. The functionalization reaction was carried out via amide coupling between the carboxylic acid of the oleic acid and the amine of PAH, thanks to the activation of the carboxylic acid of oleic acid by carbodiimide and hydroxysuccinimide in a solvent mixture of dimethyl sulfoxide (DMSO) and water. After purification by dialysis, thin-layer chromatography revealed the absence of free oleic acid in the sample. In addition, infrared spectroscopy showed the presence of covalently linked oleic acid. The determination of the degree of substitution was a difficult task to carry out due to the low solubility of the modified PAH acquired after the binding of the oleic acid and the precipitation of PAH in alcohol. Different solvents and their mixtures were tried, but water appeared to be the best compromise and the most relevant for the non-viral vector application. In that sense, the degree of substitution of oleic acid was only estimated by 1H nuclear magnetic resonance, due to the lack of interaction between the hydrophobic group and the water. Other attemps of the determination of the degree of substitution were investigated, such as elemental analysis and thermogravimetric analysis, but both techniques only resulted in demonstrating that the amount of oleic acid increased with higher molar ratio $-NH_2$: -COOH, as expected. Actually, the hydrophobic character of the oleic acid group resulted in the formation of nanoparticles in water. Interestingly, the hydrophobic groups of the modified polymer chains self-assembled in water, forming a micelle like structure with oleic acid in the middle, surrounded by PAH polymer chains. The size of the particles was determined by dynamic light scattering and transmission electron microscopy (TEM). While the hydrodynamic diameter was found to be at around 200 nm, TEM images allowed, not only particles of 10 nm particles to be observed, but also aggregates of the nanostructure with a diameter ranging from 100 to 300 nm depending on the amount of oleic acid attached. On the other hand, the surface charge was always positive, at around +40 mV.

The formation of polyplexes with siRNA was studied at different N/P ratios 2.5, 5, 10 and 15, in terms of size, surface charge and encapsulation efficiency. The polycation/siRNA complexes exhibited similar sizes as the self-assembled polymer nanoparticles in water for the highest substitution with oleic acid (PAH.OA.5, PAH.OA.10 and PAH.OA.20). On the other hand, less substituted PAH (PAH.OA.1 and PAH.OA.2) showed smaller size.

The Z potential was reduced to 30 mV after polyplex formation. was quantified by Quant-IT Ribogreen, resulting in encapsulation efficiencies greater than 90% for all polymers and N/P ratios tested. As expected, the surface charge of the polyplexes was positive but the Z potential was reduced to +30 mV after polyplex formation, as judged by aqueous electrophoresis.

SUMMARY

The transfection efficiency of oleic acid-substituted polyamine was studied in Chapter 5. First, the viability and membrane damage of A549 cells were evaluated after exposure to the polyplexes prepared with the modified polymers It was observed that the cytotoxicity of modified PAH polymers decreased with higher amount of oleic acid. However, high amounts of polymer at N/P 15 were cytotoxic in all substitutions. The ideal N/P ratio was found to be 5, with more than 95% cell viability. Internalization was evaluated by confocal microscopy and flow cytometry using fluorescently labeled probes, i.e. Atto-633-functionalized modified PAH and siRNA-6-FAM. Colocalization studies allowed both, polymer and siRNA, to be visualized inside the cells for all polyplexes prepared at a N/P ratio of 5. Flow cytometry revealed that, out of 10,000 cells, 70% showed siRNA fluorescence in all substitutions, indicating that oleic acid does not impact on the entry of polyplexes into the cell. More interestingly, the evaluation of polymer delivery efficacy by measuring GFP fluorescence after treatment with anti-GFP siRNA to A549-GFP cells (Same experiment used in Chapter 3) showed that the polyplexes prepared with PAH.OA.5 and PAH.OA.10 could achieve higher silencing performances with a protein reduction close to 70%, which is very similar to the one obtained with Lipofectamine RNAimax at around 80%.

Thus, oleic acid improved the silencing efficacy of PAH, not because of greater cellular internalization of siRNAs, but most likely by facilitating the endosomal escape.

Consequently, these vectors were tested to silence CD47 as the potential therapeutic drug to fight lung cancer. CD47 is a transmembrane protein expressed in most cells of the body, with an overexpression in certain tumors such as non-small cell lung cancer. CD47 plays a role in modulating the immune system, as it is recognized by macrophages through the SIRPα receptor located in their membrane. Through this binding, phagocytosis of the cell by the macrophage is inhibited, preventing attack of macrophages. An interesting strategy is to reduce the expression of the CD47 protein through gene silencing to evaluate if there is a reduction in tumors by phagocytosis of macrophages. The reduction of CD47 protein in A549 at the transcript (qPCR) and protein level (Western Blot, Immunofluorescence and Flow cytometry) was reduced up to 70% when PAH.OA.10 was used as polyplex, which is consistent with GFP flow cytometry data. Additionally, the same vector with a negative siRNA did not decrease expression of CD47 mRNA, ruling out any possible undesired effect of the polymer.

The good performance of the PAH.OA.10 polymer as a vector not only anticipates its application in future therapy against lung cancer, but also opens doors to new possible targets.

Chapter 1:

General introduction

1.1 Gene therapy and nanomedicine

The US Food and Drug Administration (FDA) defines gene therapy as "products that mediate their effects by transcription and/or translation of transferred genetic material and/or by integrating into the host genome and that are administered as nucleic acids, plasmids, viruses, or genetically engineered microorganisms. These products can be used to modify cells *in vivo* or can be transferred to cells *ex vivo* prior to patient administration"[1].

Traditional approaches based on chemotherapy and surgery have improved the lives of people throughout the world but there are many diseases for which these traditional methods only modulate the course of the disease but do not provide a cure. Those are genetic disorders occurring spontaneously or inherited in which, a single gene or several genes present mutations on its sequence. These mutations result in the production of malfunctioning proteins causing the disease. Applying standard drug therapy only will relieve the patient from symptoms derived from the disorder but will not erase the origin of the problem.

There are different types of genetic disorders classified by single-gene disorder (monogenic disorder), mutations in multiple genes (multifactorial genetic disorders), abnormalities in chromosomes and mitochondrial genetic disorders. Among monogenic disorders can be found cystic fibrosis, sickle-cell anemia, Duchenne muscular dystrophy. Multifactorial genetic disorders have multiple genes involved in combination with lifestyle and environmental factors, one clear example is cancer. Another example of genetic aberrations are human chromosomal disorders, which present anomalies in the chromosome number or structure and occur during early development of the fetus. The most well-known example is the Down syndrome with a trisomy in the chromosome 21. Last but not least we can find mitochondrial genetic disorders, which are caused by mutations in the DNA of mitochondria, which are inherited from female parent egg cell. These types of mutations are very rare, one example is the Pearson syndrome, which affects principally the hematopoietic stems cells in the bone marrow causing low production of red blood cells (anemia), white blood cells (neutropenia), or platelets (thrombocytopenia).

Thanks to the human genome project, it has been possible to know the base-pair sequence of most of the genes of the human being. This milestone made possible to identify the presence of mutations in any gene and open doors to multiple possible therapies.

Gene therapies can work by several mechanisms: replacing a disease-causing gene with a healthy copy of the gene, inactivating a disease-causing gene that is not functioning properly and introducing a new or modified gene into the body to help treat a disease. There are different tools to afford these mechanisms.

Inactivating or eliminating malfunctioning genes can be achieved by specific nucleases: Zinc finger nucleases (ZFNs), transcription activator-like effectors nucleases (TALENs) and the clustered regularly interspaced short palindromic repeats (CRISPR) and associated nucleases (cas), known as CRISPR/cas9 system. These are common nucleases that cut the double stranded DNA at desired

point. A gen can be deleted by making two cuts by its edges. When a double stranded break (DSB) is performed repair mechanism of the cell come into play to fix the cut. One of these mechanisms is via homologous recombination (HR). Cells can use unbroken sister chromatid or homologous chromosome as template to copy into the break site. Alternative repair is the non-homologous end-joining (NHEJ), in this process broken sites are joint without regarding the homology.

A new gene or a healthy copy can be introduced into the genome, taking advantage of homologous recombination repair mechanism. These nucleases are introduced into the cell together with the desired exogenous gene. The exogenous gene must be flanked by the same sequence of the desired locus to be inserted to, so throughout homologous recombination the new gene will be introduced into the genome after a DSB made by the specific nuclease. Other methods to introduce new genes into the genome is by transposons or by virus cassettes, in these cases a DSB in specific site is not required.

Editing the genome can indeed result in undesired outcomes, such as insertions in incorrect locations, causing the disruption of unwanted genes or unpredicted deletions. These techniques must be used with extreme caution, as any damage to the DNA chain could have irreversible consequences, potentially compromising the life of patients. As a result, it is interesting to explore the inactivation of gene expression without manipulating the DNA itself, using post-transcriptional approaches. Two primary strategies can be identified: up-regulation of a healthy copy of the gene or down-regulation of an undesired malfunctioning gene.

The first strategy involves the administration of exogenous messenger RNA (mRNA), which encodes for a deficient protein in the patient's metabolism, or a therapeutic protein involved in the treatment of the disease. This approach was successfully employed in the development of vaccines and was first used clinically to combat the COVID-19 pandemic. Due to its success, it is now being studied for implementation in other diseases, such as cancer[2].

The second strategy consists of preventing the expression of malicious gene copies by utilizing the RNA interference (RNAi) pathway. RNAi is initiated by introducing short RNA oligonucleotides into the cell, which then bind with specific messenger RNA of the targeted gene, preventing its translation. This approach can effectively silence the expression of undesired or malfunctioning genes, offering a promising alternative to direct genome editing techniques.

Nanomedicine defined as the use of nanoscale materials for drug delivery, has played an important role in the development of gene therapy, as many of the tools needed for gene editing cannot be administered on their own but need the help of nanometer-scale vehicles to transport them to the desired site of action in the body. There are many examples in literature of nanomaterials that have been developed to transport genes as delivery systems.

Over the last four decades, nanomedicine and gene therapy have advanced hand in hand in the search for solutions to genetically based diseases. Through careful design and engineering, nanomaterials can be tailored to encapsulate and protect therapeutic nucleic acids, facilitate their cellular uptake, and promote their release at the target site. As such, nanomedicine offers a

powerful strategy for the safe and effective delivery of gene therapies, with significant potential for the treatment of a wide range of genetic disorders.

1.3 Interference RNA

1.2.1 Discovery and mechanism of interference RNA

In 1998 Andrew Fire and Craig Mello published an article in which they described that introducing an exogenous doble stranded RNA (dsRNA) into the cytoplasm of *Caenorhabditis elegans* caused a gene systemic suppression[3]. They termed this phenomenon Interference RNA (iRNA).

iRNA is a naturally occurring mechanism that regulates gene expression, and it starts with a double-stranded RNA molecule (dsRNA). The origin of the dsRNA could be endogenous or exogenous, where two different type of RNA molecules are involved respectively. Although its origin is different, both molecules promote the same final, the repression of gene expression also known as *gene silencing*. The mechanism is typically post-transcriptional (PTGS) and occasionally and more rare, transcriptional (TGS). Both mechanisms are depicted in Figure 1.1.

Post-transcriptional gene silencing (PTGS) mechanism involves two types of RNAs, small interference RNA and micro interference RNA (siRNA and miRNA). Both are double stranded RNA about 18 to 25 base-pair length, with little differences between them. siRNA presents perfect base-pairing, whereas miRNA contain mismatches causing helices and terminal loops. miRNA origin is endogenous purposefully expressed from the genome as a transcript known as primary-miRNA (pri-miRNA) and siRNA derive from exogenous long dsRNA. Origin of both pathways are different but converge in the cytoplasm.

miRNA genesis occurs in the nucleus. pri-miRNA transcript is expressed, having at least 1000 base-pair length and single or clustered double-stranded hairpins. 5´and 3´termini overhang from the double-stranded region. The pri-miRNA is excised by the microprocessor complex, containing proteins Drosha, RNAse III and DiGeorge syndrome critical region gene 8 (DGCR8). DGCR8 recognizes pri-miRNA, thanks to its binding domain and Drosha perform the cleavage. The resulting 65 to 75 base-pair precursor (pre-miRNA) is exported to the cytoplasm by the Exportin-5 and RanGTP facilitators[4] (See Figure 1.1).

Both pre-miRNA and long dsRNA are associated in the cytoplasm with Dicer protein and TAR RNA-binding protein (TRBP). Dicer protein cut the terminal loop of pre-miRNA and cleavage long dsRNA, obtaining miRNA and siRNA. Both small oligonucleotides if exogenously administered can be directly bound to Dicer and TRBP protein. A third protein is recruited, from the family of Argonaute (Ago) to form the RISC-loading complex (RLC). Then the oligonucleotide is loaded into the Argonaute. Thereafter an excision in the dsRNA occurs and the guide strand (antisense) of the dsRNA is selected and the passenger strand (sense) is discarded forming the mature RNA-induced silencing complex (RISC). Guide strand in RISC complex attaches by sequence complementarity to mRNA and repression occur. In the case miRNA, sequence annealing with mRNA mismatch is some nucleotides

and RISC complex drives mRNA to P-bodies and GW-Bodies promoting its degradation and the subsequently post-transcriptional gene silencing. In the case of siRNA, guide strands usually have full complementarity to a single target mRNA and RISC complex recruit protein Ago2, which have an intrinsic slicer activity to efficiently cleave mRNA. All this induce potent and narrowly targeted gene silencing[4,5] (See Figure 1.1).

Transcriptional gene silencing (TGS) occurs in the nucleus and provoke DNA methylation and histone post-translational modifications, resulting in remodeling of chromatin around the target gene into a heterochromatic state. This causes the siRNA to silence for a longer period. TGS is observed in *Arabidopsis*, *Schizosaccharomyces pombe*, and mammalian cells. In human mechanism is not fully understood but siRNA binds to RNA-induced transcriptional silencing complex (RITS). A group of proteins, which include DNA methyltransferase 3a (DNMT3a). Then mechanism involve RNA Pol-II, and histone methylation[6,7] (See Figure 1.1).

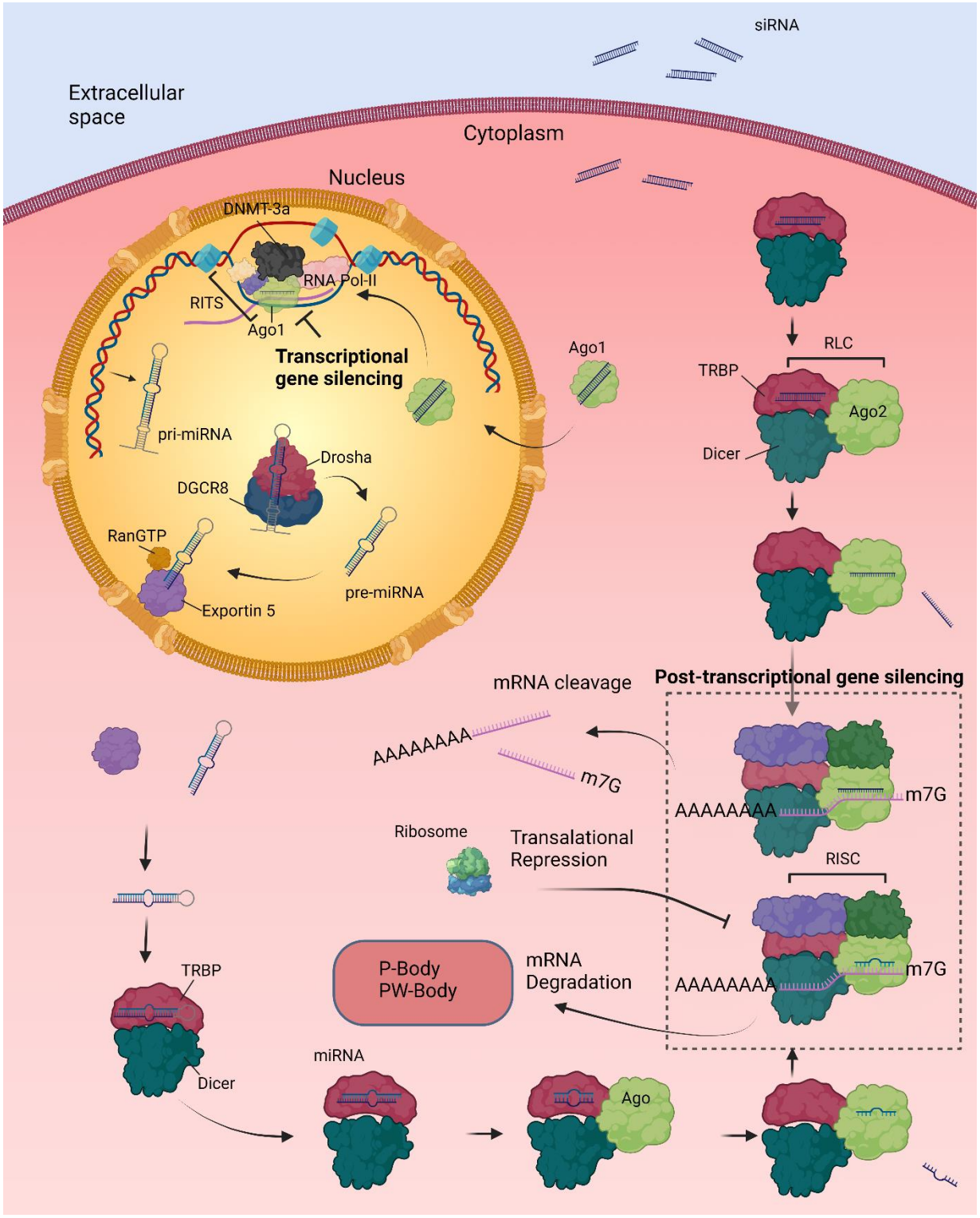

Figure 1. 1.-Scheme of cellular gene silencing mechanisms. Post-transcriptional gene silencing (PTGS), occurring in the cytoplasm and Transcriptional gene silencing (TGS) occurring in the nucleus. Image generated with Biorender.

1.2.2 RNAi based drugs

RNAi based drugs consist in introducing artificially synthesized molecules which enter in the RNAi pathways. These molecules comprise a large number of short double-banded RNA, which will bind with a specific region of the endogenous RNA or DNA previously designed. The most studied and used molecules are siRNA, miRNA and shRNA. The first two are chemically synthesized and enter

directly into the RNAi pathway once applied. The shRNA is a DNA construct, which codes for short hairpins RNA (shRNAs). The double-stranded region of shRNAs is formed through a hairpin structure and intramolecular hybridization that resembles of miRNA precursors. Dicer protein recognizes shRNA and cleaves it, forming a mature siRNA that will guide the RISC complex to bind to the specific mRNA. shRNA effect is long-term and stable while siRNA mediates only transient silencing because their concentrations in the cytoplasm are diluted over time with successive cell divisions. On the other hand, shRNAs also enter the endogenous silencing pathway at an earlier stage than siRNAs, having a higher chance of saturating the natural miRNA pathways[8]. The advantage of using a chemically synthesized molecule is that chemical modifications can be introduced to increase stability, promote efficacy, block binding to unintended targets that contain sequence mismatches (off-target effects), and reduce or abolish potential immunostimulatory effects. Conventional siRNAs are approximately 19-25 nucleotides and have 2 nucleotides overhanging in the 3‘ end of each strand that mimic Dicer cleavage products. Not every siRNA for the same target achieves equivalent levels of knockdown, large-scale siRNA screening is often performed for any given target to find the most potent candidate.

These have yielded some rules for siRNA design with high delivery efficiency[9]. 5‘ end of the antisense (guide) strand should have lower thermodynamic stability than the 5‘ end of the sense strand to be incorporated into the RISC[10]. The proportion of the nucleotides guanosine and cytidine should be around 50% or lower. Secondary structures within mRNA, ribosome and other protein binding sites could hinder access of the RISC complex to the target so these sites or nearby should be avoided[11]. Statistical analyses have also found a preference for certain nucleotides at specific positions within the siRNA, like positions 3,10,13 and 19th in sense strand should be A, U, not G and not G/C, respectively[12]. Based on these rules, practical algorithms have been introduced to select the most efficient silencing. This has led to the development of different software tools to facilitate siRNA design for the user. Different software are available for identifying the optimal target sequences for a given gene[13]: siDirect, siDESIGN center, Genscript, and Asi designer among others. Even an artificial neural network, has been used to develop a genome-wide siRNA library for humans[14]. Another interesting aspect to consider in the siRNA design is to consider splice variants and isoforms of a gene. In some approaches is important to silence all variants, meanwhile in others just a deficient isoform is required.

1.2.3 *Safety Issue*

Delivery of RNAi based drugs could provide a non-specific toxicity, a critical issue to afford. There are three sources of toxicity related to active compound of the doble-stranded oligonucleotide: Innate immune response, off-target effects and activity in non-target tissues.

1.2.3.1 *Innate immune response*

siRNA administration activates the response of the immune system. Probably due to the evolution of a defense mechanism against viral infections with long dsRNA. It is activated by two pathways: one involves recognition of cytosolic RNA-binding proteins, such as serine-threonine protein kinase

R (PKR)[15] and the other, recognition by toll-like receptors (TLR) TLR3, TLR7 and TLR8[16]. Several reports have demonstrated that this immune response can be overcome by modifying siRNA backbone with 2´-O-methyl, 2´-F and phosphorothioate backbone (Figure 1.2). Thus, avoiding TLRs binding and prevent cytokine induction while maintaining silencing activity[17,18]. Furthermore, siRNAs with non-immune stimulation could be selected after transfection of a siRNA battery in human primary cells[16,18].

1.2.3.2 *Off-target effects*

RNAi is highly specific as a result of base pairing interactions. Nevertheless, a number of studies[19,20] have demonstrated that siRNAs could bind to mRNAs of seemingly unrelated genes and knockdown their activity. It is known that only a 7-nucleotides region of the guide strand called the 'seed region' or 'seed sequence' is necessary for the binding. Therefore, such small sequence homology is enough to trigger off-target effects (OTEs) and the possibility of finding 7-nucleotide complementary regions in the entire human transcriptome are much higher than actually desired. This problem can be improved by careful comparison of candidate guide strand sequence with the entire transcriptome by using proper software. Long stretches of homology and significant overlaps with genes of concern should be avoided. However, the only way to ensure safety is via extensive testing. Here, it is critical to use primate models with large genomic sequence that overlaps with humans as the genomes of other animals have too many significant differences to provide adequate screening. Even with extensive testing, some off- target RNAi effects may be inevitable.

1.2.3.3 *Saturation of endogenous pathways*

Bioactive drugs that rely on cellular processes to exert their functions face the risk of saturating endogenous pathways. This is the case of RNAi based drugs. shRNA expressed in the nucleus accumulates the activity of Exportin-5 transporter protein (Exp5). Thus, blocks the route of endogenous pre-miRNA. A high expression of shRNAs induced cytotoxicity and ultimately caused death[8]. siRNA activity does not require Exp5, however it competes with endogenous miRNAs to be incorporated into the RISC complex. The selection of one oligonucleotide or another depends on TRBP protein selection[21]. These adverse effects have to be detected and the optimal concentration has to be used to not alter cellular processes.

1.2.3.4 *Activity in non- target tissues*

siRNAs delivered systemically to the body can accumulate in many tissues that are not the intended sites of drug activity[11]. This can lead to undesired side effects in healthy tissues. Nowadays, RNAi therapy mitigated these issues by choosing highly- disease-selective genes as the targets for RNAi silencing and by choosing delivery routes that reduce accumulation in non-target tissues. Future improvements in tissue-specific targeting of RNAi activities may ease these restrictions to allow development against additional indications. In addition, Alnylam, one the principal siRNA pharmaceutical companies, has recently developed antisense oligonucleotides that can reverse the drug activity of siRNA drugs in vivo[22].

1.2.4 *Chemical modifications*

During early days of RNAi development was evidenced that chemical modifications in oligonucleotide backbone are needed. These modifications have mainly two purposes, the reduction of immune response and the improvement of stability by reduction of degradations by endonucleases and exonucleases. The modifications can be carried out in the different moieties of the nucleotide.

Modifications in the sugar 2´carbon: 2´-O-methyl, 2´-Fluoro and 2´-O-methoxyethyl reduce immune activation, increase base pairing melting temperature (Tm) and improve nuclease resistance (See Figure 1.2).

Modification in the pentoses: Locked nucleic acids (LNA), 2´and 4´carbon are linked and unlocked nucleic acids (UNA), where 2´and 3´carbon are missing the bond. They serve to increase or decrease binding affinity to RNA respectively (See Figure 1.2).

Modifications in the phosphate backbone, using a phosphorothioate group (PS) instead of a phosphate group increases half-life stability[23](See Figure 1.2).

The replacement of the ribose by a morpholino or a peptide nucleic acid deletes or reduces the surface charge given by the backbone. This allows an increased hydrophobicity of the siRNA and more resistance against nuclease degradation (See Figure 1.2).

In late 2000s unmodified siRNAs such as bevasiranib, AGN211745, and ALN-RSV01, entered clinical trials but did not progress beyond phase II[24,25]. One reason for this was that the apparent therapeutic effect might have been due to the activation of innate immunity via the toll-like receptor 3 (TLR3) pathway, rather than the intended gene silencing mechanism. To address this issue, current clinical formulations include chemical modifications in the siRNA structure to enhance their stability and effectiveness, consequently allowing for a reduction in the administered dose.

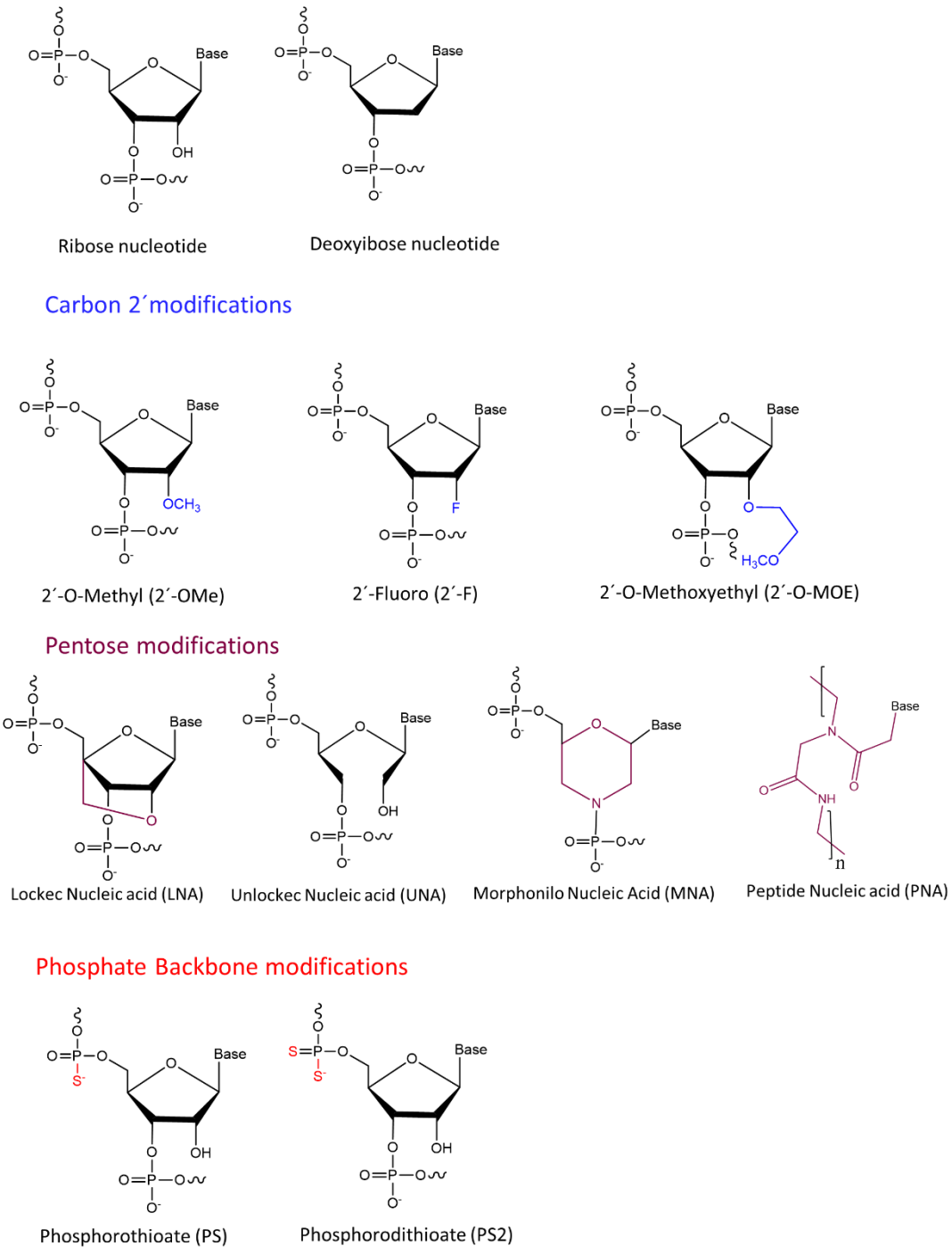

Figure 1. 2.-Structures of chemical modifications and analogs used for siRNA. According to the modification site in the nucleotide acid, these structures can be divided into carbon 2´ modifications (blue), ribose modification (Purple) and phosphate modification (Red)**.**

1.4 Barriers in RNAi delivery

The site of action of siRNAs is cytoplasm, so when they are systemically administered there are a number of barriers that will need to be overcome to achieve gene silencing. Nuclease degradation, short-live body circulation, immune recognition in blood stream, accumulation in the desired tissue, trespassing cell membrane and escape from the endosome and lysosome. By chemical

modifications, issues of stability against nucleases and immune recognition have been significantly reduced. However, other challenges still remain to be solved. For this purpose, the siRNA has to be formulated together with a vector that protects it and deliver it to their site of action.

siRNA is a molecule, 7–8 nm in length and 2–3 nm in diameter approximately with relatively high molecular weight 13-16 KDa and net negative charge. These properties make it difficult to cross the cell membrane, but their size is sufficiently small to be filtered by the glomeruli[26], as molecules smaller than 8 nm[27] are easily filtered into the urine. Once siRNAs are administered, they will be accumulated in the bladder and excreted out of the body quickly, from a few minutes up to an hour[28,29], which hampers the possibility to reach the target tissue. Even if they can avoid their elimination by urine, tissues with fenestrated blood vessels are the most common final destination of siRNAs, such as the liver, through which they end up being eliminated by the gallbladder. The negative charge of the cell membrane prevents the uptake of siRNA. Only a few types of mammalian cells are known to be transfected by siRNA, like retinal ganglion cells and neurons[30]. Common siRNAs formulations enter cells via pinocytosis and through the formation of an endosome. Once inside the cells, siRNA must escape from the endosome and lysosomes to bind to TRBP protein and enter in the RISC complex. This barrier represents the major obstacle to overcome. Only 1-2% of siRNA formulations are released into the cytoplasm and this occurred in narrow frame of time[31]. The exact mechanism of endosomal release is not fully understood. Different hypotheses of how oligonucleotides escape from endosomes are currently discussed, being the called “proton sponge effect” is the most popular one[32]. It consists of a disruption of the endosome caused by osmotic swelling. Once endosome is formed after the endocytosis, it starts to be acidified by pumping flux of protons by membrane-bound V ATPase. To compensate for the proton charges, chloride anions enter the endosome through the chloride channels. Vectors of oligonucleotide are typically designed with amino groups that can be protonated. This buffering capacity delays the acidification and induce the increase of proton influx and ions inside the vesicle leading to an osmotic imbalance. The corresponding entrance of water produce endosome swelling that disrupts the membrane and release the cargo[32,33]. However, intact endosomes have been observed after siRNA delivery with proper silencing effect[34]. Thus, another theories have proposed that deal with the direct interaction of the vector with the exoplasmic lipid leaflet causing membrane destabilization, permeability or supported nanoscale hole formation[32,35]. Hence, further understanding the escape mechanism and how to enhance the escape efficiency is of great importance for siRNA drug development[36].

1.5 Delivery systems

Delivery systems are needed to direct the oligonucleotides to its target tissue. They have an important role in the RNAi therapies because they have to provide all the characteristics that siRNA lacks to promote a silencing effect. That includes protect cargo from the nuclease degradation, confer a sufficient size to the formulation to overcome kidneys clearance. To be capable of trespass the cell membrane and promote the endosomal escape. Along the development of siRNA technology different types of carriers have been achieved. Delivery platforms are mainly classified in naked or non-vector platforms, viral-vectors or non-viral vectors (Figure 1.3).

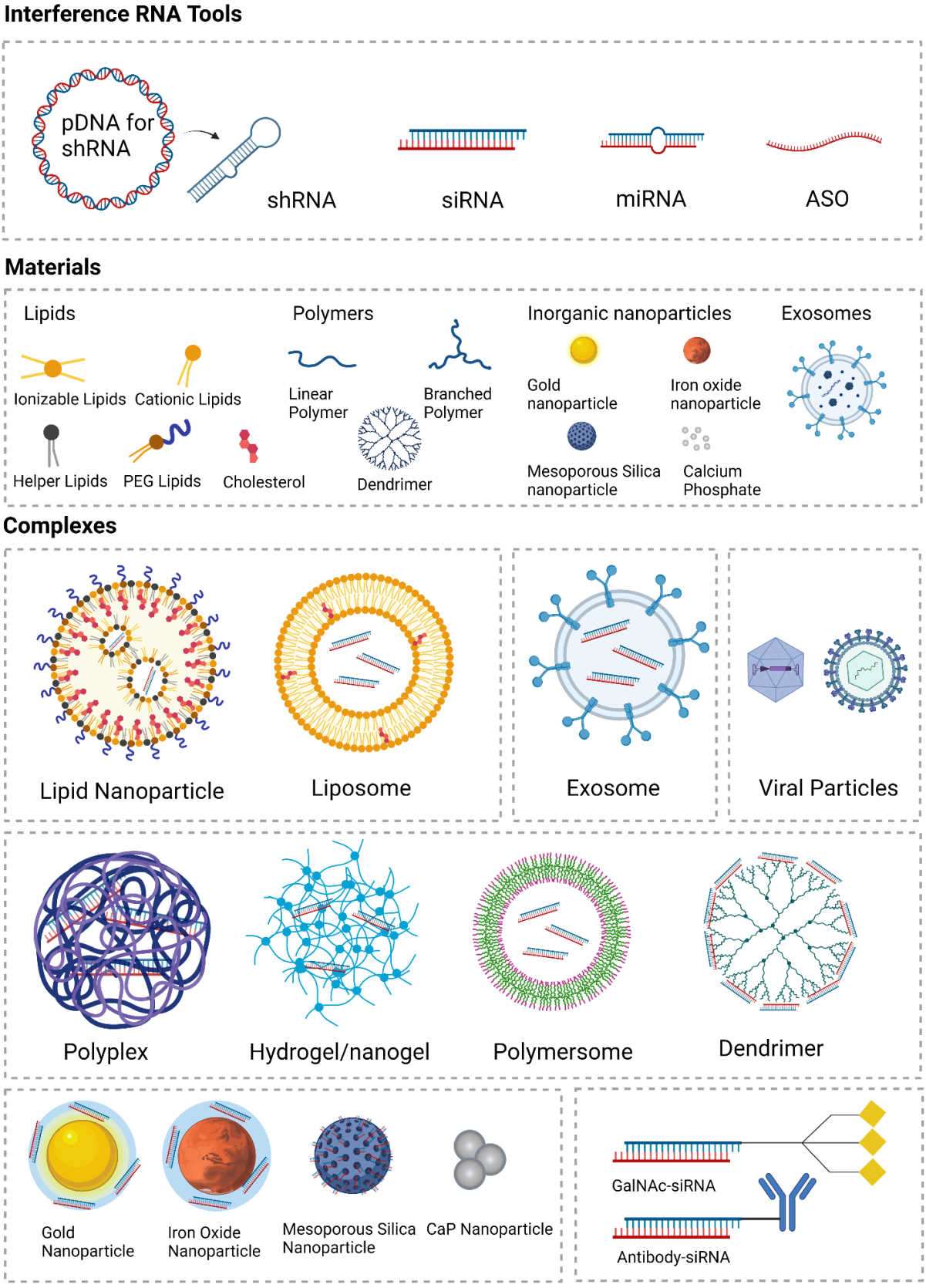

Figure 1. 3.-Scheme for the main nanoparticle design used in gene delivery. Interference RNA molecules used in therapies and materials used for construction of different nanoformulations: lipid-based nanoparticles (liposomes and LNPs), polymeric nanoparticles (polyplexes, polymersomes and dendrimers), inorganic nanoparticles and exosomes. Structures of nanoparticle complexes and conjugated iRNAs. Imaged generated with Biorender.

1.4.1 Naked siRNA

Naked siRNA delivery platforms contain only the oligonucleotide without any excipient either covalently or non-covalently attached. Because they are not protected by vehicle, modifications in siRNA structure have been conducted to render the RNA resistant to enzyme degradation and extend circulation time in the bloodstream. siRNAs are naturally filtered by the kidney, so this type of delivery can be used to treat kidney-expressed genes in renal diseases. QPI-1002 is the name given by Quark Pharmaceuticals to a siRNA designed against p53 to treat acute kidney injury. It is administered intravenously and reach kidney in a short time[37,36]. As there are some tissues that can take up naked siRNA, such as the eye and central nervous systems, siRNAs can be delivered by local injection without transfection reagents. Different groups have demonstrated efficient silencing effect against VEGF in monkeys and mice after intravitreally administration of siRNA or subretinal injection to treat age-related macular degeneration[38,39]. As well Quark Pharmaceuticals initiated clinical trials with a naked siRNA injected intravitreally against caspase-2 to treat non-arteritic anterior ischemic optic neuropathy (NAION)[40].

1.4.2 Viral vector

Viral vectors capitalize on the natural ability of viruses to penetrate cell membranes and deliver genetic material. In these vectors, the genes related to viral replication and capsid assembly are removed and replaced with the genes of interest. In the context of RNAi technology, the viral cassette is designed to carry a gene that encodes a shRNA structure, along with a promoter for RNA polymerase II (Pol II) or RNA polymerase III (Pol III). This construction will be inserted into host cell genome thanks to the mechanism of virus. The expression of the shRNA construct will be processed by the Drosha protein, resulting in a pre-miRNA mimic structure. This structure will then be exported to the cytoplasm, where it follows the miRNA pathway. The advantages of viral vectors include long-term expression of therapeutic RNAi and high transfection efficiency. There are different viral vectors based on the type of virus: Retrovirus, adenovirus, adeno-associated virus (AAV), and lentivirus. shRNA constructs in lentiviruses have demonstrated silencing β-site amyloid precursor protein cleaving enzyme 1 (BACE-1) main cause of neurodegeneration in Alzheimer's disease[41]. AAV have been used to deliver shRNA constructs against ataxin-1 in mouse models of spinocerebellar ataxia-1 (SCA1)[42]. Another example of AAV is the work by Suckau et al, who designed a shRNA construct against phospholamban, a protein involved in cardiac calcium regulation and observed restored diastolic and systolic functional parameters to normal ranges in rats with injured hearts[43].

Despite of the high efficiencies, viral vectors present important drawbacks. The loading capacity is limited, and the constructions cassettes are difficult to produce at large scale. Additionally, it has severe safety risks, inflammatory and immunogenic effects and potential oncogene formation could happen because of the insertion of the transgene in the wrong position. Due to these major safety issues non-viral vectors have gained great interest.

1.4.3 Non-viral vectors

Non-viral vectors encompass a wide variety of delivery systems that utilize different biomaterials. Approaches that combine synthetic chemistry and molecular biology have been extensively employed to develop artificial carriers capable of facilitating intracellular gene delivery. Among the non-viral vectors are lipids, polymers, inorganic nanoparticles, peptides, exosomes, and nucleic acid nanostructures.

1.4.3.1 Lipid based materials

Lipid delivery systems are mostly based of phospholipids-like structures that are dispersed in water and form spontaneously multi or single lamellar bilayer structures (vesicles) or micelles. Bilayer structure vesicles were termed as liposomes and were initially used as models of biological membranes[44], but soon were recognized as drug delivery systems due to their encapsulation capacity. In gene delivery liposomes were originally developed for DNA-based drugs, but rapidly demonstrate its potential to siRNA delivery. The complex derived from electrostatic interaction between lipid and siRNA (or another nucleic acid) is called lipoplex.

Liposomes could have different surface charges depending on the lipid composition. Cationic lipids were firstly more attractive because the electrostatic interaction with negatively charge DNA or RNA, allowing the material to be entrapped inside the vesicle. The lipid structure is formed by hydrophilic head group, a linker group and hydrophobic group made of aliphatic chains or cholesterol derivatives. The head group is typically formed by primary, secondary or tertiary amines, which gives the positive charge. Hydrophobic group could be aliphatic saturated or unsaturated or cholesterol-like structure. The linker facilitates the chemical bond between hydrophilic and hydrophobic moieties. It could have different lengths and proved to contribute to the properties of the entire molecule.

In Figure 1.4 different cationic lipid structures are shown. Lipid structure is an important determinant of the transfection efficiency and cellular toxicity. Commonly, cationic lipids were formulated together with helper lipids, cholesterol, and Polyethylene glycol (PEG)-modified lipids. Net positive-charged liposomes mediate gene delivery, but presents several drawbacks, i.e. cellular toxicity, aggregation with protein and erythrocytes and they activate immune response. For these reasons, attention has been drawn to the rational design of less toxic lipids that are known as ionizable lipids. These lipids are charged at mildly acidic pH and can be complexed with small RNAs to generate a stable nanoparticle. Under physiological pH conditions, the net charge of the particles formed is predominantly neutral to mildly cationic, and thus do not induce a strong immune response. In addition, these lipids are only destabilized by acidic environment, like the one encountered in the endosome, to release their RNA cargo[45]. Many of these lipids have a two tailored structure, but many others are multitailed. The form acquired by the vesicles in water together with siRNAs is not that of a perfect bilayer[46]. Therefore, these structures are called Lipid nanoparticles (LNP), and their inner core is formed by complexes of oligonucleotides and lipids[46] (Figure 1.6).

The principal characteristic of the ionizable lipids is its pK_a, it should be low enough to remain with low degree of protonation at neutral pH during circulation, but high enough to be protonated in early or late endosomal stages. Several combinatorial libraries[47,48,49] have been generated by using different amine head groups and different aliphatic chains achieving different pK_a values. A range between 5.4 and 7.6 resulted in an effective transfection *in vivo,* but specifically pKa values in range 6.2-6.5 achieved best efficiencies[49]. The global pKa value of the lipid nanoparticle is more important than the individual lipid components. A combination of lipids with different pKa, but overall pKa average close to 6.4, present similar results than a lipid with this pKa. There is a strong correlation between pKa value of LNPs and efficacy, however different nanoparticles with similar pKa values present different results in vivo. Rational design and screening of hundreds of lipids formulations has led to identify high efficiency lipids, listed in Figure 1.4, such as C12-200, Dlim-MC3-DMA, $304O_{13}$, 98n12-5.

Cationic Lipids

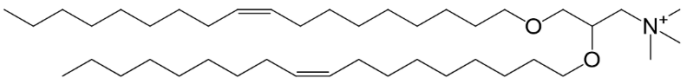

DOTMA

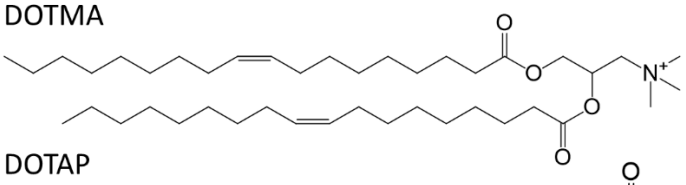

DOTAP

DOGS

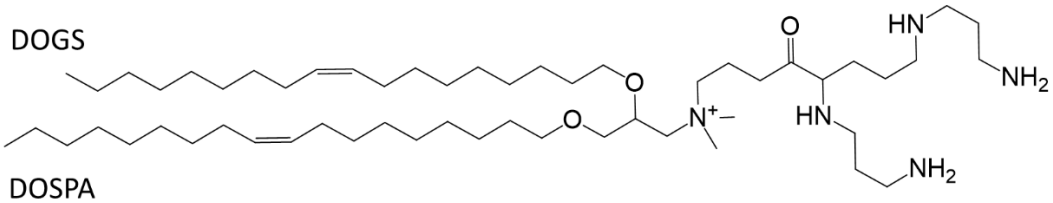

DOSPA

Ionizable Lipids

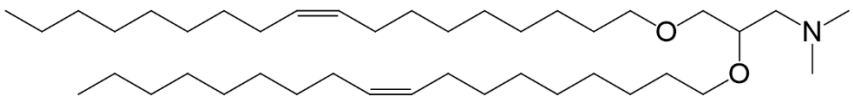

DODMA

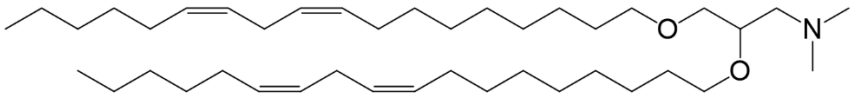

Dlin-DMA

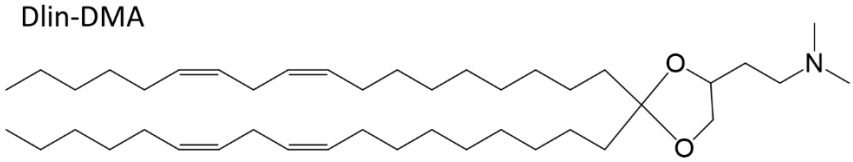

Dlin-KC2-DMA

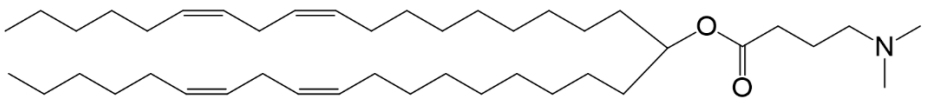

Dlin-MC3-DMA

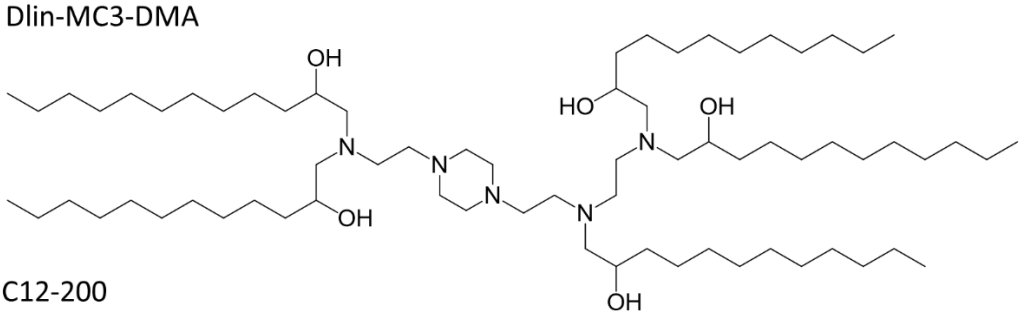

C12-200

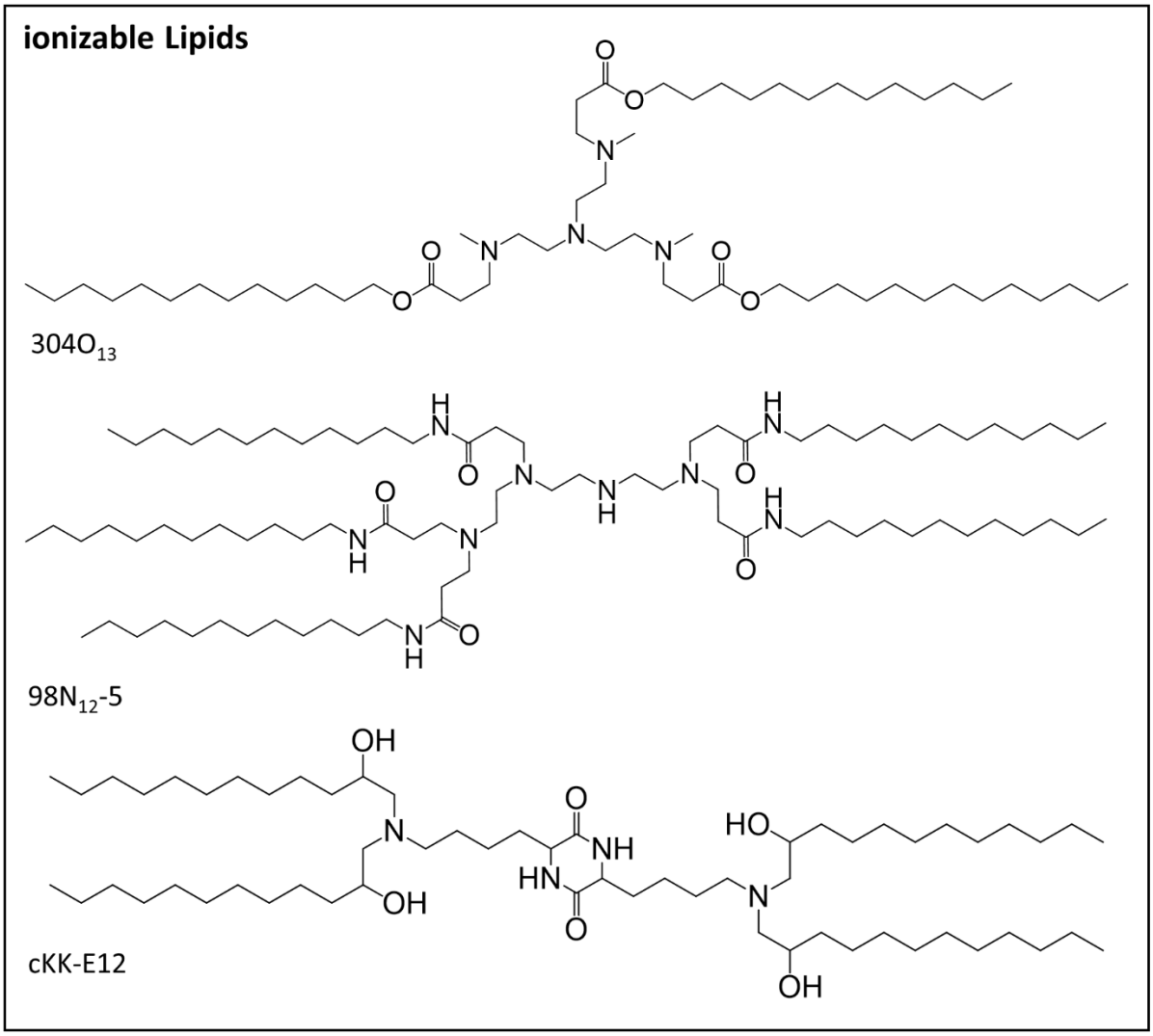

Figure 1. 4.-Chemical structures of several cationic and ionizable lipids, one of the key components of liposomes and LNPs for gene delivery.

Liposomes and lipid nanoparticles contain more components than the ionizable or cationic lipid, that help to increase stability and delivery efficiency *in vivo*, such as PEG-modified lipids (Figure 1.5). The addition of PEG shields the vesicle surface and has proved to confer several advantages: reduce particle size[50,51], prevent aggregation during storage, increase circulation time and reduce uptake by unintended targets such as red blood cells and macrophages[51,52]. For this purpose, lipids have been modified in order to have a hydrophobic core forming part of the vesicle and the PEG moiety on the outwards of the colloidal system helping in the storage stability. However, PEG shield presents some drawbacks, it reduces cellular uptake and delivery efficiency *in vitro* and *in vivo.* PEG can block interaction with the endosomal membrane and hamper endosomal release. However, it has been shown that PEG moieties detach from vesicles after certain time in the bloodstream due to the presence of lipoproteins, letting unshielded surface that interacts with targets cells[53,54]. Another crucial component of the LNPs is the helper lipids, lipids that possess neutral charge and help to stabilize the particle, reducing the amount of ionizable or cationic lipid needed to form the LNP and also help in the endosomal membrane disruption during the release (DOPC, DSPC)[55,56](Figure 1.5).

Other component, such as cholesterol, stabilizes lipid bilayers by filling in gaps between phospholipids (Figure 1.5). The lipid-to-cholesterol ratio in liposomal formulations must be carefully balanced. When cholesterol content exceeds 25%, it lowers the transition temperature of liposomal membranes containing conical-shaped lipids, thus promoting the transition from lamellar to hexagonal phase, which is only desirable at the site of cargo release[57]. Conversely, a cholesterol content of less than 10% can lead to reduced cargo release from the LNP[58,59]. Therefore, optimizing the lipid-to-cholesterol ratio is crucial for achieving the desired stability and cargo release kinetics in liposomal formulations.

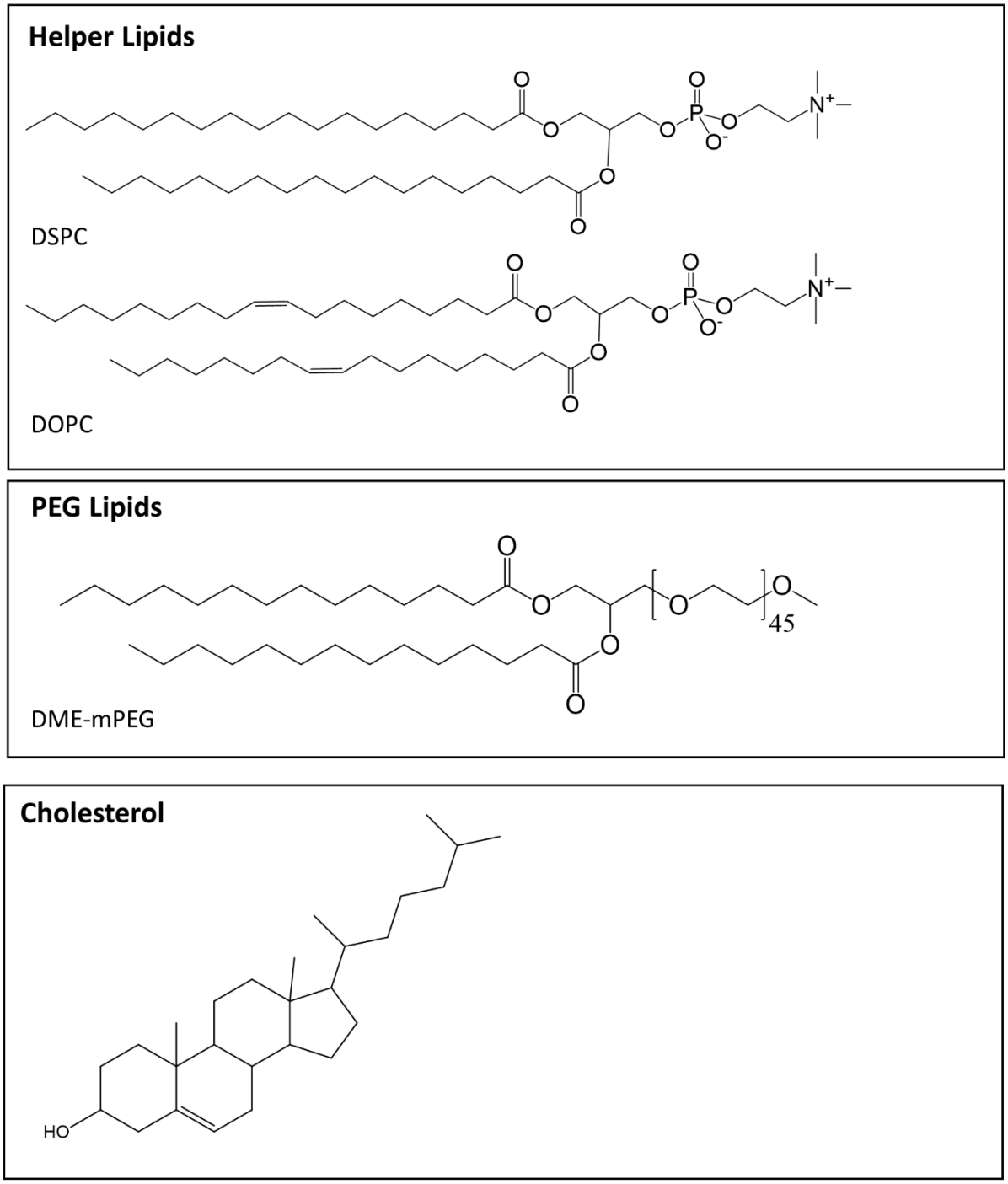

Figure 1. 5.-Chemical structure of several helper lipids, PEG-lipids and Cholesterol, components of LNP formulations.

The most used siRNA non-viral vector in clinical trials and market are LNPs, with Onpattro (commercial name of patisiran and clinical trial named as ALN-TTR02), the first RNAi based drug approved by FDA. Its composition is based on Dlin-MC3-DMA/ DSPC/cholesterol /DMG-mPEG2000 at a molar ratio of 50/10/38.5/1.5 against transthyretin (TTR) protein causing hereditary disease of transthyretin-mediated amyloidosis[49]. Regarding their production, LNPs containing siRNA are prepared by mixing an alcoholic solution (usually ethanol) containing the lipids Dlin-MC3-DMA/DSPC/cholesterol /DME-mPEG2000 and an aqueous buffer solution of sodium acetate at pH 4 containing siRNA using a T-junction mixer or microfluidic system. When lipids get in contact with water, they self-assemble into vesicle structures due to their hydrophobic character. In addition, Dlin-MC3-DMA, the ionizable lipid, is mainly protonated at pH 4, which is well below its pKa 6.4 and allow electrostatic interaction with siRNA. After this mixing step, the solution is dialyzed against PBS buffer pH 7.4. During this process DMG-mPEG orientates PEG moiety towards the outer part of the LNP (Figure 1.6). As previously mentioned, PEG lipids on the surface maintain particle stability during storage.

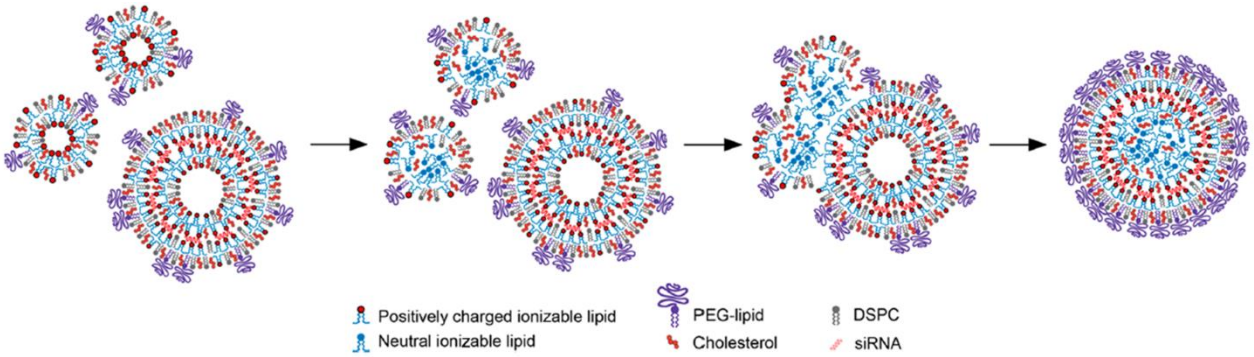

Figure 1. 6.-Mechanism of formation and structure of LNP prepared in the presence of siRNA proposed by Kulkarni et al, after CryoTEM studies, Inner core of cholesterol and neutral lipid, inner layer of siRNA and positive ionizable lipid and outer layer dominated by PEG-lipid. Figure modified from Kulkarni et al[46].

LNPs are injected intravenously once every 3 weeks to the patient at 0.3 mg per kg. Once in systemic circulation, PEG lipid is replaced by serum proteins, specifically apolipoprotein E (ApoE), which interacts with the cholesterol present in the LNPs. LNPs cross fenestrated vessels of the liver and ApoE is recognized by low density lipoprotein receptor LDLR in hepatocytes, which mediate endocytosis. Acidification of endosomes protonates Dlin-MC3-DMA causing particle disassembly. Dlin-MC3-DMA and DSPC by hydrophobic and electrostatic interaction with negatively charged endosomal lipids provoke membrane destabilization. siRNA escape from the endosome, reach cytosol and engage with RNAi machinery[11,53](Figure 1.7).

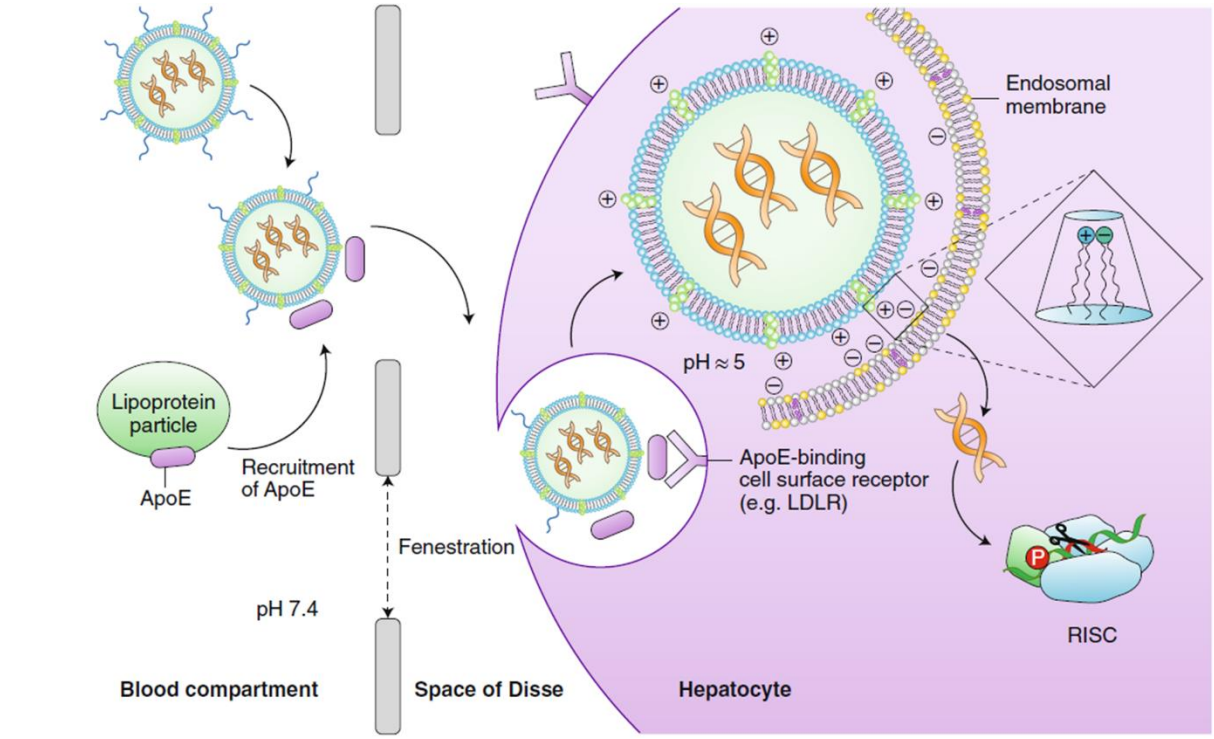

Figure 1. 7.-Model of Onpattro LNP-mediated siRNA formulation delivery *in vivo*. Upon intravenous injection, the PEG shield detaches from the LNP as it circulates through the bloodstream. Apolipoprotein E (ApoE) is recruited and adsorbed onto the surface. LNPs accumulate in the liver due to the fenestrated endothelium, where hepatocyte low-density lipoprotein receptors (LDLR) recognize the adsorbed ApoE and promote receptor-mediated endocytosis of the LNPs. Within the endosome, the ionizable lipid becomes protonated due to the low pH and interacts with negatively charged endogenous lipids, leading to the destabilization of the endosomal membrane. As a result, the siRNA is released into the cytoplasm, where it can engage with the RNAi machinery. Image extracted from *Akinc et al.*[53]

Other clinical trials are using LNP formulations with Dlin-MC3-DMA: such is the case of ALN-PCS by Alnylam pharmaceutics[60]. With other ionizable lipids such Dlin-DMA we can find TKM-080301 developed by Tekmira Pharmaceuticals, that contains anti-PLK1 (polo-like kinase 1) siRNA for the treatment of solid cancer. Arbutus Pharma started developing siRNA lipid nanoparticle formulations ARB-1467 and ARB-1740 against Hepatitis B Virus (HBV) using 3 siRNAs targeting different regions of the virus genome. However, the company suspended the studies to change to GalNac conjugate delivery system. Silence Therapeutics entered clinical trials with Atu027 using a LNP with own ionizable lipid AtuPLEX against pancreatic carcinoma[61], while MRX34 from Mirna Therapeutics was used as ionizable lipid to deliver miR-34a mimic to solid tumors[62]. However, the clinical trials of those last two candidates were discontinued at phase 1/2 because treatment did not achieve the expected results.

Despite the high knockdown efficiency achieved, LNPs present some drawbacks: Low loading efficiency, which means that more siRNA is required. Some toxicity issues related with the lipid components currently limits the maximum tolerated dose and causes concern in scenarios that require long-term use and/or repeated administration. Only liver is reached using LNPs after intravenous (IV) injection, limiting treatments only for liver diseases or for affordable local administration.

1.4.3.2 Inorganic nanoparticles

Inorganic materials have been studied for gene therapy as siRNA delivery system, such as gold nanoparticles, iron oxide nanoparticles, mesoporous silica nanoparticles and calcium phosphate nanoparticles. Inorganic nanoparticles have high surface area to volume ratio, allowing siRNA to adhere by direct conjugation or non-covalent interactions, as well as long shelf time, tunable size and shape, optical properties, remote controlled release, easy functionalization, and high loading capacity.

1.4.3.2.1 *Gold nanoparticles*

Gold nanoparticles (AuNPs) are well studied for siRNA delivery and other nucleic acids. Core of AuNP is essentially inert, nontoxic, and biocompatible, thus offering ideal conditions for the efficient and safe delivery of siRNA. siRNA could be delivered via either covalent or non-covalent chemistry. Finally, the ability to tune AuNP properties through surface modification provides useful properties for controlling NP delivery and release.

Covalent siRNA/AuNP conjugates are possible by thiol-gold covalent chemistry. Oligonucleotides are modified with a molecule containing a thiol group, that can be attached to the surface of the AuNPs. In the same way, polymers and targeting molecules could be grafted to the particle surface to enhance colloidal stability and efficacy for the treatment, respectively [63,64,65,66].

Non-covalent delivery strategies provide a versatile modular strategy for the delivery of free siRNA. AuNPs surface can be coated with different charged polymers or dendrimers[67], allowing the functionalization of drugs via electrostatic interactions. For example, cationic polymers, polyethylenimine (PEI), poly-L-Lysine (PLL) , Poly(amidoamine) PAMAMs adsorbed on the surface of AuNPs enabled electrostatic interaction with anionic siRNA[68](Example in Figure 1.8.-B). In addition, several layers of cationic polymers and anionic siRNA can be successively adsorbed on the AuNP surface (known as layer by layer technique), increasing the loading capacity[69,70].

One formulation using gold nanoparticles as delivery vector entered Phase I of clinical trials. siRNA against BCL2L12, an oncogene that prevent tumor cells from apoptosis, is covalently attached to a 13 nm AuNP together with oligoethylene glycol or PEG. Formulation NU-0129 systemically administered can cross blood brain barrier to reach glioblastoma[71,72](See Figure 1.8.-A).

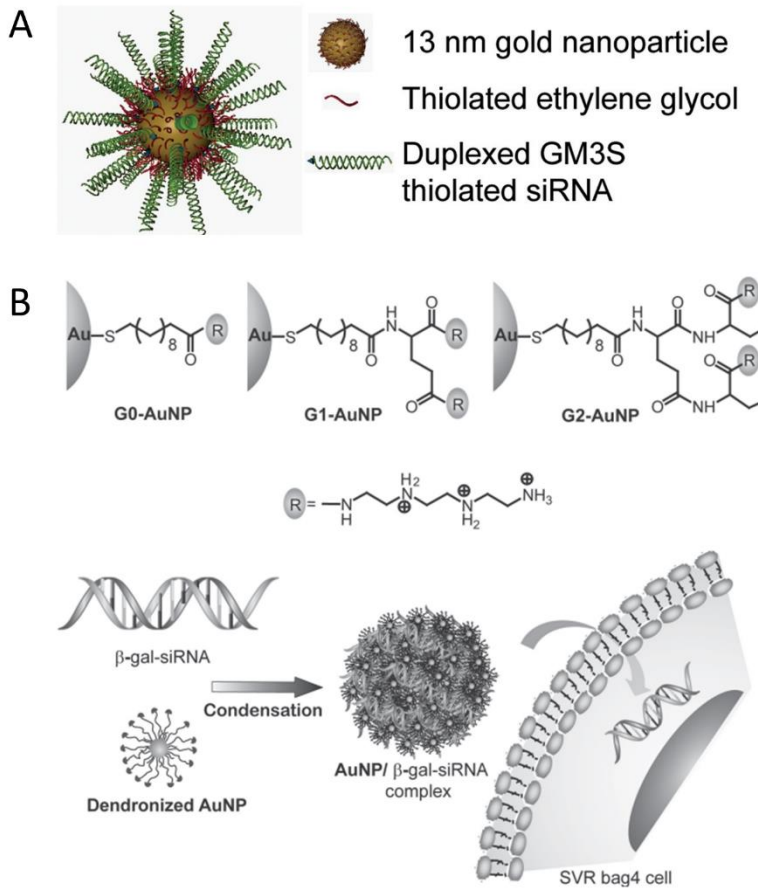

Figure 1. 8.-Representative examples of siRNA-AuNPs A) Covalently linked siRNA to AuNP via thiol. Adapted from *Randeria et Al.*[65]. B) AuNP decorated with dendrimer and complex formed with siRNA via electrostatic interaction. Adapted from *Kim et Al.*[67].

1.4.3.2.2 *Iron oxide nanoparticles*

Particles composed of Fe_3O_4 or Fe_2O_3 possess magnetic properties that can result interesting to siRNA delivery. Applying an external magnetic field can direct the nanoparticle to a specific spot, while the delivery can be monitored by Magnetic Resonance Imaging (MRI). Similarly to AuNP, siRNA can be covalently linked via thiol chemistry to the iron oxide NP or via electrostatic interaction after coating the magnetic nanoparticles (MNPs) with cationic lipids, peptides, polymer or dendrimer[73,74,75] (Examples in Figure 1.9). However, there is no candidates in clinical trials yet.

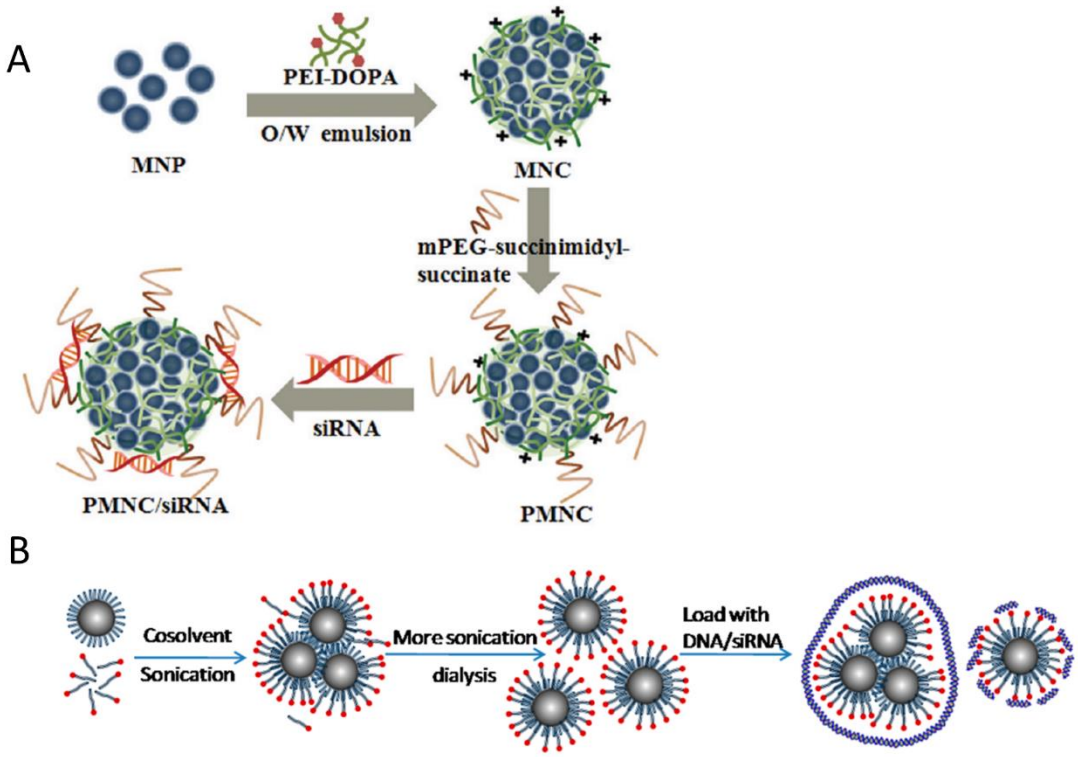

Figure 1. 9.-Examples of iron oxide nanoparticles for siRNA delivery A) Adapted from *Park et al*[73] MNPs are coated with polymer PEI and PEG B) Adapted from *Jiang et Al*[75] MNPs are coated with lipids and genetic materials are adsorbed onto the surface

1.4.3.2.3 *Mesoporous silica*

Mesoporous silica nanoparticles (MSNs) have been used to deliver a variety of drugs, including small molecules, genes, and proteins owing to the good biocompatibility and tunability of the porous architecture. It has the characteristic that drugs can be loaded in the porous and/or on the surface giving a large surface area available for encapsulation. siRNA can be attached as other inorganic particles via thiol covalent linker or by non-covalent methods. In the last one, MSNs can be coated with cationic polymers PEI, PLL and PAMAM to carry siRNA via electrostatic interactions[76,77,78](Figure 1.10). Despite a lot of preclinical research reported, no silica formulations for siRNA delivery have reached clinical trials yet.

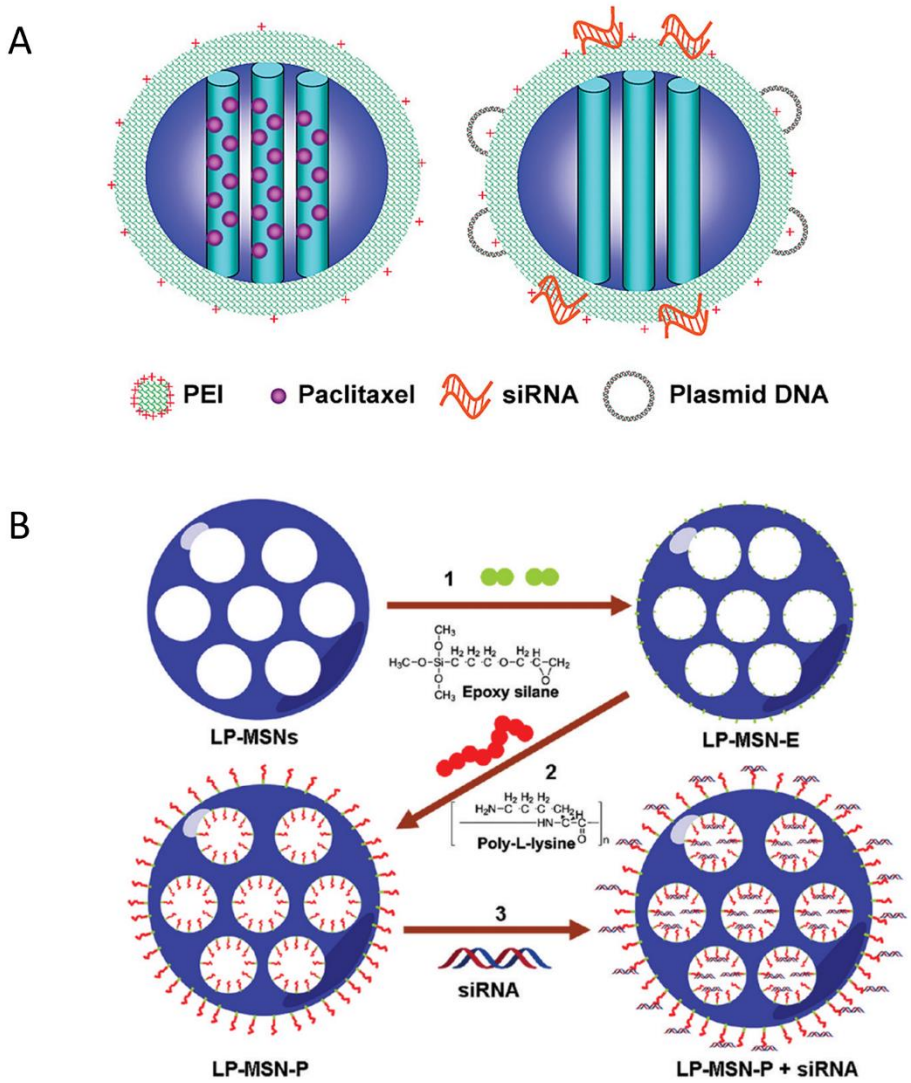

Figure 1. 10.-Examples of MSNs as gene delivery vectors A) Adapated from *Xia et al*[76] A multiple drug formulation is presented, where paclitaxel drug is carried in the interior and siRNA and plasmid on the surface thanks to the coated surface with PEI. B) Adapted from *Hartono et al*[77] pores and surface is coated with PLL to increase the encapsulation area for siRNA adsorption.

1.4.3.2.4 *Calcium phosphate CaP*

Calcium phosphate (CaP) nanoparticles are another widely studied inorganic biomaterial for gene delivery. As a natural material found in human bone and teeth, CaP presents good biocompatibility and biodegradability. As genetic materials, including siRNA, contain negatively charge phosphate groups, the interaction with cationic calcium ions result in the formation of solid nanoparticles (CaP-siRNA), that can be internalized by cells. However, low endosomal escape and uncontrolled size have been identified as critical drawbakcs[79]. To overcome these obstacles, polymers, lipids, and target ligands have been added to the CaP-siRNA nanoparticles to improve release and efficacy by directing the vectors to specific tissue, such as the one described for PMA/CaP/siRNA NPs[80]; CaP/siRNA/DOPA-HA NPs[81]; and PEG/DOPC/Anisamide/siRNA CaP NPs[82](Examples in Figure 1.11).

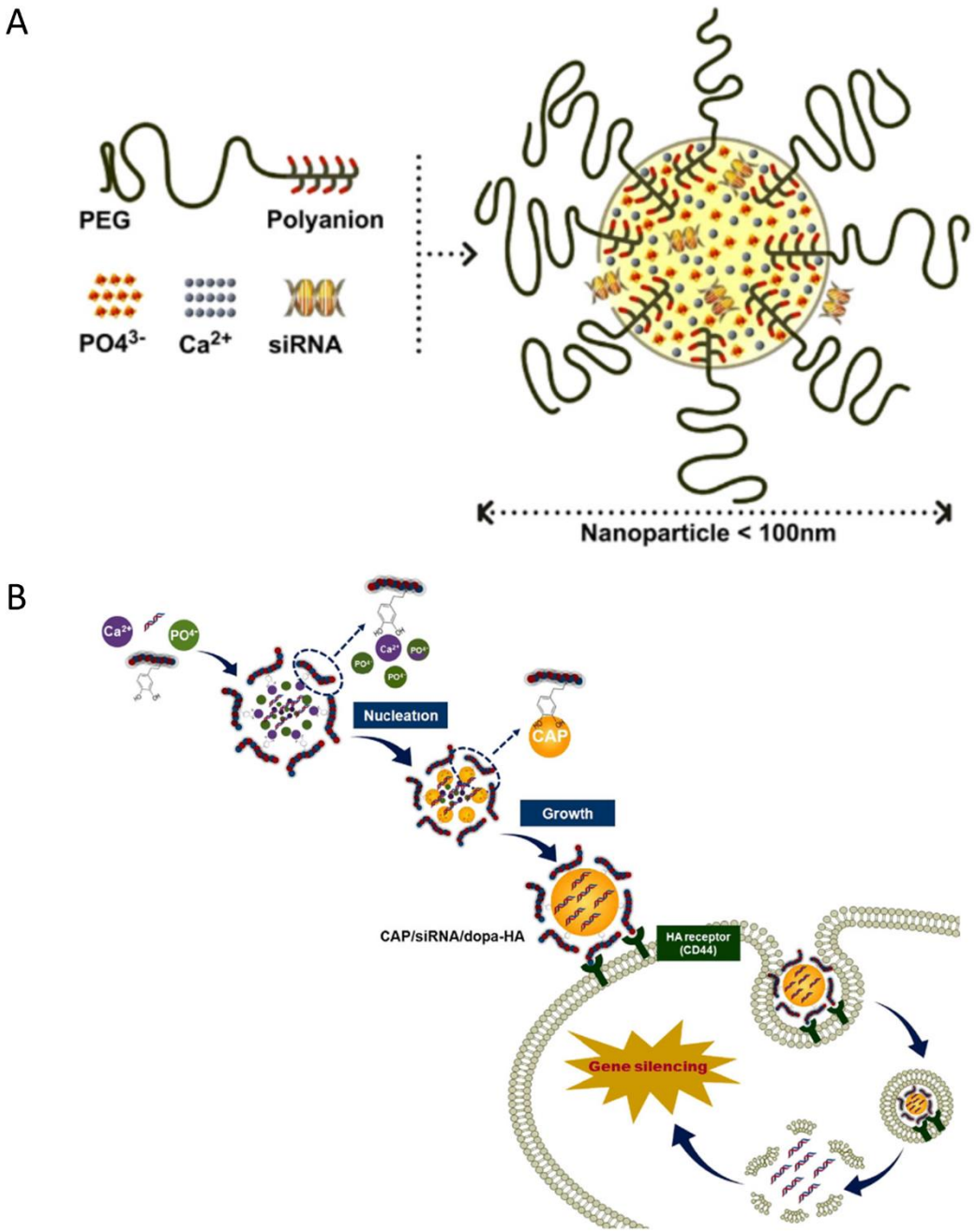

Figure 1. 11.-Examples of CaP-siRNA complexes. A) block copolymer formed by PEG and polyanion is used the CaP formulation, polyanion is trapped in the core of the nanoparticle and PEG is oriented outwards *Pittella et al.*[80] B) CaP surface coated with DOPA-Hyaluronic acid, DOPA is anchored to phosphate core, while hyaluronic acid is faced outwards, adapted from *Lee et al.*[81]

1.4.3.3 Polymer based materials

Polymers have also been extensively explored for siRNA delivery, according to published data over the last two decades. Polymers have the versatility to form different structures of delivery like polyplexes, dendrimers, hydrogels and polymerosomes. Polymeric nanoparticles are among the most promising artificial materials for nano-delivery of nucleic acids, mainly owing to their simple synthesis and functionalization, structural versatility, synthetic scalability, high transfection efficiency, gene immunogenicity and good biocompatibility[83].

Two different groups can be distinguished among the most used polymers 1) natural polymers: Chitosan, dextran, cyclodextrin and 2) synthetic polymers: polyethyleneimine (PEI), Poly-L-Lysine (PLL), Poly (lactic-co-glycolic acid) (PLGA), polyamidoamine (PAMAM), poly β-amino esters (PBAEs), polyallylamine (PAH) (Figure 1.12).

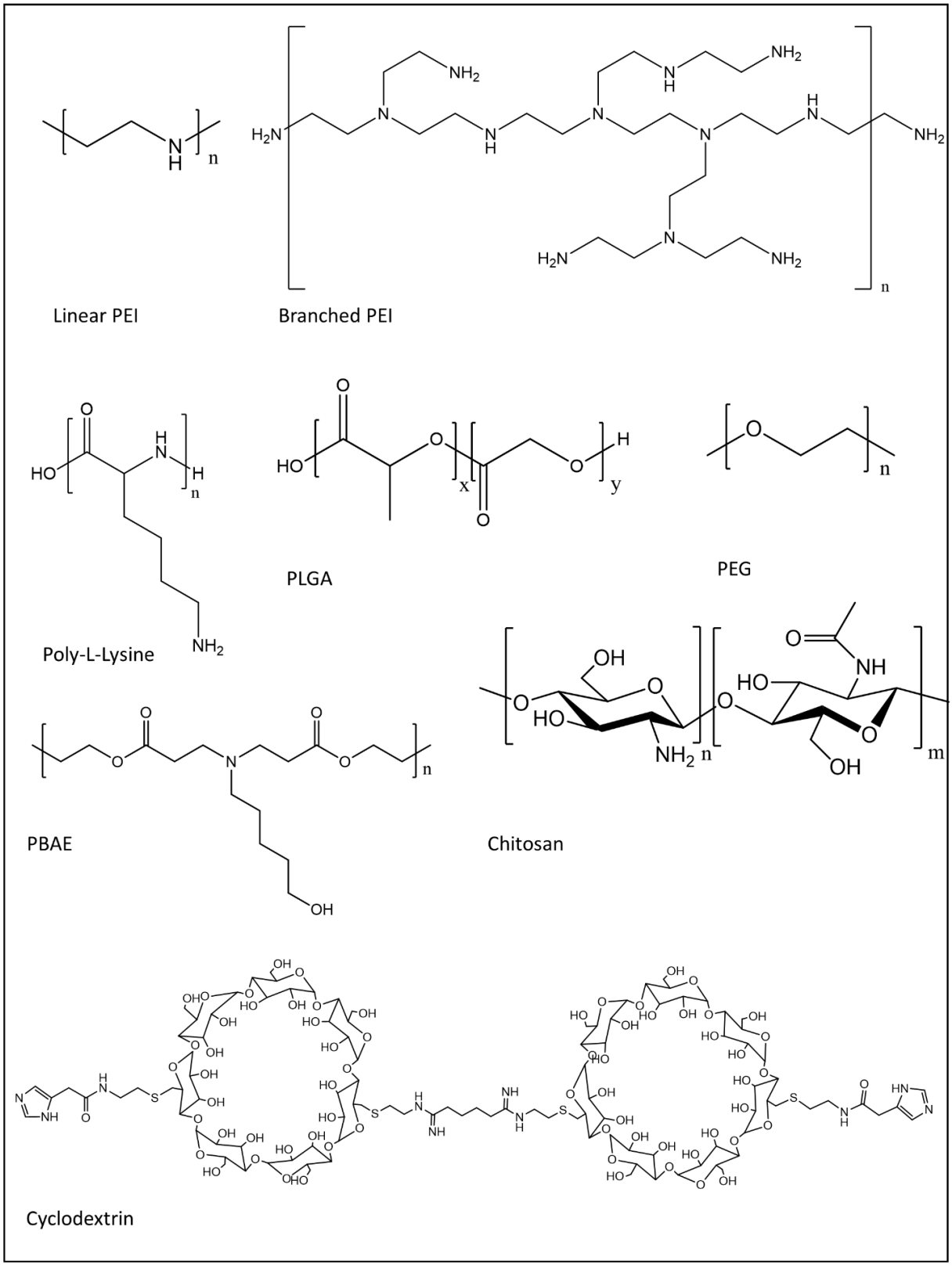

Figure 1. 12.-Chemical structure of different polymers used in gene delivery. Linear and branched poly(ethylenimine) (PEI), poly(L-Lysine) (PLL), poly(beta- amino- ester) (PBAE) and chitosan use cationic amine groups to complex the anionic phosphodiester backbone of RNA. Cyclodextrins can be incorporated into cationic polymers and then modified with different compounds. Polymers based on poly(lactic- co- glycolic acid) (PLGA) are typically modified with cationic groups. PEG is typically used to increase hydrophilicity and biocompatibility to the systems.

1.4.3.3.1 *Polyplexes*

Polyplex is the name given to a complex formed between a polymer and a nucleic acid. The complexation occurs because polymer have cationic charges, which interact with negative phosphate groups present in the nucleic acid. Cationic polymers complexes siRNA into small and compact structures. Polyplexes are formed spontaneously from mixing polymers and oligonucleotides. Different ratios of polymer relative to siRNA can be used to prepare polyplexes. The ratio of polymer to siRNA is defined by the so called N/P ratio, which is the molar ratio between the number of protonable amines and the number of phosphate groups, respectively. Typically, a higher concentration of polymer than siRNA is preferred to promote the complexation of the genetic material. Once formed, the polyplexes are expected to be good vectors to protect siRNA from nucleases, cross cell membrane and promote the release from the endosome. Different strategies based on chemical composition of the polymer are used to overcome the gene delivery barriers.

PEI

Poly(ethylene imine) is one of the most studied cationic polymers for gene delivery. It is made out repeating units of a secondary amine and two carbon aliphatic spacers. Its high cationic density results in highly condensed particles with nucleic acids. It can be linear or present different degrees of branching. Linear PEI present secondary amine and two terminal primary amines. On the other hand, branched PEI present primary, secondary and tertiary amines at estimated ratio 1:2:1. The type of amines dictates its pKa values and could have different degree of protonation at different pH values. This confers PEI a high buffering capacity, which release siRNA inside cells according to the theory of the proton sponge. These features have made PEI the gold standard of polymeric gene transfection. Different molecular weights in linear and branched PEI have been compared in terms of delivery efficiency and toxicity and for different genetic tools. Despite the good complexation and delivery, issues related to the cytotoxicity derived from high density of amines have been reported. Therefore, PEI have been modified with different chemical groups[84] or polymers, such as hyaluronic acid[85], PEG[86] and lipids[87,88,89], to lower cytotoxicity of the siRNA/PEI complexes[90] (Examples in Figure 1.13).

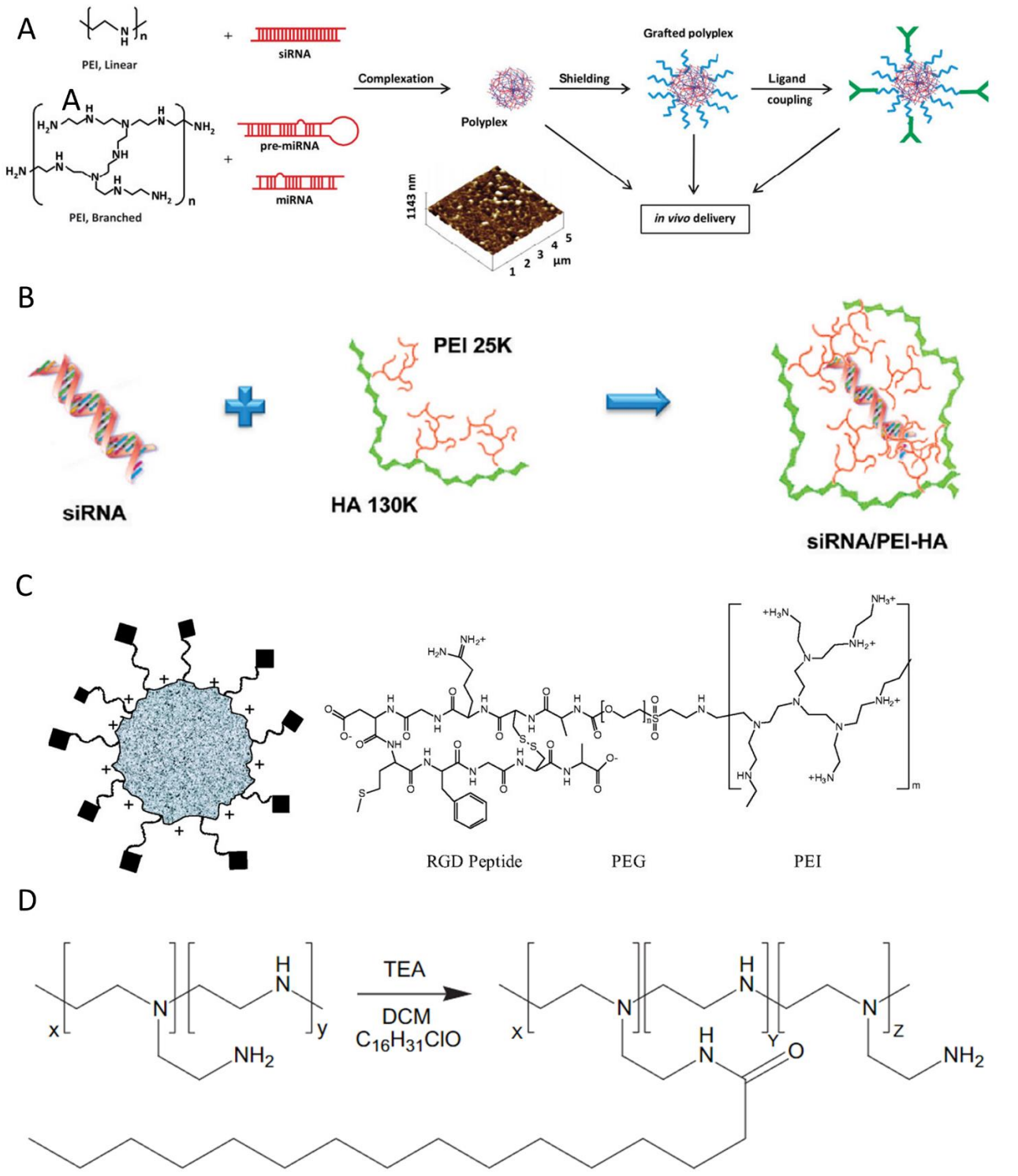

Figure 1. 13.-Examples of polyplexes based on PEI A) Scheme of complex nanoparticles based on PEI branched or linear. Extracted from *Höbel et Al*[90]. B) PEI grafted with Hyaluronic acid[85] C) Example of PEI surface decoration with targeting peptides[91] D) Grafting PEI with aliphatic chains[89]

PLL

Poly-L-Lysine, a synthetic polymer composed of L-Lysine units connected by peptide bonds (Figure 1.12), is known for its ability to form complexes with siRNA. This ability comes from the existence of a primary amine in each amino acid unit. However, the high density of these amines can provoke a cytotoxic response. To counteract this negative effect, strategies such as functionalization with polyethylene Glycol (PEG) have been documented in studies, showing a reduction in cytotoxicity[92,93].

PBAE

Poly-β-amino esters are synthetic and biodegradable polymers made by the conjugation of primary amine containing molecule and a bis (acrylate ester). PBAEs have a vast structural diversity, because different libraries of amines and bis (acrylate esters) can be used, giving different features to the polymer, such as linear or branched, with different molecular weight, hydrophobicity, and degradability that could fine tune its properties for gene delivery[94,95](Figure 1.14). The ester bonds in the backbone structure of PBAEs undergo hydrolysis in aqueous conditions, which makes PBAEs less toxic than other non-degradable cationic polymers[94]. More importantly, the presence of amino groups triggers electrostatic interactions with siRNAs, resulting in complexes suitable for delivery. Different chemical groups and modifications can be incorporated in the backbone of the polymer, such as disulfide-containing end-groups for siRNA delivery[95,96], PEG shielding for improvement of stability *in vivo*[97].

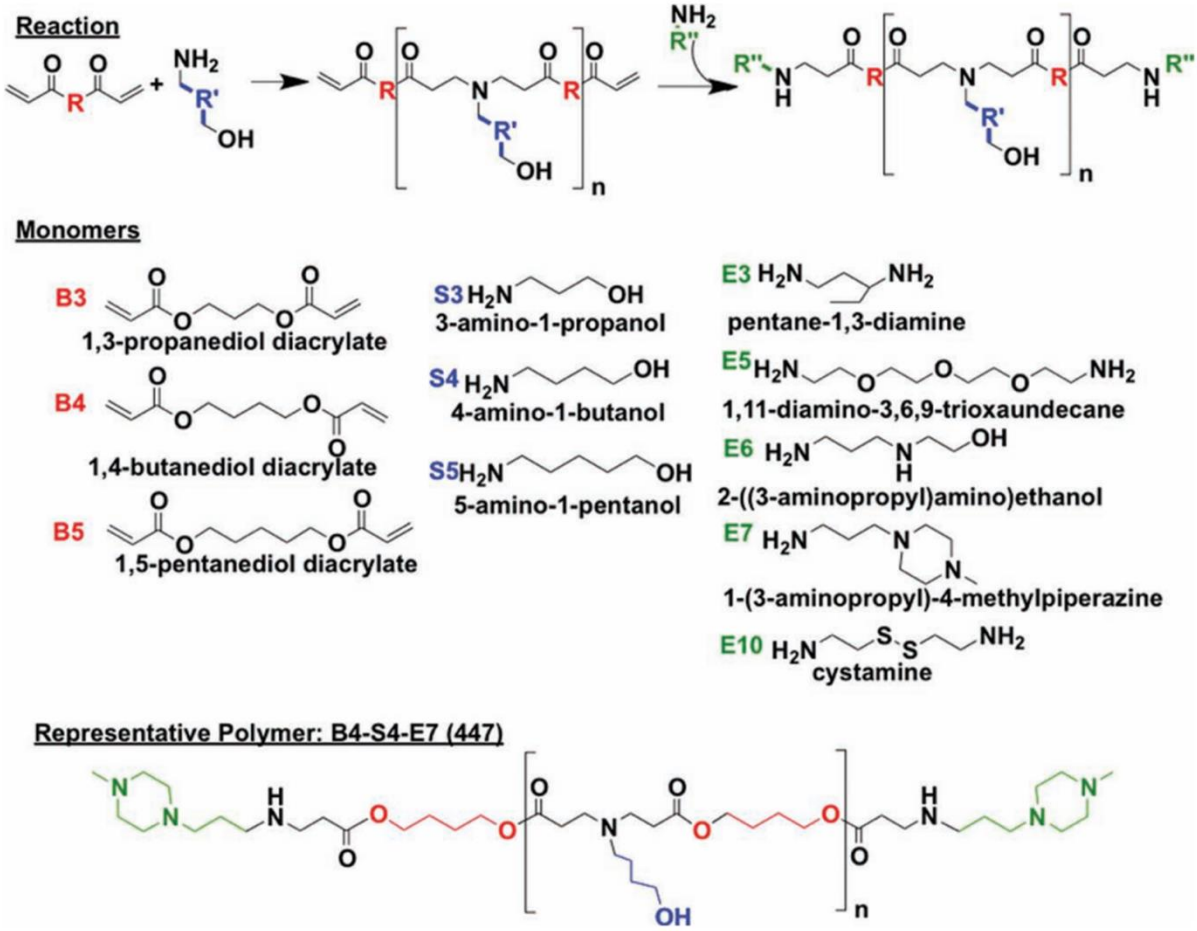

Figure 1. 14.-Monomers and reactions scheme used to synthesize PBAE library as reported by *Tzeng et Al*[95]. One backbone monomer **B** was polymerized with one sidechain monomer **S**. The diacrylate B-S base polymer was then terminated with one end-capping monomer **E**.

Chitosan

Chitosan is a polysaccharide composed of two subunits, D-glucosamine and N-acetyl-D-glucosamine (Figure 1.12). It is obtained by deacetylation of chitin, a natural polymer (only made by N-acetyl-d-Glucosamine units) that can be found in several natural sources, such as crustacean shells. Chitosan has cationic charge because of the presence of primary amines, it is biodegradable, low cytotoxic, and its capacity to deliver siRNA has been explored. Highly deacetylated chitosans are superior siRNA delivery systems compared to partially acetylated ones. Highly deacetylated chitosans have proved to provide the optimal balance between biological performance and toxicity[98].

Cyclodextrins

Cyclodextrins are cyclic oligomers of glucose, which present an amphipathic structure. The central cavity is hydrophobic meanwhile outer surface is hydrophilic. Because of these properties, cyclodextrin have been used to deliver small hydrophobic organic compounds. Its use to deliver nucleic acid was first tried in plasmids using cyclodextrin containing polycations (CDPs). In this approach, cyclodextrins are linked to each other via dimethyl suberimidate, resulting in polymers with amino groups. One of the polymer ends is linked one imidazole group, which helps in

endosomal escape (See Figure 1.12). These CDPs complexed efficiently with siRNA[99]. However, it resulted in low efficacy in vitro, the formulation required more components for stabilization. Thus, adamantane-PEG (PEG-AD) conjugations were incorporated to the formulation. Adamantane is a hydrophobic molecule which interacts with cyclic core of cyclodextrin, so that the PEG moiety faces outside the colloidal complex. PEG shield increase stability during blood circulating, but also reduces cell uptake[100,101]. To solve this problem protein transferrin, which binds to the CD71 transferrin receptor of the cell, was attached to the free end remaining in the PEG-AD. This delivery platform siRNA/CDP-PEG-AD-Tf (See Figure 1.15) has been evaluated in several animal models and was promoted to clinical trials, as RONDEL™ by Calando pharmaceuticals, now part of Arrowhead Pharmaceuticals. This formulation CALAA-01 using RONDEL platform was injected intravenously against a tumor proliferation target ribonucleotide reductase subunit 2 (RRM2). It was reported an accumulation in tumor in animal models[102]. However, after Phase I clinical trial formulation was discontinued.

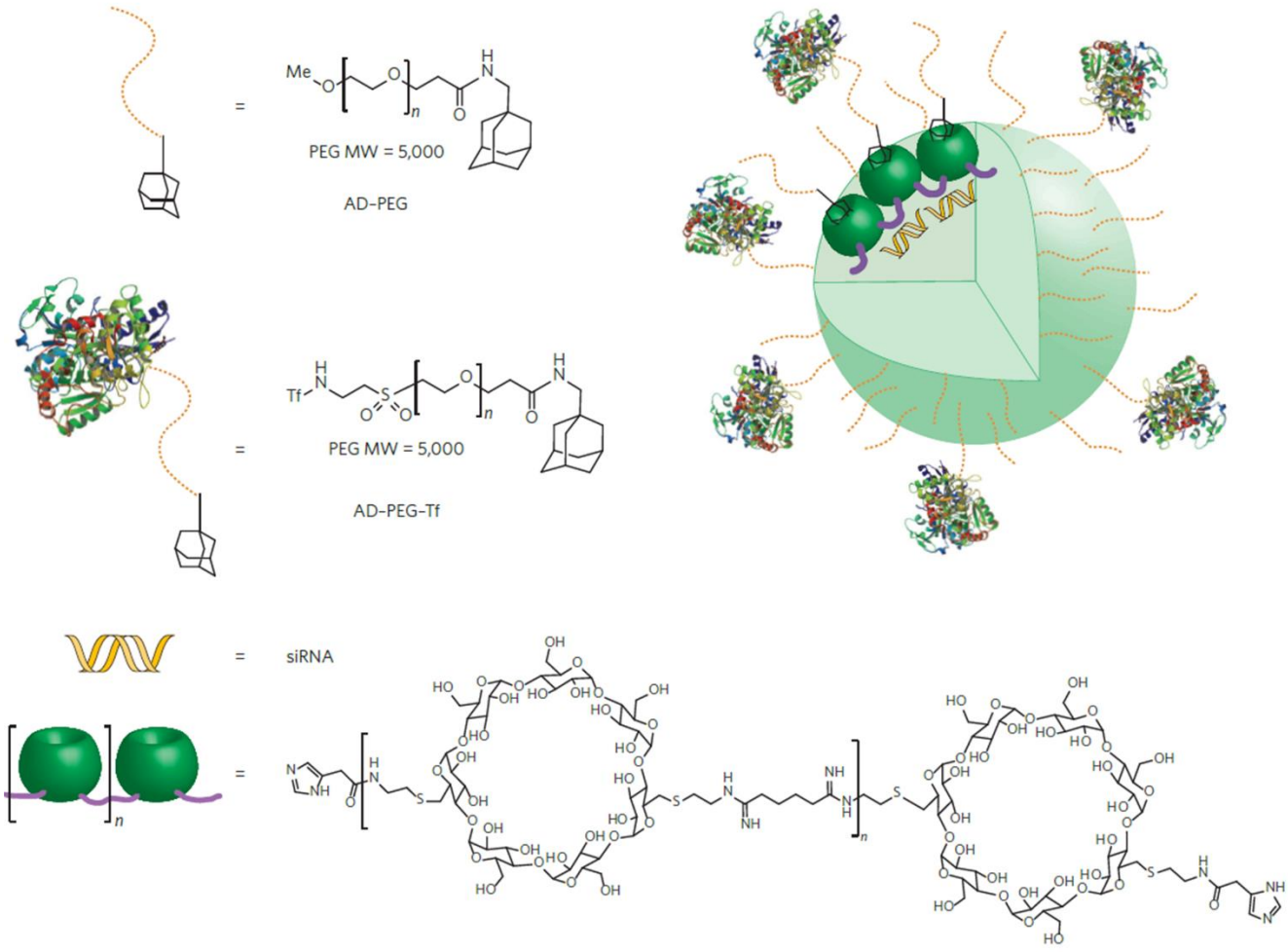

Figure 1. 15.-Cyclodextrin delivery system RONDEL™ developed by Mark E. Davis group[103]. Imaged extracted from *Kanasty et Al*[57].

1.4.3.3.2 *Other types of polymer vectors*

Polymers can form **hydrogels** by inter crosslinking of the backbones forming three-dimensional, water-swollen networks. Hydrogel properties (e.g., mechanics, degradation, drug release) are based

on the polymers and amount of cross-linker used, offering numerous design features. In the case of siRNA delivery, the use of cationic polymers is a key parameter for its retention by electrostatic interaction. Some systems are only based on the hydrogel itself and other combine carriers inside the hydrogel matrix to promote a controlled and sustained release, which is the most explored approach[104] (Figure 1.16.-A). One important feature of the hydrogels to be considered is its injectability and degradability, that both can be achieved by using judicious stimuli-responsive crosslinker (Example in Figure 1.16.-B).

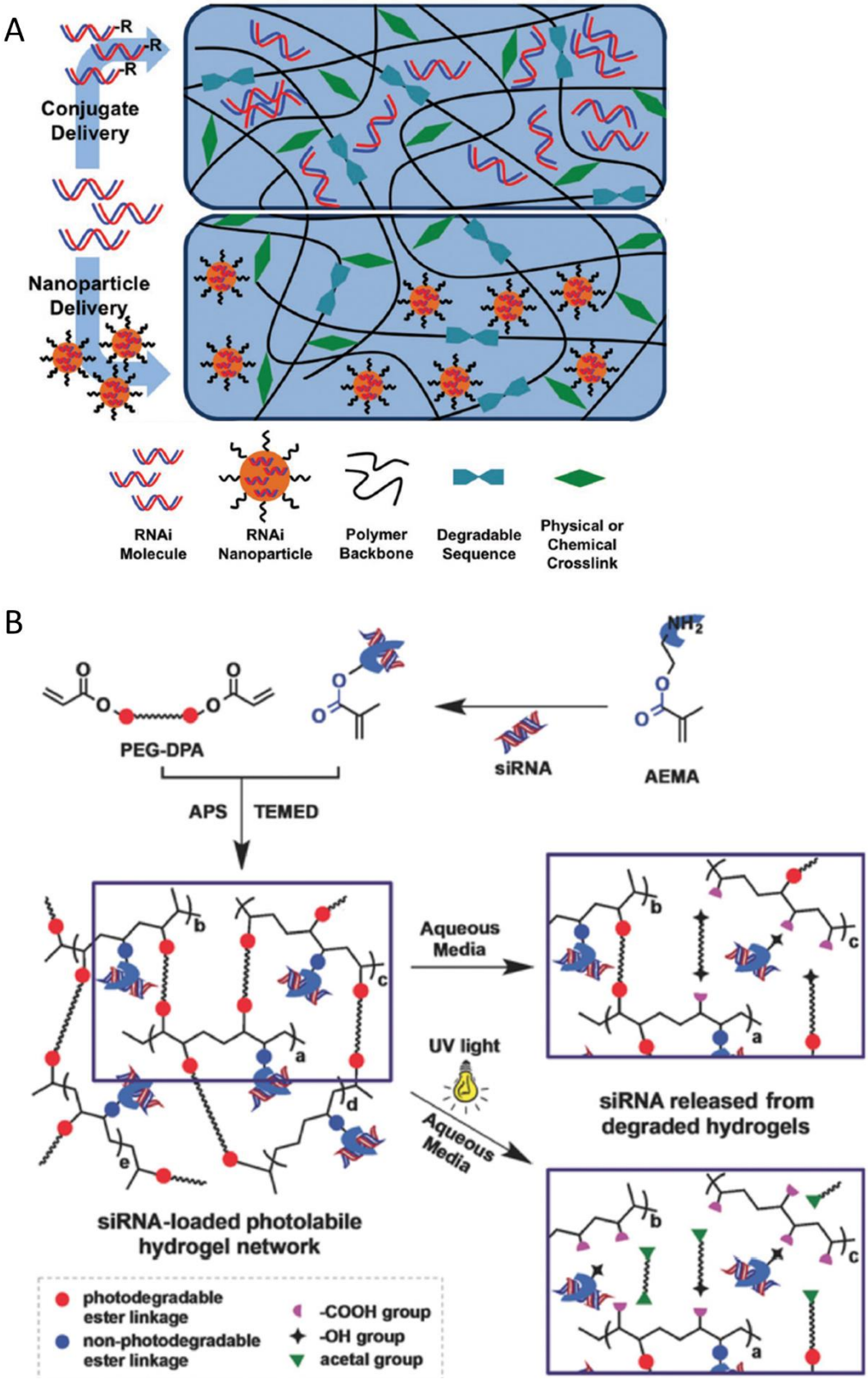

Figure 1. 16.-A) Schematic representation of hydrogels used for siRNA delivery, It could include conjugation to the polymeric matrix or first step of encapsulation in nanoparticles followed by a embedding step into the gel, reproduced from[104]. B) Photolabile siRNA delivery through hydrogels formed from PEG-o-nitrobenzene-acrylate permits siRNA release in response to UV light through o-nitrobenzene mediated photo-isomerization. Reproduced from *Huynh et Al*[105].

The company Silenseed has developed a biodegradable polymer-based gel derived from poly(lactic-co-glycolic) acid PLGA on a cylindrical shape 1 mm in diameter and 5 mm in length. It received the name of Local Drug Eluter (LODER^{TM}), being the first delivery systems that allows RNAi drugs to be directly delivered into solid tumors according to the company (Figure 1.17). LODER™ enables the slow and stable release of locally delivered drugs. Phase II of the candidate siG12D-LODER, a formulation containing siRNA anti-KRAS entrapped in LODER™, is planned for inoperable locally advanced pancreatic cancer in combination with chemotherapy. The scaffold is designed to be implanted directly into the core of a pancreatic tumor, where it gradually releases siRNA. While promising outcomes have been observed in both mice models and Phase I clinical trials, the siG12D-LODER system still needs to undergo and successfully complete Phase II clinical trials[106]. Furthermore, it is worth noting that this approach requires an invasive delivery platform, which could present challenges for patient comfort and acceptance.

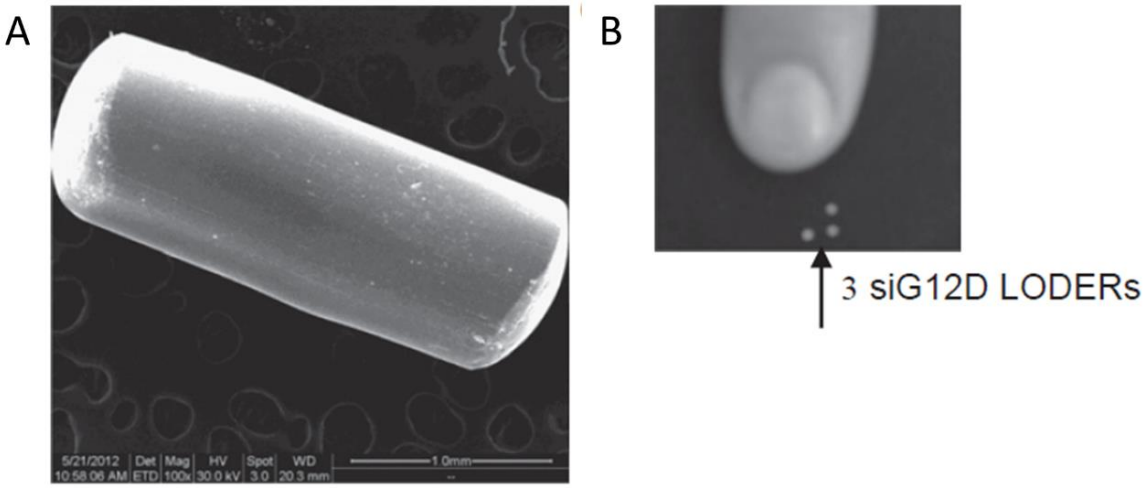

Figure 1. 17.-LODER characteristics A) SEM image of siG12D-LODER removed 45 days after implantation in vivo (1 mm scale bar) B) LODER full-size picture. Extracted from *Khvalevsky et Al*[106].

Polymersomes are polymer vesicles formed by the self-assembly of amphiphilic block copolymer via hydrophobic interactions, similarly to liposome structures[83] (Figure 1.18.-A). Amphiphilic block copolymers have two fractions, one hydrophilic and one hydrophobic. The hydrophobic moieties tend to associate to minimize their interactions with water molecules. The hydrophilic fraction f of the copolymer dictates the final morphology of the structure. When f is between 25-40% of the total mass, the individual block copolymer in water forms cylindrical shape, resulting in the formation of vesicle morphology, whereas f is more than 40% tend to form conical shapes[107]. Cylindrical shapes aggregates in liposome-like structures, while conical shapes tend to form micelles. The molecular weight of each hydrophobic and hydrophilic fraction determines the thickness of the formed membrane[108](Figure 1.18.-B). Polymersomes are prepared similar to liposomes, which include steps of film rehydration, direct hydration, solvent displacement, electroporation, polymerization-induced self-assembly, double emulsification in a microfluidic device, and flash nanoprecipitation[109] (Figure 1.18.-A). Polymerosomes are originated as AB type diblock copolymers, but their development has expanded to include ABA triblock and ABC heterotriblock structures. This diversification allows for the modulation of their physicochemical properties.

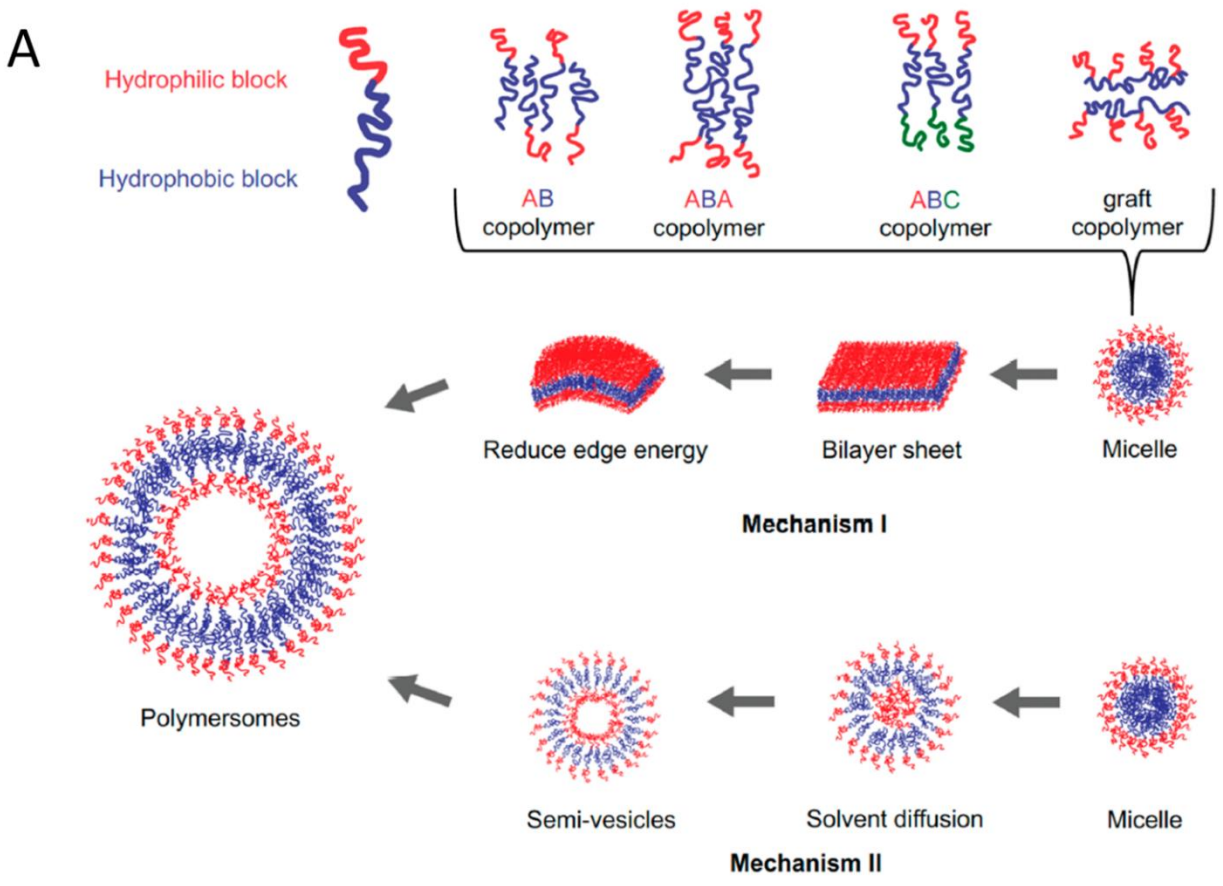

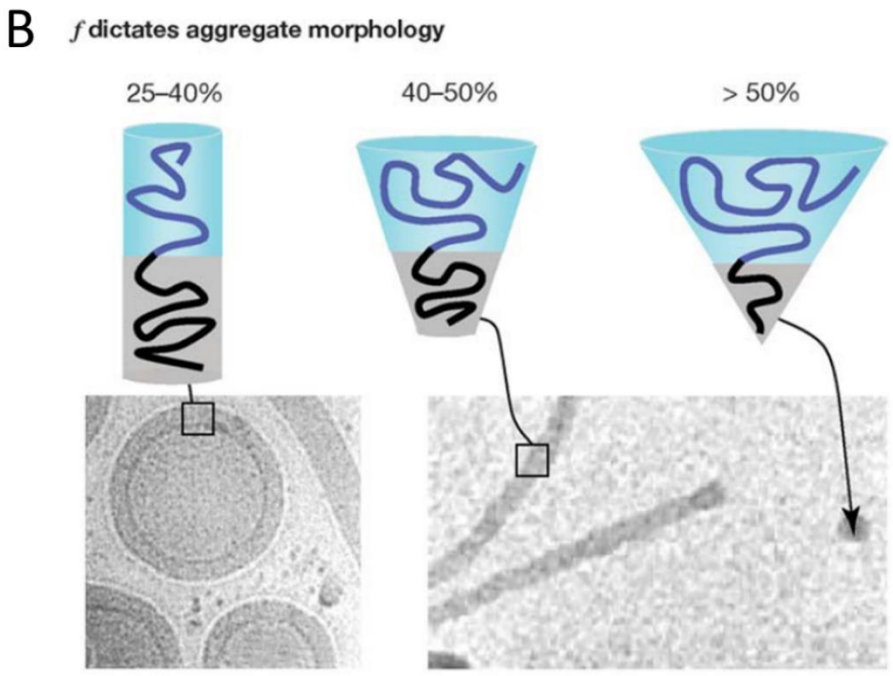

Figure 1. 18.-A) Schematic demonstration of self-assembly of block copolymers into polymerosomes via two different mechanism among all different ones[109]. B) Schematics of block copolymer fractions with respective cryogenic transmission electron microscopy images showing vesicles or worm micelles and spherical micelles[108].

Because of their ability to encapsulate a variety of substances, including small drug molecules, proteins, and nucleic acids, polymerosomes have been employed as delivery carriers in therapeutic applications. Regarding siRNA loading, several works using polymersomes have been reported. As hydrophilic block PEG has been mostly used, while different examples of hydrophobic block have been reported, such as poly(ε-caprolactone) PCL; polylactic acid PLA; polybutadiene PBD. PEG-b-PCL, PEG-b-PLA, and PEG-b-PBD-based polymersomes are good examples of siRNA formulations, which present good encapsulation and transfection efficiciency[110]. However, preferential accumulation in the liver has been shown for these examples[109]. More elaborated triblock copolymers were reported for siRNA delivery in cancer therapy, where a polycation is incorporated for siRNA entrapment. PEG-b-poly-(trimethylene carbonate-co-dithiolane trimethylene carbonate)-b-PEI, known as (PEG-b-P(TMC-co-DTC)-PEI) and cNGQ peptide functionalized diblock copolymer, cNGQ-PEG-b-P(TMC-co-DTC) were self-assembled to form polymersomes and deliver PLK1 siRNA in mouse model of orthotopic A549 cancer cells[111] (Figure 1.19). A different approach consists of a copolymer with temperature-sensitive moieties, such as poly(ethyleneoxide)-block-poly[N-isopropylacrylamide-stat-7-(2-methacryloyloxyethoxy)-4-methylcoumarin-stat-2-(diethylamino)ethyl methacrylate] [PEO-b-P(NIPAM-stat-CMA-stat-DEA)]. The hydrophilic PEO chains form the coronas of the polymersome, whereas the temperature and pH-sensitive block P(NIPAM-stat-CMA-stat-DEA) forms the dually gated heterogeneous membrane. The temperature-controlled “boarding gate” can be opened at room temperature for facile encapsulation of siRNA into polymersomes directly in aqueous solution. The “debarkation gate” can be triggered by acidic pH in endosomes via proton sponge effect[112].

Despite *in vivo* approaches found in the literature there are still no clinical trials of siRNA delivery using polymersomes. Probably due to their lack of reproducibility and complex synthesis.

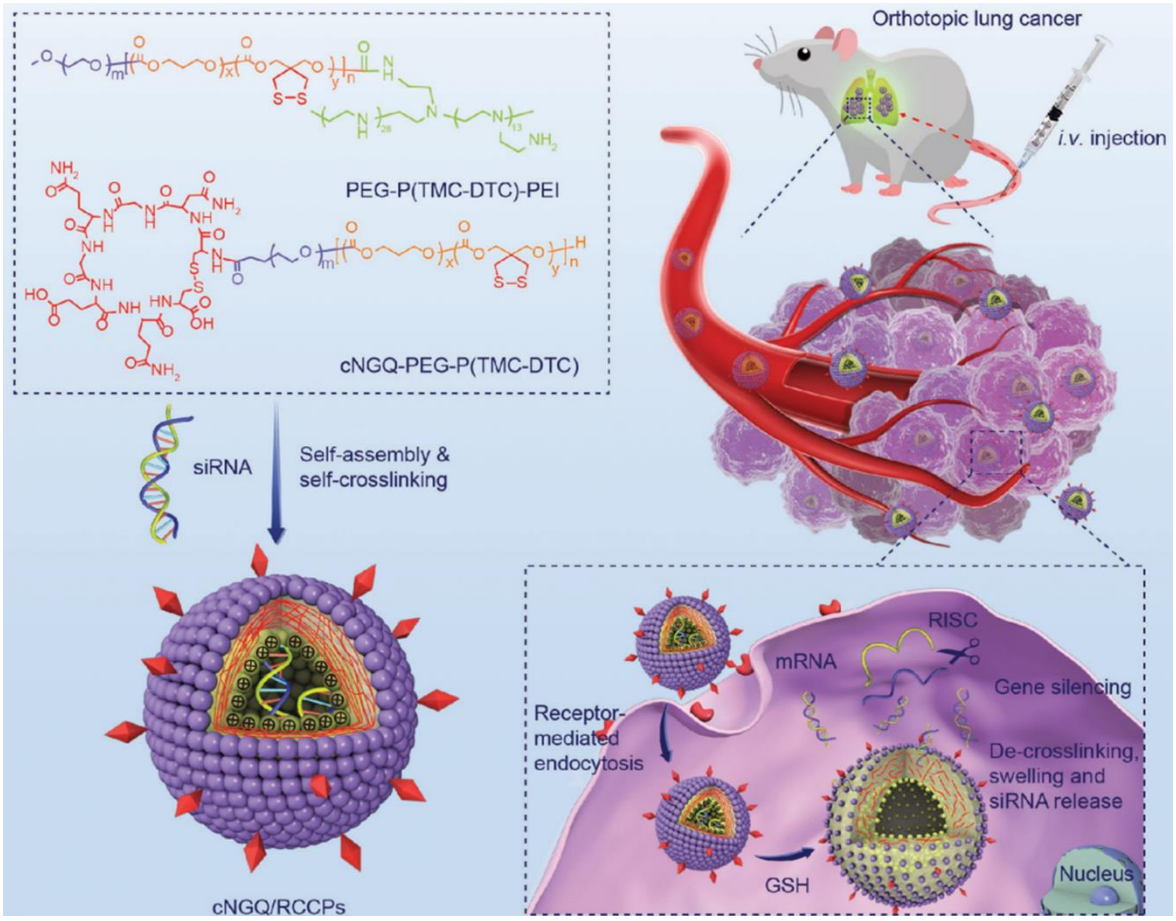

Figure 1. 19.-Targeted delivery of siRNAs by cNGQ peptide-directed, reversibly cross-linked chimeric polymersomes (cNGQ/RCCPs) to orthotopic lung tumors in mice. Reprinted from *Zou et Al* [111].

Dendrimers are polymers with a special tree-like structure. It consists of a central core molecule, from which several highly branched arms originate in a symmetrical way, adopting a spherical three-dimensional morphology. Dendrimers are classified by generations, G0 represents the core of the dendrimer, and each branching point represents the next generation, making layers surrounding the core. The last layer is the outer surface comprising different reactive groups (Figure 1.20.-A). Dendrimers can be synthesized by two approaches: convergent or divergent synthesis. Divergent method starts from a multifunctional core, which reacts with added monomers by a series of stepwise polymerization of reaction. Each monomer has 3 or more reactive points, one reacts with the core molecule leaving the rest free to react for the next generation (Figure 1.20.-B). The convergent method involves inward branching from surface to the core. Monomers react each other forming a branched structure called dendron, then each dendron is attached to the core molecule. Lower generation dendrimers have highly asymmetric shapes and possess more open structures (Figure 1.20.-C). As the chains are grown from the core, the dendrimers become densely packed, globular structures. When a critical branched state is reached, dendrimers cannot grow uniformly because of a steric constraint[113]. This type of polymerization reaction achieves chains with low polydispersity[114]. The most extensively studied dendrimer is polyamidoamine (PAMAM), since it was first synthesized in 1985[115].

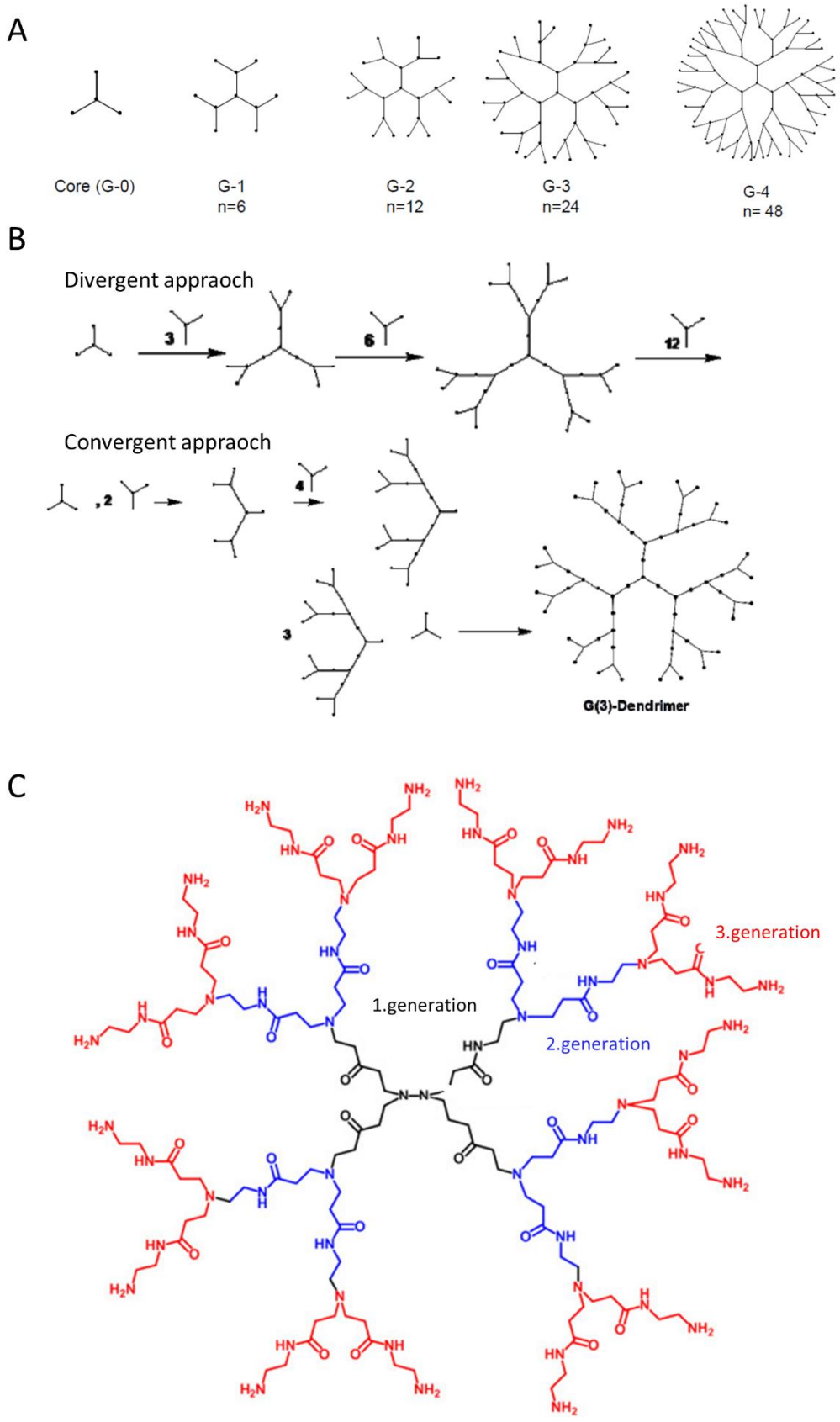

Figure 1. 20.-A) Representation of dendrimers of generations 1–4. The n denotes number of terminal functional groups[116].B) Two common synthetic approaches of dendrimer assembly. Divergent and convergent growth method[116].C) General structure of a PAMAM[117].

PAMAM is synthesized by divergent method, where the core is ammonia or commonly ethylenediamine. Then this molecule is activated with methyl acrylate by Michael addition, each amino group react with 2 acrylates monomers. Then amidation is formed between core esters resultant groups and new addition of ethylenediamine, forming the next generation.

As PAMAM is fully formed by amines interactions with nucleic acid included siRNA has been studied. Dendriplex formation has been observed in different generations, G1 with less charged density lacked siRNA complexation ability, while G4 and G7 displayed equal efficiency[118]. As a result of high cationic density PAMAM (above G4) presents high cytotoxicity and hemolysis, which limit its *in vivo* application. Surface of PAMAM has been modified with PEG (3.4 KDa) at 10% degree of substitution, achieving higher transfection efficiency and reduced cytotoxicity[119]. Other example of dendriplex include surface decoration with peptides for targeting delivery, poly(propyleneimine) generation 5 dendrimers (PPI G5), are complexed with siRNA and super paramagnetic iron oxide nanoparticles (SPION), which allow tracking by MRI for biodistribution studies. The surfaces of these complexes are decorated with PEG, which is terminally functionalized with a targeting ligand for the Luteinizing Hormone-Releasing Hormone (LHRH) receptor. This design allows the complexes to specifically target and reach cancer cells, thus enhancing the specificity and efficiency of drug delivery (Figure 1.21)[120].

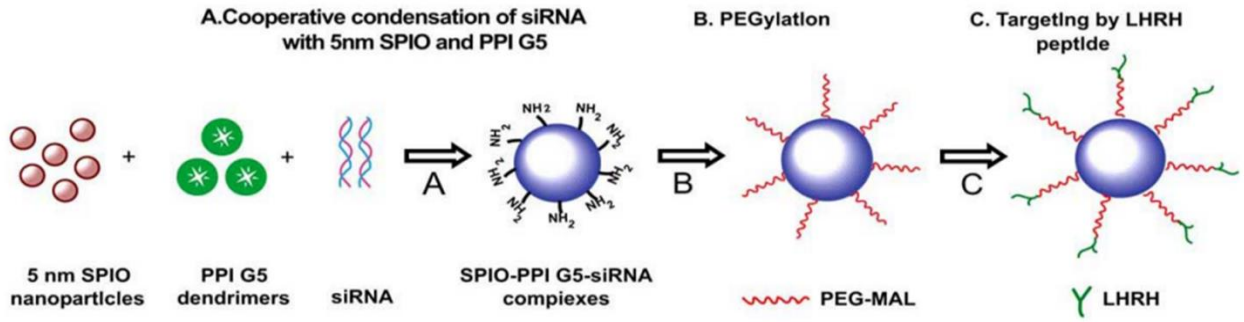

Figure 1. 21.-The preparation of tumor-targeted, stable siRNA nanoparticles. (A) Cooperative condensation of siRNA with 5 nm SPIO nanoparticles and PPI G5 dendrimers. (B) PEGylation. (C) Conjugation of LHRH peptide to the distal end of the PEG layer[120].

Despite several advantages such as low polydispersity, high complexing capacity and ease of multifunctional engineering and surface functionalization, dendrimers also present critical drawbacks like tedious synthesis and difficulties to scale-up[121]. Therefore, its translation to clinic could be hampered by its production process and relatively high quantities required for clinical trials.

1.4.4 Conjugated siRNAs

Delivery material directly conjugated with siRNA molecule by covalent chemistry is considered as a delivery system. This approach leads to well-defined, single-component systems that use only equimolar amounts of delivery material and siRNA. Conjugate delivery systems have been developed by covalently linking the sense strand of the duplex to polymers, peptides, antibodies, aptamers, cholesterol, glycans and other small molecules. Once inside cytoplasm, sense strand with

conjugated molecule is discarded. Most advanced conjugate platforms are Dynamic Polyconjugates (DPC) and n-acetylgalactosamine (GalNac) with several candidates in clinical trials and developed mostly by private companies.

1.4.4.1 *Triantennary GalNAc–siRNA*

The 3´terminus of siRNA sense strand is covalently attached to three molecules of N-acetylgalactosamine (GalNac), which are attached to a linker bound to the phosphate groups of siRNA (Figure 1.22.-A). This structure is designed for high affinity to its target, asialoglycoprotein receptor (ASPGR), in hepatocytes. ASPGR is highly and specifically expressed on hepatocyte membrane and mediates clathrin-dependent endocytosis of galactose-derived ligands[122,123] (Figure 1.22.-B). Trivalent or Tetravalent ligand exhibit higher affinity than monovalent or bivalent and space between sugar moieties and the length of the linker also play a role[124]. Study of comparison showed that subcutaneous administration achieved better performance than intravenous injection. It is assumed that subcutaneous route change the pharmacokinetic profile of GalNac-siRNA, while IV injected siRNA are excreted quickly from blood circulation to kidneys[29]. ASPGR mediated endocytosis is a safer mechanism than the lipid delivery, which lipid interaction with membrane could result cytotoxic[36]. Moreover, GalNAc–siRNA conjugates show excellent pharmaceutical properties with high tissue-targeting specificity, a higher therapeutic index and minimal or limited secondary effects. These conjugates showed an extremely long duration of action when combined with enhanced stabilization chemical modification in the siRNA structure. This allows administration only every 3 or 6 months. These good properties have led companies such as Alnylam to stop all other liposome-based programs and change to GalNac conjugates.

Using GalNAc conjugates are formulations from Alnylam in Phase III Vutrisiran, and Fitusiran and three approved by FDA Givlaari (givosiran), Revusiran, Lumasiran and Inclisiran. Other biotechnological companies have established GalNac conjugate platforms, such as Arrowhead, Dicerna, Arbutus, Silence therapeutics, etc. Nowadays GalNac platforms dominate pipelines in siRNA delivery (Table A.1 in Appendix I).

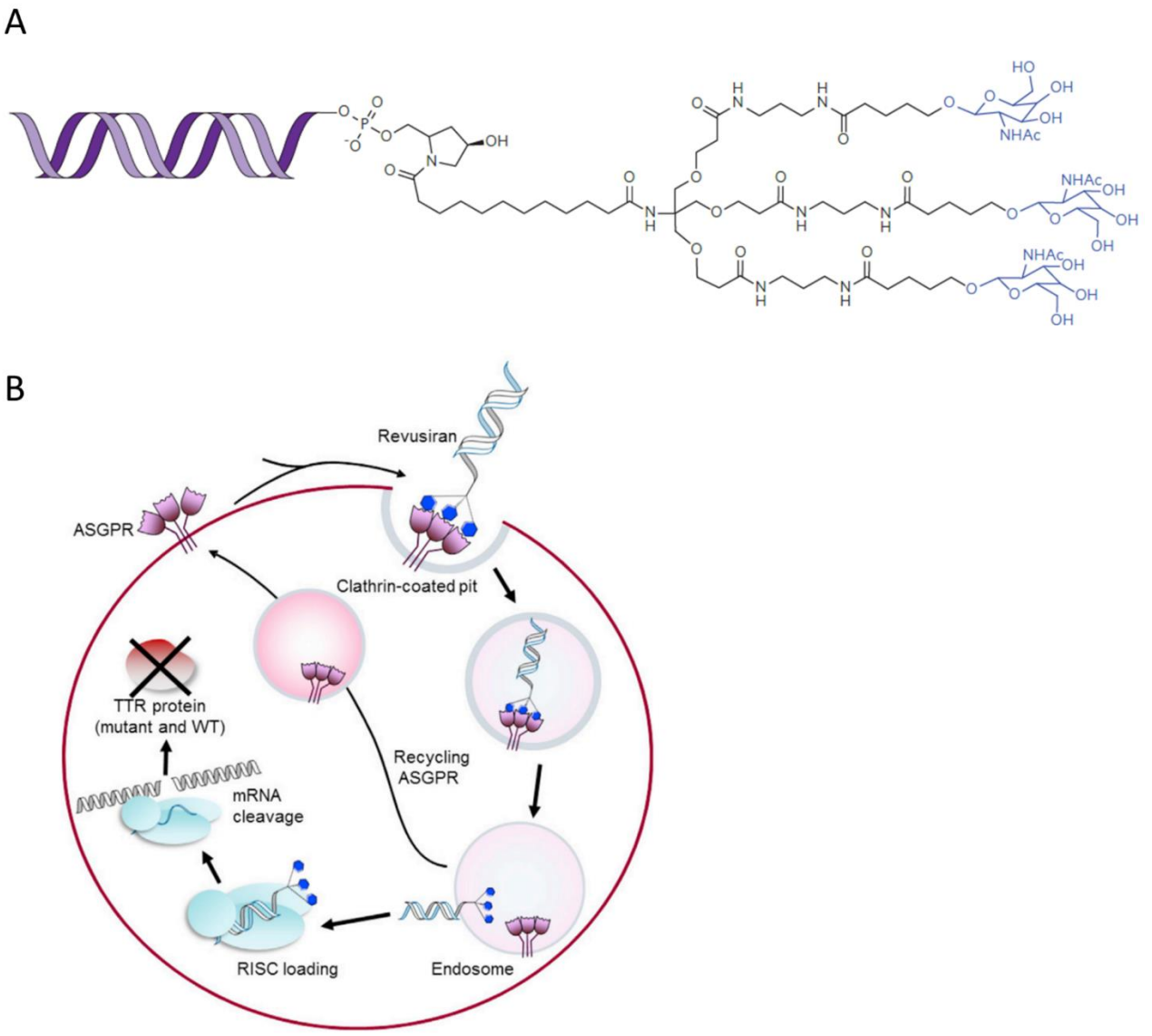

Figure 1. 22.-A) Structure of the triantennary GalNAc–siRNA conjugate used in several drug candidates from Alnylam Pharmaceuticals[57].B) Mechanism of Hepatocyte uptake and action of Revusiran. The siRNA targeting TTR mRNA is conjugated with a triantennary GalNAc. GalNAc binds to the ASGPR, which is highly expressed on hepatocytes, thus targeting revusiran to the liver. The revusiran-ASGPR complex is then taken into hepatocytes by clathrin-mediated endocytosis, where the siRNA causes TTR mRNA destruction through the RISC in the cytoplasm. The ASGPR is recycled to the cell surface for multiple rounds of siRNA uptake[125].

1.4.4.2 *Dynamic PolyConjugates (DPC™) and Targeted RNAi Molecule (TRiM™)*

DPC consists of a polymer covalently attached to siRNA by a hydrolysable disulphide linker. It is a trademark established by Arrowhead Research Corporation. The polymer poly(butyl amino vinyl ether) (PBAVE) is membrane-active polymer. PEG and target ligand GalNac are reversibly attached to PBAVE backbone via carboxylated dimethyl maleic acid linker[126]. PEG-shield protects polymer from non-desired serum interaction and extend time circulation, ligand interacts with cell receptors mediating endocytosis. Once in the endosome, carboxylated dimethyl maleic acid bonds will be cleaved by acidic environment and protonate the amino groups. siRNA covalently attached by sulfide linkage is cleaved by glutathione environment (See Figure 1.23.-A). Instead of a polymer, the backbone could be substituted by a membrane lytic peptide (MLP) and conjugated with PEG and

GalNac. Second generation of DPCs, DPC 2.0, consist of polymer/peptide backbone masked by GalNac ligand and PEG, while the siRNA is covalently linked to a molecule of cholesterol. In this case siRNA is not covalently attached to the polymer neither via electrostatic interactions (See Figure 1.23.-B). However, it was found that after co-injection both molecules reached hepatocytes and co-localized in the endosomes[127].

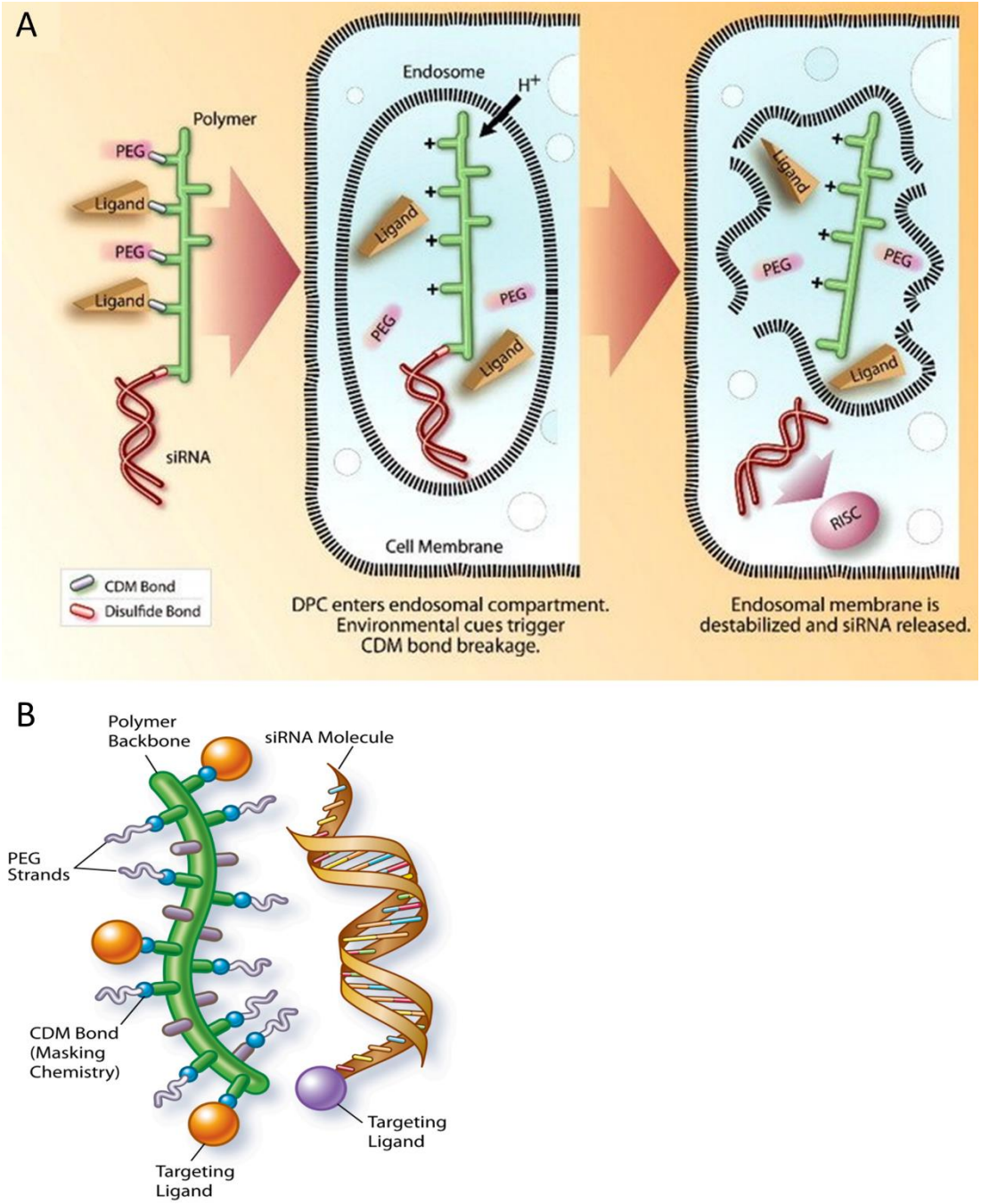

Figure 1. 23.-A) Schematic showing the siRNA Dynamic PolyConjugate DPC 1.0, its cellular uptake, disassembly in the low pH environment of the endosome, and release of the siRNA into the cytoplasm of the target cell. CDM, carboxylated dimethyl maleic acid[126]. B) New generation of DPC, DPC 2.0. typically Cholesterol-siRNA and N-Acetylgalactosamine-Polymer. Image extracted from website of Arrowhead pharmaceuticals.

Arrowhead launched clinical trials of ARC-520, ARC-521 and ARC-AAT, formulations based in DPC 2.0 to treat Hepatitis B infection and alpha-1 antitrypsin deficiency. After having reached Phase II,

long-term toxicity studies in monkeys led to two deaths using the highest dose of ARC-520. Delivery platforms were transferred to Targeted RNAi Molecule TRiM™, where siRNA is covalently conjugated with targeting ligands. GalNac, RGD motifs and avβ6 are designed to transport siRNA to hepatocytes, cancer cells and lung epithelial cells, respectively.

Hepatitis B infection and alpha-1 antitrypsin deficiency continued its evaluation with TRiM™ based formulation, ARO-AAT and ARO-HBV respectively. Nowadays, the most advanced formulation using TRiM™ technology is ARO-APOC3, siRNA conjugated to GalNac targeting Apolipoprotein C-III in hepatocytes. A reduction in ApoC3 production may result in the reduction of triglyceride rich lipoprotein. Patients with familial chylomicronemia syndrome have high levels of chylomicrons in the plasma and results in several complications, being acute pancreatitis the most serious one.

1.4.4.3 *Antibody-siRNA conjugates*

Inmunoglobulin G (IgG) antibodies conjugated with siRNA molecules are being investigated to take advantage of antibodies main properties, long circulation time and specific targeting. IgG have extended systemic circulation due to Fc (Fragment crystallize) and FcRn (neonatal Fc receptor) interactions that promote recycling and transcytosis[128] of the IgGs. Drugs conjugated with antibodies can improve its pharmacokinetics and tissue-specific targeting[129]. Antibodies can be conjugated to siRNA by non-covalent or covalent methods. In non-covalent methods, IgG are linked to cationic peptides such as nona-arginine peptides and protamine, which interact with negative charges of siRNA (Figure 1.24.-A-D). In covalent methods siRNA is linked covalently to natural residues of lysine or cysteine presented in IgG[130]. siRNA is chemically modified to expose reactive groups, which reacts directly with the antibody or via linker (Figure 1.24.-E-I). One example of siRNA-antibody conjugated platform is developed by *Sugo et al.*[131], where the antibody fragment of anti-CD71 containing sulfhydryl groups was conjugated with maleimide modified siRNA against myostatin. This conjugate showed durable gene-silencing in the heart and skeletal muscle, i.e. one month, after IV administration in normal mice. This platform was also applied to peripheral artery disease mouse model and significant levels of myostatin was reduced and muscular mass in the gastrocnemius was found.

Based on the capability of single siRNAs to reach muscular tissues, Avidity Biosciences uses siRNA covalently attached to antibodies or antibody fragments via linker. It has launched Phase I/II trial in Myotonic Dystrophy type 1 and is planning to launch clinical trials for Facioscapulohumeral Muscular Dystrophy and Duchenne Muscular Dystrophy.

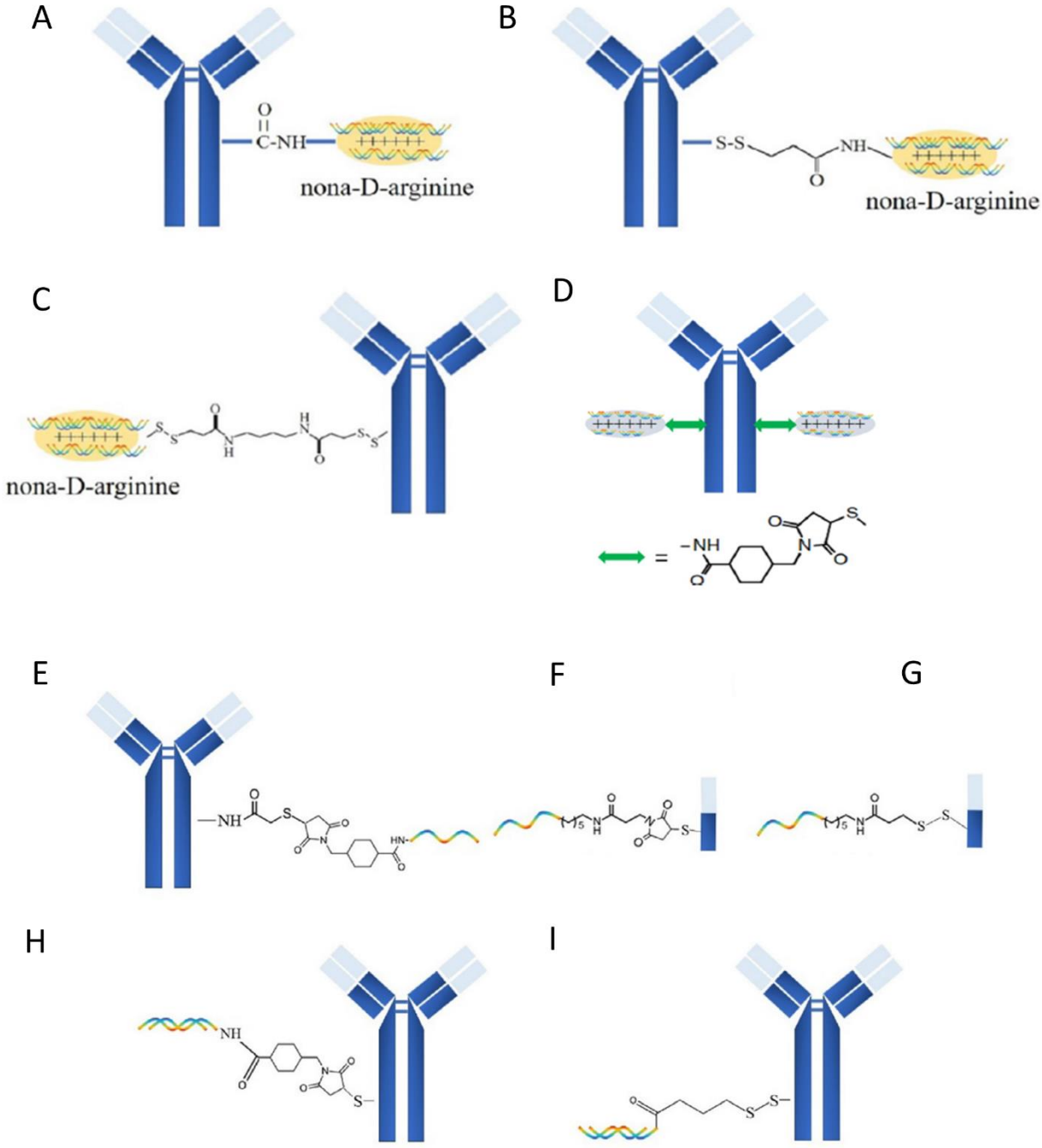

Figure 1. 24.-siRNA-antibody conjugates. Non-covalent methods: A) Antibody-carboxyl-(EDC)-amine-nona arginine-siRNAs system. B) Antibody-sulfhydryl-SPDP-amine-nona arginine-siRNAs system C) Antibody–sulfhydryl–DPDPB–sulfhydryl terminal nona arginine–siRNAs system D) Cetuximab conjugates with protamine through the reaction of sulfhydryl and maleimide. Covalent methods: E) SATA reagent-modified antibody reacts with SMCC modified siRNAs F) sulfhydryl-containing anti-CD71 Fab fragment reacts with maleimide modified siRNAs G) sulfhydryl-containing anti-CD71 Fab fragment reacts with (2-pyridyldithio) pentanoate modified siRNAs H) cysteine residues-containing antibody reacts with SMCC modified siRNAs I) cysteine residues-containing antibody reacts with SPDB modified siRNAs. Modified from *Cao et Al*[130].

1.4.5 Exosomes

Exosomes are nano-sized (40-150 nm) extracellular vesicles secreted by cells, acting as mediators in intercellular communications and material exchange. Natural cargo of exosomes are nucleic acids, proteins, lipids and other bioactive compounds (See Figure 1.25). However, exosomes can be isolated from cells and its cargo removed following several centrifugation steps and enzymatic reactions. Then they can be loaded with the desired cargo, like siRNA by electroporation[132]. The endogeneity of exosomes give them extensive and unique advantages[133] as delivery systems, due to the content of transmembrane and membrane-anchored proteins that may enhance endocytosis, thus promoting the delivery of their internal content. Hence, they are biological nanoparticles with less cytotoxicity than synthetic lipid particles. However, exosomes face considerable challenges in manufacturing scale-up, as they are produced by cells and achievement of particle homogeneity, in order to translate exosomes into the clinic, is clearly the most critical barrier. Although some researchers are perfecting cGMP manufacturing methods, others are investigating the viability of taking exosomal components and reforming them into well- controlled synthetic nanoparticles. One formulation using exosome entered Phase I of clinical trials targeting oncogene KRASG12D mutation in pancreatic ductal adenocarcinoma. The work discussed that the presence of membrane proteins such as CD47 increase circulation lifetime by avoiding exosome phagocytosis[132].

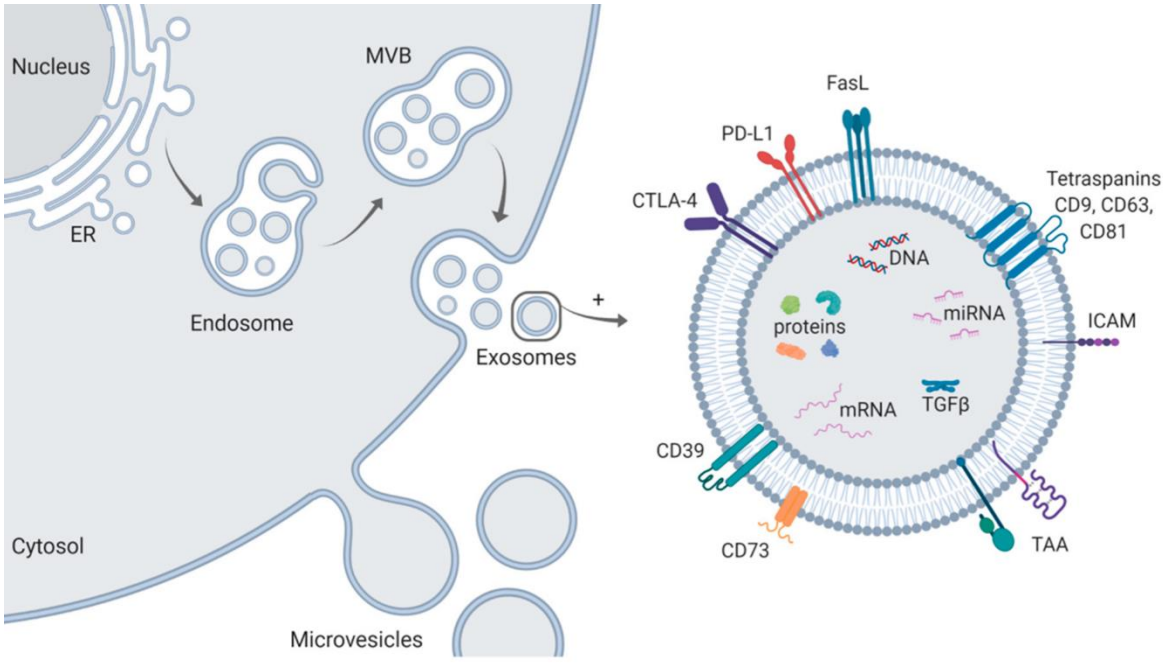

Figure 1. 25.-Schematic representation of exosome biogenesis and molecular cargo. Exosomes are formed through inward budding of the endosomal membrane resulting in the formation of multivesicular bodies (MVB). Upon fusion of MVBs with the plasma membrane, exosomes are released in the extracellular space. In contrast, microvesicles are formed by simple budding of the plasma membrane. The molecular cargo of exosomes consists of proteins, miRNA, mRNA, DNA, and lipids. On their surface, they carry the tetraspanins CD9, CD63, and CD81, commonly referred to as "exosomal markers," adhesion molecules (e.g. intercellular adhesion molecule ICAM) and—in case of TEX—tumor-associated antigens (TAA), which are specific to the cell of origin. Further, the presence of immune suppressive proteins such as CTLA-4, PD-L1, Fas-L, CD39, CD73, and TGFβ in HNSCC derived exosomes has been reported[134].

1.6 Addressable diseases and challenges by RNAi therapeutic formulations

siRNA can target any RNA by Watson-Crick base pairing. This makes siRNA a potent tool to treat any gene-dependent disorder. Among these diseases we can find infectious pathologies, caused by viruses, bacteria or protozoa; Mutation associated pathologies and miRNA regulation pathway disorders.

Viral genes that are essential for virus replication and host genes that are essential for virus entry or that play an essential role in the virus life cycle constitute attractive targets. Silencing genes relevant to viral infection, such as human pathogen respiratory syncytial virus (RSV), human immunodeficiency virus type 1 (HIV-1), influenza virus A, hepatitis B virus (HBV), hepatitis C virus (HCV), severe acute respiratory syndrome corona virus (SARS) has been achieved using RNAi[135]. For effective antiviral therapy, it is necessary to identify the essential viral factors, especially the viral proteins that are involved in disease pathogenesis. Also, identification of viral factors that are similar or share conserved sequences among different strains or even different species of viruses, belonging to the same family, has been regarded as an effective strategy to achieve a wider scope of action, using a single target. Furthermore, these factors should be distinctly different from any human proteins to avoid any harmful side effects. The most advanced case is the hepatitis virus B, with several candidates in the clinical trials (ALN-HBV02, AB-729, ARO-HBV, DCR-HBVS) See Table A.1 in Appendix I. As HBV is developed in the liver, vectors targeting hepatocytes, mostly GalNac conjugates, are used to reach the liver. siRNAs against the Hepatitis B surface antigen (HBsAg) have been shown to inhibit the antigen expression and viral replication[136,137].

In contrast to viruses, bacteria are not generally amenable to silencing by siRNA because they replicate mostly outside the host cell. However, it might still be possible to reduce morbidity and mortality from life-threatening bacterial infections by silencing host genes involved in aspects of the immune response that lead to adverse consequences. For example, reducing the expression of proinflammatory cytokines, such as tumor necrosis factor-α (TNFα)[135]. Similarly, silencing host genes involved in mediation of bacterial invasion constitutes an interesting approach. Mycobacterium is a genus of bacteria that reside in intracellular compartment of host cells, where they are protected from microbicidal attacks and elude the immune system. Moreover, they have extremely resistant cell wall. Therefore, mycobacteria such as *mycobacterium tuberculosis* and *mycobacterium leprae* are perfect candidates for treatment with RNAi-based therapeutics targeting host genes involved in mycobacterial invasion and growth inside the cells[138].

Protozoan infections are the leading cause of death in developing countries in Africa, Asia and the Americas. Protozoan infections are life-threatening diseases caused or transmitted by many protozoan species including *Plasmodium spp*. (Malaria), *Toxoplasma gondii* (Toxoplasmosis) *Trypanosoma cruzi* (Chagas disease) *Trypanosoma brucei* (African trypanosomiasis), *Leishmania donovani* (Leishmaniasis or Sleeping sickness), *Giardia lamblia* or *G. intestinalis* (Giardiasis), *Schistosoma mansoni* (Schistosomiasis), *Cryptosporidium spp*. (Cryptosporidiosis), *Entamoeba*

histolytica (Amebiasis), and *Toxocara canis* (Toxocariasis). Over the past decades, chemotherapy is the only successful standard strategy for alleviating these parasitic infections. Despite their success, clinical application of chemotherapeutic drugs has been limited due to the emergence of drug resistant parasites[139]. To overcome these challenges, RNAi-based molecules have been explored as a potential therapeutic and diagnostic tool against many intra-cellular protozoan infections. Protozoa groups of organisms are evolutionarily very distant from each other and have fundamentally different lifestyles. So, each group needs a specific strategy. Most of them as eucaryotic organisms present RNAi pathway. So, strategies are based on designing siRNAs for i) knockdown genes that will cause cell death or ii) knockdown host proteins that use protozoa to infect host cells[139].

The discovery of new disease-causing mutations in the genome identifies a number of possible therapeutic targets. Sequence aberrations can potentially be used to selectively target mutated transcripts associated with a disease. RNAi has enormous potential for the treatment of many genetic and acquired diseases. The use of RNAi-based therapeutics is especially appealing, as RNAi can be used to reduce the levels of toxic gain-in-function proteins, to inhibit the expression of disease-associated alleles without suppression of expression of wild-type alleles, and to target single-base mutation diseases, missense mutation diseases, single nucleotide polymorphisms and dysregulation of splicing process mutations associated with some genetic disorders. RNAi can also be used to modulate the expression of proteins not conventionally accessible by more traditional pharmaceutical approaches, e.g. those that lack ligand-binding domains or those that share a high degree of structural homology, both of which are difficult to target as individuals[135,140].

Moreover, the potential applications of RNAi have shown great promise in the field of cancer research. Tumors are the result of the accumulation of various types of gene mutations and the regulation of gene networks formed by the interaction of these mutated genes[141]. Knockdown of these target genes results an interesting approach to fight cancer. Advantages of RNAi technology are the rapid development of efficacious and targeted drugs for controlling tumor growth[142]. The application of RNAi in cancer is mainly via downregulation genes in tumors, modulating immune cells in the tumor microenvironment to become anti-tumoral or make tumor more sensitive to chemical drugs or immune cells.

Among cancer related genes can be found KRAS (oncogene), detection of mutations in this oncogene represents an important index for prognosis of various cancers, i.e pancreatic, lung and determining the effect of radiotherapy and chemotherapy[143]. Studies have shown that silencing PLK1 induces apoptosis[144], which is a cell cycle protein and key regulator in mitosis. EGFR (epidermal growth factor receptors), which is overexpressed in cancer cells, upon binding to specific ligand induces mitogenic signals into the tumor cell to induce cellular proliferation and resistance to apoptosis[145]. Some genes in tumors have been shown to create resistance to chemotherapy drugs, such as cisplatin. This resistance is related to the following events: improved DNA repair (e.g., Mad2), overexpression of antiapoptotic genes (e.g., BCL2, survivin), and pump-mediated drug efflux (e.g., MRP1). Fortunately, inhibition of these genes and proteins has shown high potential in restoring the efficacy of cisplatin to combat resistance and minimize off-target effects, representing

an attractive therapeutic approach[146]. Crucial genes relevant to tumor development are found within different cells that participate in the tumor microenvironment. These cells include dendritic cells, which play a critical role in immune system regulation. Silenced genes such as PD-L1, SOCS1, and STAT3 have been identified as key factors in tumor immunity regulation. Additionally, tumor-associated macrophages (TAMs) are present within the tumor and are recognized as a promising target for cancer immunotherapy. These cells exhibit important target genes that comprise chemokines, pro-inflammatory cytokines (such as IL-1β, IL-6, TNF-α), and pro-angiogenic factors that are essential in the regulation of immune response, tumor growth, and angiogenesis[147]. Another approach not so widely explored is to modulate cancer cells to be sensitive of being cleared by phagocytosis. Healthy normal tissues and cells have inherited the ability to avoid self-elimination by phagocytes through the expression of anti-phagocytosis molecules, cancer cells depend even more on similar mechanisms to evade immune eradication. Phagocytosis, is a multi-step cellular process involving target cell recognition, cellular engulfment, and lysosomal digestion, regulated by receptor-ligand interactions between the target cell and the phagocyte. One of these interactions is the SIRPα-CD47, signal-regulatory protein α (SIRPα), that is expressed on macrophages surface. It recognizes CD47 a transmembrane protein ubiquitously expressed in normal cells, which act as "don´t eat me" signal. CD47 labeled cells allow macrophages distinguish between "native" and "foreign" cells. SIRPα recognizes CD47, which leads to interruption of phagocytosis. Several cancer cells overexpressed CD47, escaping from immune system clearance. An interesting approach is to blockade this SIRPα-CD47 interaction to promote cell engulfment by macrophages. Some studies have used CD47 monoclonal antibodies for this purpose and showed increased tumor cells phagocytosis in ovarian, breast, thyroid cancer cells and self-renewing leukemia stem cells[148,149,150]. The use of siRNA in this type of therapies result quite attractive in terms of affinity and knockdown efficacy to the target gene. Despite it is emerging as new type of treatment there are some preclinical studies reported on melanoma[151] and ovarian cancer[152] by delivering siRNA.

The therapeutic potential of siRNA is mainly hampered by the delivery method and the numerous barriers encountered on its way to the cytoplasm. Consequently, the range of treatable disorders is confined by the tissues that can be reached by existing delivery systems. Figure 1.26 summarizes the current clinical trials candidates and its target organ.

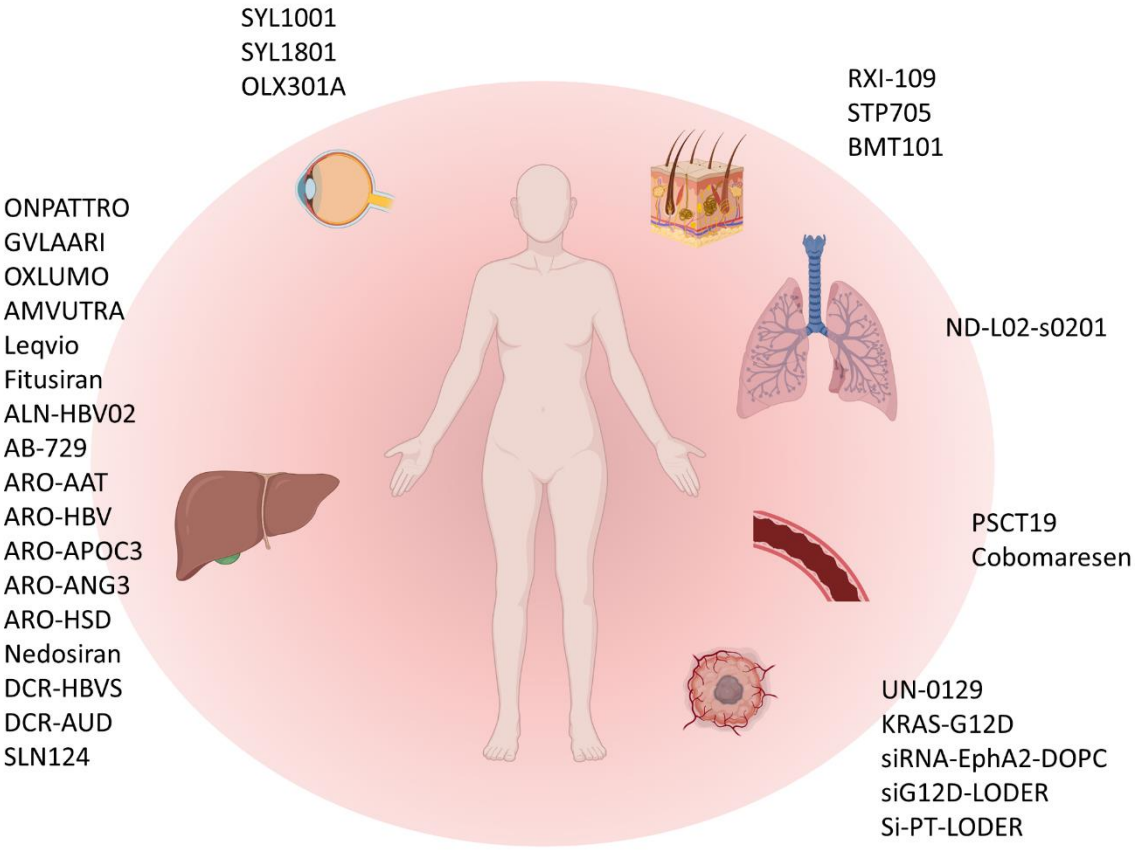

Figure 1. 26.-Current tissues targeted by siRNA therapies in the clinical stage or already approved by FDA. Imaged generated with Biorender.

As we can see (Figure 1.26), the liver is among the most readily targeted organs for drug delivery, largely due to the high efficiency of the GalNac conjugate delivery system domain. GalNac dominates the clinical trials landscape for RNAi therapeutics, with most treatable conditions being related to liver diseases due to the organ-specific delivery. However, not all therapeutic delivery requires intravenous injection. Certain areas, like the eyes and skin, can be accessed via local delivery. Eye treatments can often be administered through simple eye drops containing free siRNA, eliminating the need for carriers to achieve protein knockdown (SYL1001, OLX301A). For skin conditions, several potential treatments are currently under investigation, including oligonucleotides conjugated to cholesterol or encapsulated in polypeptide nanoparticles. Lung treatment delivery can be achieved through local administration via aerosol suspensions or dry powder inhalation, or alternatively through intravenous injection. One notable treatment currently in Phase II clinical trials is delivered intravenously using lipid nanoparticles (LNP) as a carrier(ND-L02-s0201)[153]. Tumors present a more complex scenario for drug delivery. They can be targeted either by local implantation of a therapeutic scaffold, a method known as LODER^{TM} which is invasive, or by intravenous injection. There are several materials currently undergoing clinical trials for this purpose, including liposomes (as seen in siRNA-EphA2-DOPC), exosomes (G12D-KRAS exosomes), and gold nanoparticles, such as NU-0129.

Table A.1, found in Appendix I, offers a comprehensive overview of the most advanced clinical trials concerning siRNA-based therapeutics, including details about the respective delivery vehicles used in each formulation.

Although significant progress has been made in the past decade in biomaterials and nanotechnology research for pre-clinical studies, only a few materials have advanced to clinical trials, primarily targeting the liver. To fully realize the potential of RNA interference technology, new materials are needed that can target a broader range of tissues beyond the liver. However, several challenges exist in the manufacturing process, such as lack of homogeneity, batch-to-batch variability, scale-up issues, and instability during storage. Additionally, the properties of vectors need improvement to expand the scope of future siRNA therapeutic applications. This includes increasing vehicle bioavailability, reducing the immune response, balancing vehicle stability and cargo release, optimizing loss of material during biodistribution, and improving endosomal escape. Nonetheless, the increasing number of synthetic materials for efficient in vivo transfection of cells shows the incredible potential of combining chemistry and biology (Table A.1 Appendix I). These remarkable advances inspire novel gene therapy approaches and offer hope for improving human health in the future[55].

1.7 References

1. Wirth, T., Parker, N. & Ylä-Herttuala, S. History of gene therapy. *Gene* **525**, 162–169 (2013).

2. Lorentzen, C. L., Haanen, J. B., Met, Ö. & Svane, I. M. Clinical advances and ongoing trials on mRNA vaccines for cancer treatment. *The Lancet Oncology* **23** e450–e458 (2022).

3. Fire, A. *et al.* Potent and specific genetic interference by double-stranded RNA in Caenorhabditis elegans. *Nature* **391**, 806–811 (1998).

4. Wilson, R. C. & Doudna, J. A. Molecular mechanisms of RNA interference. *Annu. Rev. Biophys.* **42**, 217–239 (2013).

5. Setten, R. L., Rossi, J. J. & Han, S. ping. The current state and future directions of RNAi-based therapeutics. *Nat. Rev. Drug Discov.* **18**, 421–446 (2019).

6. Castanotto, D. & Rossi, J. J. The promises and pitfalls of RNA-interference-based therapeutics. *Nature* **457**, 426–433 (2009).

7. Morris, K. V. Therapeutic potential of siRNA-mediated transcriptional gene silencing. Biotechniques 40, S7–S13 (2006).

8. Grimm, D. *et al.* Fatality in mice due to oversaturation of cellular microRNA/short hairpin RNA pathways. *Nature* **441**, 537–541 (2006).

9. Reynolds, A. *et al.* Rational siRNA design for RNA interference. *Nat. Biotechnol.* **22**, 326–330 (2004).

10. Sano, M. *et al.* Effect of asymmetric terminal structures of short RNA duplexes on the RNA interference activity and strand selection. *Nucleic Acids Res.* **36**, 5812–5821 (2008).

11. Setten, R. L., Rossi, J. J. & Han, S. ping. The current state and future directions of RNAi-based therapeutics. *Nat. Rev. Drug Discov.* **18**, 421–446 (2019).

12. Li, W. & Cha, L. Genetic studies of diseases: Predicting siRNA efficiency. *Cell. Mol. Life Sci.* **64**, 1785–1792 (2007).

13. Fakhr, E., Zare, F. & Teimoori-Toolabi, L. Precise and efficient siRNA design: A key point in competent gene silencing. *Cancer Gene Ther.* **23**, 73–82 (2016).

14. Huesken, D. *et al.* Design of a genome-wide siRNA library using an artificial neural network. *Nat. Biotechnol.* **23**, 995–1001 (2005).

15. Williams, B. R. Signal Integration via PKR. *Sci. STKE* **2001**, (2001).

16. Hornung, V. *et al.* Sequence-specific potent induction of IFN-α by short interfering RNA in plasmacytoid dendritic cells through TLR7. *Nat. Med.* **11**, 263–270 (2005).

17. Robbins, M. et al. 2′-O-methyl-modified RNAs Act as TLR7 Antagonists. *Mol. Ther.* **15**, 1663–1669 (2007).

18. Judge, A. D., Bola, G., Lee, A. C. H. & MacLachlan, I. Design of noninflammatory synthetic siRNA mediating potent gene silencing in vivo. *Mol. Ther.* **13**, 494–505 (2006).

19. Jackson, A. L. *et al.* Expression profiling reveals off-target gene regulation by RNAi. *Nat. Biotechnol.* **21**, 635–637 (2003).

20. Birmingham, A. *et al.* 3' UTR seed matches, but not overall identity, are associated with RNAi off-targets. *Nat. Methods* **3**, 199–204 (2006).

21. Castanotto, D. *et al.* Combinatorial delivery of small interfering RNAs reduces RNAi efficacy by selective incorporation into RISC. *Nucleic Acids Res.* **35**, 5154–5164 (2007).

22. Zlatev, I. *et al.* Reversal of siRNA-mediated gene silencing in vivo. *Nat. Biotechnol.* **36**, 509–511 (2018).

23. Braasch, D. A. *et al.* RNA interference in mammalian cells by chemically-modified RNA. *Biochemistry* **42**, 7967–7975 (2003).

24. Kleinman, M. E. *et al.* Sequence- and target-independent angiogenesis suppression by siRNA via TLR3. *Nature* **452**, 591–597 (2008).

25. DeVincenzo, J. *et al.* A randomized, double-blind, placebo-controlled study of an RNAi-based therapy directed against respiratory syncytial virus. *Proc. Natl. Acad. Sci. U. S. A.* **107**, 8800–8805 (2010).

26. Zuckerman, J. E. & Davis, M. E. Clinical experiences with systemically administered siRNA-based therapeutics in cancer. *Nat. Rev. Drug Discov.* **14**, 843–856 (2015).

27. Wartiovaara, J. *et al.* Nephrin strands contribute to a porous slit diaphragm scaffold as revealed by electron tomography. *J. Clin. Invest.* **114**, 1475–1483 (2004).

28. Huang, Y. *et al.* Elimination pathways of systemically delivered siRNA. *Mol. Ther.* **19**, 381–385 (2011).

29. Huang, Y. *et al.* Pharmacokinetic behaviors of intravenously administered siRNA in glandular tissues. *Theranostics* **6**, 1528–1541 (2016).

30. Thakker, D. R. *et al.* Neurochemical and behavioral consequences of widespread gene knockdown in the adult mouse brain by using nonviral RNA interference. *Proc. Natl. Acad. Sci. U. S. A.* **101**, 17270–17275 (2004).

31. Wittrup, A. *et al.* Visualizing lipid-formulated siRNA release from endosomes and target gene knockdown. *Nat. Biotechnol.* **33**, 870–876 (2015).

32. Bus, T., Traeger, A. & Schubert, U. S. The great escape: How cationic polyplexes overcome the endosomal barrier. *J. Mater. Chem. B* **6**, 6904–6918 (2018).

33. Zelphati, O. & Szoka, F. C. Mechanism of oligonucleotide release from cationic liposomes. *Proc. Natl. Acad. Sci. U. S. A.* **93**, 11493–11498 (1996).

34. Gilleron, J. *et al.* Image-based analysis of lipid nanoparticle-mediated siRNA delivery, intracellular trafficking and endosomal escape. *Nat. Biotechnol.* **31**, 638–646 (2013).

35. Hafez, I. M., Maurer, N. & Cullis, P. R. On the mechanism whereby cationic lipids promote intracellular delivery of polynucleic acids. *Gene Ther.* **8**, 1188–1196 (2001).

36. Hu, B. *et al.* Therapeutic siRNA: state of the art. *Signal Transduct. Target. Ther.* **5**, 101 (2020).

37. Thompson, J. D. *et al.* Toxicological and pharmacokinetic properties of chemically modified siRNAs targeting p53 RNA following intravenous administration. *Nucleic Acid Ther.* **22**, 255–264 (2012).

38. Ashikari, M., Tokoro, M., Itaya, M., Nozaki, M. & Ogura, Y. Suppression of Laser-Induced Choroidal Neovascularization by Nontargeted siRNA. **51**, 3820–3824 (2010).

39. Tolentino, M. J. *et al.* Intravitreal injection of vascular endothelial growth factor small interfering RNA inhibits growth and leakage in a nonhuman primate, laser-induced model of choroidal neovascularization. *Retina* **24**, 132–138 (2004).

40. Ahmed, Z. et al. Ocular neuroprotection by siRNA targeting caspase-2. *Cell Death Dis.* **2**, e173–e173 (2011).

41. 1. Singer, O. et al. Targeting BACE1 with siRNAs ameliorates Alzheimer disease neuropathology in a transgenic model. *Nat. Neurosci.* **8**, 1343–1349 (2005).

42. Xia, H. *et al.* RNAi suppresses polyglutamine-induced neurodegeneration in a model of spinocerebellar ataxia. *Nat. Med.* **10**, 816–820 (2004).

43. Suckau, L. *et al.* Long-term cardiac-targeted RNA interference for the treatment of heart failure restores cardiac function and reduces pathological hypertrophy. *Circulation* **119**, 1241–1252 (2009).

44. Bangham, A. D. Methods in membrane biology, vol. 7. *Trends Biochem. Sci.* **2**, 96 (1977).

45. Rietwyk, S. & Peer, D. Next-Generation Lipids in RNA Interference Therapeutics. *ACS Nano* **11**, 7572–7586 (2017).

46. Kulkarni, J. A. *et al.* On the Formation and Morphology of Lipid Nanoparticles Containing Ionizable Cationic Lipids and siRNA. *ACS Nano* **12**, 4787–4795 (2018).

47. Whitehead, K. A. *et al.* Degradable lipid nanoparticles with predictable in vivo siRNA delivery activity. *Nat. Commun.* **5**, (2014).

48. Love, K. T. *et al.* Lipid-like materials for low-dose, in vivo gene silencing. *Proc. Natl. Acad. Sci. U. S. A.* **107**, 1864–1869 (2009).

49. Jayaraman, M. *et al.* Maximizing the potency of siRNA lipid nanoparticles for hepatic gene silencing in vivo. *Angew. Chemie - Int. Ed.* **51**, 8529–8533 (2012).

50. Belliveau, N. M. *et al.* Microfluidic Synthesis of Highly Potent Limit-size Lipid Nanoparticles for In Vivo Delivery of siRNA. *Mol. Ther. Nucleic Acids* **1**, e37 (2012).

51. Bao, Y. *et al.* Effect of PEGylation on biodistribution and gene silencing of siRNA/lipid nanoparticle complexes. *Pharm. Res.* **30**, 342–351 (2013).

52. Kolli, S. *et al.* pH-triggered nanoparticle mediated delivery of siRNA to liver cells in vitro and in vivo. *Bioconjug. Chem.* **24**, 314–332 (2013).

53. Akinc, A. *et al.* The Onpattro story and the clinical translation of nanomedicines containing nucleic acid-based drugs. *Nat. Nanotechnol.* **14**, 1084–1087 (2019).

54. Mui, B. L. *et al.* Influence of Polyethylene Glycol Lipid Desorption Rates on Pharmacokinetics and Pharmacodynamics of siRNA Lipid Nanoparticles. *Mol. Ther. - Nucleic Acids* **2**, (2013).

55. Lostalé-Seijo, I. & Montenegro, J. Synthetic materials at the forefront of gene delivery. *Nat. Rev. Chem.* **2**, 258–277 (2018).

56. Paunovska, K., Loughrey, D. & Dahlman, J. E. Drug delivery systems for RNA therapeutics. *Nat. Rev. Genet.* **23**, 265–280 (2022).

57. Kanasty, R., Dorkin, J. R., Vegas, A. & Anderson, D. Delivery materials for siRNA therapeutics. *Nature Mater.* **12**, 967–977 (2013).

58. Zhigaltsev, I. V., Maurer, N., Wong, K. F. & Cullis, P. R. Triggered release of doxorubicin following mixing of cationic and anionic liposomes. *Biochim. Biophys. Acta - Biomembr.* **1565**, 129–135 (2002).

59. Takahashi, H., Sinoda, K. & Hatta, I. Effects of cholesterol on the lamellar and the inverted hexagonal phases of dielaidoylphosphatidylethanolamine. *Biochim. Biophys. Acta - Gen. Subj.* **1289**, 209–216 (1996).

60. Fitzgerald, K. *et al.* Effect of an RNA interference drug on the synthesis of proprotein convertase subtilisin/kexin type 9 (PCSK9) and the concentration of serum LDL cholesterol in healthy volunteers: A randomised, single-blind, placebo-controlled, phase 1 trial. *Lancet* **383**, 60–68 (2014).

61. Strumberg, D. *et al.* Phase I clinical development of Atu027, a siRNA formulation targeting PKN3 in patients with advanced solid tumors. *Int. J. Clin. Pharmacol. Ther.* **50**, 76–78 (2012).

62. Beg, M.S. *et al.* Phase I study of MRX34, a liposomal miR-34a mimic, administered twice weekly in patients with advanced solid tumors. *Invest New Drugs* **35**, 180–188 (2017). https://doi.org/10.1007/s10637-016-0407-y.

63. Oishi, M., Nakaogami, J., Ishii, T. & Ã, Y. N. Smart PEGylated Gold Nanoparticles for the Cytoplasmic Delivery of siRNA to Induce Enhanced Gene Silencing. **35**, 9–10 (2006).

64. Conde, J. *et al.* In vivo tumor targeting via nanoparticle-mediated therapeutic siRNA coupled to in fl ammatory response in lung cancer mouse models. *Biomaterials* **34**, 7744–7753 (2013).

65. Randeria, P. S. *et al.* siRNA-based spherical nucleic acids reverse impaired wound healing in diabetic mice by ganglioside GM3 synthase knockdown. *Proc. Natl. Acad. Sci. U. S. A.* **112**, 5573–5578 (2015).

66. Jiang, Y., Huo, S., Hardie, J., Liang, X. J. & Rotello, V. M. Progress and perspective of inorganic nanoparticle-based siRNA delivery systems. *Expert Opinion on Drug Delivery* **13**, 547–559 (2016).

67. Kim, S. T. *et al.* Dendronized gold nanoparticles for siRNA delivery. *Small* **8**, 3253–3256 (2012).

68. Song, W. J., Du, J. Z., Sun, T. M., Zhang, P. Z. & Wang, J. Gold nanoparticles capped with polyethyleneimine for enhanced siRNA delivery. *Small* **6**, 239–246 (2010).

69. Elbakry, A. *et al.* Layer-by-layer assembled gold nanoparticles for sirna delivery. *Nano Lett.* **9**, 2059–2064 (2009).

70. Lee, S. K. & Tung, C. H. A fabricated siRNA nanoparticle for ultra-long gene silencing in vivo. *Adv. Funct. Mater.* **23**, 3488–3493 (2013).

71. Jensen, S. A. *et al.* Spherical nucleic acid nanoparticle conjugates as an RNAi-based therapy for glioblastoma. *Sci. Transl. Med.* **5**, (2013).

72. NU-0129 in Treating Patients With Recurrent Glioblastoma or Gliosarcoma Undergoing Surgery - Full Text View - ClinicalTrials.gov. https://clinicaltrials.gov/ct2/show/NCT03020017.

73. Park, J. W., Bae, K. H., Kim, C. & Park, T. G. Clustered magnetite nanocrystals cross-linked with PEI for efficient siRNA delivery. *Biomacromolecules* **12**, 457–465 (2011).

74. Agrawal, A. *et al.* Functional delivery of siRNA in mice using dendriworms. *ACS Nano* **3**, 2495–2504 (2009).

75. Jiang, S., Eltoukhy, A. A., Love, K. T., Langer, R. & Anderson, D. G. Lipidoid-coated iron oxide nanoparticles for efficient DNA and siRNA delivery. *Nano Lett.* **13**, 1059–1064 (2013).

76. Xia, T. *et al.* Polyethyleneimine coating enhances the cellular uptake of mesoporous silica nanoparticles and allows safe delivery of siRNA and DNA constructs. *ACS Nano* **3**, 3273–3286 (2009).

77. Hartono, S. B. *et al.* Poly-L-lysine functionalized large pore cubic mesostructured silica nanoparticles as biocompatible carriers for gene delivery. *ACS Nano* **6**, 2104–2117 (2012).

78. Oupicky, D. *et al.* Enhanced gene and siRNA delivery by polycation-modified mesoporous silica nanoparticles loaded with chloroquine. *Pharm. Res.* **27**, 2556–2568 (2010).

79. Roy, I., Mitra, S., Maitra, A. & Mozumdar, S. Calcium phosphate nanoparticles as novel non-viral vectors for targeted gene delivery. *Int. J. Pharm.* **250**, 25–33 (2003).

80. Pittella, F. *et al.* Enhanced endosomal escape of siRNA-incorporating hybrid nanoparticles from calcium phosphate and PEG-block charge-conversional polymer for efficient gene knockdown with negligible cytotoxicity. *Biomaterials* **32**, 3106–3114 (2011).

81. Lee, M. S. *et al.* Target-specific delivery of siRNA by stabilized calcium phosphate nanoparticles using dopa-hyaluronic acid conjugate. *J. Control. Release* **192**, 122–130 (2014).

82. Li, J., Yang, Y. & Huang, L. Calcium phosphate nanoparticles with an asymmetric lipid bilayer coating for siRNA delivery to the tumor. *J. Control. Release* **158**, 108–114 (2012).

83. Mendes, B. B. *et al.* Nanodelivery of nucleic acids. *Nat. Rev. Methods Prim.* **2**, (2022).

84. Hwang, D. W. *et al.* A brain-targeted rabies virus glycoprotein-disulfide linked PEI nanocarrier for delivery of neurogenic microRNA. *Biomaterials* **32**, 4968–4975 (2011).

85. Jiang, G., Park, K., Kim, J., Ki, S. K. & Sei, K. H. Target specific intracellular delivery of siRNA/PEI-HA complex by receptor mediated endocytosis. *Mol. Pharm.* **6**, 727–737 (2009).

86. Merkel, O. M. *et al.* Nonviral siRNA delivery to the lung: Investigation of PEG-PEI polyplexes and their in vivo performance. *Mol. Pharm.* **6**, 1246–1260 (2009).

87. Beyerle, A. *et al.* Comparative in vivo study of poly(ethylene imine)/siRNA complexes for pulmonary delivery in mice. *J. Control. Release* **151**, 51–56 (2011).

88. Alshamsan, A. *et al.* Formulation and delivery of siRNA by oleic acid and stearic acid modified polyethylenimine. *Mol. Pharm.* **6**, 121–133 (2009).

89. Alshamsan, A. *et al.* The induction of tumor apoptosis in B16 melanoma following STAT3 siRNA delivery with a lipid-substituted polyethylenimine. *Biomaterials* **31**, 1420–1428 (2010).

90. Höbel, S. & Aigner, A. Polyethylenimines for siRNA and miRNA delivery in vivo. *Wiley Interdiscip. Rev. Nanomedicine Nanobiotechnology* **5**, 484–501 (2013).

91. Schiffelers, R. M. *et al.* Cancer siRNA therapy by tumor selective delivery with ligand-targeted sterically stabilized nanoparticle. *Nucleic Acids Res.* **32**, e149–e149 (2004).

92. Moriguchi, R. *et al.* A multifunctional envelope-type nano device for novel gene delivery of siRNA plasmids. *Int. J. Pharm.* **301**, 277–285 (2005).

93. Harada-Shiba, M. *et al*. Polyion complex micelles as vectors in gene therapy – pharmacokinetics and in vivo gene transfer. *Gene Ther* **9**, 407–414 (2002).

94. Karlsson, J., Rhodes, K. R., Green, J. J. & Tzeng, S. Y. Poly(beta-amino ester)s as gene delivery vehicles: challenges and opportunities. *Expert Opin. Drug Deliv.* **0**, (2020).

95. Tzeng, S. Y. & Green, J. J. Subtle Changes to Polymer Structure and Degradation Mechanism Enable Highly Effective Nanoparticles for siRNA and DNA Delivery to Human Brain Cancer. *Adv. Healthc. Mater.* **2**, 468–480 (2013).

96. Lopez-Bertoni, H. *et al.* Bioreducible Polymeric Nanoparticles Containing Multiplexed Cancer Stem Cell Regulating miRNAs Inhibit Glioblastoma Growth and Prolong Survival. *Nano Lett.* **18**, 4086–4094 (2018).

97. Kim, J. *et al.* Poly(ethylene glycol)-Poly(beta-amino ester)-Based Nanoparticles for Suicide Gene Therapy Enhance Brain Penetration and Extend Survival in a Preclinical Human Glioblastoma Orthotopic Xenograft Model. *ACS Biomater. Sci. Eng.* **6**, 2943–2955 (2020).

98. Alameh, M. *et al.* SiRNA Delivery with Chitosan: Influence of Chitosan Molecular Weight, Degree of Deacetylation, and Amine to Phosphate Ratio on in Vitro Silencing Efficiency, Hemocompatibility, Biodistribution, and in Vivo Efficacy. *Biomacromolecules* **19**, 112–131 (2018).

99. Popielarski, S. R., Mishra, S. & Davis, M. E. Structural effects of carbohydrate-containing polycations on gene delivery. 3. Cyclodextrin type and functionalization. *Bioconjug. Chem.* **14**, 672–678 (2003).

100. Bartlett, D. W. & Davis, M. E. Physicochemical and Biological Characterization of Targeted, Nucleic Acid-Containing Nanoparticles. *Bioconjug. Chem.* **18**, 456–468 (2007).

101. Mishra, S., Webster, P. & Davis, M. E. PEGylation significantly affects cellular uptake and intracellular trafficking of non-viral gene delivery particles. *Eur. J. Cell Biol.* **83**, 97–111 (2004).

102. Davis, M. E. The first targeted delivery of siRNA in humans via a self-assembling, cyclodextrin polymer-based nanoparticle: From concept to clinic. *Mol. Pharm.* **6**, 659–668 (2009).

103. Davis, M. E. The first targeted delivery of siRNA in humans via a self-assembling, cyclodextrin polymer-based nanoparticle: From concept to clinic. *Mol. Pharm.* **6**, 659–668 (2009).

104. Wang, L. L. & Burdick, J. A. Engineered Hydrogels for Local and Sustained Delivery of RNA-Interference Therapies. *Adv. Healthc. Mater.* **6**, 1–16 (2017).

105. Huynh, C. T. *et al.* Photocleavable Hydrogels for Light-Triggered siRNA Release. *Adv. Healthc. Mater.* **5**, 305–310 (2016).

106. Khvalevsky, E. Z. *et al.* Mutant KRAS is a druggable target for pancreatic cancer. *Proc. Natl. Acad. Sci. U. S. A.* **110**, 20723–20728 (2013).

107. Blanazs, A., Armes, S. P. & Ryan, A. J. Self-assembled block copolymer aggregates: From micelles to vesicles and their biological applications. *Macromol. Rapid Commun.* **30**, 267–277 (2009).

108. Discher, D. E. & Ahmed, F. Polymersomes. *Annu. Rev. Biomed. Eng.* **8**, 323–341 (2006).

109. Iqbal, S., Blenner, M., Alexander-Bryant, A. & Larsen, J. Polymersomes for Therapeutic Delivery of Protein and Nucleic Acid Macromolecules: From Design to Therapeutic Applications. *Biomacromolecules* **21**, 1327–1350 (2020).

110. Kim, Y. *et al.* Polymersome delivery of siRNA and antisense oligonucleotides. *J. Control. Release* **134**, 132–140 (2009).

111. Zou, Y. *et al.* Virus-Mimicking Chimaeric Polymersomes Boost Targeted Cancer siRNA Therapy In Vivo. *Adv. Mater.* **29**, 1703285 (2017).

112. Wang, F., Gao, J., Xiao, J. & Du, J. Dually Gated Polymersomes for Gene Delivery. *Nano Lett.* **18**, 5562–5568 (2018).

113. Gorman, C. B. & Smith, J. C. Structure-Property relationships in dendritic encapsulation. *Acc. Chem. Res.* **34**, 60–71 (2001).

114. Crayton, S. H. *et al.* 3.20 Molecular imaging. in *Comprehensive Biomaterials II* 424–466 (Elsevier, 2017). doi:10.1016/B978-0-12-803581-8.10222-X.

115. Tomalia, D. A. *et al.* A new class of polymers: Starburst-dendritic macromolecules. *Polym. J.* **17**, 117–132 (1985).

116. Biswas, S. & Torchilin, V. P. Dendrimers for siRNA delivery. *Pharmaceuticals* **6**, 161–183 (2013).

117. Bahadir, E. B. & Sezgintürk, M. K. Poly(amidoamine) (PAMAM): An emerging material for electrochemical bio(sensing) applications. *Talanta* **148**, 427–438 (2016).

118. Jensen, L. B. *et al.* Elucidating the molecular mechanism of PAMAM-siRNA dendriplex self-assembly: Effect of dendrimer charge density. *Int. J. Pharm.* **416**, 410–418 (2011).

119. Luo, D., Haverstick, K., Belcheva, N., Han, E. & Saltzman, W. M. Poly(ethylene glycol)-conjugated PAMAM dendrimer for biocompatible, high-efficiency DNA delivery. *Macromolecules* **35**, 3456–3462 (2002).

120. Taratula, O. *et al.* Multifunctional Nanomedicine Platform for Cancer Specific Delivery of siRNA by Superparamagnetic Iron Oxide Nanoparticles-Dendrimer Complexes. *Curr. Drug Deliv.* **8**, 59–69 (2010).

121. Bussy, C. *et al.* Therapeutic Applications. in *Adverse Effects of Engineered Nanomaterials* 285–313 (Academic Press, 2012). doi:10.1016/B978-0-12-386940-1.00016-7.

122. Spiess, M. The Asialoglycoprotein Receptor: A Model for Endocytic Transport Receptors. *Biochemistry* **29**, 10009–10018 (1990).

123. Khorev, O., Stokmaier, D., Schwardt, O., Cutting, B. & Ernst, B. Trivalent, Gal/GalNAc-containing ligands designed for the asialoglycoprotein receptor. *Bioorganic Med. Chem.* **16**, 5216–5231 (2008).

124. Biessen, E. A. L. *et al.* Synthesis of Cluster Galactosides with High Affinity for the Hepatic Asialoglycoprotein Receptor. *J. Med. Chem.* **38**, 1538–1546 (1995).

125. Zimmermann, T. S. *et al.* Clinical Proof of Concept for a Novel Hepatocyte-Targeting GalNAc-siRNA Conjugate. *Mol. Ther.* **25**, 71–78 (2017).

126. Rozema, D. B. *et al.* Dynamic PolyConjugates for targeted in vivo delivery of siRNA to hepatocytes. *Proc. Natl. Acad. Sci. U. S. A.* **104**, 12982–12987 (2007).

127. Wong, S. C. *et al.* Co-injection of a targeted, reversibly masked endosomolytic polymer dramatically improves the efficacy of cholesterol-conjugated small interfering RNAs in vivo. *Nucleic Acid Ther.* **22**, 399–404 (2012).

128. Roopenian, D. & Akilesh, S. FcRn: the neonatal Fc receptor comes of age. *Nat Rev Immunol* **7**, 715–725 (2007).

129. Beck, A. *et al.* Strategies and challenges for the next generation of antibody–drug conjugates. *Nat Rev Drug Discov* **16**, 315–337 (2017).

130. Cao, W. *et al.* Antibody–siRNA conjugates (ARC): Emerging siRNA drug formulation. *Med. Drug Discov.* **15**, 100128 (2022).

131. Sugo, T. *et al.* Development of antibody-siRNA conjugate targeted to cardiac and skeletal muscles. *J. Control. Release* **237**, 1–13 (2016).

132. Kamerkar, S. *et al.* Exosomes facilitate therapeutic targeting of oncogenic KRAS in pancreatic cancer. *Nat. 2017 5467659* **546**, 498–503 (2017).

133. Wang, H., Zhang, S., Lv, J. & Cheng, Y. Design of polymers for siRNA delivery: Recent progress and challenges. *View* **2**, 20200026 (2021).

134. Hofmann, L. *et al.* The emerging role of exosomes in diagnosis, prognosis, and therapy in head and neck cancer. *Int. J. Mol. Sci.* **21**, 1–22 (2020).

135. López-Fraga, M., Martínez, T. & Jiménez, A. RNA Interference Technologies and Therapeutics. *BioDrugs* **23**, 305–332 (2009).

136. Tang, Y., Liang, H., Zeng, G., Shen, S. & Sun, J. Advances in new antivirals for chronic hepatitis B. *Chin. Med. J. (Engl).* **135**, (2022).

137. Choi, H. S. J., Tonthat, A., Janssen, H. L. A. & Terrault, N. A. Aiming for Functional Cure With Established and Novel Therapies for Chronic Hepatitis B. *Hepatol. Commun.* **6**, 935-949 (2022).

138. Harth, G., Zamecnik, P. C., Tang, J. Y., Tabatadze, D. & Horwitz, M. A. Treatment of Mycobacterium tuberculosis with antisense oligonucleotides to glutamine synthetase mRNA inhibits glutamine synthetase activity, formation of the poly-L-glutamate/glutamine cell wall structure, and bacterial replication. *Proc. Natl. Acad. Sci. U. S. A.* **97**, 418–423 (2000).

139. Dyawanapelly, S., Ghodke, S. B., Vishwanathan, R., Dandekar, P. & Jain, R. RNA interference-based therapeutics: Molecular platforms for infectious diseases. *J. Biomed. Nanotechnol.* **10**, 1998–2037 (2014).

140. 1. Martin, S. E. & Caplen, N. J. Applications of RNA Interference in Mammalian Systems. *Annu. Rev. Genomics Hum. Genet*. **8**, 81–108 (2007).

141. Tian, Z. *et al.* Insight Into the Prospects for RNAi Therapy of Cancer. *Front. Pharmacol.* **12**, 1–15 (2021).

142. Mansoori, B., Shotorbani, S. S. & Baradaran, B. RNA interference and its role in cancer therapy. *Adv Pharm Bull.* **4**, 313–321 (2014).

143. Kokkinos, J. et al. Targeting the undruggable in pancreatic cancer using nano-based gene silencing drugs. *Biomaterials* **240**, 119742 (2020).

144. Zhang, L. *et al.* Gene regulation with carbon-based siRNA conjugates for cancer therapy. *Biomaterials* **104**, 269–278 (2016).

145. Binkhathlan, Z. & Alshamsan, A. Emerging nanodelivery strategies of RNAi molecules for colon cancer therapy: preclinical developments. *Therapeutic Delivery* **3**, 1117–1130 (2012).

146. Kumar, V., Yadavilli, S. & Kannan, R. A review on RNAi therapy for NSCLC: Opportunities and challenges. *Wiley Interdiscip. Rev. Nanomedicine Nanobiotechnology* **13**, 1–26 (2021).

147. Conde, J., Arnold, C. E., Tian, F. & Artzi, N. RNAi nanomaterials targeting immune cells as an anti-tumor therapy: the missing link in cancer treatment? *Mater. Today* **19**, 29–43 (2016).

148. Schürch, C. M. *et al.* Targeting CD47 in Anaplastic Thyroid Carcinoma Enhances Tumor Phagocytosis by Macrophages and Is a Promising Therapeutic Strategy. *Thyroid* **29**, 979–992 (2019).

149. Willingham, S. B. *et al.* The CD47-signal regulatory protein alpha (SIRPa) interaction is a therapeutic target for human solid tumors. *Proc. Natl. Acad. Sci. U. S. A.* **109**, 6662–6667 (2012).

150. Majeti, R. *et al.* CD47 Is an Adverse Prognostic Factor and Therapeutic Antibody Target on Human Acute Myeloid Leukemia Stem Cells. *Cell* **138**, 286–299 (2009).

151. Wang, Y. *et al.* Intravenous delivery of siRNA targeting CD47 effectively inhibits melanoma tumor growth and lung metastasis. *Mol. Ther.* **21**, 1919–1929 (2013).

152. Liu, R. *et al.* CD47 promotes ovarian cancer progression by inhibiting macrophage phagocytosis. *Oncotarget* **8**, 39021–39032 (2017).

153. Liu, Y. *et al.* Anti-hsp47 sirna lipid nanoparticle nd-l02-s0201 reverses interstitial pulmonary fibrosis in preclinical rat models. *ERJ Open Res.* **7**, (2021).

Chapter 2:

Scope, hypotheses, and objectives

This thesis was carried out under the co-supervision of Dr. Damien Dupin (Head of biomaterials unit, CIDETEC Nanomedicine) and Dr. Sergio Moya (Principal Investigator of the Soft matter Nanotechnology laboratory, CICBiomagune). First collaboration of both groups to joined forces with the objective to develop a polymeric siRNA nanocarrier to treat lung cancer. This thesis resulted in a strong effort of combining disciplines in molecular biology and biomaterials.

Polymeric nanoparticles for gene delivery have a tremendous potential for clinical translation, field dominated by lipid particles and GalNac conjugates. Polymers are easy to synthesize, modify with functional groups and scale up. As most siRNA carriers in the clinic target the liver (See Appendix I Table 1), there is a need to find a candidate with high efficiency and reduced toxicity, that could reach further tissues, even tumors.

Cancer is one of the most fatal diseases with poor prognosis and scarce solutions[1]. Among different types, lung cancer is in the top three position of the most common. However, it is the second most malignant tumor in the world, with ~1.8 million deaths in 2020, making it the greatest threat to human health[2]. Approximately 80–85% of lung cancers are categorized as non-small cell lung cancer (NSCLC). The current standard of care for early stages of NSCLC is surgery followed by adjuvant therapy. However, for locally advanced or metastatic cases, surgery is often not viable[3]. Therefore, it is imperative to develop effective and safe therapies that target the aggressive progression and metastasis of NSCLC.

Some efforts have been done to bring new siRNA-based therapies against NSCLC targeting oncogenes or reprograming immunogenic cells towards cancerous cells, such as T lymphocytes, natural killers, and tumor-associated macrophages[3]. One interesting strategy is to modified tumor cells for being eliminated by macrophages. Blocking SIRPα-CD47 interactions in mutant genes of NSCLC cells could be a promising approach. Recent studies have demonstrated that the knockdown of CD47 by siRNA reduces tumor mass in melanoma[4] and ovarian cancer[5].

CIDETEC have background expertise working with polymer-based drug-delivery systems with technology focused on single-chain polymeric nanoparticles (SCPNs) based on dextran[6,7,8]. Small and controllable size, and mimicking behavior toward proteins confers SCPNs attractive advantages as delivery platform[9].

It is proposed to explore the potential of SCPNs to deliver siRNA. It is a challenge to modify SCPNs with positive charges to interact electrostatically with negatively charged siRNAs. Nanoparticles produced so far are functionalized with negative or neutral charged groups, which are not compatible for oligonucleotides entrapment.

The group of soft matter nanotechnology has expertise in the delivery of siRNA using polycationic polymer particles[10]. The group has know-how in the biological response of nanocarriers and siRNA downregulation efficiency. It has developed a synthetic polyamine nanocarrier, with a high density of positive charges that complexes efficiently oligonucleotides. One of main issues of polycationic polymers is their cytotoxicity. Thus, a challenge is to modify the polymer backbone to reduce amine exposition without losing efficacy.

SCOPE, HYPOTHESES AND OBJECTIVES

This thesis followed two strategies with the objective of producing a novel siRNA vehicle with low cytotoxicity and high gene *silencing* efficiency. One strategy was to modify the biocompatible polymer dextran with amino groups to complex siRNA. The second strategy aimed at the chemical modification of polyamines to reduce the cytotoxicity and improve efficiency.

The first strategy covers the production of dextran-based vehicles. Here, the hypothesis is that SCPNs and dextran polymers modified with aminated molecules entrap siRNA and promote its delivery into the cells. Different amino groups were used that confers different pKa, such as cysteamine that only has one primary amine and more complex molecules, as spermine, tris(2-aminoethyl) amine or 1,4-Bis(3-aminopropyl) piperazine, which have secondary and tertiary amines. SCPNs were compared with the dextran backbone modified with the same amino molecules to evaluate the advantage of the intra crosslinking structure.

The second strategy consisted in the modification of polyallylamine, a cationic polymer, with oleic acid, conferring lipid-like properties to the polymer. Here, there are several hypotheses for the improvement of the polyallylamine as a vehicle. First one is that the grafting polyallylamine with oleic acid by carbodiimide will reduce the number of protonable amines, resulting in non-charged amide bonds with less cytotoxicity than the amines. The second one is that oleic acid contributes to weakening the electrostatic interaction between the polymer and siRNA, allowing for a better release of the cargo. The third hypothesis is that oleic acid is expected to interact with the lipid membrane of the endosomes causing a temporary instability that facilitates siRNA release[11].

Both strategies follow a common workflow for their evaluation as siRNA vectors, involving the use of different chemical, molecular biological and biomaterial techniques and approaches.

The objectives of this thesis are as follows:

1) **Chemical modification of dextran and polyamines** for enhanced transfection efficacy and reduced toxicity. The first objective involves the synthesis and physico-chemical characterization of the dextran based SCPN modified with amines and polyallylamine substituted with oleic acid. The degree of substitution of oleic acid in the original polymer backbone were quantified, as well as the amount amines linked to the SCPNs. For these purposes organic chemistry techniques were used: nuclear magnetic resonance spectroscopy (NMR), Fourier transformed Infrared spectroscopy (FTIR), Elemental analysis (EA), thin layer chromatography (TLC) and Thermogravimetric Analysis (TGA).

2) **siRNA complexing capacity and polyplex formation.** Once polymers are purified and well characterized, the capacity of complexing siRNA and form polyplexes were evaluated. For these objectives two techniques of molecular biology were used, i.e. gel retardation assay and Quant-IT-Ribogreen fluorescence. Resulting polyplexes are characterized in terms of size, shape, and surface charge. Size of the polyplexes were measured by dynamic light scattering (DLS) and by transmission electron microscopy (TEM). Also, TEM was used to observe the shape and morphology of the nanoparticles. Zeta-potential, which determines the surface charge of colloidal particles was determined by aqueous electrophoresis.

3) **Evaluate toxicological endpoints of polyplexes and study their cellular trafficking**. Cytotoxicity of the nanoparticles are studied in the human lung cancer cell line model, A549. Metabolic activity using MTS reactive was measured after treatment with different nanoparticles at different time points. In some cases fluorescence method to determine membrane integrity, known as Live/dead® were used to support viability assays. The nanoparticles were tracked inside cell using different fluorophores covalently linked to dextran-SCPNs and polyallylamine derivatives. Further characterization was performed to determine the amount of fluorophore attached: ^{1}H-NMR and UV-Visible. In some cases, fluorescence correlation spectroscopy was used to verify the covalent attachment stability of the fluorophore in solution. In order to assess the cellular entry of polyplexes, uptake experiments were conducted using the A549 cell line. Fluorophores were employed to label both the siRNA and the vehicles, along with the actin and nucleus of the cell. The intracellular localization of the polyplexes was determined using confocal laser scanning microscopy (CLSM). Additionally, flow cytometry studies were conducted to quantify the overall number of cells that had taken up the nanoparticles.

4) **Evaluate transfection efficacy of siRNA polyplexes in vitro**. To validate the nanocarrier and confirm the successful delivery of siRNA into the cytosol, the siRNA silencing capacity was examined. Specifically, A549 cells expressing GFP were treated with siRNA anti-GFP carried by the new materials, and the GFP expression levels were quantified using flow cytometry.

5) **Capacity of *silencing* CD47**. Once all candidates were evaluated, the capacity of the most promising materials were tested for *silencing* CD47, which is related in lung cancer therapy. A549 cells overexpressing CD47 were treated with generated carriers and the gene expression was measured at mRNA levels by reverse transcription quantitative polymerase chain reaction (RT-qPCR) and at protein levels by Western blot and flow cytometry.

This doctoral thesis is structured as follows: **Chapter 3** encompasses experiments involving SCPNs and dextran with various amines, as well as their corresponding biological studies. Diverse amine-containing molecules have been substituted into the dextran backbone, and their transfection performance as potential siRNA carriers was assessed.

Chapters 4 and 5 are dedicated to the study of modified polyallylamine with oleic acid. **Chapter 4** focuses on the biomaterial characterization, polyplex formation, and the determination of particle size and shape, while **Chapter 5** presents the biological studies conducted on A549 cells.

To effectively characterize and analyze the properties of the synthesized materials, a range of techniques have been employed. The fundamental principles of these techniques are discussed in Appendix II, while more specific methods are detailed in the experimental sections of each chapter.

References

1. Tian, Z. *et al.* Insight Into the Prospects for RNAi Therapy of Cancer. *Front. Pharmacol.* **12**, 1–15 (2021).

2. Lin, X. *et al.* A targeted siRNA-loaded PDL1-exosome and functional evaluation against lung cancer. *Thorac. Cancer* **13**, 1691–1702 (2022).

3. Kumar, V., Yadavilli, S. & Kannan, R. A review on RNAi therapy for NSCLC: Opportunities and challenges. *Wiley Interdiscip. Rev. Nanomedicine Nanobiotechnology* **13**, 1–26 (2021).

4. Wang, Y. *et al.* Intravenous delivery of siRNA targeting CD47 effectively inhibits melanoma tumor growth and lung metastasis. *Mol. Ther.* **21**, 1919–1929 (2013).

5. Liu, R. *et al.* CD47 promotes ovarian cancer progression by inhibiting macrophage phagocytosis. *Oncotarget* **8**, 39021–39032 (2017).

6. Gracia, R. *et al.* Synthesis and functionalization of dextran-based single-chain nanoparticles in aqueous media. *J. Mater. Chem. B* **5**, 1143–1147 (2017).

7. Gracia, R. *et al.* Biocompatible single-chain polymer nanoparticles loaded with an antigen mimetic as potential anticancer vaccine. *ACS Macro Lett.* **7**, 196–200 (2018).

8. Blanco-Cabra, *et al.* Neutralization of ionic interactions by dextran-based single-chain nanoparticles improves tobramycin diffusion into a mature biofilm. *npj Biofilms Microbiomes* **8**, 52 (2022).

9. Lyon, C. K. *et al.* A brief user's guide to single-chain nanoparticles. *Polym. Chem.* **6,** 181–197 (2015).

10. Andreozzi, P. *et al.* Exploring the pH Sensitivity of Poly(allylamine) Phosphate Supramolecular Nanocarriers for Intracellular siRNA Delivery. *ACS Appl. Mater. Interfaces* **9**, 38242–38254 (2017).

11. Bus, T., Traeger, A. & Schubert, U. S. The great escape: How cationic polyplexes overcome the endosomal barrier. *J. Mater. Chem. B* **6**, 6904–6918 (2018).

Chapter 3:

Dextran-based carriers for siRNA delivery

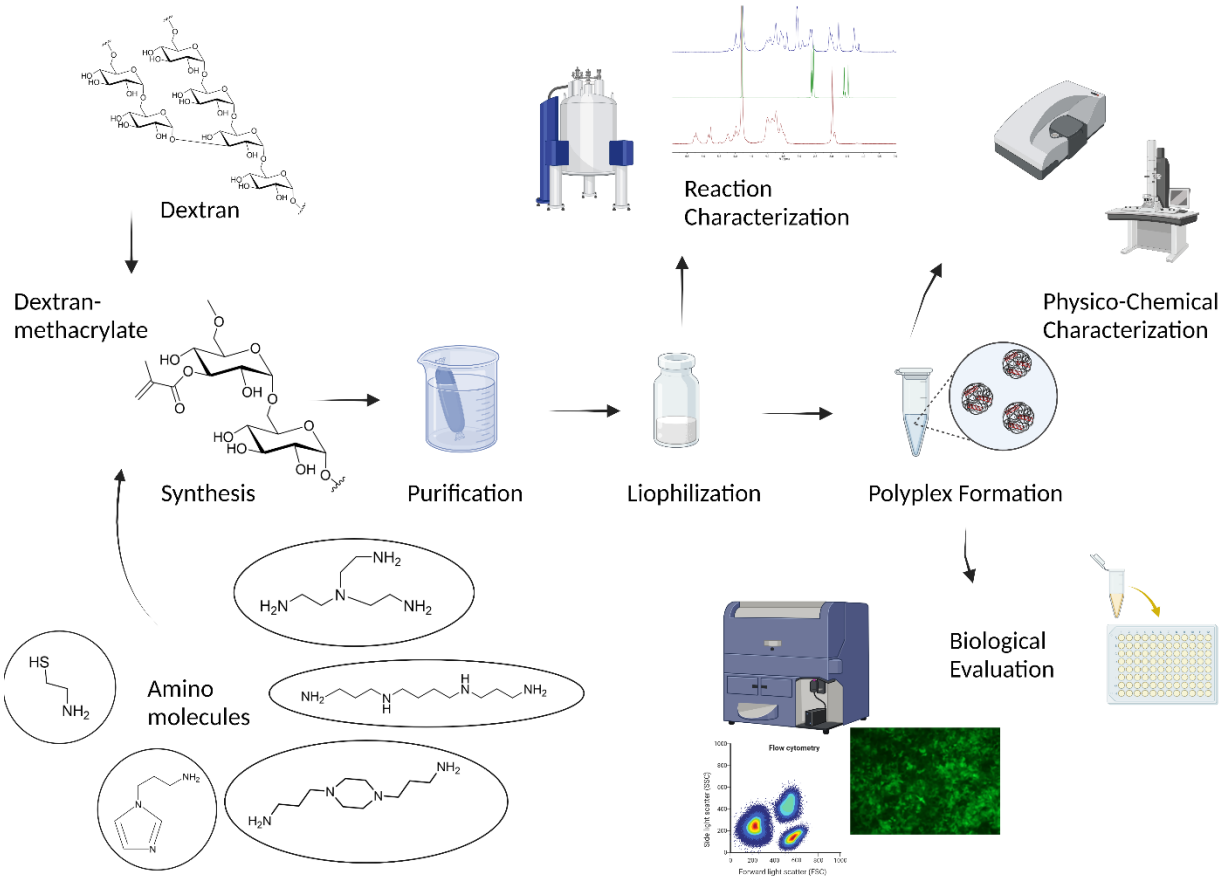

3.1 Introduction

The need of a vector for the systemic transport of siRNA has been mentioned in the introduction chapter. The development of new biomaterials plays a fundamental role in improving transport efficiency and biodistribution beyond the liver. Among different materials that can be used in nanomedicine polymers present interesting features: ease of synthesis and modification, scalability, and reproducibility. They can be modified with targeting moieties to promote specific tissue biodistribution patterns. Cationic polymers exhibit an interesting capacity to complex nucleic acids through electrostatic interactions that makes them particularly suitable for gene delivery. Polymeric vectors for gene delivery have been produced in the form of nanogels, polymerosomes or by simple self-assembly with the genetic materials. One less explored structure is the use of single chain polymer nanoparticles (SCPNs) (Figure 3.1).

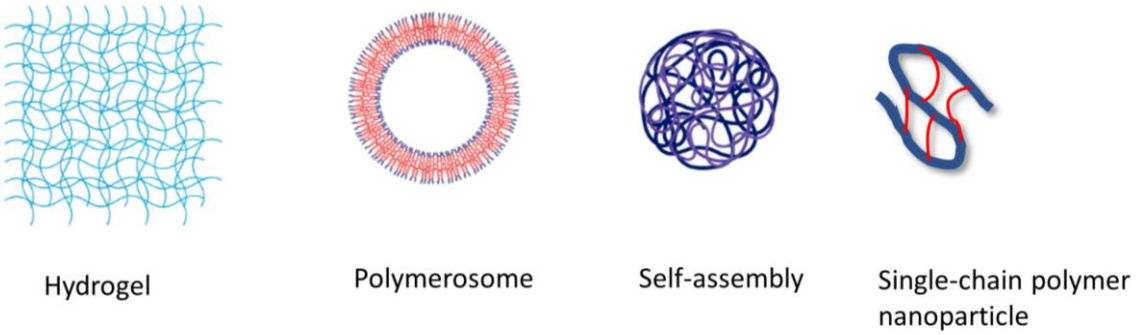

Figure 3. 1.-Scheme of different structures obtained from polymers: Hydrogels in micro or nanoscale, polymerosomes made by block copolymers, polymers that self-assemble in presence of other molecules such as nucleic acids and collapse of a single polymer chain.

SCPN refers to the collapse of one intramolecular polymer chain to form nanometric particles, in the 20 nm size range mimicking biomacromolecules, such as proteins[1]. The collapse is either achieved by self-assembly or by covalent cross-linking of functional groups on the precursor polymer or rather mediated by external cross-linkers[2]. Its small size result interesting in terms of biodistribution[2]. Different drugs have been tested with SCPN by covalent bonds or electrostatic interactions as well as the evaluation of their delivery capacity, such as folic acid[3] and antibiotics Rifampicin[4], tobramycin[5]. However, as far as we are aware, the use of SCPNs for siRNA or even nucleic acid delivery has never been reported. SCPNs are mostly based on synthetic polymers as they offer a control of the composition for the precursors compound prior to the intra-cross-linking step, allowing the SCPNs to be tuned and designed with the desired size and functionality[6].

Additionally, natural polymers are also available and are biocompatible, non-toxic and ready-to-use. In this category polysaccharides are the most commonly used worldwide. Their diversity in structure and properties is a result of their wide range of reactive groups and molecular weights (M_w), as well as their diverse chemical composition. For example, Dextran (DXT, Figure 3.2), a natural polysaccharide is made of D-glucoses linked by (1→6) bonds. It presents ramifications in (1→3) and in less proportions in (1→2) and (1→4) bonds. It is has been used as drug delivery carrier due to its

biodegradability, biocompatibility, wide availability and facile modification[7,8]. It has also a long history in clinical use as plasma volume expander and plasma substitute. As siRNA carrier, it has been explored during the last decade, in the form of nanogels[9] and self-assembly structures[10,11,12] using different type of modifications, especially with cationic molecules.

CIDETEC has developed a novel and straightforward synthetic methodology to obtain small (approximately 13 nm) dextran-based SCPNs (DXT-SCPN) through the intramolecular crosslinking of single polysaccharide chains by means of a homobifunctional crosslinker in aqueous media under mild conditions[13]. They have been used as carrier of tumor-associated carbohydrate antigen mimetic, specifically α-Tn antigen[14] and for cationic antibiotic, such as Tobramycin[5], and antimicrobial peptide[15,16,17]. DXT-SCPN was functionalized with negatively charged groups that neutralize the positive charge of the drug, allowing better penetration into the *Pseudomonas aeruginosa* biofilms and a decrease of drugs toxicity. The good electrostatic interactions of anionic SCPN with cationic antibiotics raised interest in designing DXT-SCPN with positive charges to promote interactions with nucleic acids. Exploring the potential of specifically designed DXT-SCPN as siRNA results attractive because of their small size and their facile functionalization with targeting moieties. As control, DXT homopolymer was functionalized with the same positive groups, using similar synthetic route, to evaluate the need of intra-cross-linking for non-viral vector applications.

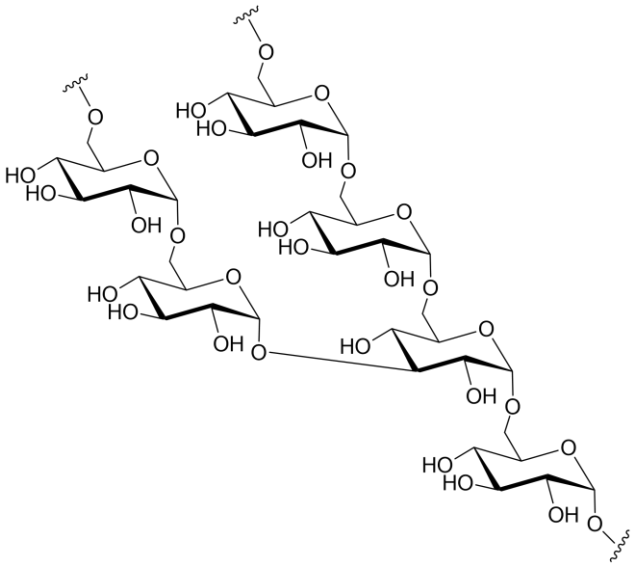

Figure 3. 2.- Structure of dextran polymer with D-glucoses linked by (1→6) bonds and ramification in (1→3).

This chapter describes the synthesis of dextran-based SCPNs and dextran homologue polymer and their functionalization with cysteamine to obtain a positively charged nanoparticles. Cationic vectors are known as good siRNA carriers by their ability to complex the siRNA electrostatically and to facilitate cell internalization to reach the cytosol. Thus, in this chapter cationic SCPN and dextran polymer have been studied *in vitro* in terms of their siRNA encapsulation, cell viability, cellular uptake and siRNA release. In addition, studies were conducted on varying the type and number of amines used for substitution by grafting different amino molecules to DXT homopolymer. Transfection of the system was evaluated with siRNA therapies, in particular to lung cancer (as the leading cause of cancer death[18]) on the A549 cell line, a human carcinoma cell lung model.

3.2 Results and discussion

3.2.1 *Synthesis of dextran-methacrylate (DXT-MA) and single-chain polymer nanoparticles*

DXT (M_w ~ 40KDa) was modified with glycidyl methacrylate (GMA) to obtain Dextran-methacrylate (DXT-MA), following the protocol established by Dijk-Wolthuis and coworkers[19]. This method consists in the transesterification of methacryloyl group from GMA to the hydroxyl group C3 of the glucose unit of dextran. This transesterification reaction became very useful because DXT-MA can undergo chemical cross-linking reactions[20], which can also be used to produce dextran-based single chain polymer nanoparticles (SCPNs)[13].

DXT-MA reaction was performed in DMSO under nitrogen atmosphere during 4 days activated by 4-(N,N-dimethylamino)pyridine (DMAP) (See Figure 3.3). Reaction was quenched by addition of 0.1M HCl and then purified by dialysis against water using 3.5KDa molecular weight cut-off (MWCO). The purified product was freeze-dried to obtain a white cotton-like solid.

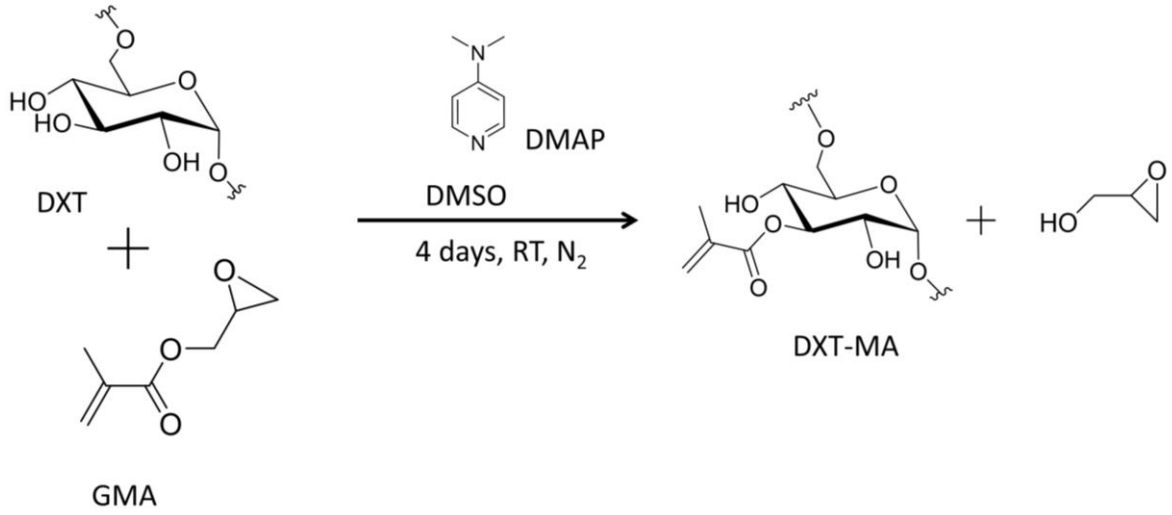

Figure 3. 3.- Scheme of synthesis of methacrylate derivatized dextran developed by Van Dijk-Wolthuis et Al. method[19],where an unexpected transesterification occurred from Glycidyl methacrylate (GMA) to the C3 of glucose unit.

As shown by ^{1}H-NMR in D_2O, pristine DXT displayed proton signals corresponding to the 6 glucose positions (H2-H7) from 3.3 to 4.2 ppm and another signal at 4.8 ppm related to the anomeric proton (H1) (Figure 3.4). On the other hand, ^{1}H-NMR spectra of DXT-MA in D_2O exhibited a signal at 1.8 ppm (m, H3, methyl) corresponding to the methyl group of the linked methacrylate group. 5 protons of the glucose remained in positions at 3.3-4.2 ppm, in the substituted ring. However, the proton in position 3 is shifted from 3.3-4.2 ppm to 5.2-5.0 ppm (3´), as well as the anomeric proton (1´) shifted to 4.9 ppm due to the presence of the methacrylate group. Characteristics peaks of alkene bond appeared in the spectra at 6.1 (m, 1H, TRANS-methacrylic-CH) and 5.7 (m,1H, CIS-methacrylic-CH) ppm (Figure 3.4).

The degree of substitution (DS) of methacrylate moiety attached to the dextran chain can be obtained from the ^{1}H-NMR spectra. DS is expressed as the percentage of substituted glucose divided by the total amount of glucose units, i.e. the sum of both substituted and unsubstituted glucoses. Thus, assuming that only one hydroxyl group per glucose is functionalized with one MA, a modified dextran having a DS of 30% means that 30% of the repeating units of glucose among the dextran chain have been modified by a methacrylate group. The detail for the calculation of MA DS is described in the Appendix III. The DS for DXT-MA obtained according to the procedure described above was calculated to be 45%, as judged by ^{1}H NMR.

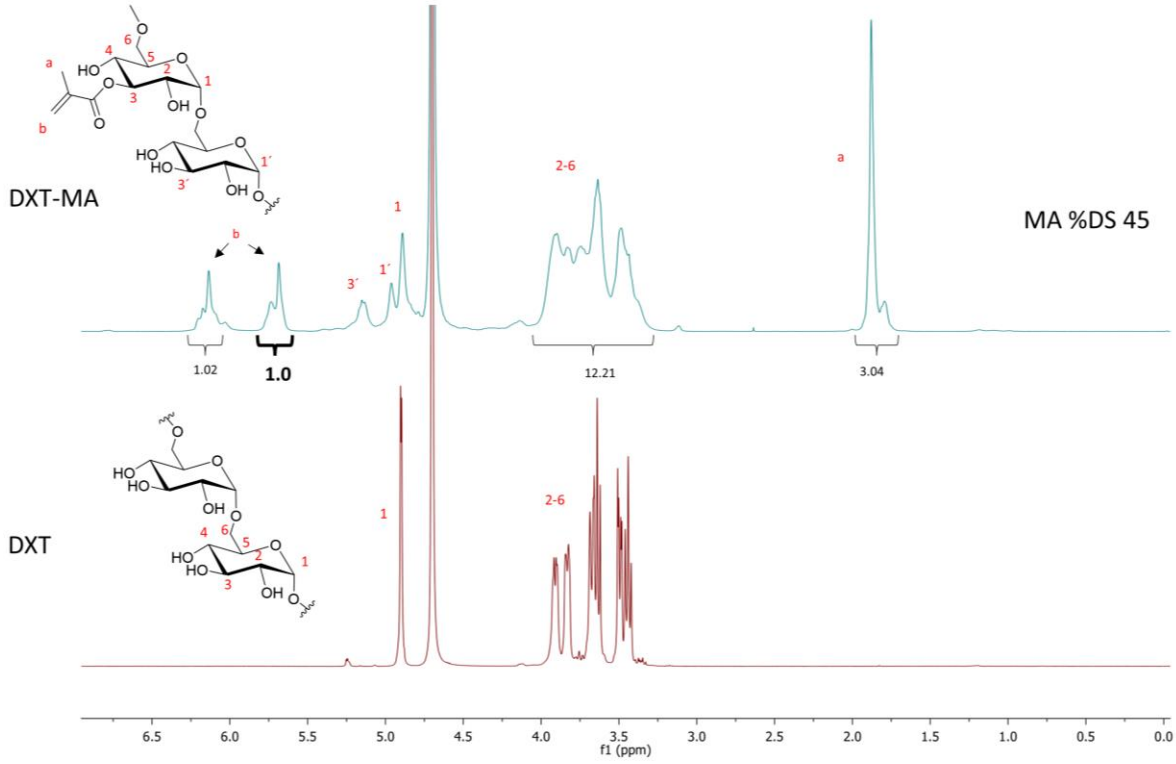

Figure 3. 4.-^{1}H-NMR spectra (D_2O 500 MHz) of Dextran 40 KDa (Bottom) and methacrylate-modified DXT-MA (Top). DXT is depicted as a linear polysaccharide (α-1,6 glucose linkages), although it is known to be branched, with side chains (α-1,3 glucose linkages) also present. Proton signals in the spectrum have been assigned to their positions in the chemical structure using letters or numbers. The integration values of each peak are also displayed for DXT-MA, with the known signal value of interest, in this case, the alkene proton, highlighted in bold. A 45% of MA degree of substitution (DS) was obtained from the integration values.

DXT-MA was used to produce DXT-SCPN-MAs with the desired size and functionality. Synthetic routes to obtain SCPNs are mainly based on intra-chain coupling or cross-linking-induced collapse of the pre-functionalized polymers. In this case, DXT-MA was reacted with 3,6-dioxa-1,8-octane-dithiol (DODT). DODT has a thiol group at both ends of the molecule, which react spontaneously with methacrylate of dextran derivative via thiol-ene Michael addition at alkaline pH in absence of any catalysts (Figure 3.5). Thiol-based Michael addition[21] is a "click" reaction, that have recently gained importance in polymer and materials synthesis[22] due to their facile use, high yield, absence of reaction by-products and selectivity under mild conditions[23,24,25]. One of the objectives of the intra-chain coupling was to let unreacted methacrylate groups that will be used in a subsequent reaction with amino molecules. Therefore, 0.5 molar equivalents of thiol group (0.25 of bifunctional

linker) compared to the total amount of MA moieties was used for the intra-chain cross-linking reaction. It is also worth mentioning that higher amount of cross-linker could result in undesired intermolecular cross-linking. Reaction was performed according to the published protocol[13] (Figure 3.5). Briefly, DODT was dissolved in methanol and the cross-linker solution was added dropwise to an aqueous dispersion of DXT-MA first dissolve in PBS (1 wt%, or 10 mg/mL) and adjusted at pH 9-9.5 with NaOH (1M) at room temperature and under atmospheric conditions. The pH was adjusted at alkaline value to increase the concentration of nucleophilic thiolates and promote the thiol-ene Michael addition. It is worth mentioning that higher pH values were detrimental to DXT-MA with the hydrolysis of the ester groups of the methacrylate moiety as judged by ^{1}H-NMR. After 24h, the reaction was stopped and the absence of non-reacted thiol groups from the cross-linker was determined by Elmann's test[26]. The resulting SCPNs were purified by dialysis against deionized water with MWCO of 3,500 Da for 5 days, refreshing deionized water twice per day. The end of purification was confirmed by monitoring the conductivity of the water, reaching the same values as the deionized water. The resulting aqueous solution was freeze-dried to obtain nanoparticles as a white solid.

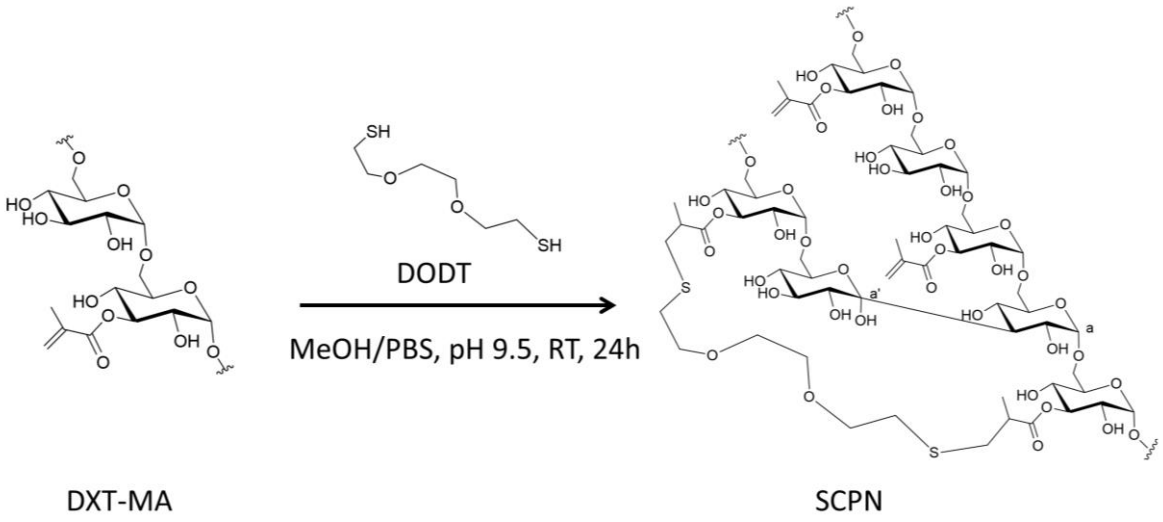

Figure 3. 5.- Schematic representation of the intra-chain cross-linking reaction of DXT-MA using a methanol solution of DODT added at a stochiometric ratio of 0.5 thiol group per methacrylate group of the DXT-MA in PBS adjusted at pH 9.5 with NaOH (1M). The reaction proceeded during 24 h at RT to obtain single chain polymer nanoparticle SCPN, based on DXT-MA. Method developed by Gracia et al.[13].

DXT-SCPN-MA was characterized by ^{1}H-NMR (Figure 3.6) where methacrylic moieties which have reacted with DODT exhibited a clear shift to 1.2 ppm of the methyl group (s,3H, crosslinker-CH_3), while the signal of the methyl group of the unsubstituted methacrylate group remained at 1.8 ppm (s, 3H, methacrylate-CH_3). New proton signals appeared in the 2.9-2.56 ppm (m, 2H, S-CH_2 and CH-CH_2) region corresponding to protons of DODT, while the protons corresponding to the ethylene glycol units are expected to appear in 3.3-4.3 ppm region, together with Glucose (Glc) protons. Obviously, the intensity of the methacrylic alkene proton signals decreased due its reaction with the thiol groups, but the peak remained present, as originally planned with the low amount of DODT added. To determine the degree of crosslinking (DC) similar method as the one applied to determine DS of DXT-MA was used using ^{1}H-NMR (Figure 3.6), see Appendix III for the detailed explanation to

calculate DC. The DC achieved is 16%, 21% of the glucose units of the pristine DXT were substituted with methacrylate and 63% were unaltered glucose. The amount of substituted glucose unit, either with methacrylate or use for the intra-chain cross-linking, sum up to 37% of substitution in total. This is 8% less than the DS calculated for DXT-MA 45%, indicating a significant hydrolysis in the ester of methacrylate induced by the cross-linking reaction pH adjusted at 9.0-9.5.

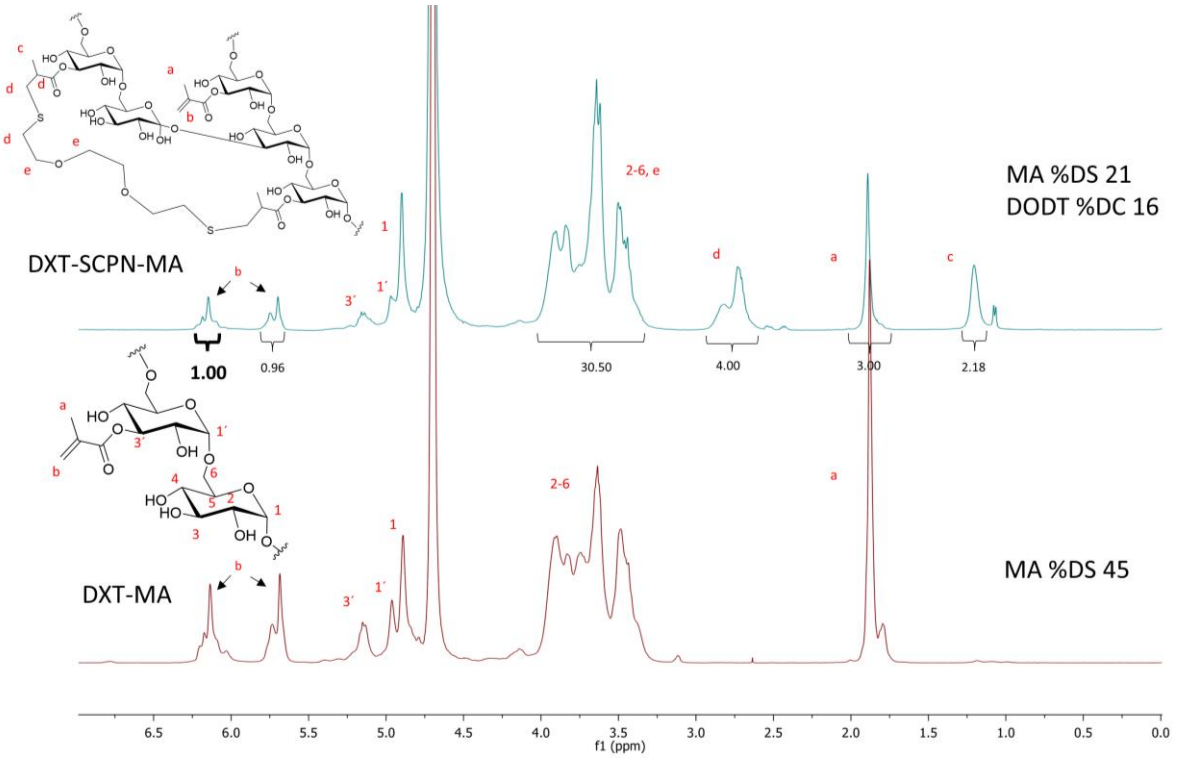

Figure 3. 6.- ^{1}H-NMR spectra of the starting material DXT-MA (Bottom) and the single-chain polymer nanoparticle DXT-SCPN-MA (Top) in D_2O at 500 MHz. Proton signals are assigned to their positions in the chemical structure using letters and numbers. The proton integral used for the DC% calculation is highlighted in bold. 16% DC is achieved while 21% DS of MA remains unreacted.

DXT-SCPN-MAs were characterized by dynamic light scattering (DLS) in order to determine the size with the support of transmission electron microscopy (TEM) (Fundamentals of the techniques are described in Appendix II). Nanoparticles in solution have the property to scatter light, which can be used to obtain the size of the nanoparticle considering the intensity and time lapse (Appendix II). The hydrodynamic diameter of DXT-SCPN-MA obtained by DLS was 14 nm with a polydispersity index (PDI) of 0.23. From 1000 nm onwards, a low intensity population appears, corresponding to the presence of a small amount of aggregates, which explains the high polydispersity (Figure 3.7). TEM micrographs display globular morphology of the SCPNs in a dry state. From TEM a number average diameter of 22 nm was determined over 100 particles (Figure 3.8).

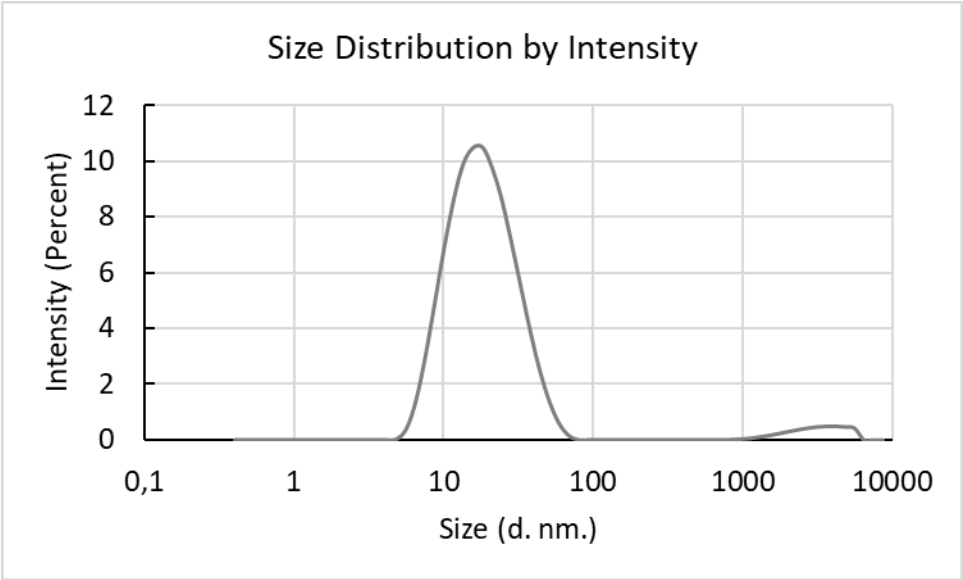

Figure 3. 7.- Size distribution graph of intensity-average diameter for DXT-SCPN-MA obtained by DLS in PBS at 10 mg/mL, pH 7.4, and 25°C.

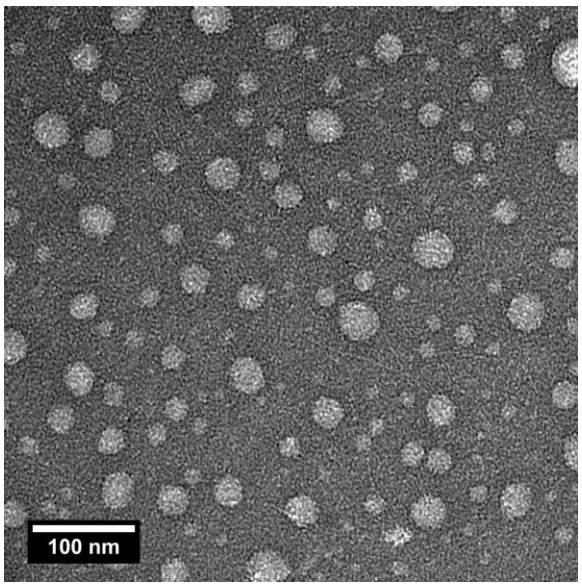

Figure 3. 8.- Transmission Electron micrographs of DXT-SCPN-MA stained with uranyl acetate 1.5% (w/v).

DXT-SCPN-MAs with free reactive methacrylate groups have been achieved were further reacted with amine-based compounds to obtain the cationic charge required for complexation with siRNA, as well as the corresponding DXT-MA polymer was subsequently reacted to obtain an intra-chain cross-linking control.

3.2.2 *Amine modification of dextran-methacrylate and single-chain polymer nanoparticle*

DXT-MA and DXT-SCPN-MA were functionalized with amino groups to confer a positive charge to the polysaccharide-based materials. Again, thiol-ene Michael addition was used to functionalize the remaining methacrylate group, i.e. 21% for SCPN and 45% for DXT-MA. Cysteamine was chosen, since it has both groups, a thiol to react with MA groups and an amine to confer the cationic

charge[27], to obtain DXT-based SCPNs substituted with cysteamine (SCPN-NH_2) and the corresponding cationic DXT (DXT-NH_2). In order to completely substitute the methacrylate moieties, 5 molar equivalents of cysteamine were used based on the amount of MA groups for each compound. pH was adjusted to 8.0 in order to minimize ester hydrolysis as much as possible but ensuring sufficient nucleophilic character of the thiolates to allow the reaction to proceed. Both reactions were carried out in saline aqueous solution to achieve a good solubility of DXT-SCPN-MA at room temperature under gentle stirring during 5 hours. Reaction was purified by dialysis 3.5 KDa MWCO against deionized water replaced twice a day during 5 days and then freeze-dried after reaching conductivity of deionized water.

^{1}H-NMR in D_2O of DXT-NH_2 and SCPN-NH_2 was performed, as shown in Figure 3.9 and 3.10, respectively. As expected, the peaks corresponding to the protons of the alkene group have disappeared, indicating that all the methacrylic groups have been functionalized. In DXT-NH_2 methyl peak shifted to 1.2 ppm (s,3H, crosslinker-CH_3), glucose ring kept its chemical shift at 3.3-4.3 ppm. However, new proton signals appeared in the 2.6-2.9 ppm (m, 5H, -S-CH_2 and -CH-CH_3) and at 3.2 ppm (s, 2H, CH_2-NH_2) corresponding to the cysteamine attached to the polysaccharide confirmed that the reaction between the MA groups and cysteamine occurred (Figure 3.9).

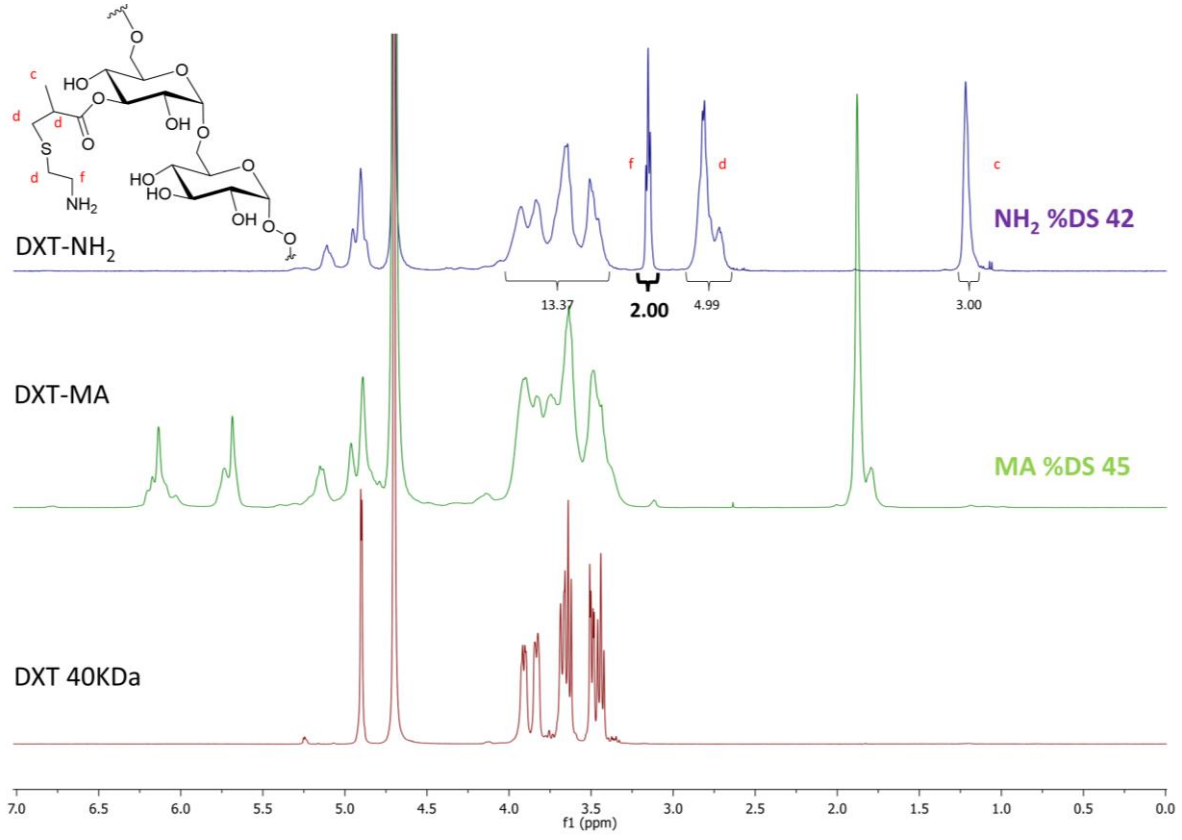

Figure 3. 9.- ^{1}H-NMR (D_2O, 500 MHz) spectra of DXT 40KDa (Bottom), DXT-MA (Middle) with 45% of methacrylate substitution and DXT-NH_2 (Top) with 42% of cysteamine substitution.

Regarding SCPN-NH_2 Figure 3. *10.*-, it is noteworthy that part of the protons from cysteamine and the ones from DODT cross-linker appeared at same chemical shift 2.56-2.9 ppm (m, 9H, CH_2-SH-CH_2, -O-CH_2-CH-SH, -CH-CH_3). However, the signal at 3.2 ppm (s, 2H, NH_2-CH_2-) corresponding only to the

cysteamine could be observed. The methyl group appeared at 1.3 ppm (s,3H,-CH-CH_3) and the glucose ring signals at 3.3-4.3 ppm (Figure 3.10).

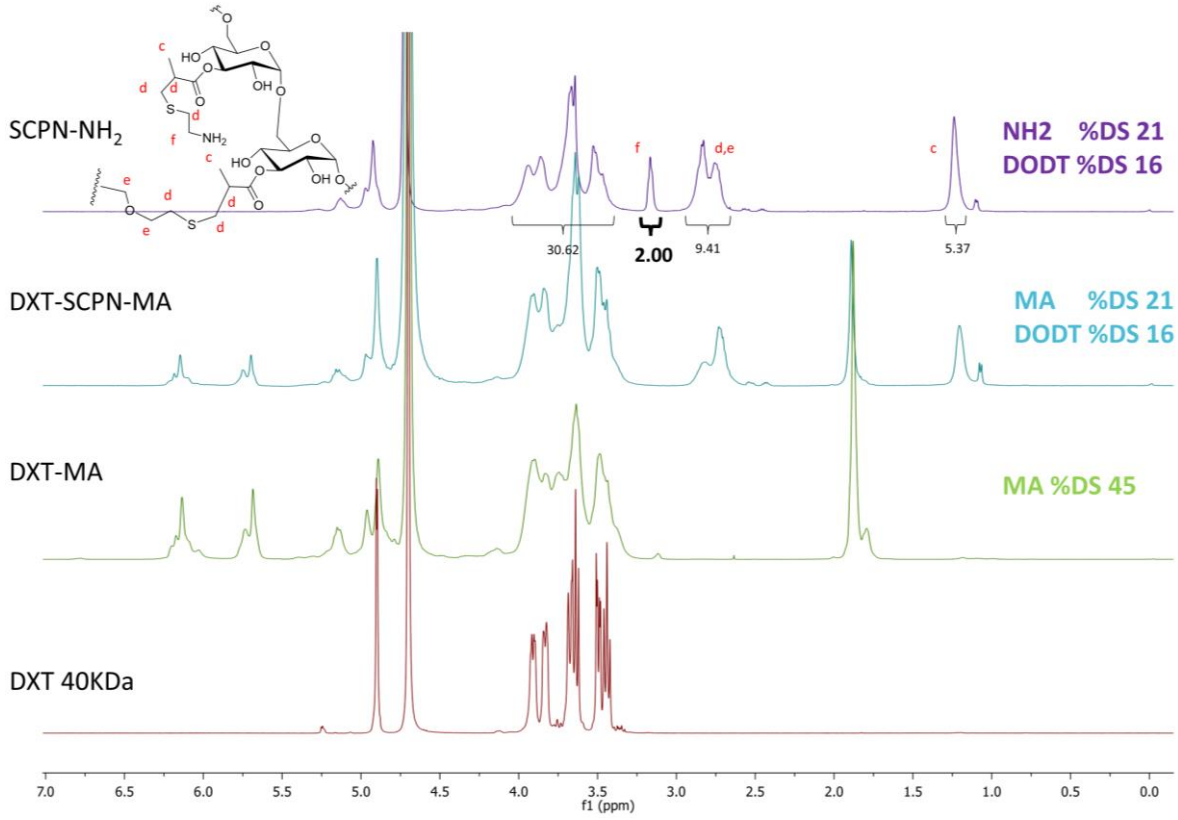

Figure 3. 10.- ^{1}H-NMR (D_2O, 500 MHz) spectra of DXT 40KDa (Bottom), DXT-MA (Lower-middle) with 45% of Methacrylate substitution, DXT-SCPN-MA (Upper-middle) corresponding to the SCPN with 16% crosslinker DODT substitution and 21% of methacrylate substitution, SCPN-NH_2 (Top) 16% crosslinker DODT substitution and 21% of cysteamine substitution.

The signal at 3.2 ppm for both in DXT-NH_2 and SCPN-NH_2 was used to calculate the DS of moieties substituted by cysteamine (See Appendix III for detailed explanation of the DS determination). DXT-NH_2 is composed of 42% of glucose units functionalized with cysteamine, which is in a good agreement with the original DS of DXT-MA at 45% of methacrylate groups. Thus, the 3% difference observed between both DS could be attributed to the hydrolysis of ester group formed to obtain DXT-MA. However, it is worth reminding that NMR resolution is usually estimated at 5% which could indicate that the difference is mainly based on the inherent error of the peak integrations. On the other hand, SCPN-NH_2 exhibited a DS for cysteamine of 21% with a DC of 16%, which correspond to the initial amount of MA (21%DS) and DODT (16% DC) groups. Thus, hydrolysis did not occur during the reaction.

As a summary, all the methacrylic groups of SCPN were successfully functionalized with a positively charged conferred by the cysteamine groups. In addition, the functionalization proved to maintain the hydrodynamic diameter of the SCPN, as judged by DLS (Table 3.1). The slight increase in size observed from 13 to 15 nm for SCPN and SCPN-NH2, respectively, is attributed to the electrostatic repulsion of the protonated amines, similarly to the one observed after carboxylate functionalization with mercaptopropionic acid[13]. On the other hand, the hydrodynamic diameter of

DXT-NH_2 polymer resulted in similar size of 15 nm compared to SCPN-NH_2. However, the corresponding PDI was much higher, i.e. 0.43, which was attributed to the lack of colloidal morphology due to the absence of intra-chain cross-linking[13]. As judged by aqueous electrophoresis, SCPN-NH_2 acquired a positive surface charge with a Z-potential at +9.53 mV compared to the one slightly negative measured for DXT-SCPN-MA at -8.5 mV. As expected, the higher number of amine groups conferred a higher positive charge to DXT-NH_2 with a Z-Potential of +30.1 mV, although the Smoluchowski equation used to determine the Z potential is not established for polymer in solution.

Table 3. 1.-Summary of the hydrodynamic diameter and Polydispersity index (PDI) measured by dynamic light scattering of DXT-SCPN-MA, SCPN-NH2 and DXT-NH_2 measured in PBS. Z-potential of the same particles determined by aqueous electrophoresis at 1 mM NaCl and pH 7 is also reported.

Sample	Z-Average (d.nm)±SD	PDI±SD	Z-potential (mV)±SD
DXT-SCPN-MA	13±0.23	0.205±0.010	-8.5±0.5
SCPN-NH_2	15±0.16	0.254±0.07	+9.53±0.6
DXT-NH_2	15±0.6	0.43±0.02	+30.1±3

3.2.3 *Cytotoxicity studies of SCPN-cysteamine and DXT-cysteamine*

It is important to keep in mind that the presence of amine and cationic charge are usually associated with cytotoxicity for the cells, as the positive amines disrupt the negatively charged cell membrane. However, the cationic character is crucial to have high RNA complexation for gene therapy delivery[28,29,30]. Thus, *in vitro* studies were carried to test the cytotoxicity of DXT-NH_2 and SCPN-NH_2 at different concentration with A549 lung cells by MTS test. The MTS test is a colorimetric assay based on the absorbance of formazan, which correlates cellular metabolic activity (See appendix II for detailed explanation of the fundamentals). SCPN-NH_2 and DXT-NH_2 were administered to A549 cells at different concentrations: 6.25, 12, 25, 50 and 500 µg/mL during 48h. At this time point metabolic activity was measured (Figure 3.11) and the absorbance intensity was normalized to the absorbance intensity of untreated cell control, which represent 100% of cell viability. Both SCPN-NH_2 and DXT-NH_2 showed good cell viability up to 50 µg/mL, with cell viability greater than 90%. At 500 µg/mL cell viability is dramatically reduced below 20% with no difference observed for the compounds tested. Thus, cytotoxicity is attributed to amine concentration. In summary, both SCPN-NH_2 and DXT-NH_2 can be administered up to 50 µg/mL.

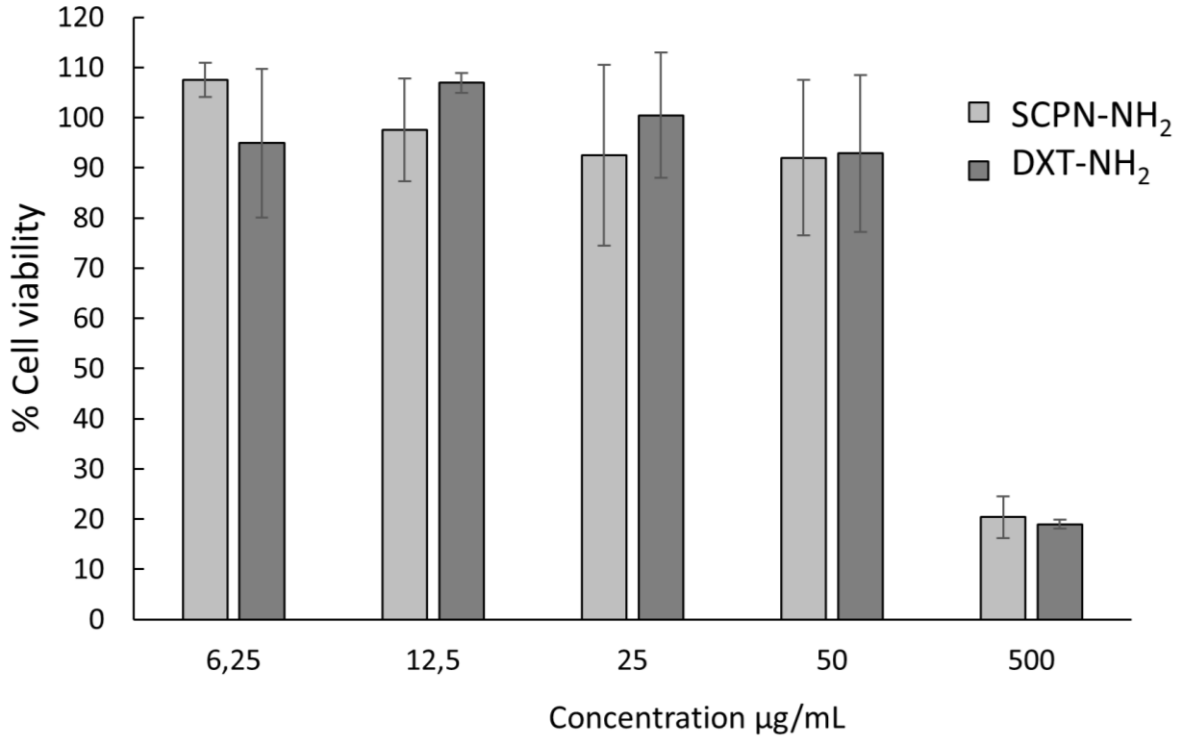

Figure 3. 11.- Cell viability assay of A549 cells treated with different concentrations of cysteamine-functionalized SCPN (SCPN-NH_2) and DXT (DXT-NH_2) after 48h. n=3, average± SD.

3.2.4 *Forming complexes of siRNA and SCPN-cysteamine or DXT-cysteamine*

As described in the introduction a polyplex is a macromolecular structure based on the electrostatic interactions of negatively charged nucleic acid and a positively charged polymer. Thus, the capacity of the synthesized SCPN-NH_2 and DXT-NH_2 to be used as a non-viral vectors to interact and complex nucleic acids was investigated using the gel retardation test (See Appendix II for detailed explanation of the technique), which consists in an electrophoresis separation in an agarose gel. siRNA is stained by GelRed®, a nucleic acid intercalant, which produces fluorescence when excited by UV light. While low M_w free siRNA will flow at a speed rate, polyplexes will be retarded because of the resulting high molecular weight of the complex. Different N/P ratios were evaluated to observe the entrapment efficiency: 0.5, 1, 2, 4 and 8 for both SCPN-NH_2 and DXT-NH_2 and compared to free siRNA. The concept of N/P ratio is defined as the ratio between the number of moles of ionizable amines present in the polymer and the number of moles of phosphates group from the siRNA. Figure 3.12 shows two images of 1% agarose gel running after 10 and 30 minutes of electrophoresis for SCPN-NH_2 (Figure 3.12.-A) and DXT-NH_2 (Figure 3.12.-B). For SCPN-NH_2 at N/P 0.5, i.e. twice the amount of phosphate groups compared to the amount of amine groups, a band at same height than the free siRNA was observed, indicating that the number of amines was not sufficient to complex all the phosphate groups, as expected. Interestingly, at N/P 1, some of the siRNA appeared to be retained by electrostatic interactions with SCPN-NH_2, preventing the oligonucleotide to migrate towards the positive pole. However, the presence of a fine and diffuse band at the level of the free siRNA confirmed that at this N/P the encapsulation was not complete. At higher N/P ratios free siRNA could not be observed, confirming that SCPN can fully encapsulate all the oligonucleotide. After 30 minutes, it can be appreciated that bands have migrated towards the opposite direction,

the negative pole, for N/P ratio > 1, indicating that the net positive charge and small size of the polyplexes based on SCPN-NH_2 can pass through the pores of the gel.

Figure 3.12.-B shows the encapsulation efficacy of siRNA by DXT-NH_2 polymer. Compared to SCPN-NH_2, full encapsulation of siRNA occurred from N/P 8 as free siRNA was observed for lower N/P ratios. Unlike the results obtained with SCPN-NH_2, after 30 minutes the polyplexes did not migrate to the negative pole which could indicate that the polyplexes obtained with DXT-NH_2 are larger and cannot diffuse through the pore of the gel.

In summary, SCPN-NH_2 proved to be more efficient to complex siRNA compared to DXT-NH_2. At similar N/P, the amount of SCPN-NH_2 was nearly double compared to DXT-NH_2 due to the final DS of amine groups being 21% and 45% for the collapse nanoparticles and the corresponding polymer, respectively. Thus, the concentration of cationic compounds could affect the encapsulation efficiency. It is also worth mentioning that the better-defined collapse morphology could help in siRNA encapsulation. However, additional studies with similar DS of amine group for both compounds should be carried out to confirm those assumptions.

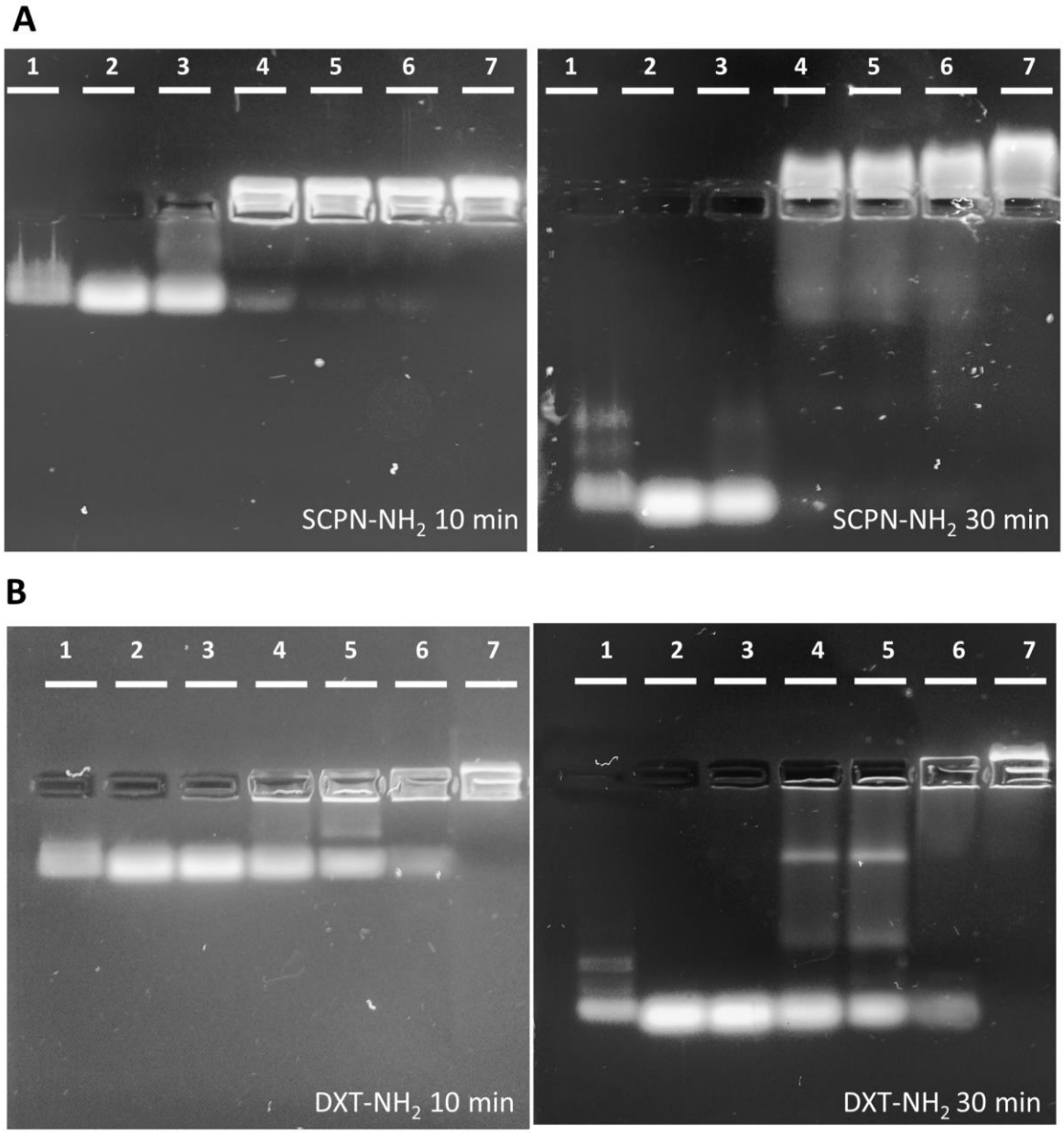

Figure 3. 12.- Agarose 1% gel retardation assay using GelRed® to stain siRNA. Wells: 1: siRNA marker; 2: free siRNA; 3: N/P 0.5; 4: N/P 1; 5: N/P 2; 6: N/P 4 and 7: N/P 8. A) SCPN-NH_2/siRNA 0.1 nmol images taken after 10 and 30 minutes of running. B) DXT-NH_2/siRNA 0.1 nmol images taken after 10 and 30 minutes of running.

The hydrodynamic diameter of the polyplexes prepared at N/P 8 with SCPN-NH_2 and DXT-NH_2, i.e. when siRNA was fully encapsulated, was determined by DLS (Table 3.2). DXT-NH_2 complexed siRNA via electrostatic interactions to form polyplexes of 117 nm, which is much higher than the hydrodynamic diameter of 15 nm obtained for the cationic polymer alone (See Table 3.1). This dramatic increase in size indicates uncontrolled aggregation of the oppositely charged compounds, as expected for polyplexes[31]. Surprisingly, only a slight increase of the hydrodynamic diameter from 15 to 27 nm was observed for the polyplexes obtained with SCPN-NH_2. This result could indicate a better control of the electrostatic interactions, surely due to the higher amount of DXT-SCPN-NH_2 used to reach N/P ratio of 8 compared to the polyplexes prepared with DXT-NH_2. Overall, the small size of the SCPN-NH_2-based polyplexes is in good agreement with the migration observed after 30 minutes in the agarose gels to the opposite pole. Regarding aqueous electrophoresis studies, Z-

potential of the polyplexes has decreased compared to the pristine SCPN-NH_2 and DXT-NH_2 and remained positive, as expected due to the complexation with negatively charged siRNA at N/P ratio 8. It is noteworthy that despite similar number of amine groups, the surface charge of SCPN-NH_2 based polyplexes was much lower at around +9 mV compared to +19 mV for the polyplexes prepared with DXT-NH_2. The collapsed conformation of SCPN might hinder some of the cationic charges, although this location within the SCPN core was not observed for the encapsulation efficiency, as all siRNA was encapsulated at lower N/P compared to DXT-NH_2-based polyplexes.

Table 3. 2.-Hydrodynamic diameter and polydispersity index measured by dynamic light scattering of different compounds in PBS 0.02 mg/mL filtered 0.4 μm. Z-potential of polyplexes at 0.02 mg/mL neutral pH in 1 mM NaCl filtered by 0.4 μm obtained by aqueous electrophoresis.

	Z-Average (d.nm)±SD	PDI±SD	Z-potential (mV)±SD
SCPN-NH_2/siRNA at N/P 8	27±0.33	0.28±0.5	+9±1.43
DXT-NH_2/siRNA at N/P 8	117±1.37	0.173±0.008	+19±1.6

The morphology of the polyplexes were studied by electron microscopy techniques. First, transmission electron microscopy (TEM) micrographs of both polyplexes prepared at N/P 8 with SCPN-NH_2 and DXT-NH_2 (see Figure 3.13) showed spherical morphology. The black contrast for DXT-NH_2-based polyplexes might indicate that the polyplexes adsorbed uranyl salts contrast agent due to their hydrophilic condition. Although the number of nanoparticles was not sufficient to give an average size value, the particles appeared to have a diameter of around 60 nm. One possible explanation for the size difference between DLS and TEM could be attributed to the sample preparation required for TEM observation. Specifically, dehydration of the sample during preparation for TEM may have caused some particles to shrink, leading to an underestimation of their size. In addition, the presence of larger complexes, aggregates or clusters of particles in the sample may have affected the DLS measurements. These aggregates would scatter more the light, resulting in an overestimation of the mean particle size. On the other hand, the SCPN-NH_2-based polyplexes (Figure 3.13.-B) appeared to maintain the shape of the unfunctionalized DXT-SCPN-MA, with a number-average diameter of around 20 nm (calculated over 100 particles), while some aggregates of around 100 nm can also be observed in the micrograph. Unlike the results observed for DXT-NH_2-based polyplexes, uranyl acetate did not penetrate inside the particles, probably due to its limited size and the relative hydrophobicity of DODT.

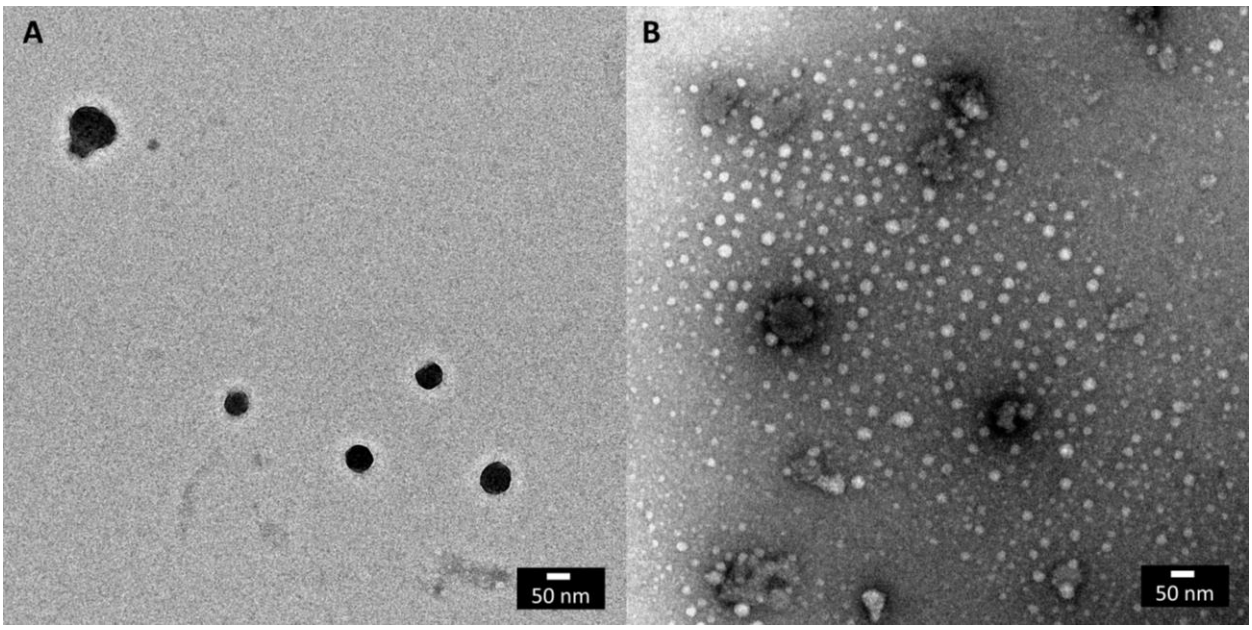

Figure 3. 13.- Transmission electron micrographs of polyplexes prepared at N/P 8 with A) DXT-NH_2/siRNA B) SCPN-NH_2/siRNA and 0.1 nmol siRNA. Both samples were stained with 1.5% uranyl acetate.

3.2.5 *Labeling with Rhodamine B SCPN-cysteamine and DXT-cysteamine*

In order to monitor the internalization of the polyplexes, DXT-NH_2 and SCPN-NH_2 were labelled with Rhodamine B (RhB) (maximum excitation and emission peak at 554 nm and 627 nm, respectively) by reacting the carboxyl group of the dye with some amine of the cysteamine attached to the glucose unit (Figure 3. 14.-). The reaction was carried out via DMTMM (4-(4,6-dimethoxy-1,3,5-triazin-2-yl)-4-methyl-morpholinium chloride) which activates the carboxylic group of the RhB and mediate the amide formation. 0.1 mol equivalents of Rhodamine B were introduced to the reaction at pH 7.4, but not above pH 8 to prevent ester hydrolysis of methacrylate moieties in the functionalized dextran. Reaction was left 16 hours at room temperature and the resulting product was purified by desalting columns PD10 and dialysis 3.5 KDa MWCO.

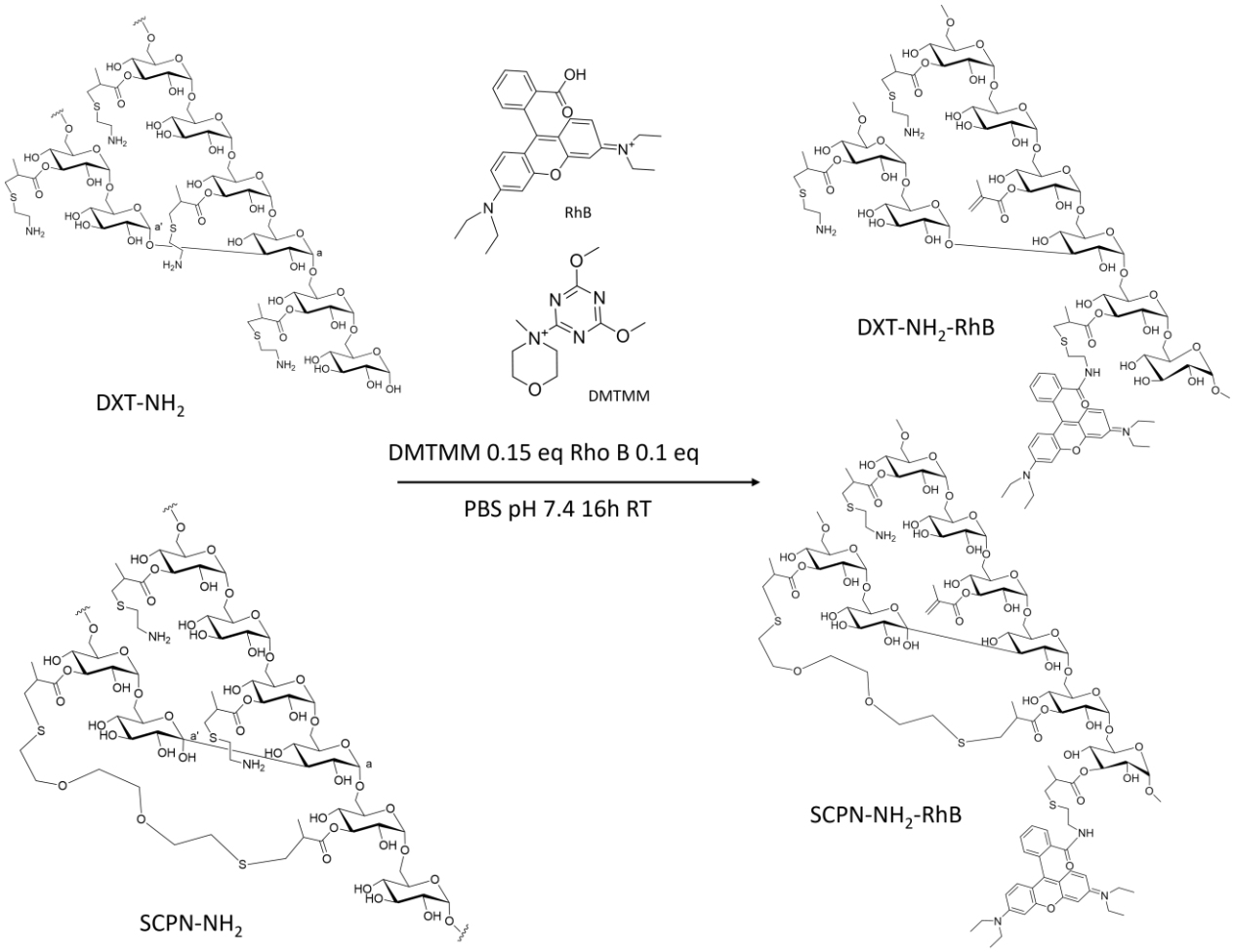

Figure 3. 14.- Schematic representation of the functionalization of DXT-NH_2 and SCPN-NH_2 with Rhodamine B using (4-(4,6-dimethoxy-1,3,5-triazin-2-yl)-4-methyl-morpholinium chloride) DMTMM activator.

^{1}H-NMR studies were attempted to determine the amount of RhB successfully grafted but the concentration of Rhodamine achieved was too low for this technique (data not shown). Then, the amount of RhB linked to the dextran was determined by absorbance using a calibration curve (Figure 3.15) with mathematical fitting shown with the following equation:

$$y = 0{,}0799x$$

Being y the absorbance at 554 nm of excitation and X concentration in µg/mL

The mean absorbance of triplicates of 1 mg/mL DXT-NH_2-RhB and SCPN-NH_2-RhB were used to extract the concentration of RhB in each polymer. The concentration of Rhodamine B was represented as percentage of the total weight of the polymer by dividing the obtained concentration of Rhodamine B and the concentration of dextran. 0.67% and 0.47% weight of Rhodamine B substitution were obtained for SCPN-NH_2-RhB and DXT-NH_2-RhB, respectively.

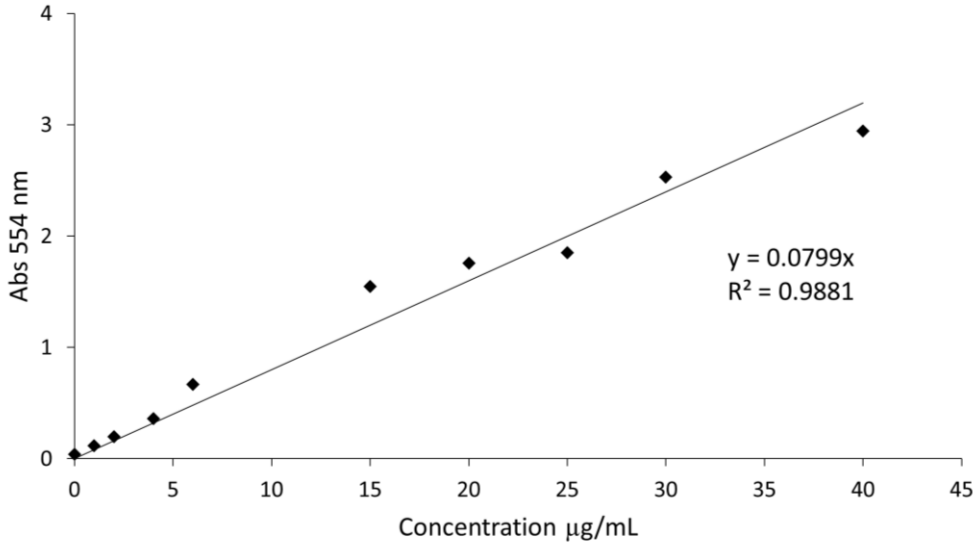

Sample	[Polymer/SCPN] µg/mL	M1	M2	M3	MEAN	[RhodB] µg/mL	% RhB wt
SCPN-NH2-RhB	1000	0.542	0.54	0.527	0.53633333	6.7126	0.67
DXT-NH2-RhB	1000	0.374	0.376	0.378	0.376	4.706	0.47

Figure 3. 15.- Calibration curve of known concentrations of rhodamine B: 0, 1, 2, 4, 6, 8, 10, 15, 20, 25, 30 and 40 µg/mL. Rhodamine B concentration in SCPN-NH_2 and DXT-NH_2 was extracted from the equation. Rhodamine was expressed of wt% from the total mass of polymer/SCPNs.

3.2.6 *Uptake of SCPN-NH_2-RhB and DXT- NH_2-RhB*

The capacity of polyplexes prepared with SCPN-NH_2 and DXT-NH_2 to enter to the cells was evaluated by confocal laser scanning microscopy (CLSM) studies (See appendix II for fundamentals of the technique) using the RhB labelled compound previously prepared and siRNA labelled with 6-carboxyfluorescein (6-FAM) at N/P 8. Polyplexes were administered to human cell line A549 during 24 hours at a final concentration of 200 nM siRNA and final polymer concentration of 20 µg/mL in OptiMEM medium. After incubation, cells were washed and fixed with paraformaldehyde 4% and nucleus was stained with Hoescht 33342. Emissions from different fluorophores were represented in separate channels along with a merged channel, as depicted in Figure 3.16. The yellow channel corresponds to RhB linked to the polymer chain, the green channel represents 6-FAM labeled siRNA, and the blue channel indicates Hoescht 33342 bound to the nucleus.

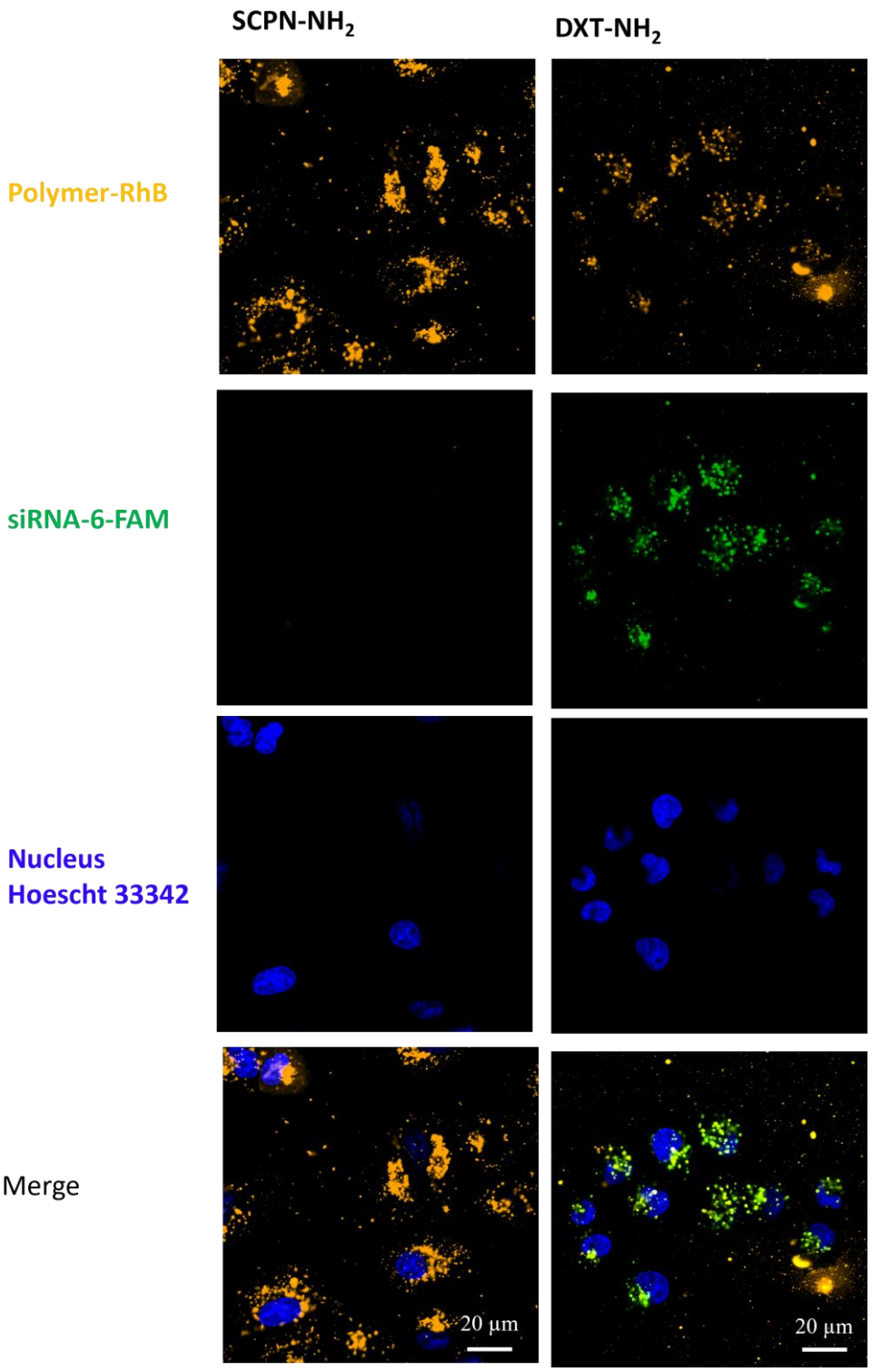

Figure 3. 16.- Confocal laser scanning microgrpahs representing the uptake study by A549 cells 24h after administration of polyplexes of siRNA-6-FAM prepared SCPN-NH_2 or DXT-NH_2/siRNA at N/P 8. Final siRNA concentration of 200 µM per well were used. SCPN-NH_2 and DXT-NH_2 functionalized with rhodamine B are represented in yellow channel, siRNA-6-FAM in green Chacnel and nucleus stainned with Hoescht33342 in blue channel. All chanels are displayed together in merged Channel.

As judged by CLSM, both SCPN-NH_2 and DXT-NH_2 displayed in yellow are located inside the cell, surrounding the nucleus. The main difference between the two systems is that the siRNA (in green) only co-localizes with the carrier in the case of DXT-NH_2. In the case of SCPN-NH_2 no siRNA was found inside the cell. Two hypotheses could explain this unexpected result: one suggests a rapid

release of the siRNA and the subsequent degradation within 24 hours. The second assumption is the loss of interaction between SCPNs and siRNA before the entry to the cell due to the components of cellular medium. The first hypothesis is addressed by measuring delivery efficiency, shown in the following section 3.2.7 and it can be already mentioned that the siRNA was not delivered. Thus, the second hypothesis seems more plausible. Although a special low-serum medium, OptiMEM, was used; displacement caused by the components of the medium could occur, dissociating the siRNA from SCPN-NH_2. The reasons are unknown, but unlike for DXT-NH_2 polymers, SCPNs have a rigid structure conferred by intra-chain cross-linking. This rigidity prevents SCPNs from changing their conformation and possible adaptation of its conformation upon the surrounding medium, causing siRNA detachment. However, further studies should be performed to determine the causes of siRNA displacement and its inability to be translocated into cells by SCPN.

3.2.7 *siRNA delivery efficiency of SCPN-NH_2 and DXT-NH_2*

As mentioned in the introduction, a successful vector for oligonucleotides should protect its cargo from RNases, enhance short-term circulation, exhibit low cytotoxicity and immune response, penetrate the cell membrane, and escape the endosome. It is crucial to note that cellular entrance does not guarantee an efficient cargo release. Consequently, endosomal escape has been identified as a significant barrier for siRNA delivery[32,33]. The transfection efficacy of both DXT-NH_2 and SCPN-NH_2-based polyplexes was investigated *in vitro*. For this purpose, green fluorescent protein (GFP), which is a protein originally from jellyfish with a fluorescence emission in the green spectra, 500 nm, when excited by light with a wavelength from 300-500 nm, was used as a reporter. Enhanced GFP (eGFP), a fluorescently improved version, was introduced in the genome of A549 cell line, causing the cells to continuously emit fluorescence. When treated with an efficient carrier delivering anti-eGFP siRNA, A549-eGFP self-fluorescence is expected to be reduced by silencing protein expression. Fluorescence intensity quantification was performed using flow cytometry (refer to Appendix II for the underlying principles of this technique). Mean fluorescence of 10,000 transfected cells was compared among different carriers, Lipofectamine RNAimax as positive control and non-treated cells as negative control. Polyplexes were exposed to cells during 24 h, after this time, cells were washed and refreshed with new medium full (10% FBS, 1% P/S). It is important to point out that protein reduction might be optimal 48 h later and last from 5-7 days, depending on the cell type and protein[34,35]. So, treated cells were measured by flow cytometry after 96 h after transfection. Mean fluorescence of cells treated with different polyplexes and controls were normalized to non-treated cells, which represent a 100% of expression (Figure 3.17).

As expected, free siRNA cannot trespass cell membrane and no reduction in GFP expression is observed. Positive control Lipofectamine RNAimax reduced GFP expression as low as 20% of expression. Unfortunately, DXT-NH_2- and SCPN-NH_2-based carriers did not present any significant decrease in expression in any of N/P ratios.

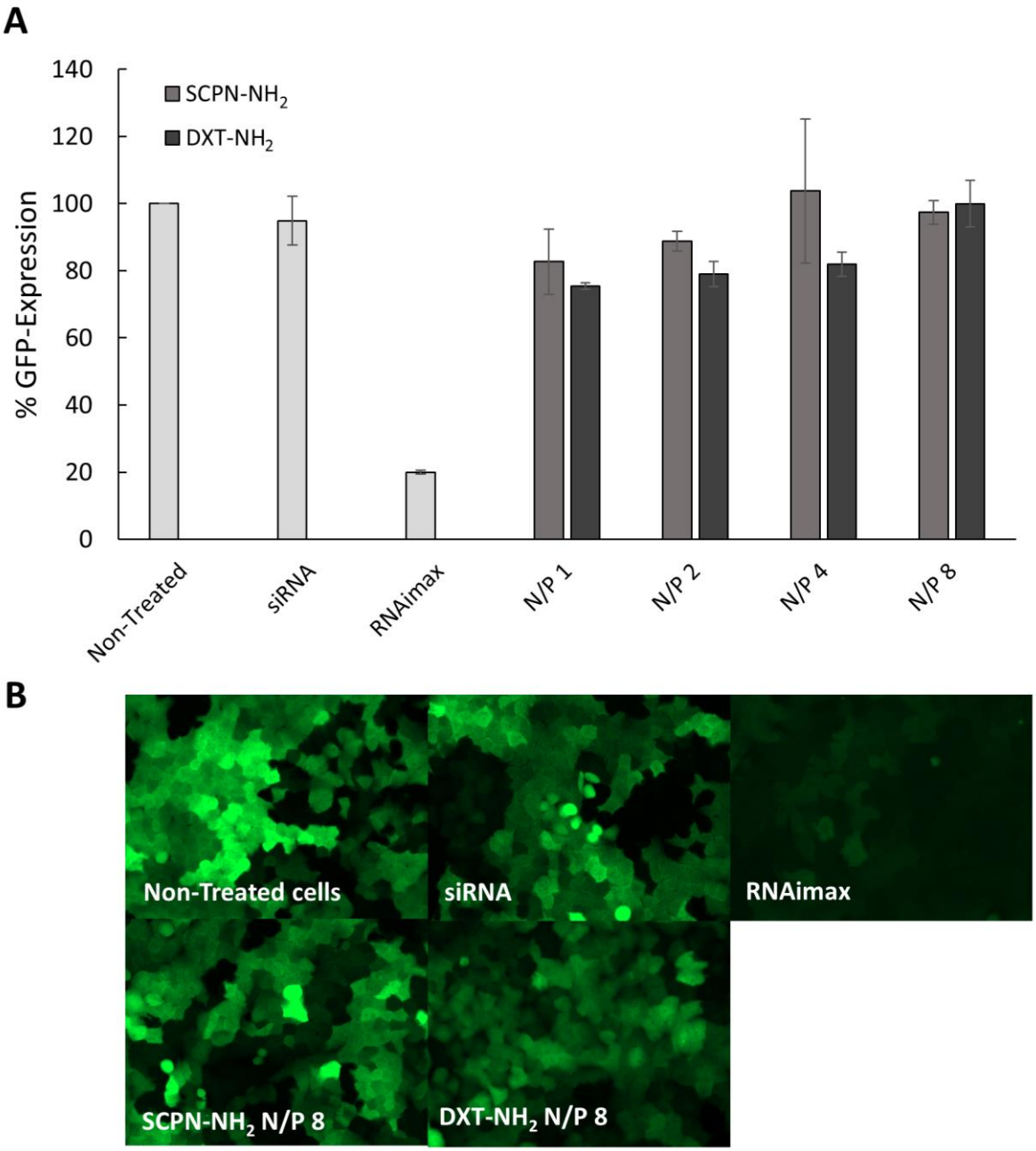

Figure 3. 17.- siRNA delivery efficiency studies. A549-GFP cells were treated during 24h with free siRNA anti-GFP, polyplexes based on siRNA anti-GFP with SCPN-NH_2 or DXT-NH_2, and positive control Lipofectamine RNAimax complexed with siRNA anti-GFP. The siRNA anti-GFP was maintained constant at 200 nM concentration for all the candidates and N/P ratios 1,2,4 and 8 studied. A) Mean Fluorescence relative to the control of non-treated cells, n=3 percentage flow cytometry± SD B) confocal Laser Scanning micrographs of N/P 8 ratios 96 h after being treated with siRNA anti-GFP.

The findings suggest that the assumption dealing with a rapid siRNA release from SCPN-NH_2 based polyplexes was incorrect, and it is likely that the siRNA did not enter the cell due to weakened interactions with the cationic carrier. Although a low serum medium, OptiMEM, was employed, trace amounts of proteins may have affected the electrostatic assembly of the polyplex. To verify the loss of polyplex stability in this medium, gel retardation assays in the presence of proteins should be conducted. However, such experiments may not be relevant at this stage, as DXT-NH_2 also failed to demonstrate effective siRNA delivery, even though colocalization of the oligonucleotide within the cell was observed.

It is important to remember that the mechanism of escape from endo-lysosomal compartments by polyplexes still remains unclear. Different assumptions and theories have been postulated, with the most popular being the so-called “proton sponge” hypothesis, claiming an escape by rupture of the endosome membrane through osmotic swelling. It was the first effort to explain the excellent transfection efficiency of poly(ethylene imine)[33]. Moreover, it is assumed that a unique mechanism based on the ability to capture protons and to buffer the endosomal pH is the basis of endosomal escape. Probably buffering capacity acquired by DXT-NH_2 is not sufficient to promote endosomal disruption due to the relative low amount of amine offered by the cysteamine and/or the pKa of those primary amines might be too high which did not result in an efficient buffering effect during endosomal pathway. In that sense, the presence of secondary and/or tertiary amines with a lower pKa could improve the buffering capacity of the polymer. On the other hand, a strong complexing ability between amino-dextran and siRNA could lead to insufficient unpacking of oligonucleotide that could cause the poor transfection performances. In the current study 40 KDa dextran was used, but a recent study showed that lower molecular weight dextran of 10 and 20 KDa achieved greater efficiency[25]. In order to achieve a better delivery efficiency and determine the key features of dextran polymer to deliver siRNA, different amine-containing molecules and lower molecular weight dextran were used. The same flow cytometry technique described above was performed for rapid screening of the transfection performances for the obtained polymers. Overcoming the barriers of entrapment, RNAse protection, cellular uptake and endosomal release are answered by simply measuring siRNA activity. The new cationic dextran derivatives will be only tested in the polymer version and not in SCPN form, as the internalization studies previously obtained with SCPN-NH_2 were not satisfactory.

3.2.8 *Screening of functionalized dextran polymer with different amino groups and different molecular weights.*

The effect of the type of amine group was studied by using different functionalizing groups to dextran 40 KDa polymer. Also, a couple of low-molecular weight dextran were used to achieve better transfection effect, as previously shown[25].

Imidazole group (Figure 3.18) present in histidine side chain has a pKa close to pH 6.0, which is close to endosomal pH values at 6.5 and suspected to have a buffering effect during endosomal protonation[36]. Histidine-rich peptides and histidylated polymers H-polylysine[37], H-chitosan[38], show evidences of increasing pDNA transfection efficiency. Even imidazole containing polymer, such as polyvinylimidazole[39] showed good gene delivery capacity. Thus, incorporating imidazole groups to dextran polymer could enhance the siRNA delivery efficiency of the system.

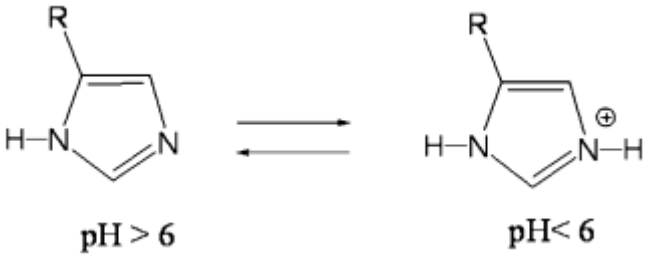

Figure 3. 18.- pH dependence of the imidazolium protonation state. Extracted from Midoux et Al.[40]

Similarly, spermine is a tetra-amine linear molecule, containing two primary amines and two secondary amines (Figure 3.19), that is involved in cellular metabolism and present in all eukaryotic cells[41]. It reversibly complexes DNA and is routinely used in DNA isolation[42]. It has been grafted to different polymers to modulate delivery efficiency[43,44]. The presence of four amine group per molecule significantly increases the content of ionizable amine per substituted repeating unit in dextran backbone. Sterically speaking, its linear structure and length (14-atoms) is expected to increase the spacing between siRNA and polymer backbone which could facilitate its release due to weaker interactions. All these features make it an interesting candidate to improve delivery efficiency of DXT-based cationic carriers. On the other hand, tris(2-aminoethyl)amine is tetra-amine branched-like molecule with one tertiary amine and three primary amines (Figure 3.19). Its branched structure resembles to the first generation of dendrimers and may help for siRNA entrapment and buffering capacity, similarly to the results achieved between linear and branched PEI, where the latter present better buffering capacity due to the presence of three type of amines[45]. Piperazine is a six-membered nitrogen-containing heterocycle, widely used in medicinal chemistry[46]. The presence of 2 tertiary amines and cyclic structure may improve siRNA delivery. It is noteworthy that this compound is used for the synthesis of cationic lipids for the lipid nanoparticles (LNPs)[47,48] and also for polymer substitution[49]. These four molecules containing chemical groups mentioned above were selected (Figure 3.19). The functionalization of DXT with M_w of 40KDa with the selected molecules was performed via thiol-Michael addition. First, the amino-containing molecules were reacted with Traut's reagent to offer a thiol group that will then react with the alkene of DXT-MA (See Figure 3.20)[50]. On the other hand, DXT of 6 and 20 KDa were used to study the effect of the molecular weight of the cationic DXT-NH_2 on the transfection efficiency. For this purpose, cysteamine was used via Michael addition, similarly as described above (Section 3.2.2). Finally, a screening of the siRNA transfection with the different cationic DXT candidates were carried out via flow cytometry.

Name (abbreviation)	Molecule Structure
1-(3-aminopropyl)imidazole (Imidazole)	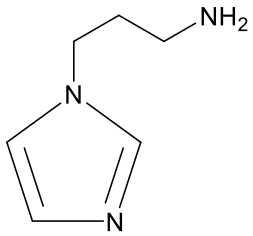
Spermine (Sper)	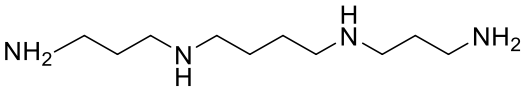
Tris (2-aminoethyl)amine (TAEA)	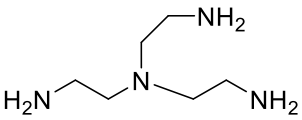
3,3'-(piperazine-1,4-diyl)bis(propan-1-amine) (Piperazine)	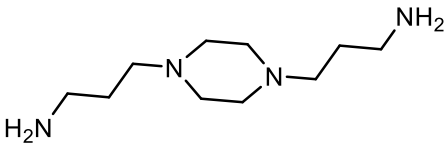
Cysteamine	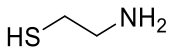

Figure 3. 19.- Amino molecules used to substitute dextran polymer modified with methacrylate groups DXT-MA.

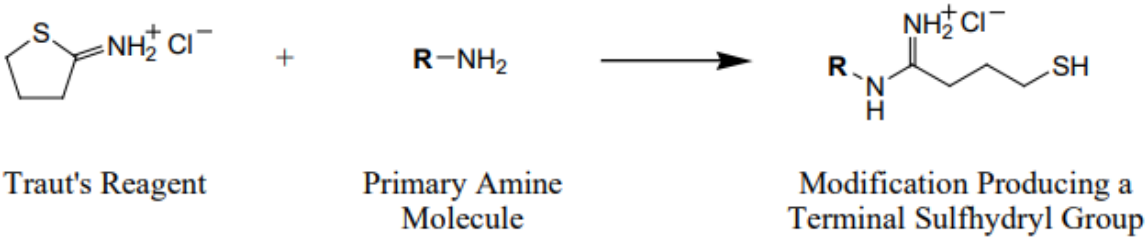

Figure 3. 20.- Structure of 2-Iminothiolane (Traut´s reagent) and reaction scheme with primary amines.

Traut´s reagent was mixed with DXT-MA and the amine containing molecules: i) 1-(3 aminopropyl) imidazole, ii) Spermine, iii) Tris (2-aminoethyl) amine, and 3,3'-(piperazine-1,4-diyl) bis(propan-1-amine) at pH 8 in PBS in a one pot reaction (Figure 3.21) to avoid as much as possible the hydrolysis of the ester groups, at molar ratio of 1:2:4 (Methacrylate:2-Iminothilane: primary amine, respectively). DXT-MA with 54% DS were used for all the reactions and the product, purified by

dialysis, was freeze-dried and stored at 4°C before use. All products obtained were characterized by ^{1}H-NMR in D_2O (Figures 3.22-26).

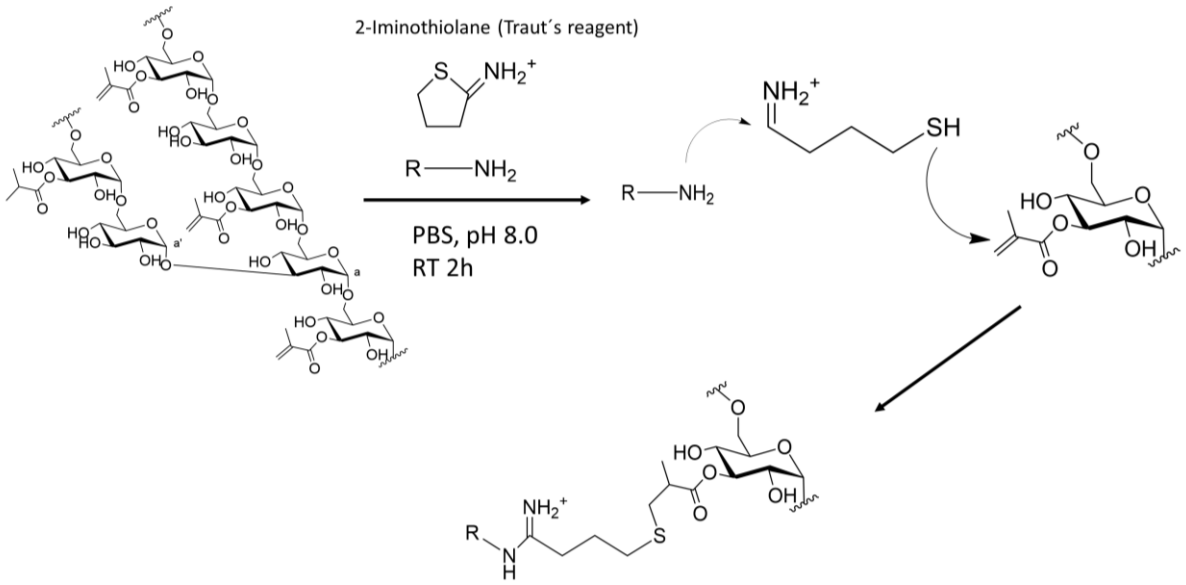

Figure 3. 21.- Schematic representation of DXT-MA one pot reaction with Traut´s reagent and amine-containing molecules (Table 3) in saline conditions and pH 8. A sulfhydryl group is coupled, which react with alkene of the methacrylate groups via thiol-Michael addition.

Figure 3.22 shows the spectra of imidazole molecule, DXT-MA and DXT substituted with 1-(3-aminopropyl) imidazole (DXT-imidazole). Imidazole molecule present 6 peaks: 1.91 ppm (qu, 2H, -CH_2-CH_2-NH_2), 2.57 ppm (t,2H, -CH_2-NH_2), 4.08 ppm (t,2H, -CH_2-CH_2-CH_2-NH_2) corresponding to aminopropyl and 7.02 ppm (s,1H, -C=CH-N), 7.17 ppm (s,1H, -N-CH=C) and 7.69 ppm (s, 1H, N-CH=N) to the imidazole ring. Peaks of glucose, methacrylate, 1-(3-aminopropyl) imidazole, as well as 2-iminothiolane moieties, are found on the DXT-imidazole spectrum. Methacrylate groups were not fully substituted owing to the presence of alkene protons at 5.7 and 6.22 ppm. Degree of substitution of unsubstituted glucoses units were calculated by integrating imidazole peak 7.17 ppm by 1H and using the values obtained from integrations 6.22 ppm (methacrylate) and 3.45-4.1 ppm (glucoses) peaks, detailed calculations are shown in Appendix III.

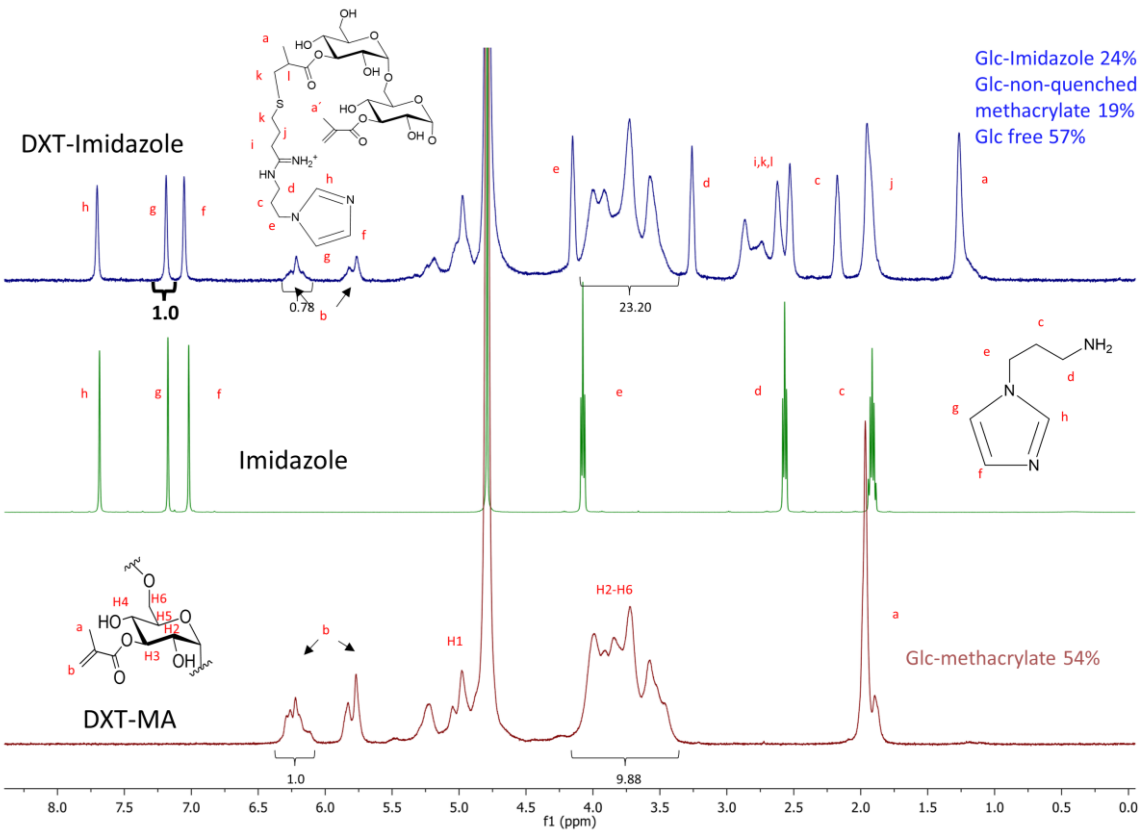

Figure 3. 22.- ^{1}H-NMR spectra of DXT-MA (Bottom), 1-(3-aminopropyl) imidazole (Middle) and DXT-imidazole (Top) in D_2O, 500 Mhz. Starting from 54% DS of methacrylate groups, the final DS with imidazole is 24% DS while 19% of the glucose functionalized with MA groups did not react.

DS of 24% was obtained for DXT functionalized with imidazole group, meaning that 53 units of the 222 glucose units of DXT have imidazole as pendent group. Also, it means that there is still 19% of the glucose units with unreacted methacrylate groups and 57% are unsubstituted glucose units. Taking into account that the original DXT-MA had DS of 54%, it appears 11% of MA groups have been hydrolyzed.

Figure 3.23 displays the dextran-spermine spectrum. Spermine molecule alone shows four main peaks: 1.47 ppm (s, 4H, CH_2-CH_2-NH-), 1.6 ppm (qu, 4H, -CH_2-CH_2-NH_2), 2.55 ppm (t, 8H, -CH_2-NH-), 2.62 ppm (t, 4H,-CH_2-NH_2). Spectrum of dextran-spermine shows peaks for glucose units, methacrylate, 2-iminothiolane and spermine moieties. Since the methacrylate groups were all reacted, as judged by the absence of signal at 5.7 ppm, the methyl group was considered as the reference proton of spermine for the calculation of DS, see appendix III. DXT-MA was substituted with a 30% DS of spermine. As it has been started from 54% of MA, a 24% loss of methacrylates was found which was attributed to the hydrolisis of the ester occurred due to the pH 8 and surely catalyzed by the amine present in the functionalizing molecule.

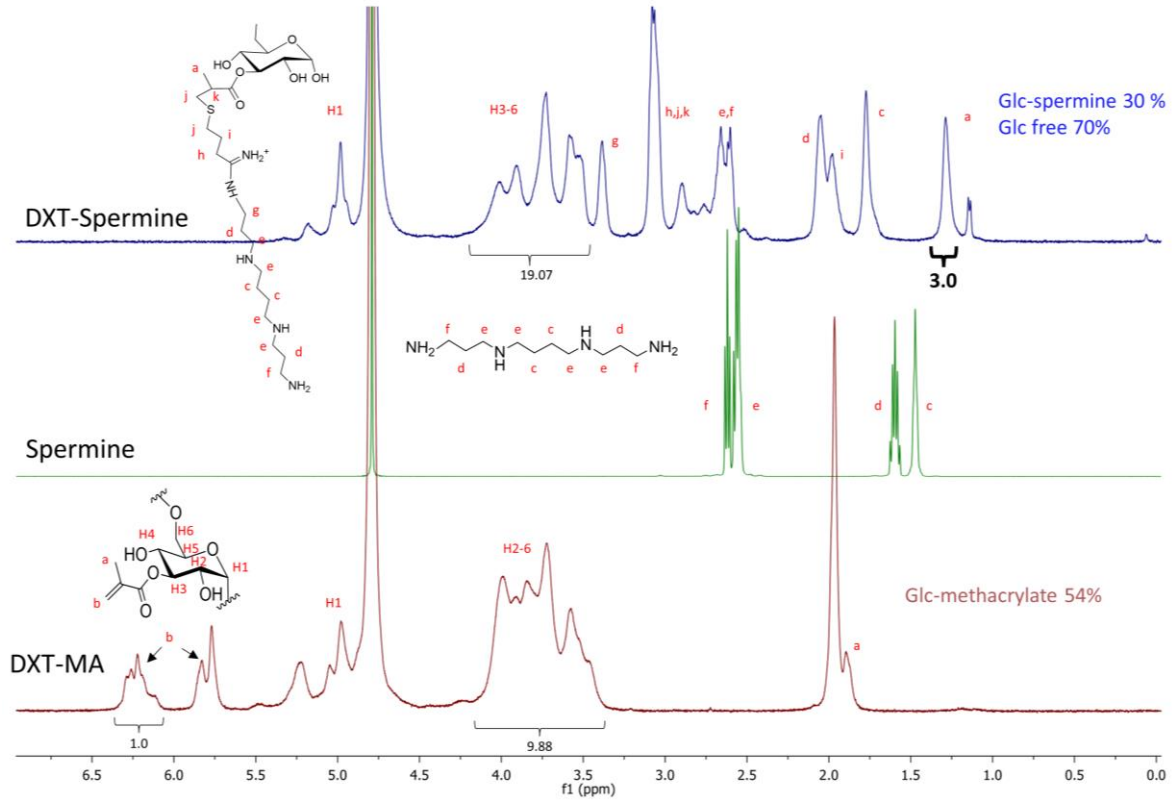

Figure 3. 23.- ^{1}H-NMR spectra of DXT-MA (Bottom), spermine (Middle) and DXT-spermine (Top) in D_2O, 500 Mhz. Starting from 54% DS of methacrylate groups 30% DS of spermine were achieved.

Figure 3.24 shows the spectra of the product obtained by reacting DXT-MA with tris (2-aminoethyl) amine in the presence of Traut's reagent. TAEA presents two peaks at 2.56 ppm (t, 6H, -CH_2-N-) and 2.72 ppm (t, 6H, -CH_2-NH_2). Dextran substituted with TAEA did not show the presence of peaks corresponding to unreacted methacrylate. It appears that 20% of DXT-MA was substituted with TAEA (See detailed calculation in Appendix III), and the 34% of the methacrylate group suffered hydrolisis.

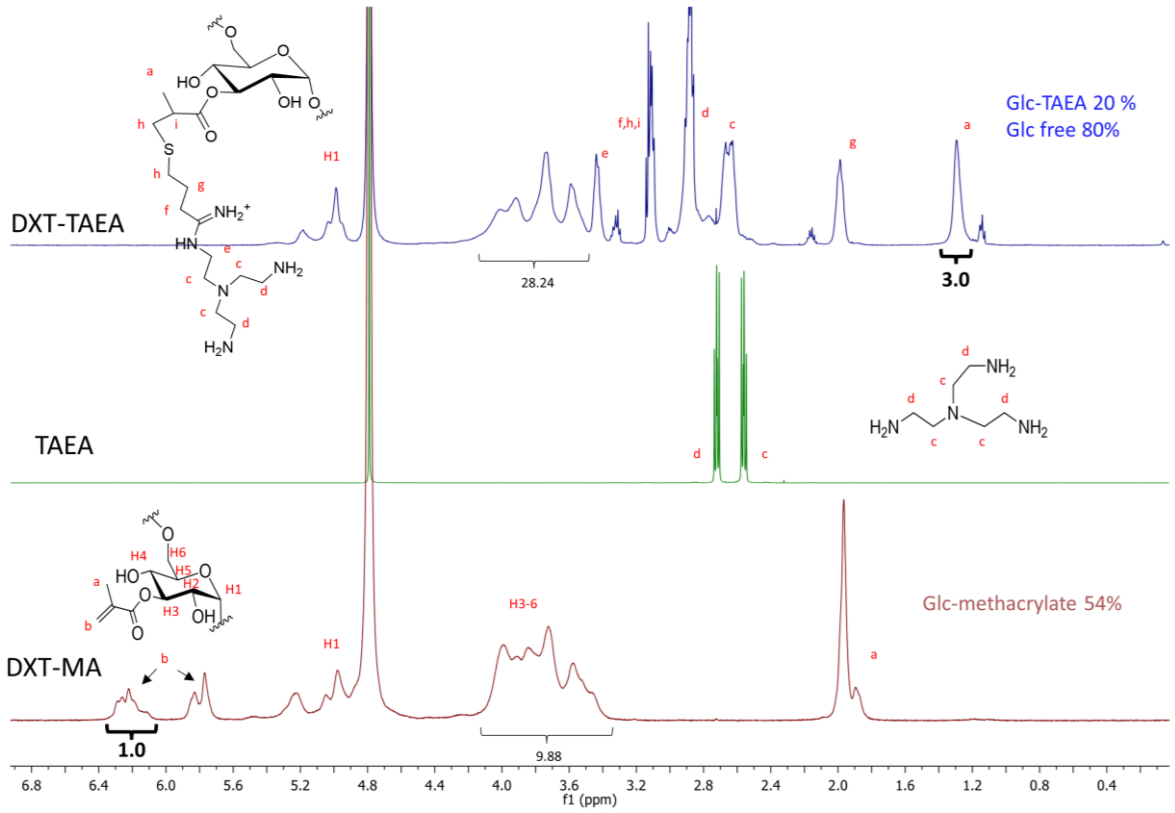

Figure 3. 24.- ^{1}H-NMR spectra of DXT-MA (Bottom), tris (2-aminoethyl) amine (Middle) and DXT-TAEA (Top) in D_2O, 500 Mhz. Starting from 54% DS of methacrylates groups 20% DS of TAEA were achieved.

Figure 3.25 shows the 3,3'-(piperazine-1,4-diyl) bis(propan-1-amine) substitution in dextran polymer. Piperazine molecule present 4 peaks: 1.54 ppm (qu, 4H, $-CH_2-CH_2-NH_2$), at 2.29 ppm are overlapped two signals: inner ring (s, 8H $-CH_2-N-$ ring) and outer $-CH_2$ (t, 4H, $-CH_2-N-$) and one last peak at 2.53 ppm (t, 4H, $-CH_2-NH_2$). Methacrylate reacted completely and similarly to the other functionalization, methyl peak at 1.29 ppm was integrated as piperazine proton value. Dextran-MA has been substituted with 21% of piperazine and a 33% of hydrolysis occurred (See detailed calculation in Appendix III).

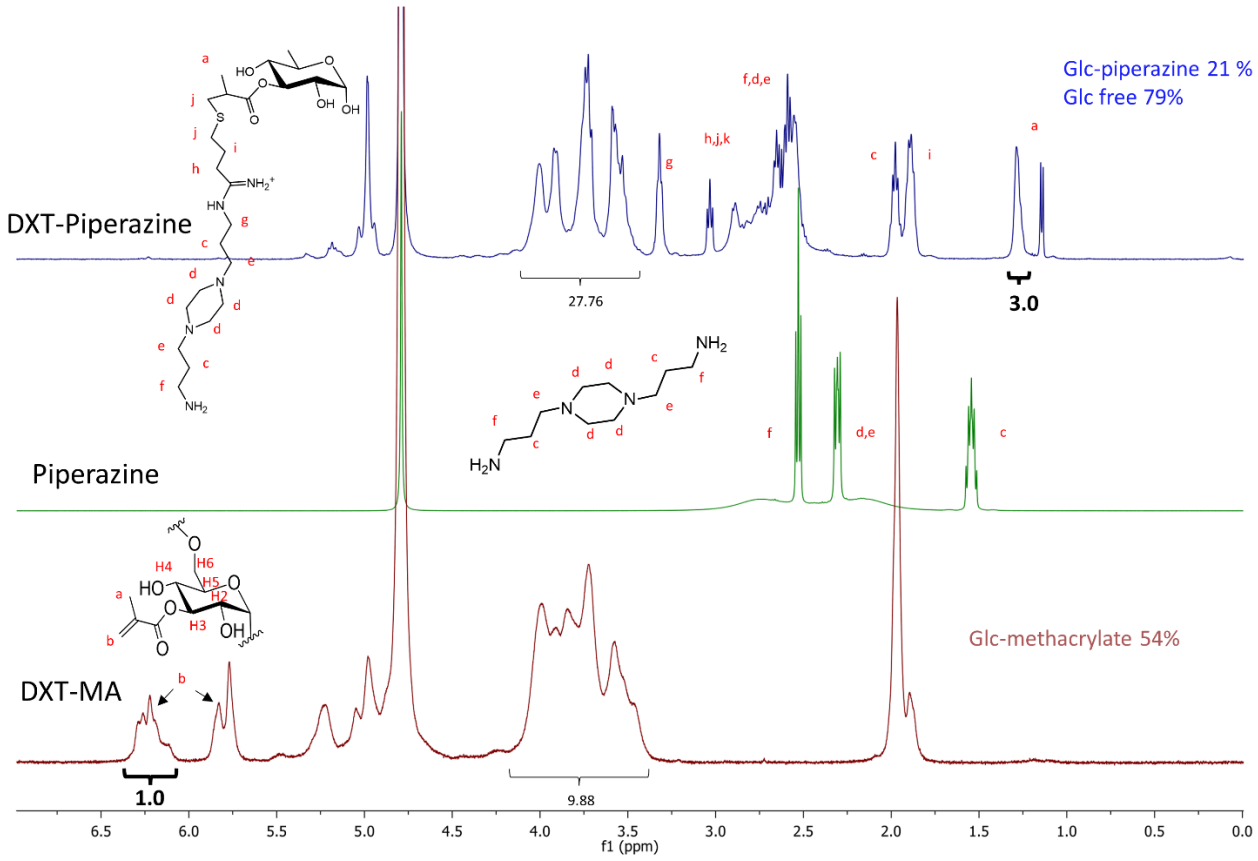

Figure 3. 25.- ^{1}H-NMR spectra of DXT-MA (Bottom), 3,3'-(piperazine-1,4-diyl) bis(propan-1-amine) (Middle) and DXT-piperazine (Top) in D_2O, 500 Mhz. Starting from 54% DS of Methacrylate groups 21% DS of piperazine were achieved.

Since dextran-imidazole has unreacted methacrylates, a further reaction with spermine via Traut's reagent was conducted following the same protocol and the resulting ^{1}H-NMR spectrum is shown in figure 3.26. As already mentioned in Figure 3.23, spermine present 4 peaks and new signals appeared in dextran-imidazole-spermine compared to starting material dextran-imidazole (Figure 3.22). Signals of methacrylate alkene protons were reduced but not completely eliminated, meaning that unreacted methacrylate groups remained after that second functionalization. Dextran has been substituted with 24% DS of imidazole and 15% DS of spermine. 6% of methacrylate are still reactive and unaltered glucose represents 54% of the polymer. In this case, the amount of hydrolysis was quantified to be around 10% (See detailed calculation in Appendix III).

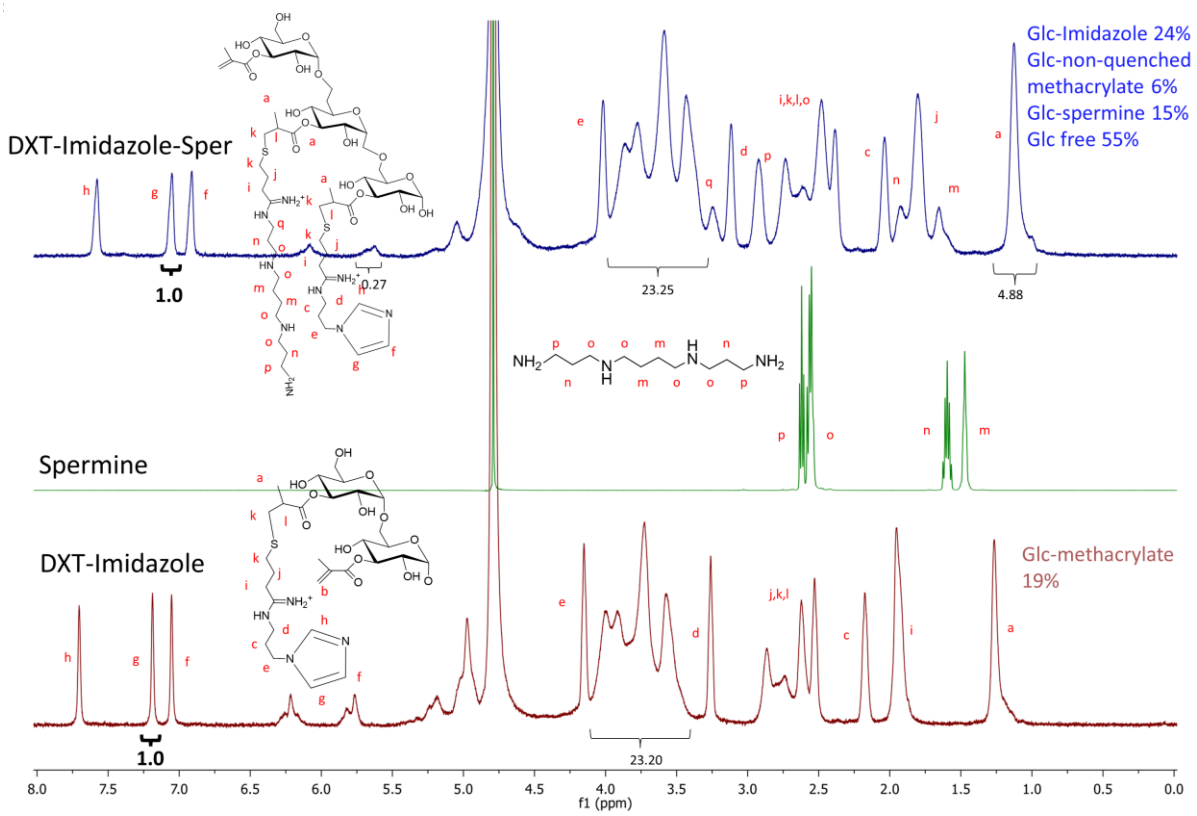

Figure 3. 26.- ^{1}H-NMR spectra of DXT-imidazole (bottom), spermine (Middle) and DXT-imidazole-spermine (Top) in D_2O, 500 Mhz. Starting from 54% DS of Methacrylate groups 21% DS of piperazine were achieved.

On the other hand, the effect of DXT molecular weight was studied in the delivery efficiency. Cysteamine substitutions have been performed on dextran-methacrylate with M_w of 6 and 20 KDa. The same procedure used for the 40 KDa reaction with glycidyl methacrylate was used with those low molecular weight DXT, obtaining DS of 37% and 43% for 6KDa and 20KDa DXT-MA, respectively. Subsequently, using the same technique and molar equivalents as for the 40KDa polymer, cysteamine was coupled by Michael addition. 1:5 eq MA:-SH 8h, RT pH 8. Both polymers were dialyzed against water using 3.5KDa MWCO. White cotton-like solid was obtained after freeze-drying. The ^{1}H-NMR spectra of 6KDa and 20KDa DXT-NH_2 are displayed in Figure 3.27 and 3.28.

DXT-NH_2 o 6 KDa was functionalized with 17% of cysteamine, while 20% of hydrolysis of MA groups was observed, as judged by ^{1}H-NMR (See appendix III for DS determination), while DXT-NH_2 of 20 KDa was functionalized with 17% cysteamine, while 3% of methacrylate group remained unreacted and 80% of glucose units were not substituted.

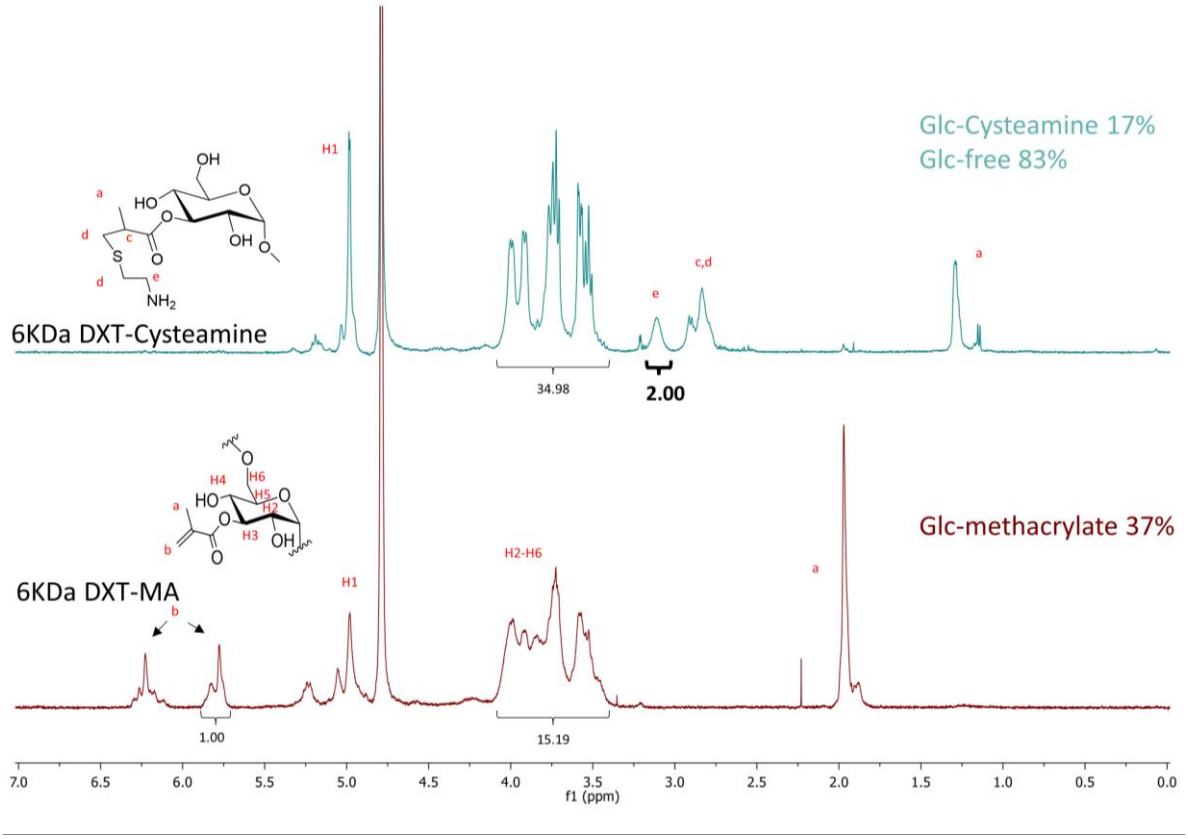

Figure 3. 27.- ^{1}H-NMR Spectra of a 6KDa cysteamine-DXT-MA functionalization. DXT-MA 6KDa (Bottom), DXT-cysteamine (Top). Starting from 37% DS of methacrylate groups and achieving 17% DS of cysteamine in D_2O, 500 MHz.

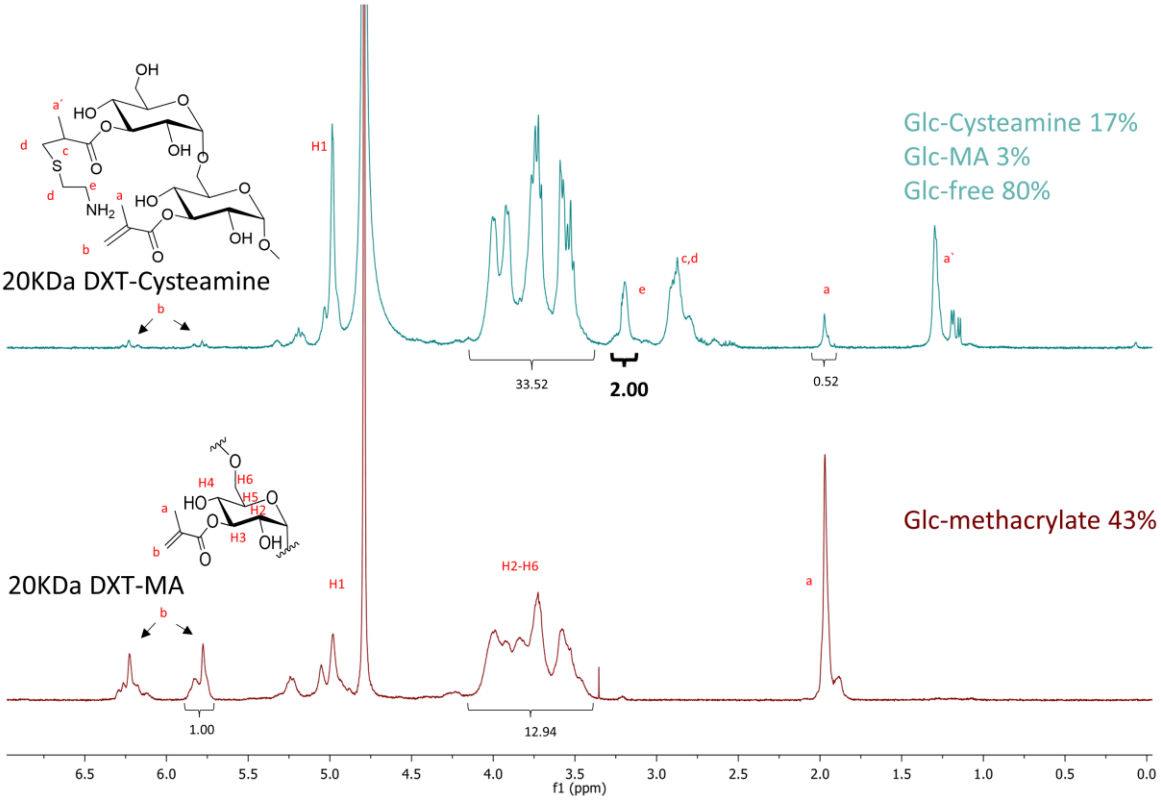

Figure 3. 28.- ^{1}H-NMR Spectra in D_2O 500 MHz of a 20 KDa cysteamine-DXT-MA functionalization. DXT-MA 20KDa (Bottom) and DXT-cysteamine (Top). Starting from 43% DS of methacrylate groups and achieving 17% DS of cysteamine, 3% DS of methacrylate were not reacted.

Finally, a production of highly substituted cysteamine-dextran was attempted in order to obtain sufficient amine to promote the buffering capacity at endosomal pH. A reaction with the double amount of glycidyl methacrylate was carried out and subsequently reacted with cysteamine, following same conditions for DXT-NH_2 in section 3.2.2. ^{1}H-NMR spectra for both polymers are displayed in Figure 3.29. However, only a 57% of cysteamine conversion was obtained, which is not much different than the 42%DS obtained for DXT-NH_2.

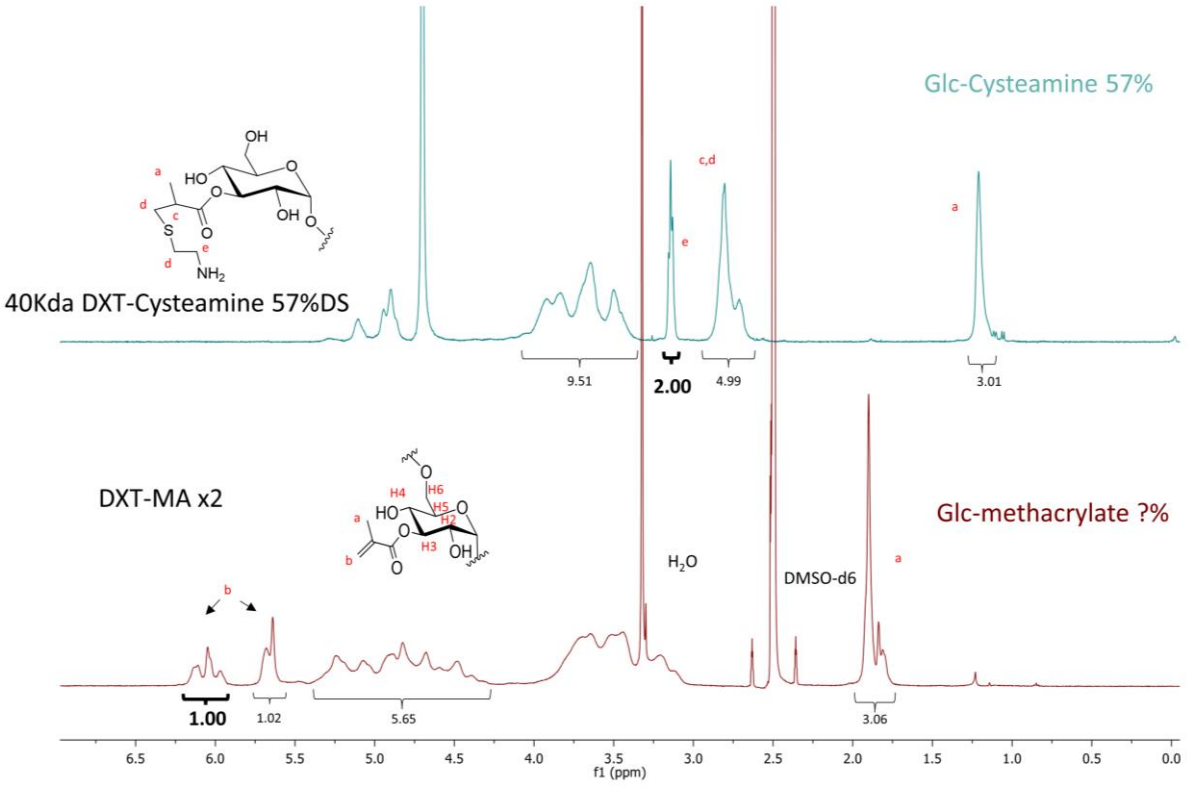

Figure 3. 29.- ^{1}H-NMR Spectra of a 40 KDa cysteamine-DXT-MA functionalization. DXT-MA (Bottom) in DMSO-d6 and DXT-cysteamine (Top) in D_2O. DXT-MA was insoluble in water the %DS of methacrylate could not be calculated. DXT-cysteamine reaction achieved 57%DS.

Polyplex with the different candidates were formed at N/P ratio 10 to study the interactions with siRNA. Size and Z-potential were measured and shown in Table 3. As expected, all the polyplexes obtained with the different amine functionalization have a positive Z-potential due to the presence and high quantity of amine groups at such N/P ratio. Regarding more into detail, dextran substituted with 57% DS of cysteamine have a Z-potential of +33.5 mV, which is the highest Z-potential achieved by cysteamine compared to polyplexes of DXT-NH_2 (section 3.2.4), which presents 42% DS and +19 mV, but it is noteworthy that N/P ratio were different, 10 and 8 respectively. Z-potential increased much more in polyplexes when dextran is substituted with other amino molecules. Polyplexes obtained with DXT-Spermine exhibited a Zeta potential of +46.5 mV at N/P 10, DXT-TAEA at around +30 mV and DXT-Piperazine +28 mV at same N/P 10. At the same DS of cysteamine and N/P ratio, the polyplexes obtained with 6KDa DXT have lower Z-potential than the one produced with 20 KDa, i.e. +3.7 mV and +17.3, respectively, which indicate that cationic 6KDa DXT-cysteamine is neutralized by the negative charge of siRNA despite using a 5 fold excess of polymer molecules to achieve the same N/P ratio.

In terms of their size, polyplexes substituted with amino molecules presented values between 100 to 200 nm and PDIs from 0.17 to 0.4 (Table 3.3). Low molecular weight 6KDa DXT-NH_2 formed the largest polyplexes with a hydrodynamic diameter of 272 nm. On the other hand, polyplexes obtained with DXT-NH_2 20KDa presented a hydrodynamic diameter of 245 nm, which is slightly higher than the hydrodynamic diameter of the polyplexes obtained with DXT-NH_2 40KDa at 198 nm,

although N/P are 10 and 8 respectively (Table 3.2). As it is mentioned in *Tang et Al. (2014)*[25] size of dextran complexes are influenced by binding ability and positive charge. Polymers with higher molecular weight present better binding ability, which leads to a higher complexation and consequently a smaller particle.

Table 3. 3.-Degree of substitution (%DS) obtained with the different amine molecules. Z-average and Z-potential of polyplexes with siRNA at N/P 10 ratio. Every dextran used has 40KDa molecular weight, unless other molecular weight is indicated.

Name, abbreviation and modified polymer abbreviaton	**%DS of -NH2 molecule**	**Z-average (d.nm) ±SD /PDI of N/P 10 polyplex**	**Z-potential (mV) ±SD of N/P 10 polyplex**
1-(3-aminopropyl)imidazole **Imidazole** DXT-Imidazole	24	170±4.5/0.178	29.2±1.64
Spermine **Sper** DXT-Sper	30	176±1.3/0.22	46.5±1.84
Spermine-Imidazole DXT-spermine-Imidazole	24 Imidazole 15 spermine	182±4.3/0.35	48.3±2.3
Tris (2-aminoethyl)amine **TAEA** DXT-TAEA	20	177±1.9/0.22	31.8±1.73
3,3'-(piperazine-1,4-diyl)bis(propan-1-amine) **Piperazine** DXT-Piperazine	21	261±5.6/0.35	28.4±1.61
Cysteamine (6KDa DXT) 6KDa DXT-Cysteamine	17	272±19.4/0.17	3.71±0.34
Cysteamine (20KDa DXT) 20KDa DXT-cysteamine	17	245±25.7/0.41	17.3±1.85
Cysteamine 40KDa DXT-cysteamine 57DS	57	198±3.8/0.22	33.5±1.48

The performance of the different candidates listed in Table 3.3 to release siRNA and transfect A549-eGFP cells was studied at N/P ratios 3, 10 and 30 (Figure 3.30). A simplified and rapid method described in section 3.2.7 was performed to screen *in vitro* all the candidates prepared by quantifying eGFP fluorescence after siRNA treatment by flow cytometry. siRNA amount was maintained at 0.1 nmol for all the experiments and the results were expressed as relative expression of GFP. As expected, free siRNA did not have the ability to knockdown the protein and Lipofectamine RNAimax, as positive control, achieved up to 80% of GFP reduction. None of the polyplexes prepared with the cationic polymers resulted in more than 50% of GFP reduction. The lower molecular weight 6 KDa and 20 KDa did not help siRNA-anti-GFP to *silence* GFP gene, neither did the DXT-NH_2 with high DS. The most efficient polyplexes was the one obtained with DXT modified with piperazine, but only achieving transfection of 50% of the protein expression. The polyplexes prepared with DXT-spermine exhibited 70% of GFP expression, whereas the use of DXT-imidazole as vector did not show any reduction at all. Unfortunately, the combined functionalization of DXT with Imidazole-spermine did not show any synergy as for the delivery of siRNA, only the effect conferred by the spermine functionalization appeared to improve transfection.

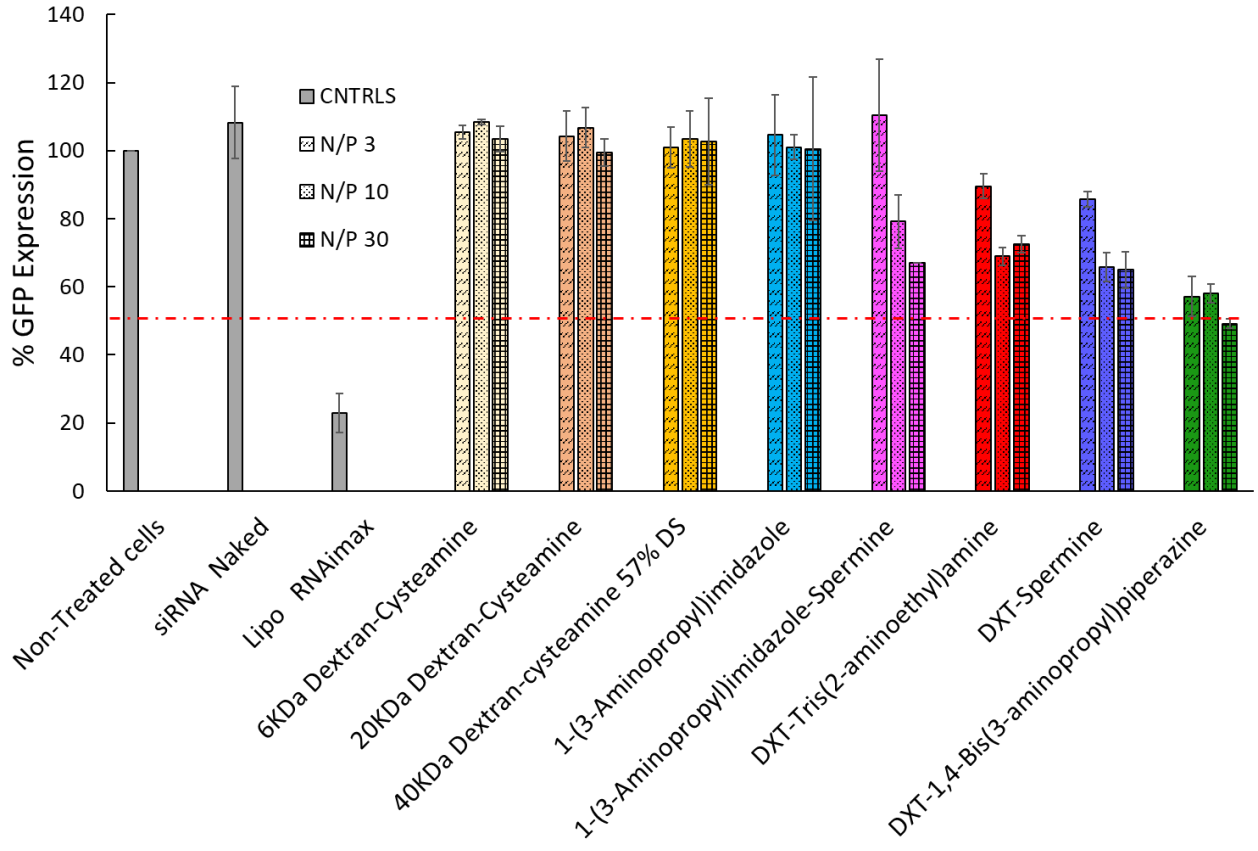

Figure 3. 30.- siRNA delivery efficiency test. A549-GFP cells were treated during 24h with free siRNA, dextran derivatives and positive control Lipofectamine RNAimax complexed with siRNA anti-GFP 200 nM final well concentration. N/P ratios 3, 10 and 30 were used. GFP expression represent mean Fluorescence normalized to the control of non-treated cells, n=3 percentage ± SD.

Previous studies have reported that polyplexes prepared with low molecular weight DXT (6 and 20 KDa) exhibit superior transfection efficiency compared to those prepared with higher molecular

weight (70 KDa) counterparts[25]. However, in our study the low molecular weight DXT polyplexes did not show any notable effect on transfection efficiency. This discrepancy may be attributed to the use of different grafted molecules, cysteamine in our study and peptide in the reported work. We substituted DXT with molecular weights of 6, 20, and 40 KDa with cysteamine at substitution levels of 17%, 17%, and 42% DS, respectively, but siRNA release would not be achieved, possibly due to the low degree of substitution. Interestingly, even 40 KDa DXT with the highest DS of cysteamine at 57% did not result in any GFP Knockdown, suggesting that siRNA release was hindered due to the insufficient buffering capacity of cysteamine, which is necessary for promoting endosomal escape. 40 KDa dextran was substituted with spermine, TAEA, Piperizine, and Imidazole to achieve 30, 20, 21, and 24% DS, respectively. These molecules contain more than one amine group and have secondary or tertiary amines, which may improve the buffering capacity and steric disposition of the polymer system to enhance siRNA release. However, results indicate that delivery properties are still not sufficient to promote more than 50% of protein knockdown. Among the substitutions, the presence of two tertiary amines showed the highest protein *silencing* performances. It is also important to point out that the synthesis route used to introduce the amino molecules is not the most efficient, since hydrolysis of the ester of the methacrylate group to glucose was observed, indicating a lack of stability and reproducibility of the amine functionalized DXT. Some studies have demonstrated the formation of more stable bonds by grafting spermine via glucose ring opening[10,44] and in a different approach, researchers achieved better siRNA release by introducing an acidic-pH-sensitive linker between the amino moiety and the dextran backbone[51,11]. This strategy takes advantage of the pH encountered in endosomal conditions to cleave the functionalizing group and promote siRNA release. To improve the efficiency of siRNA delivery, further work should focus on understanding the siRNA delivery process, including cell uptake, oligonucleotide complexation, and buffering capacity tests. A better understanding of the siRNA route could guide the synthesis of more efficient materials for siRNA delivery and gene knockdown.

3.3 Conclusions

The good results obtained for the formulation of negatively charged SCPNs with cationic antibiotics via electrostatic interactions led to develop polyplexes formulations based on positively charged SCPNs with negatively charged siRNA. DXT-SCPNs was functionalized with positive charges using cysteamine. The benefit of small size of SCPN was evaluated as siRNA carrier and compared to its non-crosslinked DXT-NH_2 homologue. Collapse of intrachain was achieved by cross-linking with dithiol molecule DODT via thiol-ene Michael addition of previously modified methacrylate-dextran. 16% of DODT substitution was achieved and the remaining methacrylate groups (21%) were subsequently substituted with cysteamine via same thiol-ene Michael addition. The homologue DXT-NH_2 polymer was substituted with cysteamine achieving 42% DS. Both molecules in water exhibit a hydrodynamic diameter of around 15 nm, but crosslinking led to better size distribution with 0.2 PDI compared to 0.4 obtained for polymer, while both candidates proved to be cytocompatible for A549 cells at concentration up to 50 μg/mL. Both structures formed polyplexes entrapping siRNA, where N/P ratios of 8 was required to achieve the highest entrapment efficiency. The polyplexes obtained with SCPN-NH_2 had a hydrodynamic diameter of 27 nm, while larger

polyplexes of 117 nm were obtained with DXT-NH_2, as judged by DLS studies. As expected, surface charge of materials were positive and appeared to be slightly reduced when formulated with siRNA at N/P ratio of 8 for both systems, as judged by aqueous electrophoresis studies. Despite an efficient complexing, SCPN-NH_2 did not show any siRNA uptake by A549 cells, whereas the polymer showed co-localization of material and oligonucleotide in the interior on CLSM observation. The absence of internalization was attributed to the rigid structure achieved by crosslinking hindering some of the cationic charges of the polymer chains to the siRNA, leading to weak reduced amount of electrostatic interaction and dissociation in the presence of medium, similarly to the one reported for anionic SCPN with cationic antibiotics. Delivery studies demonstrate that neither SCPN-NH_2 nor DXT-NH_2 could promote endosomal escape and release siRNA into A549-GFP cells. Taking into account those uptake studies, further studies with SCPN substitutions were discarded and DXT polymer was selected to study the effect of other cationic modifications. In order to promote endosomal escape dextran 40 KDa were functionalized with different amino molecules: spermine, Imidazole, TAEA and Piperazine. Those compounds were all selected for the presence of different type of amine groups that were expected to offer buffering capacity and improve transfection performances. In addition, 6KDa and 20KDa DXT were functionalized with cysteamine to study the effect of M_w on transfection, as it was previously published that lower molecular weights resulted in improved siRNA release. All different candidates formed polyplexes with positive charge and sizes from 170 to 270 nm at N/P 10 ratio. However, the maximum protein silencing did not exceed 50% while lowering the molecular weight of DXT-NH_2 did not show any improvement in term of transfection. Double functionalization of DXT with spermine and imidazole did not show any improvement for the polyplexes performances neither. The low number of amines could be the main reason for poor delivery due to low buffering capacity for endosomal escape. The functionalization strategy did not appear to be the most efficient reactions due to the low DS achieved and the hydrolysis of the ester groups observed. Thus, a new functionalization strategy to improve the stability and increase the degree of substitution could result interesting. In order to solve the issue regarding the low number of amines per polymer chain a polyamine-based system was considered, as well as its hydrophobic modification to improve siRNA delivery efficiency, as shown in the following chapters.

3.4 Material and methods

3.4.1 *Materials*

Dextran 40 KDa was purchased to **Pharmacosmos**. Glycidyl methacrylate (GMA), dimethyl sulfoxide (DMSO) (98%), 4-(4,6-dimethoxy-1,3,5-triazin-2-yl)-4-methylmorpholinium chloride (DMTMM·HCl) (96%) and 2,2'-(ethylenedioxy) diethanethiol [3,6-dioxa-1,8-octane-dithiol (DODT)] (95%), Cysteamine ~95% (ref:M9768), 1-(3-aminopropyl) imidazole 97% (ref: 272264), Tris (2-aminoethyl) amine (TAEA) 96% (ref: 225630), Spermine 97% (ref: S3256) , 3,3'-(piperazine-1,4-diyl)bis(propan-1-amine) 99% (ref: 239488), 2-Iminothiolane hydrochloride >98% (ref: I6256), Gel Loading Buffer (ref: G2526), Triton™ X-100 (ref: X100), Rhodamine B 95% (ref: R6626), Agarose low EEO (Ref: 9539), Dextran 6KDa (31388-25G), Dextran 20KDa were purchased from **Sigma Aldrich**. 4-(Dimethylamino)pyridine (DMAP) was purchased from **Acros-Organics**. Phosphate-buffered saline (PBS) was purchased from **Scharlau**. PD-10 desalting columns (ref:17085101) was purchased

from **GE Healthcare**. µ -Slide 8 Well plate (ref: 80826) was purchased from **Ibidi.** Lipofectamine RNAimax (Ref: 13778030), Nuclease-free water (ref: AM9932), Opti-MEM™ Reduced Serum Medium no phenol red (ref: 11058021), Fetal bovine Serum FBS (ref:10500-064 Gibco), Trypsin-EDTA (0.25%) phenol red (ref: 25200056 Gibco), Penicillin-Streptomycin 10,000 U/mL (ref: 15140122 Gibco), Trypsin-EDTA (0.5%), no phenol red (Ref: 15400054, Silencer™ 6-FAM-labeled Negative Control No. 1 siRNA (ref:AM4620), Hoechst 33342 Solution (ref: 62249), Blasticidina S HCl 10 mg/ml (ref: A1113903), DTNB (Ellman's Reagent) (5,5-dithio-bis-(2-nitrobenzoic acid) (ref: 22582), Deuterium oxide 99.8% D (Ref: 426931000), methyl-sulfoxide-d6 99.9%D (Ref: 16629100), SnakeSkin™ dialysis membrane 3500 MWCO 22 mm ø, Dextran 20KDa (J61216) were purchased from **Thermo Fisher**. A549 human lung carcinoma cell line (CCL-185), EMEM Eagle's Minimum Essential Medium (ref: 30-2003) were purchased from **ATCC**. A549 / GFP stable cells (Blasticidin) (ref: SC043-Bsd) was purchased from **GeneTarget**. siRNA negative control (sense 5´UUC UCC GAA CGU GUC ACG UdTdT3´ antisense 5'-ACG UGA CAC GUU CGG AGA AdTdT-3'), siRNA anti-eGFP (sense 5´-CAA GCU GAC CCU GAA GUU CdTdT-3´ antisense 5´-GAA CUU CAG GGU CAG CUU GdTdT-3´) were purchased by demand to **BioSpring Biotechnolgie GmbH.** CellTiter 96® AQueous One Solution Cell Proliferation Assay MTS (ref: G3580) to **Promega**. GelRed®10,000x water (ref: 41003) was purchased to **Biotium**. 4% Paraformaldehyde aqueous solution (Ref:1574) was purchased from **Electron Microscopy Sciences**.

3.4.2 *Methods*

2.4.2.1 Synthesis of dextran-methacrylate DXT-MA 45% DS

Dextran methacrylated polymer (DXT-MA) was synthesized following a slightly modified published procedure[19]. First, dextran (DXT-40, 2g, 0.05 mmol, 1 eq) was dissolved in 60 mL of dimethyl sulfoxide (DMSO) under a nitrogen atmosphere. To this solution, 400 mg of 4-(N,N-dimethylamino)pyridine (DMAP, 3.27 mmol, 65 eq) was added. Then, 2 mL of glycidyl methacrylate (GMA, 15 mmol, 300 eq) was incorporated and the mixture was stirred at room 3 days. The reaction was stopped by adding an equimolar amount of 1M HCl solution 1.6 mmol, 3.28 mL to neutralize DMAP. The modified dextran solution was subjected to purification by dialysis against ultrapure water using a membrane with a molecular weight cutoff (MWCO) of 3,500 Da. The dialysis process was carried out at room temperature for a period of 10 days. To ensure effective purification, the dialysis solution was refreshed with 5 liters of deionized water twice per day. During the dialysis process, the conductivity of the eluent was monitored as an indicator of the purification progress. A conductivity value below 2 µS/cm was considered acceptable, indicating that the product had been sufficiently purified. Then, solution was freeze-dried to obtain white cotton-like solid.

3.4.2.2 Synthesis of single-chain polymer nanoparticles. SCPN

Synthesis based on Gracia et al (2017)[13], 500 mg of DXT-MA (1.0918 mmol Glc-MA) was dissolved in 50 mL PBS adjusted to pH 9.5. A solution of 0.15 M of cross-linker 3,6-dioxa-1,8-octane-dithiol (DODT) (0.25 -SH mol equivalents 0.273 mmol) was prepared by adding 49 µL of stock DODT to 1 mL of PBS adjusted to pH 9.5, same amount 1:1 of methanol was added to the mix, 1 mL. The 2 mL mixture was added dropwise using a syringe pump at 0.226 mL/h during 8 h at room temperature under constant stirring. After addition, the reaction was maintained stirring at room temperature for 12 h more. Then, the disappearance of the -SH groups from the cross-linker DODT was verified by Ellman´s test. 6 mL was removed from reaction and purified by dialysis for further characterization and remaining 44 mL were used to further reaction with cysteamine. A conductivity value below 2 µS/cm was considered acceptable, indicating that the product had been sufficiently purified.

3.4.2.3 Functionalization of DXT-MA with cysteamine (DXT-NH_2)

Dextran methacrylate polymer was functionalized with cysteamine. Briefly, 500 mg (1.0918 mmol 1 eq mol glc-MA) of DXT-MA 45%DS was dissolved in 50 mL PBS and adjusted to pH 8. Then, 421 mg (5.459 mmol 5 eq mol -SH) cysteamine was dissolved in 20 mL of PBS and adjusted to pH 8. Both solutions were mixed together and stirred 5 h at room temperature. Purification was made by dialysis 3,5 KDa MWCO against ultrapure water for 5 days, conductivity below 2 µS/cm was checked to consider the product purified. The resulting aqueous solution was freeze-dried obtaining a white cotton-like solid.

3.4.2.4 Functionalization of SCPN with cysteamine (SCPN-NH_2)

Functionalization of SCPN with cysteamine was directly made from already prepared DXT-SCPN-MA solution (500 mg 1.0198 mmol Glc-MA). SCPN solution was adjusted to pH 8. One batch reaction was achieved by adding 421 mg of cysteamine (5 eq mol 5.459 mmol -SH) previously dissolved in 25 mL PBS and adjusted to pH 8. Reaction was stirred during 5h at room temperature and subsequently purified by 3.5 KDa MWCO dialysis. A conductivity below 2 µS/cm indicates that the product has been purified and subsequently freeze-dried.

3.4.2.5 Functionalization of DXT-MA with amines via Traut reaction

The functionalization of DXT-MA was performed in one pot reaction following the stoichiometry 1:2:4 MA:Traut:Amine molar equivalents. The amine compounds used are listed in figure 3.19 [1-(3-aminopropyl) imidazole/spermine/ Tris (2-aminoethyl) amine/3,3'-(piperazine-1,4-diyl)bis(propan-1-amine)]. 100 mg of 54% DS DXT-MA was dissolved in 2 mL PBS and pH was adjusted to 8.0. Corresponding amount of Traut´s reagent and amino molecule was dissolved in 2 mL PBS separately and adjusted to pH 8.0. The three solution was mixed and pH 8.0 was confirmed. The mix was stirred at room temperature during 2h. The reaction was purified by dialysis 3.5 KDa MWCO against deionized water during 7 days refreshing water twice a day. A conductivity value below 2 µS/cm was considered acceptable, indicating that the product had been sufficiently purified. After dialysis compound were freeze-dried, a cotton-like white solid was obtained.

3.4.2.6 Nuclear Magnetic Resonance NMR

Samples were kept 4°C freeze-dried, minimum amount of 5 mg are dissolved in 0.6-1 mL of the proper deuterated solvent. Mostly deuterium dioxide. NMR spectra were recorded on a Bruker AVANCE III spectrometer at 500 MHz and 25°C. Chemical shifts (δ) are expressed in ppm. Splitting patterns: b, broad; s, singlet; d, doublet; t, triplet; q, quartet; qu quintet, m, multiplet.

3.4.2.7 Polyplex formation

siRNA and vectors were complexed for different applications: gel retardation assay, DLS measurements, TEM, uptake and delivery efficiency studies. Different N/P ratios were performed for different occasions. The N/P ratio is defined as moles of nitrogen present in the vector divided by moles of phosphates in the siRNA. N/P ratios 0.5, 1, 2, 4 and 8 were carried out for SCPN-NH_2 and DXT-NH_2 and N/P 3, 10 and 30 for DXT-amine substitutions and 6KDa and 20KDa DXT-cysteamine. In every case, same amount of siRNA 0.1 nmol is maintained and the amount of material is varied to achieve the indicated N/P. Briefly, corresponding amount of polymer was dissolved in 50 µL RNAse-free water to achieve desired N/P ratio. The corresponding amount of siRNA (0.1 nmol) was added to polymer aqueous solution and then mixed by pipetting up-down or by a

short vortex. Samples were incubated during 15 minutes at room temperature (RT), to allow both molecules to form complexes.

3.4.2.8 Gel retardation assay

Agarose gel at 1% w/v in TAE 1x buffer was casted in Bio-Rad Mini-sub G T cell. GelRed was used as siRNA intercalant, which was added into the agarose solution at 0.8x before solidification. Meanwhile gel solution was cooled down, polyplexes were formed as described above for testing SCPN-NH_2 and DXT-NH_2 capacity at N/P ratios of 0.5, 1, 2, 4 and 8. Once Gel was solidified in the cell, then was covered by TAE buffer 1x. Samples were mixed with gel loading buffer and loaded in the wells of the gel. In addition to each polyplex at N/P ratios, free siRNA and siRNA marker were added to the gel. Then cell was connected to power supply and run at 80V during 10 minutes and then back again until 30 minutes.

3.4.2.9 Dynamic Light Scattering DLS

DLS analyses were conducted using a Zetasizer Nano ZS, ZEN3600 Model (Malvern Instruments Ltd). All measurements were performed in disposable sizing cuvettes at a laser wavelength of 633 nm and a scattering angle of 173°. Each measurement was repeated three times per sample at 25°C. SCPN measurements were done in PBS at 10 mg/mL concentration pH 7.4 and filtered by 0.44 µm. DXT with cysteamine was done in PBS at 10 mg/mL and DXT substituted with different amines were performed in PBS at different concentrations from 0.02 to 5 mg/mL. When SCPNs and DXTs were complexed with siRNA concentration was reduced and varied from 0.02 to 2 mg/mL.

3.4.2.10 Z-potential measurements

Z-potential measurements were performed with Zetasizer Nano ZS, ZEN3600 Model (Malvern Instruments Ltd). Disposable folded capillary cells DTS1070 was filled with 750 µL of sample solution. Different materials were dissolved in NaCl 1 mM pH 7 at different concentrations depending on the material from 0.5 to 10 mg/mL and then filtered by 0.4 µm. 3 measurements at 25ºC 30 sub-runs.

3.4.2.11 Transmission electronic microscopy TEM

TEM analyses of single-chain polymeric nanoparticles (SCPNs) were performed in a TECNAI G2 20 TWIN microscope operating at an accelerating voltage of 200 KeV in a bright-field image mode. One drop of the sample dispersion in water (~3 µL, 0.035 mg/mL) was deposited on a carbon film supported on a copper grid (300 mesh). The sample was hydrophilized by a glow discharge process just prior to use. The sample was stained by dropping an aqueous solution of uranyl acetate (1.5% w/v) onto a copper grid. After staining, the sample was spin-dried at room temperature. TEM analyses of polyplexes of DXT-NH_2/siRNA and SCPN-NH_2/siRNA were carried out in a JEOL JEM 1010 (120kV) system equipped with a GATAN US1000 CCD camera (2k x 2k). One drop of the sample dispersion in water (5 µL of N/P 8 0.1 nmol siRNA) was deposited on a carbon film supported on a copper grid (300 mesh) and hydrophilized by a glow discharge process just prior to use. The staining was carried out for 120 seconds with uranyl acetate (1.5% w/v) and the sample was dried at room temperature overnight.

3.4.2.12 Cell culture

A549 human pulmonary cell line was maintained using EMEM´s Medium supplemented with 10% v/v Fetal bovine Serum FBS and 1% v/v Penicilin-Strptomicine (P/S). A549 stably expressing eGFP (A549-eGFP) were kept in EMEM´s medium 10% FBS, 1% P/S and 10 µg/mL Blasticidin.

3.4.2.13 Cytotoxicity by MTS assay

Cytotoxicity of DXT-NH_2 and SCPN-NH_2 were evaluated for the A549 cell line after 48 hours exposition to the cells. Cells were seeded in 96-well using EMEM supplemented with 10% FBS and 1% Penicillin-Streptomycin and incubated 24 hours. When cells were confluent, DXT-NH_2 and SCPN-NH_2 were added to the cell culture at different concentrations: 6.25, 12.5, 25, 50 and 500 µg/mL and 4 technical replicates. After 48 hours incubation at 37ºC and 5% CO2, MTS CellTiter 96® AQueous One Solution was conducted. A corresponding volume of MTS solution was added to each well and incubated during 2 hours at 37ºC and 5% CO2. Absorbance of the Formazan resulting product was measured at 490 nm in plate reader Synergy HT by Biotek.

3.4.2.14 Functionalization of DXT-NH_2 and SCPN-NH_2 with Rhodamine B (DXT-NH_2-RhB) (SCPN-NH_2-RhB)

Rhodamine B, (ex: 554 em: 627) was selected as fluorophore for tracking DXT-NH_2 and SCPN-NH_2. 20 mg of both polymers were dissolved in PBS and pH was adjusted to 7.4. 1.6 mg of Rhodamine B (0.1 eq mol) and 1.4 mg (0.15 eq mol) of DMTMM (4-(4,6-dimethoxy-1,3,5-triazin-2-yl)-4-methyl-morpholinium chloride) was added to the solution. DMTMM is a precursor that activates carboxylic acid and mediates amide coupling. Reaction was stirred for 16 h at room temperature. After that, it was purified by PD10 columns and the solutions collected were freeze-dried. The resulting solid powder was characterized by ^{1}H-NMR to confirm the presence of the dyes on DXT-NH_2 and SCPN-NH_2. However, this method was not valid to detect Rhodamine B. So, Rhodamine B was determined by UV-Absorbance. Calibration curve was performed by making different concentrations of Rhodamine B in PBS: 0, 1, 2, 4, 6, 8, 10, 15, 20, 25, 30 and 40 µg/mL and measuring the absorbance at 554 nm. Absorbance was plotted in Y-axis and Concentrations in X-axis. Standard curve was prepared and the fitting equation was used to detect the Rhodamine B concentration in 1 mg/mL of DXT-NH_2-RhB and SCPN-NH_2-RhB. Amount of RhB was expressed as % wt in the samples.

3.4.2.15 Uptake study by Confocal Laser Scanning Microscopy

A549 cells were cultured in 8-well ibidi plates at 30.000 cell/well. 24h after DXT-NH_2 and SCPN-NH_2 labeled with Rhodamine B were used to form polyplexes with siRNA-6-FAM at N/P ratio of 8 as described above. Final concentration of siRNA per well was 200 nM. Resulting polyplexes were exposed to confluent cells during 24h of transfection. Then, cells were washed with DPBS, fixed with 4% v/v paraformaldehyde (PFA) and permeabilized with 0.5% v/v Triton-X-100 washing with DPBS between steps. After that cell nucleus was stained with dilution of 1:2000 Hoechst 33342. Fixed cells ready for imaging were embedded in DPBS. Ibidi plates were set up on confocal laser scanning microscopy (CLSM) Zeiss LSM 510. CLSM images were acquired by exciting at 405, 488 and 561 nm excitation laser lines, with a 63x objective. Taken images was processed by ZEN 3.3 software and ImageJ.

3.4.2.16 siRNA delivery efficiency by flow cytometry

Delivery efficiency of siRNA inside cells was assessed by measuring the siRNA silencing of eGFP protein by flow cytometry. A549 cells stably expressing eGFP (A549-eGFP) were seeded in 24-well plates at 60,000 cells/well using EMEM 10% v/v FBS 1% v/v P/S and 10 µg/mL Blasticidin. Transfection was performed using polyplexes of different carriers: DXT-NH_2 and SCPN-NH_2 anti-eGFP at ratios N/P 1, 2, 4 and 8. DXT amine derivatives: DXT-Imidazole, DXT-spermine, DXT-TAEA, DXT-piperazine, DXT-spermine-imidazole, 6 KDa-DXT-cysteamine, 20 KDa-DXT-cysteamine and 57%DS-DXT-cysteamien at ratios N/P 3, 10 and 30. In every case 0.1 nmol of siRNA was used to achieve a final concentration of 200 nM per well. Lipofectamine RNAimax was used as positive control and polyplexes were prepared following the protocol provided by the manufacturer, using same amount of siRNA. Cells media were substituted by OptiMEM and complexes were distributed into the wells. After 24 hours incubation, cells were washed and refreshed with full growth media EMEM 10% FBS 1% P/S. Cells were incubated between 72-96 hours after transfection to obtain an effective protein reduction. Once incubation finished cells were lifted with 0.25% trypsin/EDTA without phenol red. Trypsin effect was blocked with DPBS 10% FBS and the resulting cells solution was transferred to a flow cytometer´s tube. Samples were measured with a Flow Cytometer FACS diva canto II. FITC filter was applied to count GFP expressing cells. Software BD FACS Diva was used to measure the mean fluorescence intensity of 10,000 events per condition. Data is presented as relative GFP expression normalized to the intensity of the non-treated cells, considered 100% of GFP-expression. Every condition had 3 technical replicates.

3.5 References

1. Huo, M. *et al.* Single-chain polymer nanoparticles: Mimic the proteins. *Polymer* **66**, A11–A21 (2015).

2. Kröger, A. P. P. & Paulusse, J. M. J. Single-chain polymer nanoparticles in controlled drug delivery and targeted imaging. *J. Control. Release* **286**, 326–347 (2018).

3. Sanchez-Sanchez, A. *et al.* 'Michael' Nanocarriers Mimicking Transient-Binding Disordered Proteins. *ACS Macro Lett.* **2**, 491–495 (2013).

4. Pia P. Kröger, A. P. P., Hamelmann, N. M., Juan, A., Lindhoud, S. & Paulusse, J. M. J. Biocompatible single-chain polymer nanoparticles for drug deliverya dual approach. *ACS Appl. Mater. Interfaces* **10**, 30946–30951 (2018).

5. Blanco-Cabra, et al. Neutralization of ionic interactions by dextran-based single-chain nanoparticles improves tobramycin diffusion into a mature biofilm. *npj Biofilms Microbiomes* **8**, 52 (2022.

6. Hanlon, A. M., Lyon, C. K. & Berda, E. B. What Is Next in Single-Chain Nanoparticles? *Macromolecules* **49**, 2–14 (2016).

7. Mehvar, R. Dextrans for targeted and sustained delivery of therapeutic and imaging agents. *J. Control. Release* **69**, 1–25 (2000).

8. Heinze, T., Liebert, T., Heublein, B. & Hornig, S. Functional Polymers Based on Dextran. in *Polysaccharides II* (ed. Klemm, D.) 199–291 (Springer Berlin Heidelberg, 2006). doi:10.1007/12_100.

9. Raemdonck, K. *et al.* Biodegradable dextran nanogels for RNA interference: Focusing on endosomal escape and intracellular siRNA delivery. *Adv. Funct. Mater.* **19**, 1406–1415 (2009).

10. Cohen, J. L. *et al.* Acid-degradable cationic dextran particles for the delivery of siRNA therapeutics. *Bioconjug. Chem.* **22**, 1056–1065 (2011).

11. Krishnamachary, B., Penet, M. F. & Bhujwalla, Z. M. Acid-degradable dextran as an image guided siRNA carrier for COX-2 downregulation. *Theranostics* **8**, 1–12 (2018).

12. Nagane, K., Jo, J. I. & Tabata, Y. Promoted adipogenesis of rat mesenchymal stem cells by transfection of small interfering rna complexed with a cationized dextran. *Tissue Eng. - Part A* **16**, 21–31 (2010).

13. Gracia, R. *et al.* Synthesis and functionalization of dextran-based single-chain nanoparticles in aqueous media. *J. Mater. Chem. B* **5**, 1143–1147 (2017).

14. Gracia, R. *et al.* Biocompatible single-chain polymer nanoparticles loaded with an antigen mimetic as potential anticancer vaccine. *ACS Macro Lett.* **7**, 196–200 (2018).

15. Falciani, C. *et al.* Antimicrobial peptide-loaded nanoparticles as inhalation therapy for Pseudomonas aeruginosa infections. *Int. J. Nanomedicine* **15**, 1117–1128 (2020).

16. Ritter, D. *et al.* In vitro inhalation cytotoxicity testing of therapeutic nanosystems for pulmonary infection. *Toxicol. Vitr.* **63**, 104714 (2020).

17. van der Weide, H. *et al.* Therapeutic efficacy of novel antimicrobial peptide AA139-nanomedicines in a multidrug-resistant klebsiella pneumoniae pneumonia-septicemia model in rats. *Antimicrob. Agents Chemother.* **64**, (2020).

18. Kris, M. G. *et al.* Adjuvant systemic therapy and adjuvant radiation therapy for stage I to IIIA completely resected non-small-cell lung cancers: American society of clinical oncology/cancer care Ontario clinical practice guideline update. *J. Clin. Oncol.* **35**, 2960–2974 (2017).

19. Van Dijk-Wolthuis, W. N. E., Kettenes-van Den Bosch, J. J., Van Der Kerk-van Hoof, A. & Hennink, W. E. Reaction of dextran with glycidyl methacrylate: An unexpected transesterification. *Macromolecules* **30**, 3411–3413 (1997).

20. Kim, S. H. & Chu, C. C. Synthesis and characterization of dextran-methacrylate hydrogels and structural study by SEM. *J. Biomed. Mater. Res.* **49**, 517–527 (2000).

21. Mather, B. D., Viswanathan, K., Miller, K. M. & Long, T. E. Michael addition reactions in macromolecular design for emerging technologies. *Prog. Polym. Sci.* **31**, 487–531 (2006).

22. Hoyle, C. E., Lowe, A. B. & Bowman, C. N. Thiol-click chemistry: A multifaceted toolbox for small molecule and polymer synthesis. *Chem. Soc. Rev.* **39**, 1355–1387 (2010).

23. Kakwere, H. & Perrier, S. Orthogonal 'relay' reactions for designing functionalized soft nanoparticles. *J. Am. Chem. Soc.* **131**, 1889–1895 (2009).

24. Li, G. Z. *et al.* Investigation into thiol-(meth)acrylate Michael addition reactions using amine and phosphine catalysts. *Polym. Chem.* **1**, 1196–1204 (2010).

25. Tang, Q. *et al.* Dextran-peptide hybrid for efficient gene delivery. *Langmuir* **30**, 5202–5208 (2014).

26. Riddles, P. W., Blakeley, R. L. & Zerner, B. [8] Reassessment of Ellman's reagent. *Methods Enzymol.* **91**, 49–60 (1983).

27. Abbas, S. S., Kelly, N. L., Patias, G., Hanna, J. V. & McNally, T. Cysteamine functionalised reduced graphene oxide modification of maleated poly(propylene). *Polymer* **203**, 122750 (2020).

28. Putnam, D., Gentry, C. A., Pack, D. W. & Langer, R. Polymer-based gene delivery with low cytotoxicity by a unique balance of side-chain termini. *Proc. Natl. Acad. Sci. U. S. A.* **98**, 1200–1205 (2001).

29. Paul, A., Eun, C. J. & Song, J. M. Cytotoxicity mechanism of non-viral carriers polyethylenimine and poly-l-lysine using real time high-content cellular assay. *Polymer* **55**, 5178–5188 (2014).

30. Clamme, J. P., Azoulay, J. & Mély, Y. Monitoring of the formation and dissociation of polyethylenimine/DNA complexes by two photon fluorescence correlation spectroscopy. *Biophys. J.* **84**, 1960–1968 (2003).

31. Andreozzi, P. *et al.* Exploring the pH Sensitivity of Poly(allylamine) Phosphate Supramolecular Nanocarriers for Intracellular siRNA Delivery. *ACS Appl. Mater. Interfaces* **9**, 38242–38254 (2017).

32. Varkouhi, A. K., Scholte, M., Storm, G. & Haisma, H. J. Endosomal escape pathways for delivery of biologicals. *J. Control. Release* **151**, 220–228 (2011).

33. Bus, T., Traeger, A. & Schubert, U. S. The great escape: How cationic polyplexes overcome the endosomal barrier. *J. Mater. Chem. B* **6**, 6904–6918 (2018).

34. Bartlett, D. W. & Davis, M. E. Insights into the kinetics of siRNA-mediated gene silencing from live-cell and live-animal bioluminescent imaging. *Nucleic Acids Res.* **34**, 322–333 (2006).

35. Chen, W., Smeekens, J. M. & Wu, R. Systematic study of the dynamics and half-lives of newly synthesized proteins in human cells. *Chem. Sci.* **7**, 1393–1400 (2016).

36. Pichon, C., Gonçalves, C. & Midoux, P. Histidine-rich peptides and polymers for nucleic acids delivery. *Adv. Drug Deliv. Rev*. **53,** 75–94 (2001).

37. Putnam, D., Gentry, C. A., Pack, D. W. & Langer, R. Polymer-based gene delivery with low cytotoxicity by a unique balance of side-chain termini. *Proc. Natl. Acad. Sci. U. S. A.* **98**, 1200–1205 (2001).

38. Jin, H. *et al.* Urocanic acid-modified chitosan-mediated PTEN delivery via aerosol suppressed lung tumorigenesis in K-rasLA1 mice. *Cancer Gene Ther.* **15**, 275–283 (2008).

39. N. Danilovtseva, E. *et al.* Poly(1-vinylimidazole) Prospects in Gene Delivery. *Chinese J. Polym. Sci. 2019 377* **37**, 637–645 (2019).

40. Midoux, P., Pichon, C., Yaouanc, J. J. & Jaffrès, P. A. Chemical vectors for gene delivery: A current review on polymers, peptides and lipids containing histidine or imidazole as nucleic acids carriers. *Br. J. Pharmacol.* **157**, 166–178 (2009).

41. Allen, J. C. Biochemistry of the polyamines. *Cell Biochem. Funct.* **1**, 131–140 (1983).

42. Jere, D. *et al.* Akt1 silencing efficiencies in lung cancer cells by sh/si/ssiRNA transfection using a reductable polyspermine carrier. *Biomaterials* **30**, 1635–1647 (2009).

43. Jiang, H. L. *et al.* Chitosan-graft-spermine as a gene carrier in vitro and in vivo. *Eur. J. Pharm. Biopharm.* **77**, 36–42 (2011).

44. Hosseinkhani, H., Azzam, T., Tabata, Y. & Domb, A. J. Dextran-spermine polycation: An efficient nonviral vector for in vitro and in vivo gene transfection. *Gene Ther.* **11**, 194–203 (2004).

45. Höbel, S. & Aigner, A. Polyethylenimines for siRNA and miRNA delivery in vivo. *Wiley Interdiscip. Rev. Nanomedicine Nanobiotechnology* **5**, 484–501 (2013).

46. Magriotis, P. A. Recent progress toward the asymmetric synthesis of carbon-substituted piperazine pharmacophores and oxidative related heterocycles. *RSC Med Chem* **11**, 745–759 (2020).

47. Whitehead, K. A. *et al.* Degradable lipid nanoparticles with predictable in vivo siRNA delivery activity. *Nat. Commun.* **5**, (2014).

48. Ni, H. *et al.* Piperazine-derived lipid nanoparticles deliver mRNA to immune cells in vivo. *Nat. Commun.* **13**, 1–9 (2022).

49. Capel, V. *et al.* Water-soluble substituted chitosan derivatives as technology platform for inhalation delivery of siRNA. *Drug Deliv.* **25**, 644 (2018).

50. Traut, R. R. *et al.* Methyl 4-Mercaptobutyrimidate as a Cleavable Gross-Linking Reagent and Its Application to the Escherichia coli 30S Ribosome. *Biochemistry* **12**, 3266–3273 (1973).

51. Cui, L. *et al.* Conjugation chemistry through acetals toward a dextran-based delivery system for controlled release of siRNA. *J. Am. Chem. Soc.* **134**, 15840–15848 (2012).

Chapter 4:

Synthesis of polyallylamine-based carriers for siRNA delivery

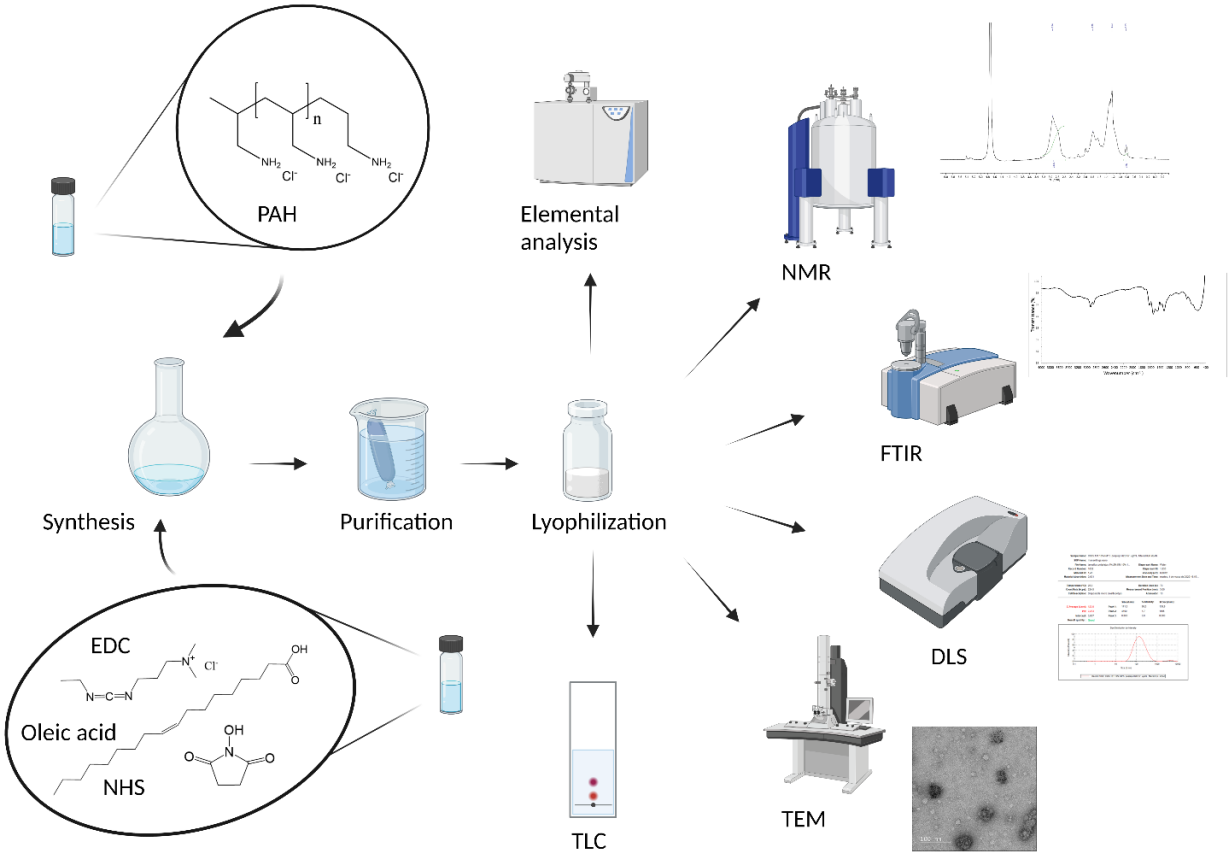

4.1 Introduction

As highlighted throughout this thesis, new biomaterials for siRNA delivery beyond the liver are needed to reach tissues or tumours only accessible by intravenous injection. Polymers have a great potential to fill this gap due to their versatility, ease of synthesis, modification, and scalability. Considering the poor delivery efficiency obtained with dextran functionalized with different amine groups explained in Chapter 3, cationic polymers were chosen as next strategy. Polycations have been studied along the last decades and have shown good complexation and release of siRNA. Polyplex formation between siRNAs and polycations results from the electrostatic interaction of positively charged amines groups from the polymers with the negatively charged phosphate groups of the nucleic acid.

Among the cationic polymers less explored for nucleic acid delivery we find polyallylamine (PAH). PAH is a synthetic linear polymer with one primary amine in each monomer units (See Figure 4.1). Polyallylamine respond to pH[1], it is highly hygroscopic, and commonly commercialized in its salt form of polyallylamine hydrochloride (PAH). Its high density of amines brings the capacity to complex pDNA and siRNA[1,2,3]. However, the delivery efficiency reported for PAH so far has been relatively low and often associated with significant cytotoxicity, as consequence of its positive charge. Several modifications of the cationic pendant chain of PAH have been investigated to improve the release of the siRNA inside the cells, e.g. cholesterol[4,5], methylglycolate[2] and several acrylates[6], and thus improving transfection efficiency.

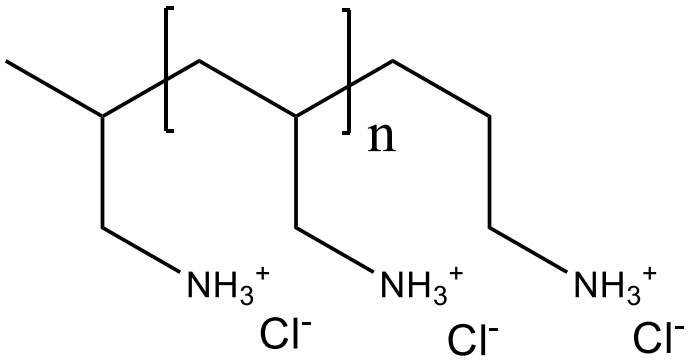

Figure 4. 1.-Scheme of chemical structure of polyallylamine hydrochloride (PAH). n = repeating units, depending on the molecular weight.

Grafting aliphatic chains of different length to cationic polymers, such as the well-studied polyethyleneimine, has proved to improve nucleic acid delivery[7,8]. Actually, *lipidoids* or cationic lipid libraries have been created using small amino molecules composed of 1 to 6 amines (putrescine, N-Propylethylenediamine, 1-(2-Aminoethyl)piperidine) conjugated to aliphatic chains, saturated or unsaturated, from C10 to C18 length. Those candidates have been tested to look for the best efficient cationic lipid in terms of siRNA delivery[9,10,11,12,13]. Lately, they have been formulated together with other lipids forming lipid nanoparticles (LNPs) and liposomes.

The role of lipids in the enhancement of small amines and polyamines as efficient siRNA carriers has been clearly demonstrated. However, polyallylamine modified with aliphatic chains has not been studied as siRNA vector yet.

In order to improve the transfection efficiency of polyallylamine-based vectors of siRNA, oleic acid (C18) was selected to modify the polycation. To study the influence of the aliphatic chain on complexation and transfection, polyallylamines with different degree of substitution of oleic acid have been produced by carbodiimide chemistry. The new materials were evaluated in terms of size, surface charge, siRNA encapsulation efficiency, cell uptake, cytotoxicity and protein knockdown. This study was divided in two chapters, Chapter 4, where the synthesis and characterization of the different materials are explained as well as the study of the interaction with siRNA and Chapter 5 to cover the biological studies of the resulting polyplexes.

4.2 Results and discussion

4.2.1 Synthesis of oleic acid substitutions of polyallylamine

PAH (~17.5 KDa) was covalently modified with oleic acid via amide bonds using carbodiimide chemistry. 5 different molar substitutions were targeted with increasing amounts of oleic acid, i.e. 5 different ratios of amine from PAH to carboxylates from oleic acid: NH_2: COOH at 1:0.01, 1:0.02, 1:0.05, 1:0.1 and 1:0.2. The polymers were named as its expected degree of substitution, PAH.OA.1, PAH.OA.2, PAH.OA.5, PAH.OA.10 and PAH.OA.20, respectively. Hereafter, polymers will be mentioned as their names, despite the DS obtained is not exactly matching the expected one. The synthesis protocol followed was inspired from previous works[14,15,16,17] for other functionalization of polyamines with aliphatic chains, including some modifications to adapt to OA characteristics. The synthesis was performed as follows: The different amounts of oleic acid were firstly activated with 1-Ethyl-3-(3-dimethylaminopropyl) carbodiimide (EDC) and n-hydroxysuccinimide (NHS) 30 minutes in DMSO in a molar ratio of NHS/EDC: COOH 10:1. The resulting succinimidyl oleate is reactive with primary amines of the polyallylamine, which was added dropwise dissolved in water to the DMSO solution. The mixture was stirred during 3 days at 37ºC. These two solvents were found to be the best option in terms of solubility, as polyallylamine homopolymer is poorly dissolved in any other solvent than water. For the same reason, the polymer aqueous solution was added dropwise to the DMSO solution to avoid solubility issues as much as possible (Figure 4.2).

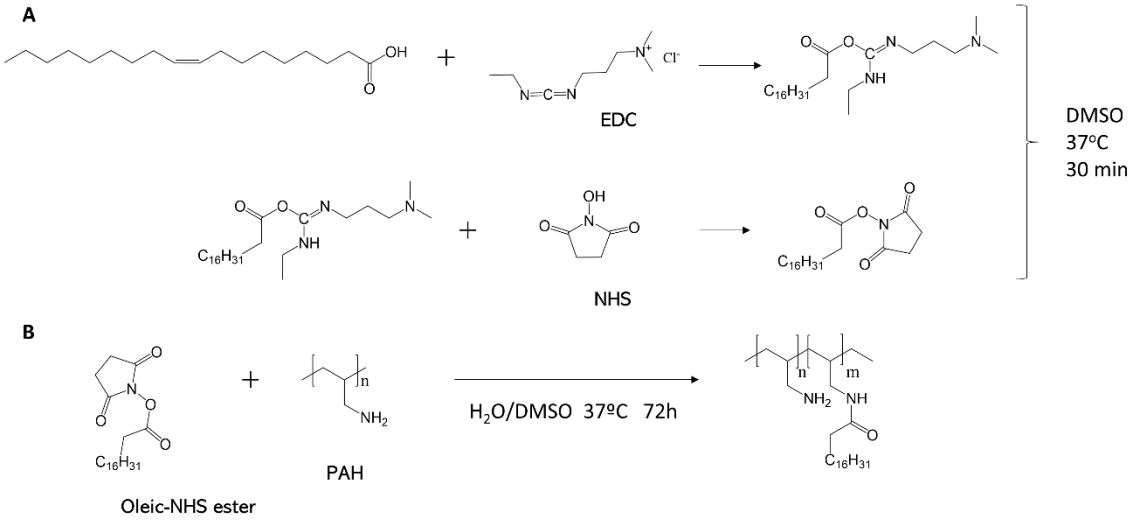

Figure 4. 2.-Schematic representation of the functionalization reaction of PAH with OA using carbodiimide chemical route assisted by 1-Ethyl-3-(3-dimethylaminopropyl) carbodiimide (EDC) and n-hydroxysuccinimide (NHS). **A)** Firstly, Succinimidyl oleate is formed by the coupling of carbodiimide to the oleic acid, followed by succinidime attachment. **B)** Later, polyallylamine dissolve in water was added dropwise to the oleate mixture to form oleic acid-functionalized polyallylamine (PAH.OA).

Then, the reaction mixture was purified by intensive dialysis against ultrapure water with a cut-off membrane of 3.5 KDa to eliminate the non-reacted oleic acid, EDC, NHS and possible by-products. The dialysis process was sustained over a period of 10 days until the conductivity of the water reached values equivalent to those of the pure water, indicating the successful elimination of undesired products or impurities. After dialysis, the purified product was freeze dried, obtaining a white, cotton-like, solid and stored at 4°C prior its use.

4.2.2 Characterization of oleic acid-functionalized polyallylamine

The slight turbidity observed for the different freeze-dried PAH-OA in water indicated that the functionalized polymers were not fully soluble, because of the hydrophobicity conferred by the grafted oleic acid. Different organic solvents, DMSO, ethanol, methanol, chloroform, ethyl acetate, acetone and mixtures ethanol/water and DMSO/water were attempted to dissolve the functionalized PAH-OA. However, the best results in terms of solubility were acquired in water. The slight turbidity observed in aqueous solution indicates the self-assembly of the PAH.OA via hydrophobic interactions between the OA functional groups.

Firstly, thin layer chromatography (TLC, See Appendix II for fundamentals of the technique) was carried out to determine the presence of free oleic acid in the samples purified by dialysis (Figure 4.3). In TLC, the mobile phase (Hexane:Ethyl acetate, see material and methods 4.4) drags the unreacted OA while the PAH is trapped in the silica. Then, potassium permanganate ($KMnO_4$) is used to stain both molecules. Figure 4.3 shows that free oleic acid could not be observed for polyallylamine derivatives. Thus, the dialysis process can be considered to have been sufficient to remove all, or at least most, of the unreacted OA.

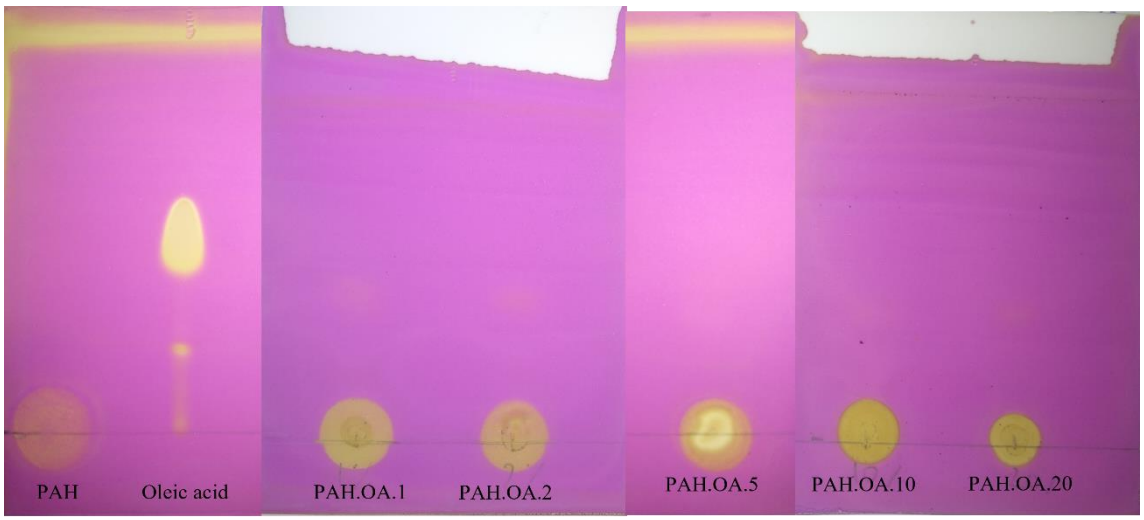

Figure 4. 3.-Thin layer chromatography of PAH (dissolved in pure H_2O), Oleic acid (MeOH), PAH.OA substitutions (pure H_2O) using a Hexane:ethyl acetate: acetic acid solution at 80:19:1 molar ratio as mobile phase and silica gel as stationary phase.

Fourier transformed infrared (FT-IR) spectroscopy has been used to identify the chemical groups for polyallylamine oleic acid derivatives (PAH.OA.1, PAH.OA.2, PAH.OA.5 PAH.OA.10, and PAH.OA.20) and compared to PAH and OA alone (Figure 4.4). The band observed at 2900 cm^{-1} corresponding to the stretching vibrations of -CH_2-CH- bonds appeared as a broad peak in PAH, while the two sharp peaks at 2850 cm^{-1} and 2920 cm^{-1}, corresponding to -CH_2-CH_3 and -CH_2-CH_2- stretching vibrations were attributed to the oleic acid. Thus, the presence of those signals from OA on the purified samples confirmed that the functionalization of PAH has been successful. Interestingly, the intensity of these peaks in the spectra of PAH.OA derivatives appear to increase with the quantity of oleic acid grafted onto the polyallylamine backbone. However, FTIR spectroscopy cannot provide a quantitative analysis without the use of a reference standard. More importantly, a broad band in the range 3400-3200 cm^{-1} is observed for PAH and PAH.OA polymers, corresponding to N-H and O-H stretching, but not for free OA, as no amine groups neither water are present in the sample. Additionally, the carbonyl group (C=O) of free OA displayed a signal at 1700 cm^{-1}. In the PAH.OA derivatives, the carbonyl group forms part of the amide bond resulting from the functionalization and was shifted to 1736 cm^{-1}. In conclusion, the FTIR studies confirm the successful grafting of OA on polyallylamine via amide coupling. However, a quantitative analysis could not be obtained with that technique to determine the degree of substitution of OA on PAH.

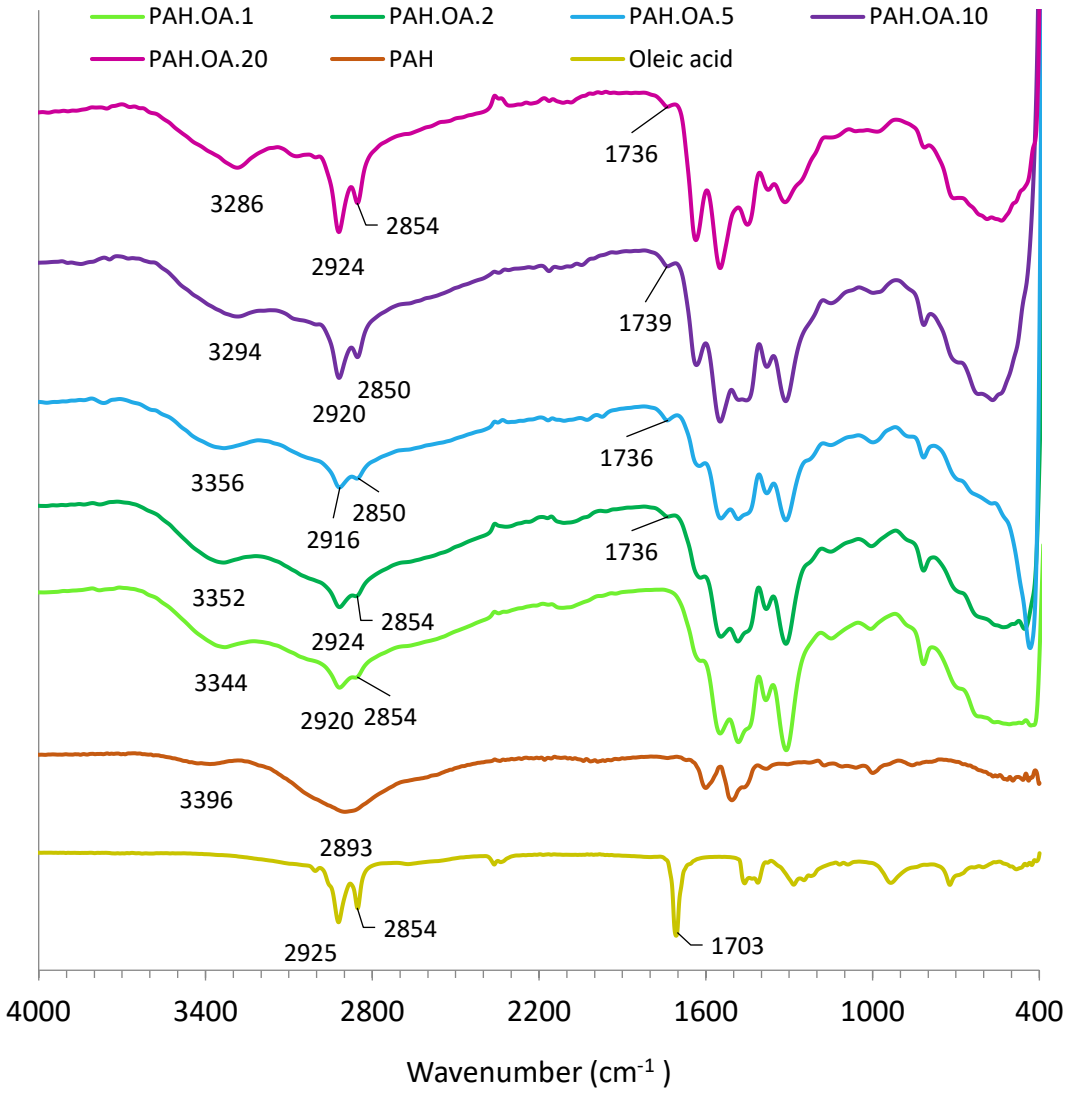

Figure 4. 4.-Fourier Transform Infrared (FT-IR) spectra of various polyallylamine oleic acid (PAH.OA) derivatives. The spectra are presented as a plot of the percentage of transmittance versus wavenumber (cm^{-1}). Key vibrational peaks, denoting distinct molecular vibrations, are labelled directly on the graph.

The PAH derivatives were further characterized using ^{1}H-NMR spectroscopy. Despite the observed aggregation in water, these studies were performed in deuterium oxide (D_2O), acknowledging that the ^{1}H-NMR results might potentially underestimate the OA DS due to the lack of solubility conferred by OA substitution. Both, the unmodified PAH and the oleic acid, dissolved in D_2O and deuterated methanol (MeOD) respectively, were also characterized by ^{1}H-NMR to provide reference spectra. The stacked ^{1}H-NMR spectra of the different PAH.OA derivatives are depicted in Figure 4.5.

Pristine PAH dissolved in D_2O presents 3 main peaks at 1.5 ppm (m, 2H, -CH_2-), 2.1 ppm (m, 1H, -CH-) and 3.0 ppm (m,2H, -CH_2-NH_2). Free OA in MeOD presents 6 peaks at 0.9 ppm (t, 3H,-CH_3), 1.33 ppm (d, 20H,-$(CH_2)_n$-), 1.6 ppm (t, 2H, -(CH_2-CH_2-C=O), 2.0 ppm (d, 4H, -CH_2-HC=CH), 2.29 ppm (t, 2H, -CH_2-C=O) and 5.30 ppm (t, 2H, HC=CH).

While PAH is highly soluble in water, it was previously mentioned that PAH.OA exhibited turbidity in aqueous solution. More importantly, the solubility in water appeared to decrease with higher amount of oleic acid attached to the polymer chain, especially evidenced for PAH.OA.20.

On the ^{1}H-NMR spectrum, PAH.OA modified polymers present characteristic peaks corresponding to both molecules. Despite the clear overlapping of some peak at 1.33, 1.6, 2.0 and 2.29 ppm, the signal at 0.9 ppm corresponding to methyl group of oleic acid was sufficiently separated from the signal corresponding to the protons of the PAH backbone at 3.0 ppm to allow the quantification of the amount of OA grafted. In addition, this peak at 3.0 ppm integrates for modified and unmodified PAH monomers units. Thus, the integration of this peak has been used to calculate the degree of substitution (%DS) of oleic acid in polyallylamine. DS expresses the number of amines, or monomer units, substituted with OA compared to the total number of amines, or monomer, present in the polymer. Thus, a polymer with a degree of substitution of 10% means that 10% of the repeating units of the PAH polymer have been modified with OA. The calculations of DS for different PAH derivatives are described in the Appendix IV.

The degree of substitution of every polymer was calculated (Figure 4.5): 1%, 2%, 6%, 14% and >14% DS for PAH.OA.1, PAH.OA.2, PAH.OA.5, PAH.OA.10 and PAH.OA.20, respectively. Due to relatively low solubility of PAH.OA, it is important to keep in mind that these values might be underestimated.

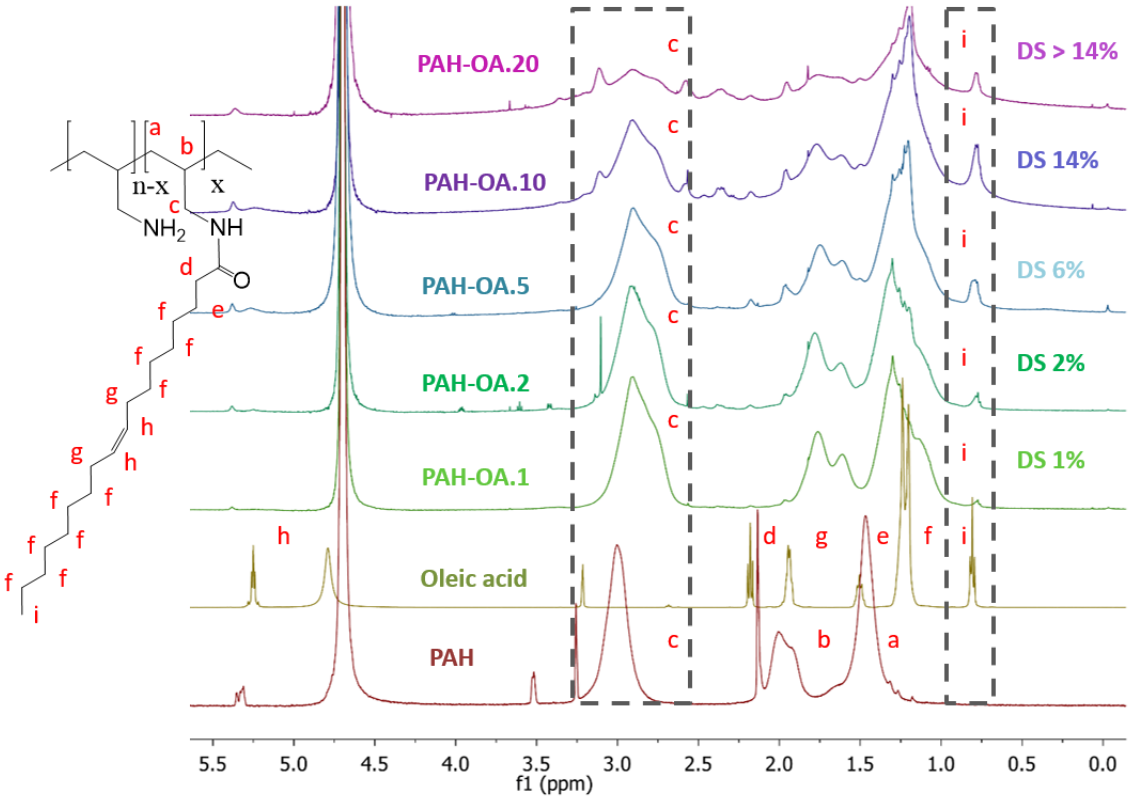

Figure 4. 5.-^{1}H-NMR spectra of PAH (D_2O), OA (MeOD) and the modified polymers: PAH.OA.1, PAH.OA.2, PAH.OA.5, PAH.OA.10 and PAH.OA.20 (D_2O). Degree of Substitution (%DS) were calculated by comparing integration from i and c peaks in the Appendix IV.

Elemental analysis measurements were performed to estimate the quantity of oleic acid grafted onto the polymer and support data found by ^{1}H NMR technique (See appendix II for fundamentals of technique). To this end, 10 mg of each sample were subjected to a comprehensive drying process under vacuum for 5 days, aimed at eliminating as much hygroscopic water as possible. The elemental analysis results, providing the weight percentage of Carbon (C), Hydrogen (H), Nitrogen (N), and Oxygen (O) in the samples, are summarized in Table 4.1.

Table 4. 1.- Elemental Analysis (CHNO) of polyallylamine and the derivatives of PAH.OA.1, PAH.OA.2, PAH.OA.5, PAH.OA.10 and PAH.OA.20. Weight percent (%W) obtained experimentally.

%W of Elements				
Polymer	**N**	**C**	**H**	**O**
PAH	**12.71**	**33.93**	**8.91**	**9.81**
PAH.OA.1	**14.37**	**44.95**	**9**	**18.77**
PAH.OA.2	**14.06**	**46.52**	**9.55**	**15.73**
PAH.OA.5	**13.06**	**47.64**	**8.91**	**16.17**
PAH.OA.10	**11.86**	**53.15**	**9.78**	**15.79**
PAH.OA.20	**10.71**	**60.1**	**10.42**	**11.37**

It is noteworthy to mention that the oxygen element should be only present in the grafted polymers. However, a considerable amount of oxygen was also detected in the pristine PAH, likely due to its hygroscopic nature and its propensity to absorb water, despite the intensive drying process. On the other hand, PAH.OA substituted polymers present a decreased hygroscopicity as the number of grafted aliphatic chains increases. As a result, the oxygen and hydrogen content cannot be reliably used to estimate the quantity of grafted oleic acid on the polymer.

On the other hand, it is worth pointing out that the amount of carbon increases with increasing amount of oleic acid substitution in the polymer, as a result from the additional 18 Carbon atoms added by the grafted OA. Nevertheless, as depicted in Table 4.1, the combined total weight of Carbon, Nitrogen, Oxygen, and Hydrogen does not account for 100% of the sample composition. Thus, it is clear that some additional elements, such as the chlorine counter ions of the protonated amines, have not been considered in the study. For this reason, the exact quantification of the degree of substitution of OA for PAH.OA cannot be determined, but only an estimation or trend can be drawn.

Other attempt to determine the DS of OA was thermal gravimetric analysis (TGA), a technique predicated on the differential decomposition temperatures of oleic acid and PAH (for a detailed explanation of the technique, refer to Appendix II). A series of samples, including PAH, OA, and all PAH.OAs, were subjected to TGA to monitor potential weight changes under increasing temperature.

As depicted in Figure 4.6, PAH displays three distinct decomposition temperatures: 200°C, 360°C, and 480°C. The initial weight loss of 5% observed at 200°C is attributed to the decomposition of lower molecular weight polymer side chains (-CH_2-NH_2). Subsequent degradation between 300°C and 430°C results in a weight loss of approximately 20%, which is associated with the decomposition of the high molecular weight polymer side chain (-CH_2-NH_2). Finally, the substantial weight loss of 75% observed at 485°C corresponds to the decomposition of the polymer backbone. This is consistent with previously reported polymer backbone/pendant chain ratios[18].

On the other hand, the main decomposition temperature of OA was observed at 150°C, 90% loss in weight. The remaining 10% decomposes between 220°C and 400°C. The first decomposition temperature of OA was thought to be sufficiently different from PAH thermal decomposition footprint to be used to determine DS.

Thus, for the PAH.OA derivatives, the decomposition profiles can be broadly divided into two groups: low oleic acid substitution (PAH.OA.1, PAH.OA.2, and PAH.OA.5) and high oleic acid substitution (PAH.OA.10 and PAH.OA.20). The low-substitution group exhibits a single decomposition stage from 100°C to 180°C, likely corresponding to the loss of oleic acid, as decomposition temperature match with the oleic acid . From 180°C to 450°C, corresponding to both grafted and ungrafted side chains (-CH_2-NH_2) of polyallylamine, approximately 60-70% of the weight is lost. While several substages are discernible within this range, they cannot be assigned to specific moieties' degradation. The final stage, from 450°C to 800°C, corresponds to the main polyallylamine chain's degradation, which occurs more slowly than in the pristine polymer, requiring higher temperatures for complete decomposition.

Highly substituted PAH.OA.10 and PAH.OA.20 do not exhibit a distinct first stage corresponding to oleic acid loss, suggesting that a high degree of grafting modifies the thermal degradation fingerprint. However, above 200°C, the decomposition follows a similar pattern to that of the low-substitution polymers. From 0°C to 450°C, decomposition occurs gradually, with up to 60% of the weight lost. From 450°C to 800°C, the polyallylamine is completely degraded.

Given the absence of a distinct oleic acid loss stage in substituted polymers, it is not possible to quantify the degree of substitution based on TGA data.

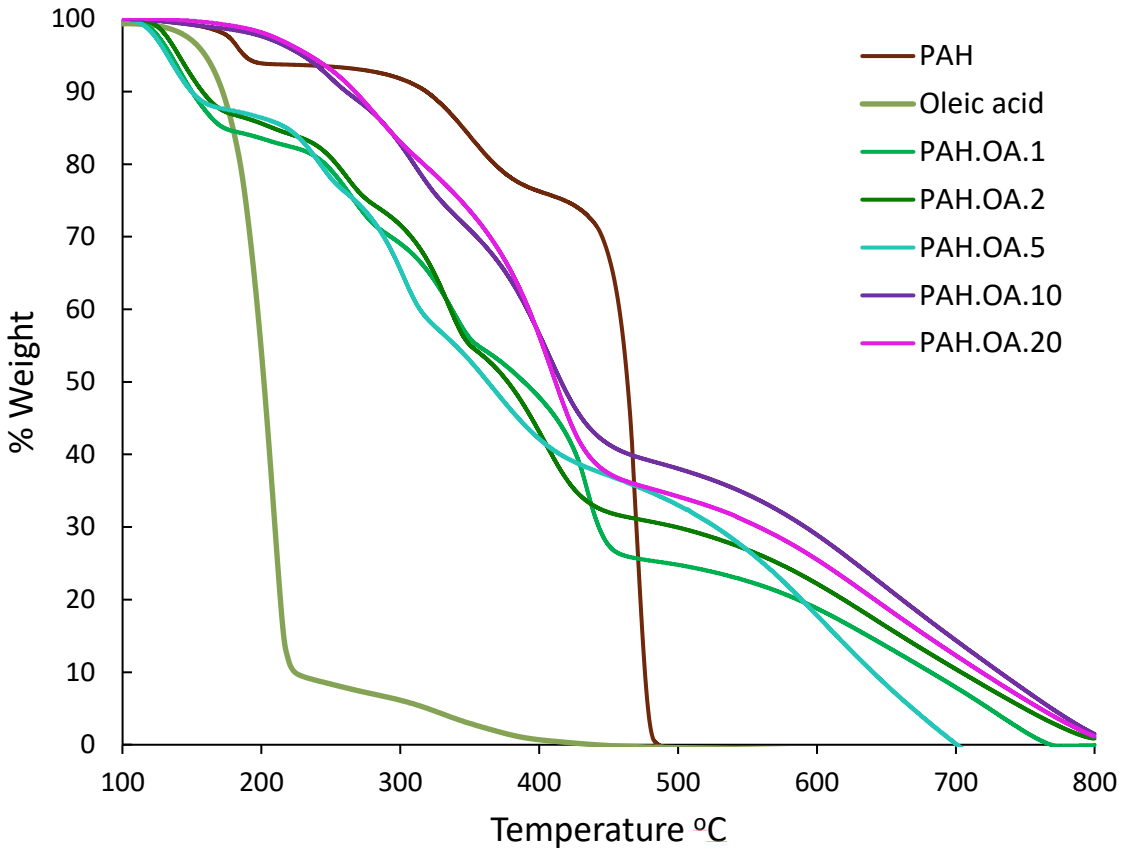

Figure 4. 6.-TGA curves of oleic acid, PAH, and PAH.OA derivatives ranging from 100°C to 800°C. Four distinct thermal decomposition patterns are observable corresponding to PAH, Oleic acid, low oleic acid substituted PAH (PAH.OA.1, PAH.OA.2 and PAH.OA.5), and high oleic acid substituted PAH (PAH.OA.10 and PAH.OA.20).

Overall, our data from various analytical techniques affirm the successful grafting of increasing quantities of oleic acid onto polyallylamine. TLC analysis revealed the absence of any free oleic acid, suggesting that all oleic acid peaks detected in ^{1}H-NMR correspond to grafted aliphatic chains. Furthermore, FTIR spectroscopy confirmed the presence of oleic acid through the progressive sharpening of peaks associated with -CH_2-CH_3 and -CH_2-CH_2 stretching vibrations.

The challenge of finding an appropriate solvent for the polymers complicated our analysis, yet an estimation of %DS of oleic acid was possible using ^{1}H-NMR in D_2O. The data from TGA and elemental analysis support these findings, demonstrating an increase in oleic acid grafting through changes in the elemental composition and shifts in thermal decomposition patterns between low- and high-substitution polymers. This comprehensive suite of techniques provides strong evidence of successful oleic acid grafting onto polyallylamine, setting the stage for exploration these modified polymers as potential siRNA vectors.

4.2.3 Characterization of nanoparticles formed by PAH.OA. substitutions

As mentioned in the previous section, the functionalization of PAH with OA affected the water solubility, conferring amphiphilic character to the polymer as the aqueous solution appeared turbid. Such turbidity is often attributed to the formation of aggregates or nanoparticles via self-assembly of the amphiphilic polymers via hydrophobic interactions among oleic acid chains. Thus, to

determine the size of those self-assembled objects dynamic light scattering (DLS) studies were carried out. The hydrodynamic diameter observed by DLS, assuming that all the self-assembled objects are spherical, for PAH, PAH.OA.1, PAH.OA.2, PAH.OA.5, PAH.OA.10 and PAH.OA.20 are shown in Table 4.2.

Table 4. 2.-DLS measurements of self-assembled nanoparticles in water of PAH.OA derivatives. Z-Average (hydrodynamic diameter in nanometres ± standard deviation)) and polydispersity index (PDI) are reported from different concentration of polymers corresponding to equivalents N/P ratios 2.5,5, 10 and 15. Z-potential (ZP) results expressed in milivolts (mV) of self-assembled nanoparticles formed by PAH.OA derivatives measured by aqueous electrophoresis. Results are shown as mean of 5 measurements ± standard deviation. Samples loaded into 700 µL of NaCl 10 mM pH 7 and measured by diffusion barrier technique.

	%DS Oleic acid	polymer concentration (µg/mL)	Z-average±SD	PDI	ZP Mean±SD (mV)
PAH	0	20	N/A	0.9	N/A
		39	N/A	1	6,05
		79	N/A	1	5,97
		118	N/A	0.956	7,07
PAH.OA.1	1	20	133±21	0.312	40.4±2
		41	170±7	0.275	42.11±2
		81	267±11	0.269	43.5±1
		121	311±18	0.23	40.3±1
PAH.OA.2	2	21	178±13	0.174	40.5±2
		42	249±21	0.196	43.8±2
		89	322±13	0.217	42.9±2
		127	292±11	0.209	43.2±1
PAH.OA.5	6	23	93±24	0.462	33.6±2
		45	126±14	0.391	40.6±1
		91	137±2	0.405	41.9±1
		136	110±2	0.409	41.5±1
PAH.OA.10	14	28	131±9	0.447	34.4±2
		57	94±5	0.388	41.9±3
		113	117±1	0.43	41.6±2
		170	144±10	0.476	55.6±1
PAH.OA.20	>14	34	181±11	0.273	40.1±2
		67	122±2	0.231	40.8±2
		134	147±1	0.224	50.7±2
		201	134±1	0.211	53.7±1

Different concentrations of polymer have been used to do the measurements, corresponding to equivalent N/P ratio 2.5, 5, 10 and 15 that will be studied later. N/P ratio is explained in chapter 3, but it will have reminded later in detail, it is the relation between polymer and siRNA to form polyplexes. As protonable amines are reduced with the oleic acid substitution, different concentrations are used for the different PAH.OA derivatives to match same N/P ratio.

At a first glance, no significant differences in size is found among different concentrations corresponding for same polymer substitution. First, it is important to point out that pristine PAH is

totally dissolved in water and does not form nanoparticles. Thus, the lack of light scattering does not allow a sufficiently good quality for DLS measurement. PAH.OA.1 and PAH.OA.2 lowest OA substitutions form particles from 100 to 300 nm and are polydispersed, PDI 0.2-0.3 approximately. PAH.OA.5 and PAH.OA.10 form smaller particles around 100 nm, (93 to 144 nm) but polydispersity increased to 0.4 approximately. PAH.OA.20 around 150 nm (from 134 to 181 nm), exhibiting a PDI of 0.2. It can be elucidated that an increase in oleic acid amount tend to form smaller nanoparticles. However, concentration does not influence in size of nanoparticles, at least for the concentrations studied, ranging from 20 to 200 μg/mL. So, size depend exclusively on the type of the polymer, that in this case the difference is the amount of oleic acid. These results suggest that polymers with a higher hydrophobic payload could shield the hydrophobic domains from water more effectively due to stronger hydrophobic interactions. This data aligns well with previous studies on PAH substitutions with other hydrophobic groups, further reinforcing our findings[15].

Zeta potential, a measure of the surface charge of a particle, critically reflects the particle's interactions with its environment. It is calculated from the electric potential generated in the outer layer of ions that envelop the nanoparticles. Detailed principles of zeta potential measurements are discussed in Appendix II.

Since polyallylamine (PAH) is a polycation, it naturally exhibits a positive surface charge. The zeta potentials of PAH and its oleic acid derivatives, PAH.OA.1, PAH.OA.2, PAH.OA.5, PAH.OA.10, and PAH.OA.20, were measured under neutral pH conditions in a 10 mM NaCl solution at the same concentrations used for the Z-average measurements (See Table 4.2). Given that zeta potential measurements rely on the electrophoretic movement of particles, a prerequisite for accurate data is the presence of well-dispersed particles. As such, the zeta potential for pristine PAH could not be measured due to its complete dissolution in water. However, the self-assembled PAH.OA exhibit high positive zeta potentials, ranging from +34 to +53.7 mV, across different polymer concentrations and degrees of substitution. This observation highlights that the PAH.OA complex maintains its positive charge, even with the loss of cationic amine groups during amide bond formation.

Interestingly, higher zeta potential values were observed at higher concentrations for PAH.OA.10 and PAH.OA.20 compared to PAH.OA.1, PAH.OA.2, and PAH.OA.5, despite number of protonable amines were kept constant among different derivatives to maintain same N/P ratios. This phenomenon can be rationalized by the increased stabilization of polymer assembly due to lipid interactions, leading to better-defined particles and subsequently a higher net zeta potential. As PAH is totally dissolved in water and does not scatter the light, the less oleic acid substitution the more moieties of the complex are dissolved in water, scattering light in a poorer way. Additionally, lipid moieties in the complex may shield cationic charges, preventing their repulsive interactions and thus stabilizing the complex[8]. This increase in internal hydrophobic interactions can potentially lead to a displacement of positive charges from the inner to the outer layers of the complex, rendering the surface more positive[19].

Transmission electron microscopy (TEM) was employed to examine the morphology, size, polydispersity, and degree of aggregation of PAH.OA derivatives. These observations were made

after staining the samples with ammonium molybdate 12% w/v pH 7 to provide contrast against the grid background. Detailed principles of this technique are provided in Appendix II.

The concentrations of polymer for an N/P ratio of 10 for each polymer were selected for imaging. The resulting micrographs are presented in Figure 4.7. The pristine PAH did not form any discernible nanoparticles, resulting in an amorphous structure. Conversely, the substituted PAH.OA polymers exhibited a formation of spherical nanoparticles. The low substituted polymers, PAH.OA.1 and PAH.OA.2, displayed larger sizes, with an average of approximately 30 nm. In contrast, the more densely substituted polymers, PAH.OA.5, PAH.OA.10 and PAH.OA.20, formed smaller nanoparticles, averaging around 10 nm. However, larger aggregates were also noted in these samples, ranging from 50 to 150 nm as determined by TEM imaging. This finding aligns well with the DLS data (93 to 181 nm). One potential aspect contributing to these observed sizes may be the loss of water during the drying process, which would reduce the sample size. Therefore, DLS measurements are referred to as "hydrodynamic". In addition, DLS measurements are an intensity-based technique. Consequently, larger aggregates, which scatter light more intensively than smaller particles, can give the impression of an oversized sample.

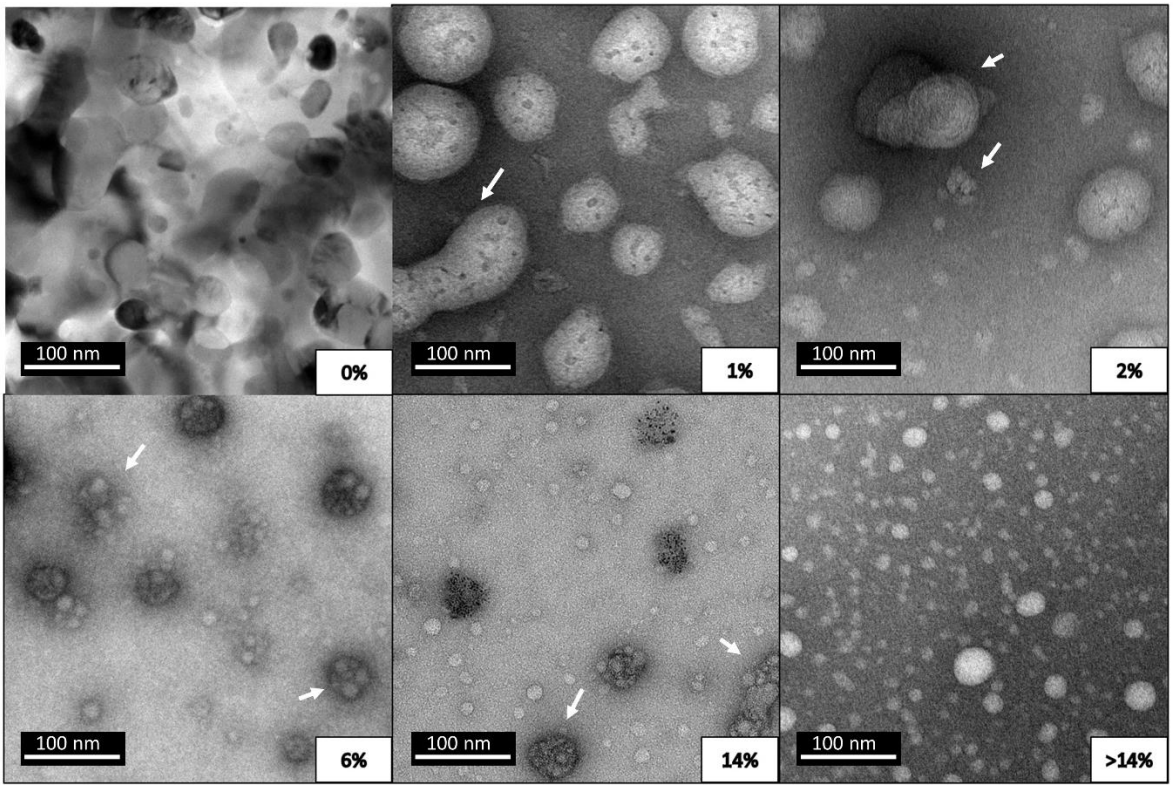

Figure 4. 7.-Transmission electronic micrographs of PAH.OA polymers dissolved in water at 100 µg/ml filtered 0.44 µm and stained with ammonium molybdate pH 7 12% w/v. Images representing different percentage of oleic acid substitution A-F: PAH, PAH.OA.1(1%), PAH.OA.2(2%), PAH.OA.5(6%), PAH.OA.10(14%) and PAH.OA.20 (>14%). Aggregates are indicated with white arrows.

The advanced techniques such as small-angle x-ray scattering (SAXS) or small-angle neutron scattering (SANS) would indeed provide insightful data regarding the potential micellar structure of PAH-oleic acid derivatives. However, the techniques employed in this study provide sufficient evidence to speculate about the particle formation process in aqueous media, as depicted in Figure

4.8. The oleic acid molecules seem to orient inward, forming a hydrophobic core that resists interaction with water. This core is maintained by hydrophobic interactions among the oleic acid chains. As evidenced by DLS measurements, an increase in oleic acid content leads to further compaction of the chains, resulting in smaller particle sizes. As observed through TEM, the size of these compacted particles is approximately 10 nm. However, these particles tend to aggregate, forming larger structures that range in size from 50 to 100 nm.

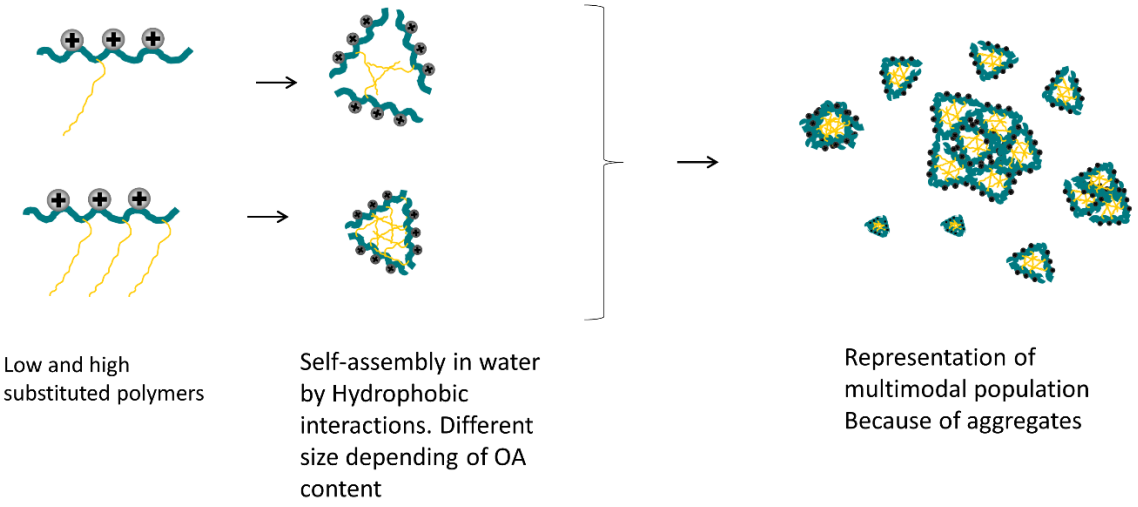

Figure 4. 8.-Schematic of the self-assembly process of polyallylamine nanoparticles grafted with oleic acid. A first stage of hydrophobic interaction occurs when polymer is dissolved in water. An assemble into a nanoparticle happens due to the strength of hydrophobic interactions. Nanoparticles formed aggregate in larger structures. This explanation is based on DLS and TEM results.

4.2.4 Complexation of siRNA by PAH.OA. substitutions

To assess the complexation capacity of oleic acid-polyallylamine (PAH.OA) derivatives with siRNA, various N/P ratios were explored. N/P ratio, which stands for nitrogen/phosphorus ratio, is a crucial determinant of the complexation efficiency and cytocompatibility of the resulting complexes, often called polyplexes. The N/P ratio represents the ratio of the number of moles of ionizable (protonable) amines present in the polymer to the number of moles of phosphate groups in the siRNA. These protonable amines form electrostatic interactions with the negatively charged phosphate backbone of the siRNA, facilitating the formation of polyplexes.

Choosing the right N/P ratio is critical: too low a ratio might result in inadequate siRNA entrapment, while too high a ratio could potentially affect cell viability due to an excess of cationic groups. Therefore, we tested four different N/P ratios—2.5, 5, 10, and 15—to establish the optimal balance.

For each N/P ratio tested, the amount of siRNA was kept constant at $1x10^{-4}$ µmol, while the amount of PAH.OA was varied accordingly. This approach allowed us to evaluate the influence of varying N/P ratios on the complexation capacity of the PAH.OA derivatives. The quantity of polymer necessary to every N/P ratio has been calculated from N/P ratio equation:

$$\frac{N}{P} = \frac{mol\ polymer\ x\ nº\ of\ protonable\ amines}{mol\ siRNA\ x\ nº\ of\ phosphates} \qquad \textbf{equation 4.2.4.1}$$

$$mol\ polymer = \frac{mol\ siRNA\ x\ nº\ of\ phosphates\ x \frac{N}{P} ratio}{nº\ of\ protonable\ amines}$$

SiRNA typically comprises a duplex oligonucleotide that is 16-23 base-pairs (bp) long, with an average length of 21 bp. This means that a duplex of 21 bp siRNA contains 42 phosphate groups, considering one phosphate group per nucleotide. To determine the quantity of protonable amines in the polymer, it is necessary to subtract the number of amide groups formed post-oleic acid grafting from the total number of Nitrogen atoms in the polymer. The number of amide groups can be calculated by multiplying the number of monomers by the degree of substitution obtained through ^{1}H-NMR for PAH.OA. An example for N/P 10 is given below for PAH.OA.10 using equation 4.2.4.1. The molar quantity for the rest of PAH.OA substitutions are shown in table 4.3:

$$187\ amines \qquad \text{PAH mol} = \frac{1x10^{-4}\mu mol\ x\ 42\ x\ 10}{187} = 2.245x10^{-4}\ \mu mol$$

$$PAH.OA.10\ \%DS\ 14\ x\ 187 = 26.\ \ 187 - 26 = 161\ amines$$

$$PAH.OA.10 = \frac{1x10^{-4}\mu mol\ x\ 42\ x\ 10}{161} = 2.61x10^{-4}\mu mol$$

In order to calculate the weight of the polymer to be added, the quantities derived above are multiplied by the respective molecular weights of each polymer.

The assembly of polyplexes and their subsequent analysis using DLS and TEM provided insights into their size and morphology, as detailed in Table 4.3 and Figure 4.9. The Z-potential also was determined (Table 4.3) to assess the surface charge and to compare with the self-assembled nanoparticles from substituted polymers (See Table 4.2). At a first glance, there is little variations across different N/P ratios any given oleic acid substitutions. Notably, pristine PAH formed nanoparticles in the presence of siRNA, exhibiting a hydrodynamic diameter ranging from 101 to 123 nm and a PDI between 0.28-0.43.

Regarding PAH.OA.1 and PAH.OA.2, a reduction in size and polydispersity was observed for the corresponding polyplexes in the presence siRNA compared to the modified polymers in aqueous solution (Table 4.2). PAH.OA.1 polymer exhibited a hydrodynamic diameter ranging from 133 to 311 nm with a PDI between 0.23 and 0.31 at varying concentrations. However, the corresponding polyplexes at different N/P ratios displayed a hydrodynamic diameter between 162 and 207 nm with a narrower PDI range of 0.12 to 0.15. The higher N/Ps showed a major reduction in size. Similarly, PAH.OA.2 polymer in aqueous solution resulted in nanoparticles have been also slightly reduced in size from 178-322 nm to 215-256 nm and PDI from 0.17-0.21 to 0.11-0.28. These results suggest that the self-assembled nanoparticles of PAH substituted with a low amount of OA undergo

reorganization due to electrostatic interaction in the presence of siRNA, leading to smaller, more compact nanoparticles.

On the other hand, PAH substituted with a higher degree of oleic acid (i.e., PAH.OA.5, PAH.OA.10, and PAH.OA.20) displayed minimal changes upon the addition of siRNA. However, a reduction in PDI when comparing polymers and polyplexes was noted, indicating a decrease in polydispersity (Table 4.3). Despite this, the PDI remained relatively high, suggesting that size changes may not be significant.

Specifically, PAH.OA.5 polymer sizes ranged from 93 to 137 nm, and polyplexes ranged from 120 to 178 nm. PAH.OA.10 showed a size range from 94 - 144 nm, with polyplexes ranging from 123-132 nm. PAH.OA.20 polymers measured between 122-181 nm, and polyplexes were between 122-142 nm. In the case of highly substituted polymers, the polyplexes did not show a smaller size than the polymers themselves, which was contrary to the lower substituted versions. It appears there is a limit to the compaction of the polymer chains, which is reached by PAH.OA.5, PAH.OA.10, and PAH.OA.20. Therefore, it is likely that siRNA may not further compact the polymer chains.

The Z-potential of polyplexes was determined by aqueous electrophoresis (see Table 4.3). It was found that pristine PAH-based polyplexes exhibited a positive zeta potential, which varied between +15.9 and +31 mV. Unlike PAH alone, these polyplexes formed nanoparticles and it was possible to measure the zeta potential. Polyplexes constituted with PAH.OA.1 and PAH.OA.2 displayed marginally higher positive zeta potential values relative to PAH, ranging from +22.7 to +35 mV.

On the other hand, polyplexes obtained with PAH.OA.5, PAH.OA.10, and PAH.OA.20 exhibited negative charge for N/P ratio 2.5 at -20, -9.12, and -1 mV, respectively. However, for N/P 5, 10 and 15 the Z-potential turns more positive than PAH. In N/P 2.5 low amount of polymer is added, thus more quantity of siRNA is located over the surface of the polyplex achieving negative Z-potentials. When the amount of polymer respect to siRNA increases, the more polymer is facing out the complex and siRNA is entrapped between polymer chains.

For a constant N/P, it appears that a trend to increased Z-potential is observed with higher oleic acid substitution. For instance, at an N/P ratio 10 polyplex showed an increasing Z-potential value from +22.6, +32.4, +35, +32.8, +40.7 and +47.1 for PAH, PAH.OA.1, PAH.OA.2, PAH.OA.5, PAH.OA.10 and PAH.OA.20, respectively. As discussed in section 4.2.3 concerning polymers, despite same number of protonable amines are present in the solution, it seems that higher oleic acid substitution confers a more positive surface charge than lower OA substitutions. This can be attributed to lipid interactions that stabilize the polymer assembly, making more defined particles, fact that is further emphasized by the presence of siRNA.

In general, the polymers and polyplexes exhibit highly positive Z-potential values. This was to be expected, due to the high density of primary amines in the polyallylamine. However, when comparing the same concentration of a particular OA derivative for both the polyplex and the polymer, a reduction in surface charge is noted, likely due to the addition of siRNA.

Table 4. 3.-Polyplexes at N/P ratios 2.5, 5, 10 and 15. Amount of polymer necessary for $1x10^{-4}$ µmol siRNA to match the N/P ratio. Z-Average (hydrodynamic diameter in nanometers ± standard deviation)), polydispersity index (PDI) and Z-potential from polyplex.

	%DS Oleic acid	N/P	polymer (µmol)	polymer (µg)	Concentration polymer for DLS (ug/mL)	Z-average mean ±SD	PDI	ZP mean±SD (mV)
PAH	0	2,5	$5,61x10^{-05}$	0.98	20	123±6	0.429	31.1±2
		5	$1,12x10^{-04}$	1.97	39	154±5	0.394	23.3±3
		10	$2,25x10^{-04}$	3.93	79	141±3	0.409	22.6±4
		15	$3,37x10^{-04}$	5.90	118	101±8	0.278	15.9±1
PAH.OA.1	1	2,5	$5,68x10^{-05}$	1.14	20	162±13	0.147	22.7±4
		5	$1,14x10^{-04}$	2.29	41	169±5	0.123	32.1±1
		10	$2,27x10^{-04}$	4.57	81	207±29	0.119	32.4±2
		15	$3,41x10^{-04}$	6.86	121	201±11	0.133	33.1±2
PAH.OA.2	2	2,5	$5,74x10^{-05}$	1.16	21	256±4	0.279	30.2±2
		5	$1,15x10^{-04}$	2.31	42	198±10	0.209	30.5±2
		10	$2,30x10^{-04}$	4.62	89	233±6	0.205	35±3
		15	$3,44x10^{-04}$	6.93	127	215±6	0.11	34±2
PAH.OA.5	6	2,5	$5,97x10^{-05}$	1.26	23	120±18	0.264	-20±1
		5	$1,19x10^{-04}$	2.53	45	137±4	0.209	27.9±3
		10	$2,39x10^{-04}$	5.06	91	178±7	0.405	32.8±2
		15	$3,58x10^{-04}$	7.59	136	150±2	0.348	33.8±2
PAH.OA.10	14	2,5	$6,52x10^{-05}$	1.49	28	132±1	0.205	-9.12±6
		5	$1,30x10^{-04}$	2.97	57	123±2	0.273	36.7±1
		10	$2,61x10^{-04}$	5.94	113	133±3	0.261	40.7±3
		15	$3,91x10^{-04}$	8.92	170	131±2	0.375	39.8±1
PAH.OA.20	>14	2,5	$7,00x10^{-05}$	1.78	34	122±3	0.168	-1±6
		5	$1,40x10^{-04}$	3.56	67	116±3	0.206	35.1±3
		10	$2,80x10^{-04}$	7.12	134	136±6	0.279	47.1±2
		15	$4,20x10^{-04}$	10.68	201	142±3	0.233	49.7±5

As it was done for the self-assembled polymer nanoparticles, polyplexes were observed under transmission electron microscope after being stained with ammonium molybdate 12% w/v, pH 7. Micrographs of polyplexes formed with PAH, PAH.OA.1, PAH.OA.2, PAH.OA.5, PAH.OA.10 and PAH.OA.20 at N/P ratio 10 are shown in Figure 4.9.

PAH-based polyplexes displayed a round-shaped nanoparticles with a diameter from 20 to 80 nm in size (Figura 4.9.-A). Nanoparticles have absorbed molybdate in contrast to oleic acid substitutions due to there is no hydrophobic core preventing the entry of water.

Polyplexes with low OA substitutions, specifically PAH.OA.1 and PAH.OA.2, exhibited a smaller size compared to their corresponding self-assembled polymers. The average size was determined to range from 10 nm to 30 nm, based on measurements taken over a sample of 100 particles. It is

important to mention that aggregated polyplexes were also observed by TEM but could not be appreciated in Figure 4.9.-B and 4.9.-C.

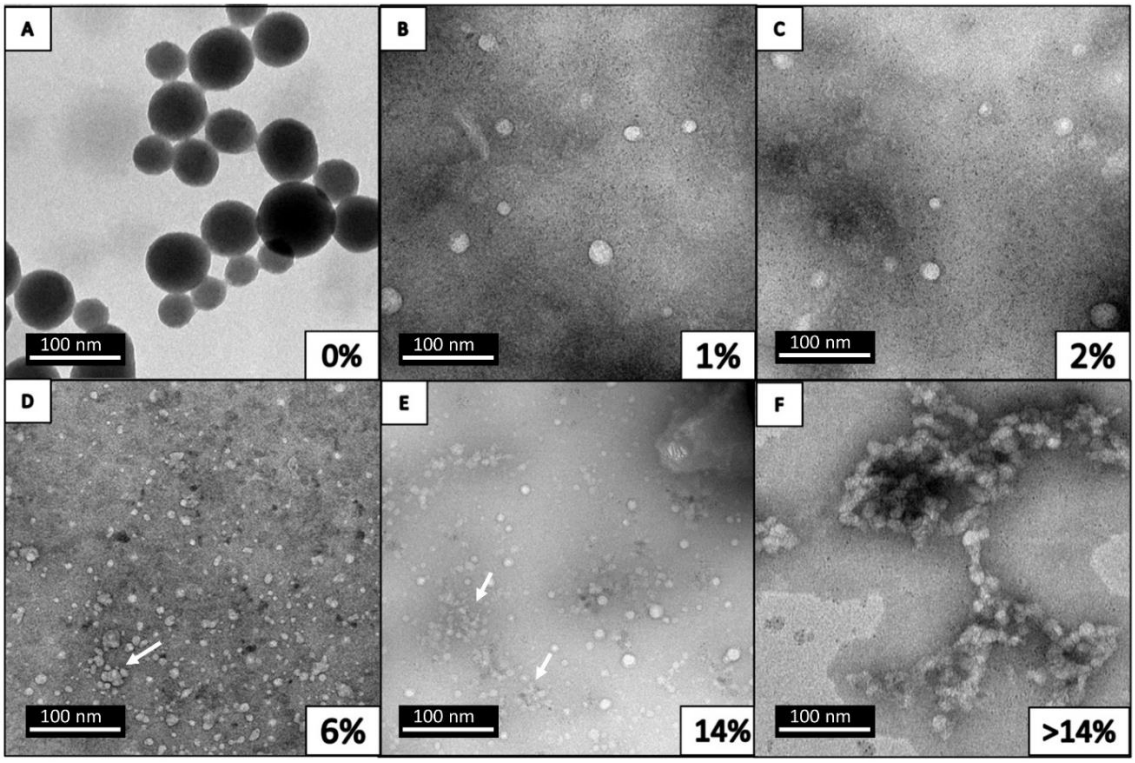

Figure 4. 9.-Transmission electronic micrographs of PAH.OA/siRNA polyplexes dissolved in water at 100 µg/ml filtered 0.44 µm and stained with ammonium molybdate pH 7 12% w/v. Images representing different percentage of oleic acid substitution A-F: PAH, PAH.OA.1(1%), PAH.OA.2(2%), PAH.OA.5(6%), PAH.OA.10(14%) and PAH.OA.20 (>14%). White arrows indicate aggregates. In the case of PAH.OA.20 (>14%) aggregates were found over all the sample.

On the other hand, the size of polyplexes formed by PAH.OA.5, PAH.OA.10 and PAH.OA.20 did not change significantly compared to the corresponding self-assembled polymers. The diameter of the polymers was 10 nm, whereas the corresponding polyplexes measured 12 nm, based on a count of 100 nanoparticles. However, it is clear from the TEM images in Figure 4.9.-D, 4.9.-E, 4.9.-F that, despite their small and spherical morphology, aggregates were present in the sample ranging from 100 to 300 nm. In the case of PAH.OA.20 (Figure 4.9.-F), those aggregates were present in whole area observed by TEM. The differences in size between TEM and DLS are attributable to DLS-intensity-based detection methodology, which tends to give more weight to large aggregates, as explained in section 4.2.3.

The polyallylamine derivatives are initially dissolved in water prior to the addition of siRNA, leading to the formation of self-assembled structures as outlined above. Various concentrations are employed to achieve different N/P ratios, with the siRNA concentration kept constant. Depending on the content of aliphatic chains, hydrophobic interactions yield nanoparticles of varying sizes. Upon the addition of siRNA, electrostatic interactions are promoted between protonated amines and phosphates. A rearrangement of the structures occurs, leading to the formation of complexes which, in the case of low hydrophobic interactions, are smaller in size.

The new structures so called polyplexes have sizes ranging from 12 nm to 30 nm among different OA substitutions, as observed by TEM. However, larger aggregates were also observed in the samples achieving larger sizes from 100 to 250 nm. These observations are congruent with DLS measurements, in which the light intensity corresponding to large structures is detected.

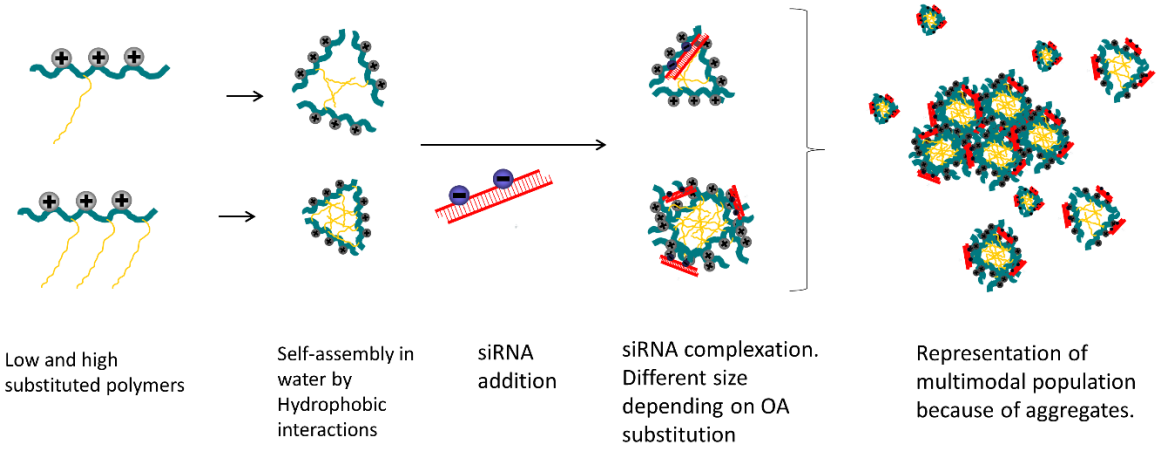

Figure 4. 10.-Schematic representation of polyplex formation based on DLS and TEM results. Aliphatic chains interact each other with different force depending on the OA content achieving different sizes. siRNA is later added to the solution at proper N/P ratio and electrostatic interaction occurred configuring the nanoparticles. The so called polyplexes, achieved smaller sizes than polymer self-assembly in the low substituted ones. The nanoparticles interact each other forming aggregates.

The encapsulation of siRNA within the polyplexes was assessed using the Quant-IT™ Ribogreen fluorophore. The underlying principle of this technique is detailed in Appendix II. Briefly, the highly sensitive Invitrogen fluorescent marker binds with free RNA molecules in solution, but not when the RNA is complexed with a polymer. The same quantity of siRNA is used to form complexes with differently substituted polymers. Polyplexes were treated with a solution of 50 mg/mL heparin/1% Triton-X-100 to neutralize the electrostatic interactions between PAH.OA and siRNA, disassembling the polyplexes, to force its release. Thus, the percentage of siRNA encapsulation was calculated from the ratio between untreated and treated samples. As follows in this equation 4.2.4.2:

$$Encapsulation\ efficiency(100\%) = 100 - \left(\frac{(U_{Sample} - U_{Blank})}{(T_{sample} - U_{Blank})} * 100\right)$$ **Equation 4.2.4.2**

Usample represents fluorescence intensity of samples untreated with Heparin/Triton-X-100 solution.
Tsample represents fluorescence intensity of polyplexes treated with Heparin/Triton-X-100 solution.
Blank represents buffer with Quant-IT™ without RNA, as Quant-IT™ fluorophore exhibits minor fluorescence intensity in aqueous media when it is not bound.

In Figure 4.11 it is clear that for all N/P ratios encapsulation over 80% was achieved with all the cationic polymers used to form the polyplexes. It is interesting to point out that those encapsulation efficiencies were much higher than the lipofectamine RNAimax, commercial siRNA transfect agent considered the gold standard. This is attributed to the strong interactions between the cationic

polymer and the negatively charged phosphates of the siRNA, facilitated by the high protonated amine density offered by the PAH and PAH.OAs (Table 4.3). The same number of protonable amines was kept constant in solution for the different OA substitutions to maintain the N/P ratio, which results in a higher polymer concentration in the more substituted derivatives. Despite this, encapsulation efficiency remained at similar levels across the board, suggesting that oleic acid does not significantly influence encapsulation capacity.

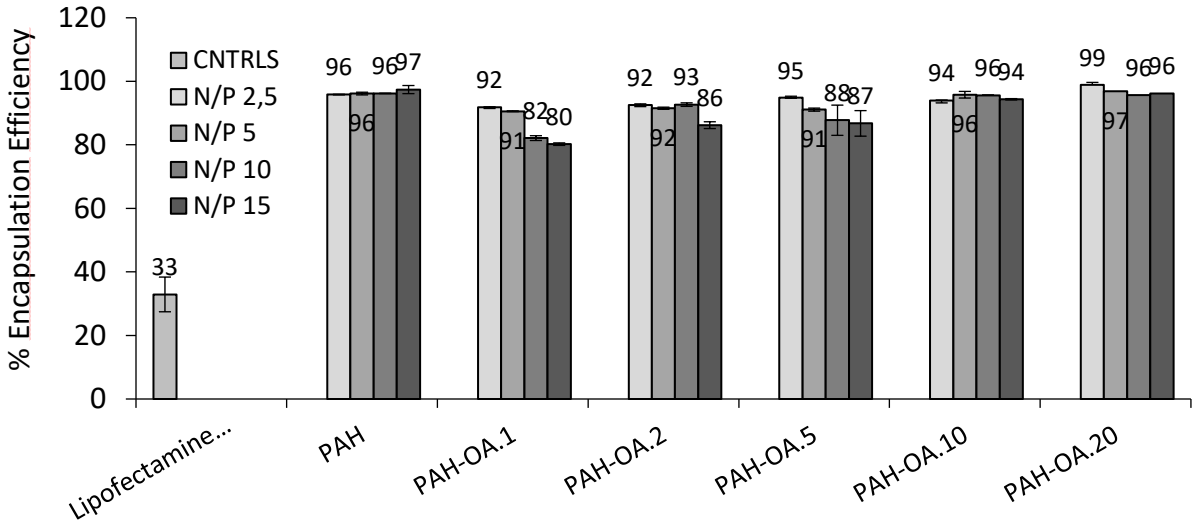

Figure 4. 11.-Encapsulation efficiency of PAH, Lipofectamine RNAimax and PAH.OA substitutions measured by Quant-IT™ Ribogreen fluorophore. Each measurement is based on a n=3, and the error bars represent the standard deviation. The percentage of encapsulation is indicated above each column.

4.3 Conclusions

This chapter covers the synthesis and characterization of new vectors for siRNA based on polyallylamine functionalized with oleic acid. Different grades of oleic acid have been grafted to the polymer chain to study the influence of oleic acid in siRNA delivery. The presence of oleic acid is confirmed by several techniques ^{1}H-NMR, FTIR and elemental analysis. However, exact degree of substitution cannot be elucidated due to the difficulties encountered in solubility being water the best compromise, as it was not soluble in common organic solvents. ^{1}H-NMR allowed a close approximation of oleic acid content in the 5 new different polymers named PAH.OA.1, PAH.OA.2, PAH.OA.5, PAH.OA.10 and PAH.OA.20 according to the percentage of OA expected.

Slight turbidity found in water suggest the self-assembly of the grafted polymers. Dynamic light scattering studies confirm the presence of nanoparticles in water with sizes depending on the OA content, being low substituted ones larger than high substituted. In contrast to pristine PAH that dissolves in water completely. TEM studies and polydispersity index of dynamic light scattering results revealed that aggregates are formed from small nanoparticles (10 nm high OA content and 30 nm low OA content approx) to large structures (100 to 300 nm approx. depending on the OA content). Surface charge is positive around +40 to +50 mV in all derivatives.

To study the interaction between the polymers and siRNA, four N/P ratios were tested: 2.5, 5, 10, and 15. Each polymer and N/P ratio achieved an encapsulation efficiency exceeding 80%. The nanoparticles of polymers with siRNA, displayed a change in size for low substituted polymers (PAH.OA.1 and PAH.OA.2), achieving smaller sizes compared to their self-assembled counterparts. However, the size of highly substituted polymers (PAH.OA.5, PAH.OA.10 and PAH.OA.20) barely changed. Aggregates were still observed after siRNA addition and surface charged remained positive, although a reduction of 10 mV was found.

In the next chapter, polyplexes will be evaluated as siRNA vehicles, testing different aspects such as cytotoxicity, cell uptake and siRNA release. The impact of OA content in a polymer with a high density of amines will be assessed, with a particular focus on enhancing siRNA delivery.

4.4 Material and methods

4.4.1 Materials

Polyallylamine Hydrochloride PAH (average M_w ~17,500 GPC vs. PEG std.) (Ref: 283215). Oleic acid OA (Ref: 364525) N-Hydroxysuccinimide NHS (Ref: 130672), Ammonium molybdate (Ref: 277908-5G) were purchase from **Sigma Aldrich**. 1-(3-Dimethylaminopropyl)-3-ethylcarbodiimide hydrochloride 98% (EDC), Ref: 171440500, was purchased from **Acros Organics™**. siRNA negative control (sense 5´UUC UCC GAA CGU GUC ACG UdTdT3´ antisense 5'-ACG UGA CAC GUU CGG AGA AdTdT-3') were purchased by demand to **BioSpring Biotechnolgie GmbH**. Lipofectamine RNAimax (Ref: 13778030), Nuclease-free water (ref: AM9932), Quant-iT™ RiboGreen™ RNA Assay Kit (Ref: R11490), Deuterium oxide 99.8% Deutered (D_2O) (Ref: 426931000) were purchased from **Thermo Fisher**. TLC Silicagel 60 F_{254} (Ref: 105554) was purchased from **Merck**. DMSO, Snakesskin 3.5 KDa, Methanol-d4, 99 6 % Deuterated (MeoD) (ref:325360500) was purchase from **Acros Organics®**.

4.4.2 Methods

4.4.2.1 Synthesis oleic acid-substituted polyallylamine

PAH of 17.5 KDa, was substituted covalently with oleic acid via the carbodiimide/N-hydroxysuccinimide following the protocol of previous works[14,15,16,17]with different changes. Different molar ratios of -NH_2/-COOH were tested 1:0.01, 1:0.02, 1:0.05, 1:0.1 and 1:0.2. Hereafter named PAH.OA.1, PAH.OA.2, PAH.OA.5, PAH.OA.10 and PAH.OA.20. The corresponding molar amounts of oleic acid were dissolved in 48 mL DMSO. EDC and NHS were added to the oleic acid solution at 10:10:1 molar ratio EDC:NHS:-COOH. The solution was stirred at 37°C for 30 minutes to achieve preactivated NHS-esters of oleic acid. 100 mg of PAH were dissolved in 12 mL of deionized water (diH_2O) and added dropwise to the DMSO solution during 1 h. The mixture of water/DMSO was stirred for 72 hours at 37°C. Polymer was purified by dialysis against deionized H_2O for 10 days changing water twice a day. Finally, the dialyzed aqueous solution was freeze-dried until obtaining a white cotton-like powder. Free oleic acid presence was assessed by thin layer chromatography.

4.4.2.2 Thin layer chromatography

Principles of thin layer chromatography TLC is explained in Appendix II. As mobile phase a mixture of Hexane:ethyl acetate:acetic acid in a 80:19:1 proportion was used and as stationary phase silica gel 60 from Merck. 5 mg of PAH and lyophilizates of PAH.OA.1, PAH.OA.2, PAH.OA.5, PAH.OA.10 and PAH.OA.20 were dissolved in 1 mL of pure water and 5 mg of oleic acid in 1 mL methanol. These samples were spotted onto silica plates and allowed to dry. Subsequently, the plates were placed in a chamber with the mobile phase. Once the mobile phase reached near the top of the plate, the plate was removed from the chamber and left to dry. The dried plate was then stained with $KMnO_4$. The bands were visualized and documented with an image capture.

4.4.2.3. ^{1}H Nuclear Magnetic Resonance

5 mg of PAH and or freeze-dried PAH.OA.1, PAH.OA.2, PAH.OA.5, PAH.OA.10 or PAH.OA.20 were dissolved in 700 μL D_2O and 5 mg oleic acid in 700 μL of MeOD. NMR spectra were recorded on a Bruker AVANCE III spectrometer at 500 MHz and 25°C. Chemical shifts (δ) are expressed in ppm. Splitting patterns: s, singlet; d, doublet; t, triplet; q, quartet; qu, quintuplet m, multiplet. The degree of substitution of amines substituted by lipids was calculated comparing the methyl protons of the oleyl chain 0.8 ppm and multiplet at δ 2.8–3.3 ppm. See spectra in the result section of 4.2.2. Figure 4.5 and calculations in the Appendix IV.

4.4.2.4. Attenuated Total reflection Fourier Transformed Infrared Spectroscopy ATR-FTIR

Freeze-dried samples were placed under vacuum for 5 days to remove all the remaining water. Then, a small piece of each sample was put on the holder of the ATR-FTIR instrument (ATR module GladiATR™, Pike Technologies connected to FTIR 4000 Jasco) and scanned from 4500 to 400 wavenumber (cm^{-1}) with a resolution of 4 cm^{-1}.

4.4.2.5 Elemental analysis

10 mg of freeze-dried samples PAH, PAH.OA.1, PAH.OA.2, PAH.OA.5, PAH.OA.10 and PAH.OA.20 were placed under vacuum for 5 days to remove absorbed water. Polymers were kept under Argon inert atmosphere and send to the Elemental Analysis service of the University of the Basque Country (UPV). Polymers were analyzed for abundance of Nitrogen, Carbon, hydrogen and Oxygen using Euro EA CHNSO analyzer from Eurovector. Weight percentage of elements C, H, N and O in the samples were received as results.

4.4.2.6 Thermogravimetry analysis TGA

PAH, Oleic acid, and lyophilized samples of PAH.OA.1, PAH.OA.2, PAH.OA.5, PAH.OA.10 and PAH.OA.20 were analysed by thermogravimetry analysis (TGA). Principles of TGA are explained in Appendix II. Samples were dried under vacuum and kept in air-free atmosphere until analysis. Similar weighs from 1 to 3 mg were placed on the baskets of TGA 5500 TA instruments, temperature was set up until 800°C with a slope of 10°C/min. All samples were combusted in a furnace under N_2 atmosphere. Data were started to be recorded from 100°C up to 800°C. The results obtained shown the percentage of weight lost by the sample in function of the temperature applied.

4.4.2.7 Preparation of siRNA/PAH.OA polyplexes

Freeze-dried polymers were dissolved in RNAse-free H_2O with the help of vortex and a sonication bath to achieve a stock solution of 1 mg/mL. siRNA/polymer complexation was performed for the following N/P ratios: 2.5, 5, 10, 15. The N/P ratio is defined as moles of protonable amines present in the polymer divided by moles of phosphates in the siRNA. Corresponding amount of polymer necessary to keep the N/P ratio for a constant amount of 0.1 nmol siRNA was calculated, see result in Table 4.3. The quantity of polymer is obtained from 1 mg/mL stock solution, the volume that contain the appropriate mass of polymer was diluted in RNAse-free water to achieve a total volume of 50 µL. Volume of siRNA corresponding to 0.1 nmol was added to polymer aqueous solution and then mixed by pipetting up-down or by a short vortex. Samples were incubated during 15 minutes at room temperature (RT), to allow both molecules to form the complexes.

4.4.2.8 Size by Dynamic Light Scattering DLS

Freeze-dried samples of PAH and PAH.OA derivatives were dissolved in RNAse-free H_2O with the help of vortex and a sonication bath to obtain a stock solution of 1 mg/mL. The measurements of the polymers were obtained by diluting the stock solution to 100 µg/mL concentration sample in a total volume of 200 µL. The measurement of the polyplexes was achieved by previously forming the complexes at different N/P ratios 2.5, 5, 10 and 15 as described above scaling-up to 200 µL. Both samples, polymers and polyplexes were filtered through 0.44 µm, before placing the volume in a disposable low volume cuvette (BRAND® UV cuvette micro-7592). The measurements were conducted in a Zetasizer nano ZS ZEN3600 Model (Malvern Instruments Ltd.) at a laser wavelength of 633 nm and a scattering angle of 173° to obtain the hydrodynamic diameter.

4.4.2.9 Z-potential measurements

Z-potential measurements were performed by the diffusion barrier technique method described by Malvern Analytical, see Appendix II. Z-potential disposable cuvette DTS1070 is previously filled with 700 µL of NaCl 10 mM and then the sample is loaded in the U-bend region at the bottom of the cuvette using a long pipette-tip, see Appendix II and reference[20]. The samples were either polymer or polyplex at 5 mg/mL concentration of the different PAH and PAH.OA derivatives dissolved in pure H_2O at neutral pH. Polyplexes were prepared as described above, maintaining the N/P ratio, but scaling-up the quantity of polymer to 5 mg/mL. Five measurements at 25°C per sample were taken at 20 maximal sub-runs using Zetasizer nano ZS ZEN3600 Model (Malvern Instruments Ltd.)

4.4.2.10 Transmission Electron Microscopy TEM

Free polymer and polyplexes of PAH and PAH.OA derivatives were prepared at final concentration of 100 µg/mL polymer in RNAse free H_2O. Samples were filtered through 0.44 µm and 5 µL were transferred onto a carbon film coated copper grid (400 mesh), previously hydrophilized by glow discharge. After 5 minutes incubation, solution was removed with filter paper. Sample were negatively stained with 5 µL of ammonium molybdate pH 7 12% w/v after 5 minutes incubation. Grids were washed with pure water and kept drying overnight. Transmission electron microscopy measurements were performed with a JEOL JEM 1010 microscope operating at an acceleration voltage of 100 kV and images were taken. The number-average diameter was calculated by ImageJ platform analysis using gaussian curve fitting after counting at least 100 nanoparticles.

4.4.2.11 Quant-IT Ribogreen

Quant-IT Ribogreen assay was used to quantify siRNA encapsulation. The fundamental principles of Quant-IT-Ribogreen method are described in Appendix II. Polyplexes of PAH and PAH.OAs at 4 different N/P 2.5, 5, 10 and 15 were prepared exactly as described above for 50 µL total volume. Then, the protocol provided by manufacturer was followed for two groups of samples: Untreated and Treated samples with a solution of 50 mg/mL heparin and Triton-X-100 1% in DPBS during 10 minutes at 70^{o}C. Fluorescence was quantified using a Synergy HT plate reader by Biotek, with excitation at 480 nm and emission at 520 nm. Then, encapsulation efficiency (EE) was calculated as follows, equation 4.2.4.2:

Encapsulation efficiency EE (%) = 100 - (((Usample-Ublank) / ((Tsample-Tblank) x 100)

U=Untreated T=treated with Heparin solution

4.5 References

1. Andreozzi, P. *et al.* Exploring the pH Sensitivity of Poly(allylamine) Phosphate Supramolecular Nanocarriers for Intracellular siRNA Delivery. *ACS Appl. Mater. Interfaces* **9**, 38242–38254 (2017).

2. Boussif, O. *et al.* Synthesis of polyallylamine derivatives and their use as gene transfer vectors in vitro. *Bioconjug. Chem.* **10**, 877–883 (1999).

3. Di Silvio, D. *et al.* Self-assembly of poly(allylamine)/siRNA nanoparticles, their intracellular fate and siRNA delivery. *J. Colloid Interface Sci.* **557**, 757–766 (2019).

4. Huang, Y. *et al.* Elimination pathways of systemically delivered siRNA. *Mol. Ther.* **19**, 381–385 (2011).

5. Oskuee, R. K., Ramezanpour, M., Gholami, L. & Malaekeh-Nikouei, B. Cholesterol improves the transfection efficiency of polyallylamine as a non-viral gene delivery vector. *Brazilian J. Pharm. Sci.* **53**, (2017).

6. Oskuee, R. K., Mahmoudi, A., Gholami, L., Rahmatkhah, A. & Malaekeh-Nikouei, B. Cationic liposomes modified with polyallylamine as a gene carrier: Preparation, characterization and transfection efficiency evaluation. *Adv. Pharm. Bull.* **6**, 515–520 (2016).

7. Neamnark, A. *et al.* Aliphatic lipid substitution on 2 kDa polyethylenimine improves plasmid delivery and transgene expression. *Mol. Pharm.* **6**, 1798–1815 (2009).

8. Remant Bahadur, K. C., Landry, B., Aliabadi, H. M., Lavasanifar, A. & Uludağ, H. Lipid substitution on low molecular weight (0.6-2.0 kDa) polyethylenimine leads to a higher zeta potential of plasmid DNA and enhances transgene expression. *Acta Biomater.* **7**, 2209–2217 (2011).

9. Whitehead, K. A. *et al.* Degradable lipid nanoparticles with predictable in vivo siRNA delivery activity. *Nat. Commun.* **5**, (2014).

10. Love, K. T. *et al.* Lipid-like materials for low-dose, in vivo gene silencing. *Proc. Natl. Acad. Sci. U. S. A.* **107**, 1864–1869 (2009).

11. Akinc *et al.* A combinatorial library of lipid-like materials for delivery of RNAi therapeutics. *Nat Biotechnol* **26**, 561–569 (2008).

12. Semple, S. C. *et al.* Rational design of cationic lipids for siRNA delivery. *Nat. Biotechnol.* **28**, 172–176 (2010).

13. Jayaraman, M. *et al.* Maximizing the potency of siRNA lipid nanoparticles for hepatic gene silencing in vivo. *Angew. Chem. Int. Ed.* **51**, 8529–8533 (2012).

14. Incani, V., Lin, X., Lavasanifar, A. & Uludağ, H. Relationship between the extent of lipid substitution on poly(l-lysine) and the DNA delivery efficiency. *ACS Appl. Mater. Interfaces* **1**, 841–848 (2009).

15. Thompson, C. J. *et al.* The effect of polymer architecture on the nano self-assemblies based on novel comb-shaped amphiphilic poly(allylamine). *Colloid Polym. Sci.* **286**, 1511–1526 (2008).

16. Park, C., Vo, C. L. N., Kang, T., Oh, E. & Lee, B. J. New method and characterization of self-assembled gelatin-oleic nanoparticles using a desolvation method via carbodiimide/N-hydroxysuccinimide (EDC/NHS) reaction. *Eur. J. Pharm. Biopharm.* **89**, 365–373 (2015).

17. Chen, Z., Zhang, T., Wu, B. & Zhang, X. Insights into the therapeutic potential of hypoxia-inducible factor-1α small interfering RNA in malignant melanoma delivered via folate-decorated cationic liposomes. *Int. J. Nanomedicine* **11**, 991–1002 (2016).

18. Zhao, H., Wu, X., Tian, W. & Ren, S. Synthesis and thermal property of poly(allylamine hydrochloride). *Adv. Mater. Res.* **150–151**, 1480–1483 (2011).

19. Simon, M., Wittmar, M., Bakowsky, U. & Kissel, T. Self-Assembling Nanocomplexes from Insulin and Water-Soluble Branched Polyesters, Poly[(vinyl-3-(diethylamino)- propylcarbamate-co-(vinyl acetate)-co-(vinyl alcohol)]-graft- poly(l-lactic acid): A Novel Carrier for Transmucosal Delivery of Peptides. *Bioconjug. Chem.* **15**, 841–849 (2004).

20. Corbett, J. C. W., Connah, M. T. & Mattison, K. Advances in the measurement of protein mobility using laser Doppler electrophoresis - the diffusion barrier technique. *Electrophoresis* **32**, 1787–1794 (2011).

Chapter 5:

Evaluation of modified oleic acid-polyallylamine as siRNA carrier

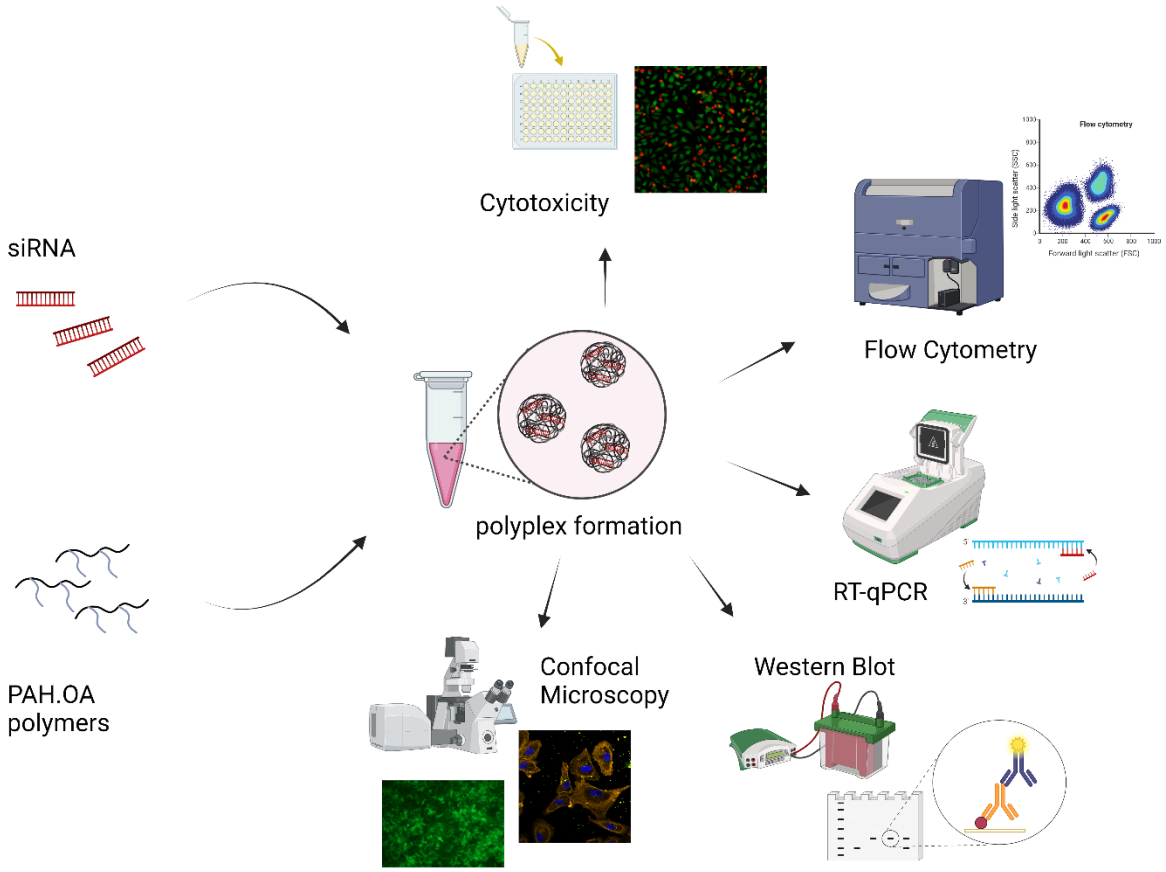

5.1 Introduction

In the previous chapter, we explored and synthesize novel materials based on oleic acid-functionalized polyallylamine homopolymers (PAH.OA). The incorporation of oleic acid confers to these polymers an amphiphilic character, facilitating their self-assembly into nanoparticles in aqueous media. The positively charged surface of PAH.OA enables these polymers to form complexes with siRNA, entrapping almost the total quantity added to the solution (0.1 nmol) at N/P ratios ranging from 2.5 to 15.

The application of siRNA therapies reaches different genetic disorders. Thus, it has rapidly gained attention to cancer therapies due to the large potential for translation and high complementary with other therapeutic approaches. Among types of cancer, lung cancer, especially non-small cell lung cancer (NSCLC) is the leading cause of cancer death[1]. Efforts have been made on bringing new siRNA-based therapies against cell lung cancer (NSCLC) by targeting oncogenes related to tumor angiogenesis (VEGF), tumorigenesis downstream pathways (KRAS) and tumour maintenance proteins that confer resistance to chemotherapy (BCL2)[2].

Some therapeutic approaches involve reprograming immunogenic cells towards cancerous cells, such as T lymphocytes[3], natural killers[4] and tumour-associated macrophages[5]. Another interesting strategy is to modified tumour cells to be genuinely eliminated by macrophages[6]. This can be done by knocking-down CD47 protein, which is a transmembrane protein ubiquitously expressed in normal cells and overexpressed in some cancer cells.

CD47 protein acts as a “don´t eat me signal”, which is recognized by signal regulatory protein α (SIRPα) expressed in macrophages and promoting the inhibition of phagocytosis. CD47-labelled cells are recognized by macrophages as “native” cells, while CD47-deficient cells are identified as “foreign” cells and are eliminated by engulfment (Figure 5.1). With the presence of mutant genes, NSCLC and other types of cancers overexpress CD47. Therefore, downregulating CD47 levels in lung tumour cells holds promise for NSCLC treatment.

Recent studies have demonstrated the efficacy of blocking SIRPα/CD47 interactions with monoclonal anti-CD47 antibodies[6,7] and a limited number of studies have examined CD47 knockdown in ovarian cancer[7], melanoma[8], and lung cancer[9] by using siRNA therapy. In every case a good delivery system is employed to achieve protein *silencing*.

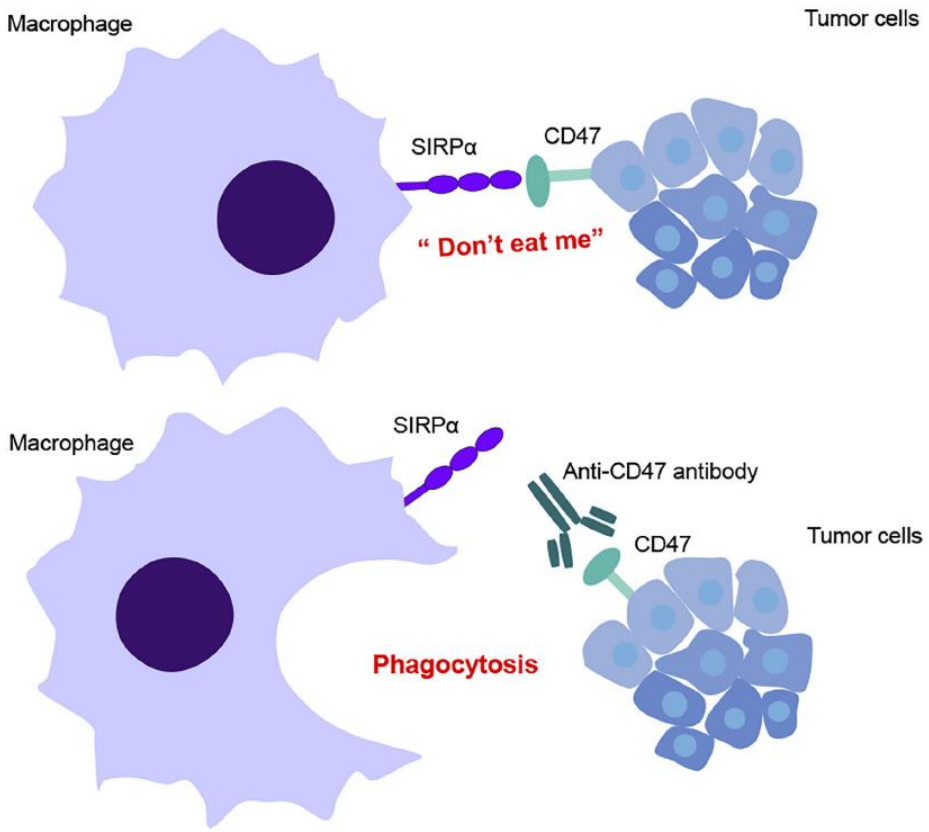

Figure 5. 1.-The interaction between SIRPα and CD47 regulates phagocytic activity of macrophages. This mechanism is used by many cancers as an immune evasion. Some treatments, which consist in blocking CD47 with monoclonal antibodies resulted in significantly tumor burden decrease in mice models. Image extracted from *Huang et al*[10].

A good siRNA performance is correlated with endo-lysosomal escape, as significant protein knockdown can only be achieved if the siRNA is delivered into the cytosol. Several barriers must be overcome by siRNA administered intravenously to reach the cytoplasm. The first barriers rely on its administration to blood stream: renal clearance, nuclease degradation, unwanted activation of immune response and cytotoxicity. Then, siRNA must be delivered at the desired tissue, trespass cell-membrane and escape from the endosome. To ensure efficient transfection, a carrier or vector is thus required. The different types of siRNA carriers have been discussed previously (See General Introduction).

In this chapter, we evaluate the performances of PAH.OA, described in Chapter 4, as siRNA delivery vectors for lung cancer cells. Cytotoxicity, cell membrane penetration and endosomal escape *in vitro* using cell model of lung carcinoma A549 was investigated. In detail, the effect of OA DS on the cytotoxicity of the material was studied and the capacity to enter the cell was evaluated by labelling the polymer and the siRNA with different fluorophores to carry out co-localization studies inside the cell. The pathway of cell entry was also studied as understanding this uptake mechanism is vital for the development of new delivery vehicles. The endosomal escape represents the most difficult barrier, and it is evaluated by flow cytometry, using the same method, which was presented in chapter 3. Finally, CD47 gene messenger RNA and protein levels have been measured to evaluate the therapeutic potential of selected PAH.OA and the possibility to modulate tumour cells so that they can be engulfed by native macrophages.

5.2 Results and discussion

5.2.1 Cytotoxicity of PAH.OA polyplexes

The optimal density of amine groups for a nucleic acid carrier has been widely discussed[11,12,13]. Amino groups in polycations complex nucleic acids but also cause cytotoxicity. Several modifications in the polycations have been performed aiming at reducing toxicological endpoints. Polyethylene glycol grafting has been frequently employed for modifying polycations such PEI[14,15,16], PLL[17,18], or chitosan[19] and reduce their toxicity. Other chemical modifications of polycations such as hydrophobic modifications can be beneficial for increasing cell viability[20]. The cytotoxicological impact of PAH.OA has been assessed in the pulmonary adenocarcinoma cell line A549. Metabolic activity (MTS) and cell membrane damage (Live/Dead) were measured after treating cells with the PAH.OA/siRNA polyplexes (Figure 5.2 and 5.3). All the polyplexes prepared transport the same amount of siRNA, i.e. 200 nM concentration delivered to the cells. Therefore, cytotoxicity only depends on the amount of polymer and OA DS.

The principles of the Live/Dead assay were explained in detail in Appendix II. Briefly, this assay involves the staining of cells with two dyes, Calcein AM and Ethidium homodimer-1 (EtdH-1). Calcein AM is non-fluorescent and can easily diffuse into cells through the plasma membrane. Upon entry, it is converted by intracellular esterases into calcein, which has a strong fluorescence activity, indicating cell viability. On the other hand, EtdH-1 cannot penetrate an intact plasma membrane and only enters cells with compromised membranes, binding strongly to DNA in the nucleus.

A549 cells were treated with PAH.OA/siRNA polyplexes, and the cytotoxicity was evaluated 24h after. Confocal images of A549 cells treated with Live/Dead kit was taken and displayed in Figure 5.2. The images show live cells and dead cells stained in green and red, respectively. Polyplexes were prepared at N/P ratios of 2.5, 5, 10, and 15 using PAH, PAH.OA.1, PAH.OA.2, PAH.OA.5, PAH.OA.10, and PAH.OA.20.

At low N/P ratios 2.5 and 5 cells are predominantly green (Figure 5.2), corresponding to non-cytotoxic outcomes. On the other hand, at N/P ratio 15 cells were stained red, indicating cell membrane damage for all polymers except PAH.OA.20. Regarding N/P 10, cell membrane damage was evident for polymers PAH and PAH.OA.1, while an increased number of live cells (green) was observed with increasing OA substitution, specifically for PAH.OA.2, PAH.OA.5, PAH.OA.10 and PAH.OA.20. These observations suggest that a higher OA DS enhances the cytocompatibility of the cationic PAH homopolymer.

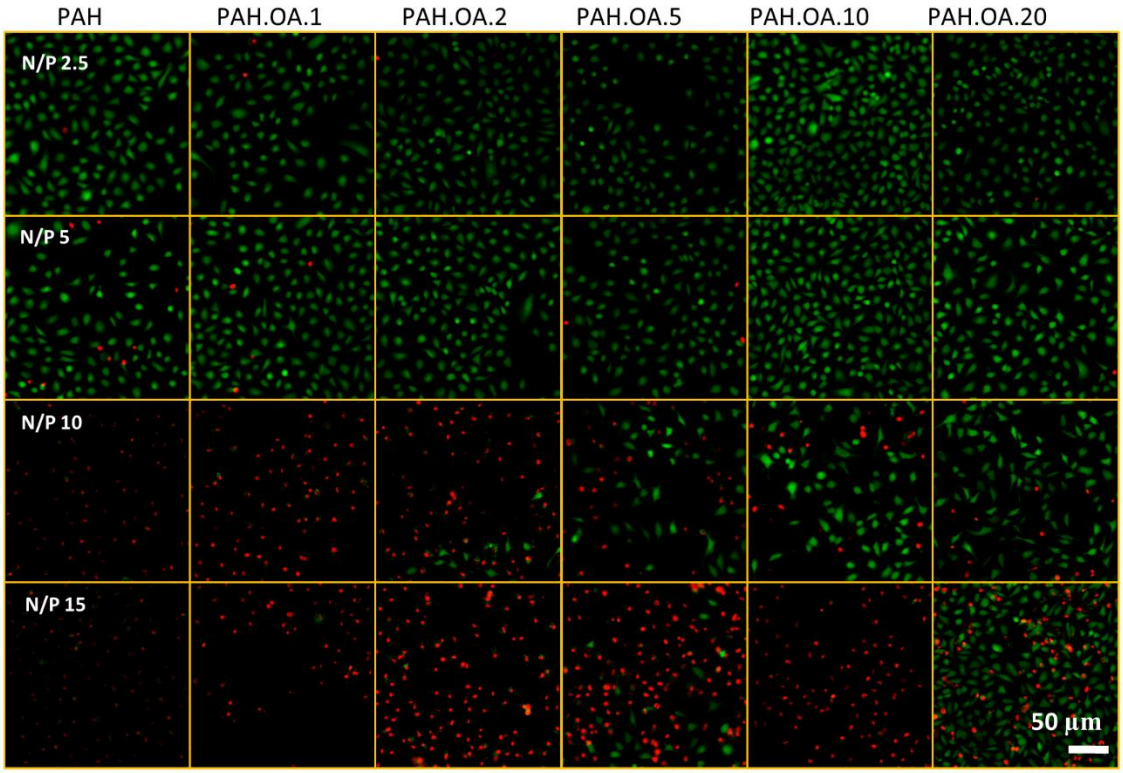

Figure 5. 2.-Live/Dead assay in A549 cells 24h after transfection with polyplexes based on polyallylamine with the different oleic acid substitutions at N/P ratios 2.5, 5, 10 and 15. Green staining corresponds to living cells and red to dead cells.

A second complementary method to evaluate polymers cytotoxicity is the measurement of cell viability by the MTS assay which is based on a tetrazolium compound that is reduced by viable cells to the coloured product formazan. The reduction is carried out by NAPDH and NADH, molecules characteristic of the metabolic activity of the cells. The absorbance of formazan is directly correlated with the number of viable cells in the culture.

The same polymers and N/P ratios as the one used for Live/Dead assay were administered to the cells and exposed to MTS after 24h. Absorbance data was normalized to control experiments, consisting of non-treated cells, and the data are expressed as percentage of viability.

As shown in Figure 5.3, low N/P ratios 2.5 and 5, which correspond to the lowest polymer concentrations, were not cytotoxic for all the polyplexes tested. Cell viability was greater than 80% compared to non-treated cells. In contrast, polyplexes prepared at the highest N/P ratio 15 presented low cell viability, less than 5%, for PAH, PAH.OA.1, PAH.OA.2 and PAH.OA.5. However, cells treated with polyplexes prepared with PAH.OA.10 and PAH.OA.20 showed viability greater than 70%.

For polyplexes prepared at N/P 10, PAH and PAH.OA.1 exhibited significant cytotoxicity, having less than 40% of cell viability. However, viability increases with higher oleic acid substitutions: 40%, 50%, 80%, 90% of cell viability is obtained for PAH.OA.2 and PAH.OA.5, PAH.OA.10 and PAH.OA.20, respectively. These results are in good agreement with those obtained for the Live/Dead assay,

further validating that the cytotoxicity of polyplexes decreases when prepared with PAH having an increasing OA DS.

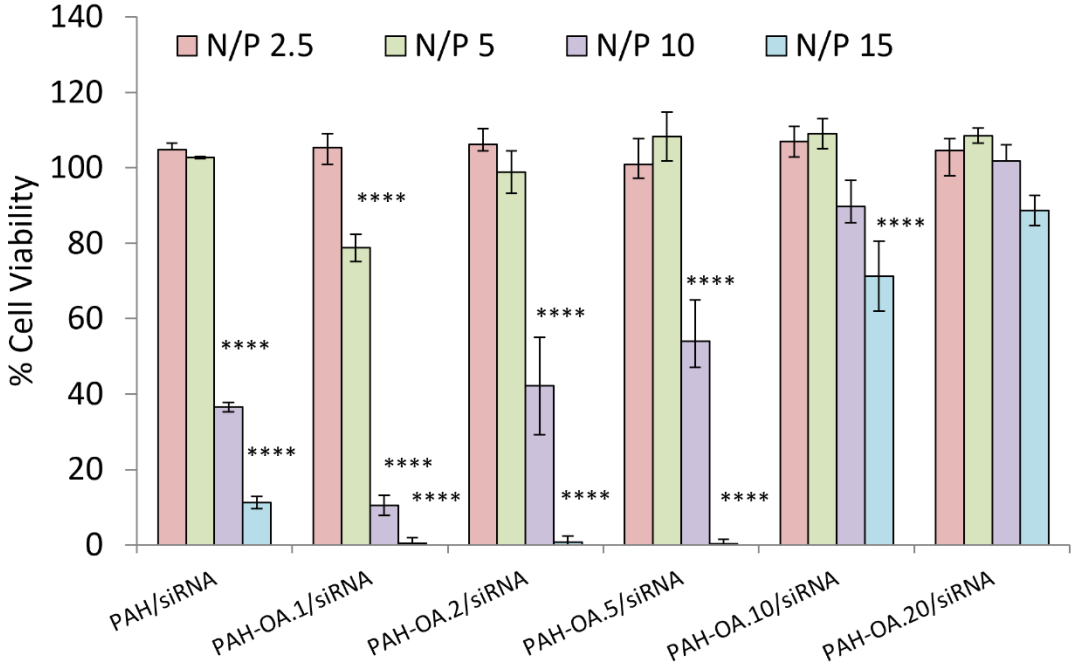

Figure 5. 3.-MTS assay to determine metabolic activity of A549 cells 24h after transfection with PAH and PAH.OA.1, PAH.OA.2 and PAH.OA.5, PAH.OA.10 and PAH.OA.20 at N/P ration of 2.5, 5, 10 and 15. n=3 error bars represent standard deviation. Statistical analysis One-way ANOVA against control non-treated cells, representing 100%. P-valor * < 0.05 ** < 0.01 *** < 0.001 **** < 0.0001.

At low concentration of polymer corresponding to N/P 2.5 and 5, cells are exposed to lower number of cationic amine groups, which is reflected in the greater cell viability and lower cell membrane damage. On the other hand, the highest concentration of polymer corresponding to N/P 15 are cytotoxic for the cells at any degree of substitution of PAH.OAs, except for PAH.OA.20. Interestingly, polyplexes prepared at N/P 10 showed an inflection point, where an effect of OA is clearly observed. Cell viability increases with the amount of OA, as well as cell membrane damage is reduced. This effect is attributed to the reduction of the number of available amine groups, as well as the formation of nanoparticles by self-assembly as shown in section 4.2.4, where a significant amount of the primary amines is shielded. Similar results were obtained with the hydrophobic modifications of PEI[21,22] that showed lower cytotoxicity because of the reduction of the number of primary amine groups. Nevertheless, high concentrations of polymer resulted in cytotoxic polyplexes, as shown by the decrease in cell viability observed at N/P ratio of 15. Thus, further experiments were performed only with polyplexes prepared with PAH and PAH.OA at N/P ratio of 5 which did not show significant cytotoxicity.

5.2.2 Internalization of PAH.OA. polyplexes

As it is mentioned in the introduction, one of the first barriers a carrier will face is the cell membrane. A good carrier should enter the cell and trespassing the cell membrane. Nanoparticle-cell interactions are modulated by physicochemical properties of the nanoparticles including size, shape, surface charge and surface chemistry. Studies carried out with gold nanoparticles, which controlled shape and size, showed that size of approximately 50 nm and spherical shape result in the most efficient cell uptakes. However, smaller and larger size have also shown internalization and transfection efficiency[23]. Nanoparticles with neutral surface coatings, such as PEG, exhibited low interaction with cells and consequently displayed minimal internalization. While negatively-charged nanoparticles report certain internalization, positively-charged nanoparticles are the most effective in crossing cell-membrane barrier. Cationic particles are known to bind to negatively charged groups on the cell surface (e.g., sialic acid) and translocate across the plasma membrane[23].

As it is reported in Chapter 4, the polyplexes based on PAH.OA are spherical nanoparticles from 10 to 30 nm with the presence of aggregates of around 150 nm with a positive charge, up to +40 mV, as judged by aqueous electrophoresis studies. Despite their broad size distribution, they have demonstrated good siRNA entrapment capacities without causing cytotoxicity at low N/P ratios. As such, their ability to cross cell membranes was evaluated in vitro using the A549 cell line. The internalization of polyplexes was measured by confocal scanning laser microscopy and flow cytometry. Both techniques are based on fluorescently labelled samples. For this purpose, 6-carboxyfluorescein siRNA (siRNA-6-FAM) was acquired, and polyallylamine derivatives were labelled by the atto-633 fluorophore by Atto-tec.

Atto-633-NHS ester fluorophore was bound to primary amines of polyallylamine at a feed ratio of 1 molecule fluorophore per 2000 monomers of polymer. Reaction was conducted following manufacturer instructions and was purified by size exclusion chromatography and dialysis. Figure 5.4 shows the ^{1}H-NMR spectra of the freeze-dried labelled polymers: PAH, PAH.OA.1, PAH.OA.2, PAH.OA.5, PAH.OA.10 and PAH.OA.20. The same peaks as the one observed for the polymers described in Chapter 4 (Figure 4.5, Chapter 4) were identified with the difference that small and fine peaks appeared from 3.5 to 3.8 ppm corresponding to Atto-633 protons. Although the presence of the fluorophore in the freeze-dried polymer was confirmed, it was still to demonstrate that the dye was covalently attached to the polymer chains. This is very important as free fluorophore could lead to false positive internalization results when observed under confocal microscope, i.e. only free fluorophore is detected into the cells. To ensure the successful functionalization of atto633 to the polymer chain, fluorescence correlation spectroscopy (FCS) (see Appendix II) was used. FCS is a technique based on fluctuation of fluorescence intensity in small time span in Brownian motions produced by a fluorophore or any particle carrying a fluorophore of particles in solution. Correlation of the same value of fluctuations in time allows to extract the diffusion coefficient of the fluorescent molecule. As for DLS, the correlation function of small particles or free dye decays faster than that of larger particles, as they move faster. Autocorrelation function G(τ) and diffusion coefficients, corresponding to dye concentration and particle size, respectively, of different polymers at the same concentration (PAH, PAH.OA.1, PAH.OA.2, PAH.OA.5, PAH.OA.10 and PAH.OA.20) and Atto633 are

shown in Figure 5.5. Despite some difference in G(τ) value between the samples, indicating the different concentration of fluorophore measure, the most important data is the clear shift of the diffusion coefficient observed from 360 $\mu m^2/s$ for Atto633 down to < 17.34 $\mu m^2/s$ for PAH/PAH.OA, which indicate the successful functionalization of the polymer chain with the dye.

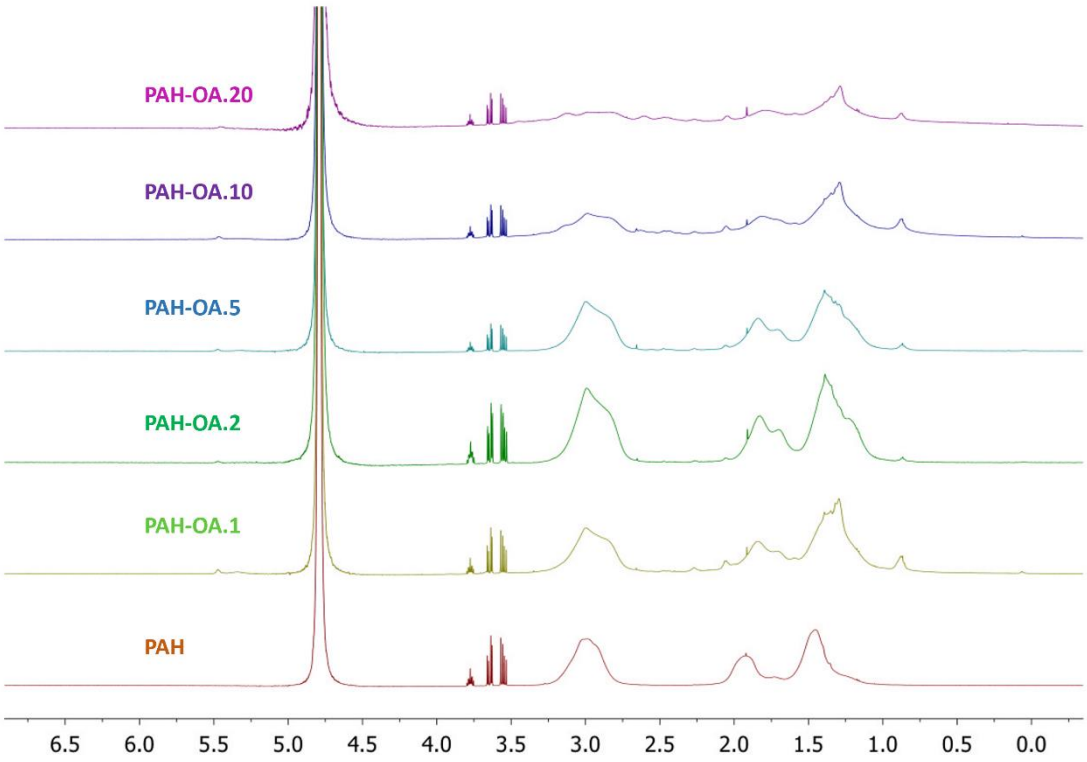

Figure 5. 4.-^{1}H-NMR spectra of labelled PAH and PAH.OA polymers with Atto633 fluorophore in D_2O (from bottom to top: PAH, PAH.OA.1, PAH.OA.2, PAH.OA.5, PAH.OA.10 and PAH.OA.20).

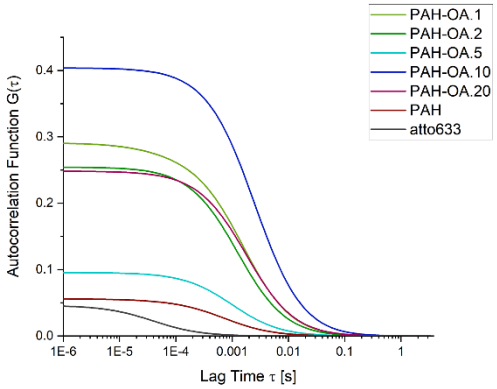

Species	Lag time τ [μs]	Diffusion coefficient [$\mu m^2/s$]
ATTO 633	39.71 ± 0.41	360
PAH	736.179 ± 6.11	17.34 ± 0.16
PAH-OA.1	1578.63 ± 38.90	8.55 ± 0.21
PAH-OA.2	1263.61 ± 26.00	10.68 ± 0.22
PAH-OA.5	1006.13 ± 18.2	13.42 ± 0.25
PAH-OA.10	2522.84 ± 60.8	5.35 ± 0.13
PAH-OA.20	1789.36 ± 91.1	7.55 ± 0.39

Figure 5. 5.-Fluorescence correlation spectroscopy of free Atto633 fluorophore in solution or after reaction with PAH and PAH.OAs polymers. Autocorrelation function and coefficient diffusion of fluorophore 633 linked to polymers. The higher the coefficient diffusion, the smaller the size.

Thus, the first experiment to evaluate internalization consisted in treating cells with labelled polymers and siRNA and then localizing them within the cell by confocal laser scanning microscopy (CLSM) (see Appendix II for the explanation of the fundamentals). In this technique, laser-excited

samples emit fluorescence, which is subsequently captured by specific detectors to generate an image. Importantly, the absorption and emission spectra of the selected fluorophores for the samples 6-FAM and atto633 for siRNA and PAH/PAH.OA, respectively – do not overlap, and are also distinct from those of Hoescht 33342 and Actin Red, which were used to stain the nucleus and actin cytoskeleton, respectively.

Polyplexes of labelled polymers and fluorescent siRNA were formed in RNAse free water at N/P 5, as a good compromise between cytotoxicity and positive charges to promote the siRNA translocation. A549 cells were exposed to $1x10^{-4}$µmol of siRNA during 24 h in serum-reduced OptiMEM medium, as it should allow sufficient time for internalization to occur. After staining the nucleus and actin cytoskeleton of the A549 cells with Hoescht 33342 and Actin Red®, respectively, the cells were observed using CLSM to monitor the internalization of polyplexes.

In Figure 5.6, green, red, blue and yellow channels correspond to siRNA-6-FAM, atto633-polymers, cell nucleus and cell actine cytoskeleton, respectively. The merged channel 2 comprises the four channels observed together. Confocal images reveal co-localization of siRNA and polymer (yellow dots), indicating polyplex stability in the cell medium after 24h. Some polyplexes were observed to colocalize with the cells, while others were located outside the cell area. Regardless of the degree of substitution, all polyplexes exhibited similar localization patterns.

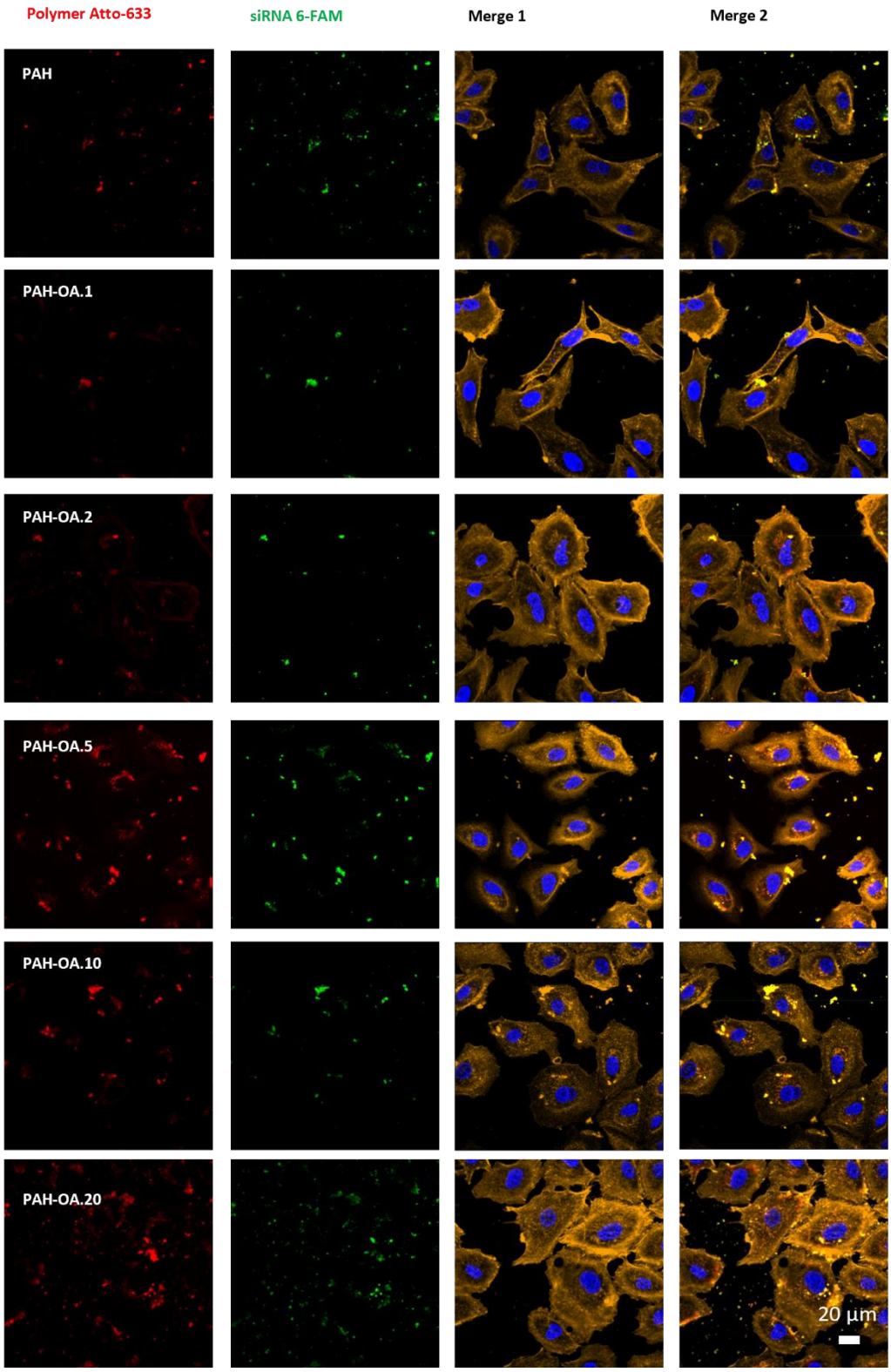

Figure 5. 6.-Confocal micrographs of A549 cells 24 hours after being transfected with fluorescently labelled polyplexes PAH.OA/siRNA at N/P 5. PAH, PAH.OA.1, PAH.OA.2, PAH.OA.5, PAH.OA.10 and PAH.OA.20 labelled with atto-633 fluorophore emission at 635 nm (red channel) and siRNA-6-FAM emission at 520 nm (green channel). After transfection cells were fixed and treated with Hoescht 33342 and ActinRed®. Merge 1 channel correspond to cells with labeled actin (yellow) and nucleus (blue). Merge 2 channel correspond to channels of siRNA, polymer and marked cells. Scale bar 20 µm.

To confirm internalization and rule out mere surface adherence of the polyplexes, Z-stack imaging technique was conducted in the confocal. This technique involves acquiring a series of images at varying heights along the Z-axis within the same orthogonal plane, which can then be used to construct a 3D image. This comprehensive view allows for the confirmation of polyplex presence within the cells. Figure 5.7 provides a detailed orthogonal view in the X-Y axis with two representative cross-sections. From these cross-sections, images along the X-Z (bottom) and X-Y (right-hand side) axes show that polyplexes are indeed localized within the cells. Despite some polyplexes being present on the cell membrane, it can be affirmed that the polyplexes are internalized, highlighted by the white circles and arrows. The smallest polyplex nanoparticles are expected to be rapidly internalized by the cells, c.a. within two hours, while larger particles or aggregates should exhibit a slower cell uptake, as previously reported PEI[24] which showed that different uptake pathways are taking place depending on the particles size.

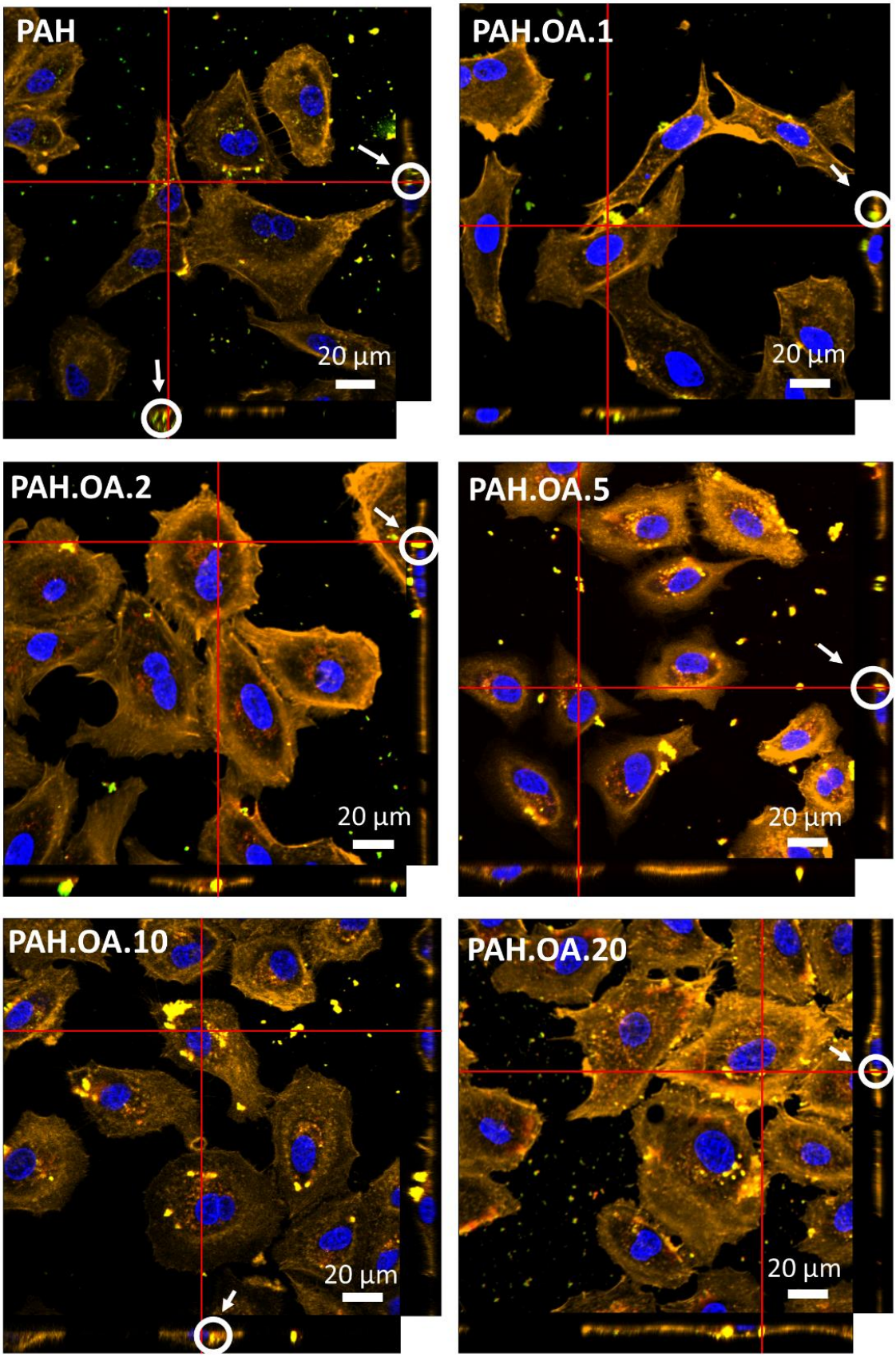

Figure 5. 7.-Orthogonal view of merge 2 channel from Figure 5.6 confocal micrographs. A549 cells 24 hours after being transfected with fluorescently labeled polyplexes PAH.OA/siRNA at N/P 5. Cross section done in the red lines images are represented as X-Z and Y-Z axis images located at right-hand side and bottom of each micrographs. White arrows and circles indicate polyplexes inside cells.

In addition to CLSM, internalization was also assessed quantitatively using flow cytometry, which allows the percentage of cells that have incorporated siRNA to be determined. In this analysis, A549 cells were treated with polyplexes containing fluorescent siRNA-6-FAM at an N/P ratio of 5 for 24 h. The cells were then collected and analysed using a flow cytometer.

Figure 5.8.-A illustrates the raw data obtained for 10,000 cells per condition, with the population of live cells and singlets being selected. A histogram of the 6-FAM fluorescence intensity for the singlet population is plotted, with untreated cells demonstrating low or no fluorescence intensity, as expected. A gate is then established on the histogram from the end of the intensity peak of the control population (refer to P3, top-right graph in Figure 5.8.-A). Consequently, any cells within this gate are considered positive for siRNA internalization.

The percentage of the 10,000 cells falling within this gate is then calculated for the different polyplexes prepared with PAH, PAH.OA.1, PAH.OA.2, PAH.OA.5, PAH.OA.10, and PAH.OA.20, as shown in Figure 5.8.-B. Remarkably, over 70% of the A549 cells were positive for 6-FAM, indicating that all the polyplexes were able to penetrate the cell membrane. Interestingly, no significant difference was observed among the various degrees of substitution studied. This suggests that OA DS does not impact significantly the penetration of the cell membrane and cell uptake. This result is in good agreement with the study involving linear PEI 2KDa with aliphatic substitutions, suggesting that the aliphatic chains did not offer additional interactions with the cell membrane[25].

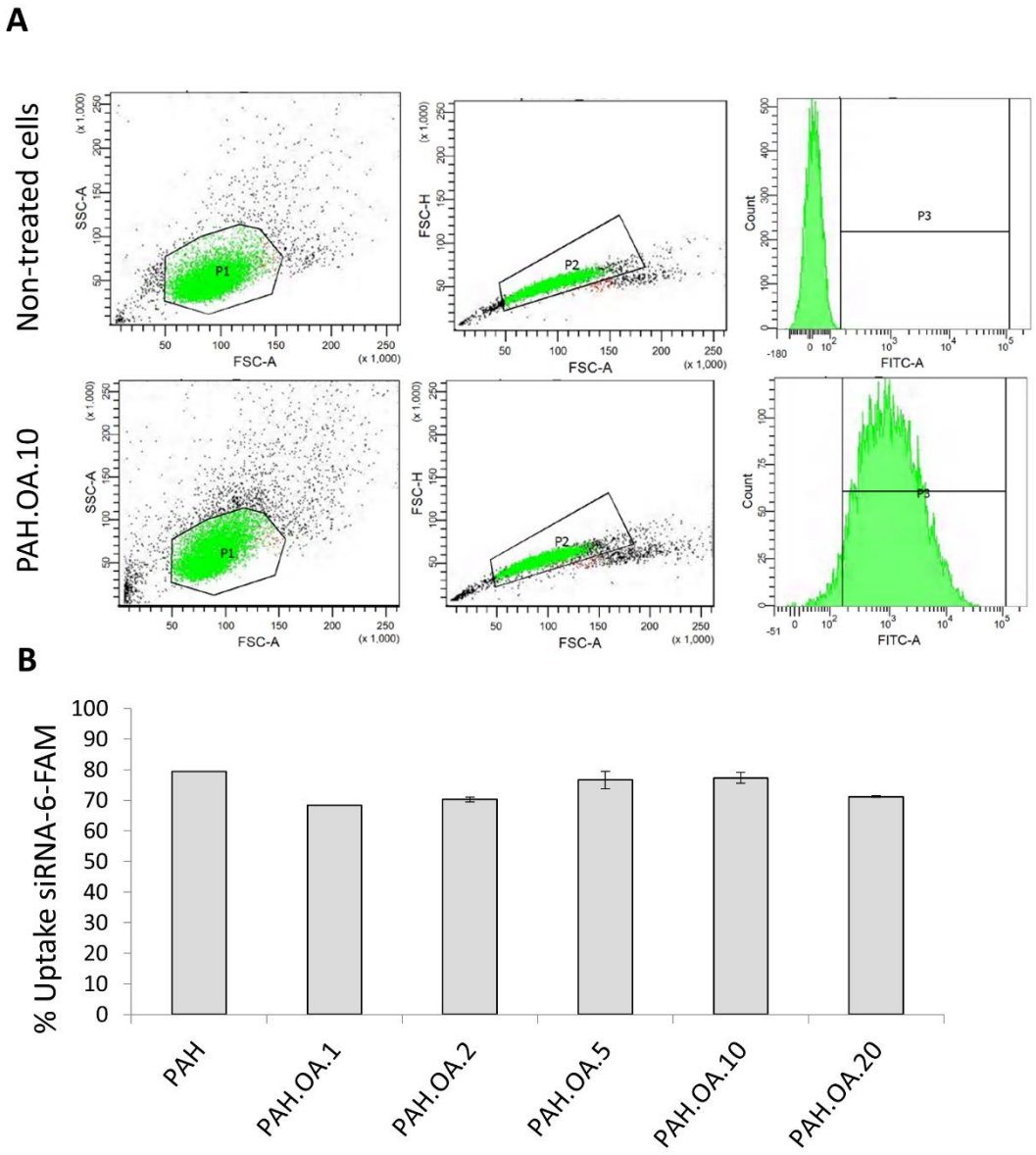

Figure 5. 8.-Flow cytometry analysis of uptaken siRNA-6-FAM in A549 cells after 24h of transfection with PAH.OAs/siRNA polyplexes at N/P 5. A) Raw data extracted from Flow cytometer. Hierarchy of populations. FSC vs SSC P1, live cells, FSC-H vs FSC-A P2, Singlets, FITC-A histogrma P3, fluorescent cells. Gate of P3 was set up from non-treated cells, in which the percentage of fluorescent cells is 0%. B) Analysed data representing percentage of fluorescent cells of a total of 10,000 events. n=3, error bars represent standard deviation.

5.2.3 siRNA delivery by PAH.OA

As previously shown, all PAH.OAs polymers prepared can entrap efficiently siRNA and can be internalized inside cells. However, achieving cytosol delivery presents a significant challenge, primarily due to the need to escape from the endosome. To test the delivery efficiency of our system in cancer cells, the silencing performances of the encapsulated siRNA was investigated with the same technique as described in Chapter 3.

Specifically, siRNA against eGFP protein was administered to human A549 pulmonary adenocarcinoma cells that overexpress the green fluorescence protein (A549-eGFP cells). A reduction in eGFP fluorescence corresponds to a successful delivery and silencing efficiency by the

carrier. Cells were transfected with PAH.OA/siRNA anti-eGFP at N/P ratios of 2.5, 5, and 10, while N/P ratio of 15 was excluded from the assay due to the cytotoxicity observed previously (Figure 5.3 and 5.4).

Cell fluorescence was measured by flow cytometry 96 hours post-transfection. Figure 5.9.-A presents raw flow cytometry data for 10,000 cells that were passed through the cytometer, with only live and singlet populations selected for GFP fluorescence measurement. Mean fluorescence intensity was compared among different PAH.OAs used to prepare the polyplexes at the stated N/P ratios. A shift to lower intensity was observed when siRNA was applied. PAH exhibited a broad distribution, reflecting the presence of cells with high and low eGFP intensity, indicative of low transfection efficiency. In contrast, cells treated with PAH.OA.10 showed a decrease in the number of cells at high intensity, attributable to superior transfection efficiency.

Fluorescent microscopy images of A549-eGFP cells after transfection (Figure 5.9.-B) showed that lower number of fluorescent cells could be distinguished with PAH.OA.10-based polyplexes compared to the non-treated cells and the one treated with the polyplexes prepared with PAH. Mean intensity data are treated and displayed as relative eGFP expression of the non-treated cell control, which represent 100% of expression.

Figure 5.9.-C shows that low transfection efficiency is obtained for any of the polyplexes formed at N/P 2.5 with an expression of eGFP above 70%. Treatment with polyplexes prepared with PAH, PAH.OA.1 and PAH.OA.2 at N/P 5 and N/P 10 resulted in transfection efficiency down to 50%. However, it is important to remember that some cytotoxicity was observed for those polyplexes at N/P 10 (Figure 5.2 and 5.3). Therefore, the most reliable data for effective transfection are derived from polyplexes prepared at N/P 5, with a clear improvement observed as the degree of substitution increased. More interestingly, the transfection efficacy increased significantly for polyplexes prepared with PAH.OA.5 and PAH.OA.10 reducing eGFP expression the most up to 60% and 70%, respectively. These results confirmed the beneficial effects of OA substitution. However, this trend appeared to reach a limit as the polyplexes prepared with PAH.OA.20 exhibited low transfection efficiency, indicating that an optimum degree of substitution is required to offer the best transfection efficiency for the resulting polyplexes. Altogether, the best transfection efficiencies were obtained when the cells were treated with polyplexes prepared with PAH.OA.10 at N/P 5 and N/P 10. The results obtained indicate that the cationic character of the polyplexes allow their internalization by the cells and the presence of OA groups, confers the ability to escape from the endosome and release. Similar results have been reported for PEI aliphatic substitutions with hydrophobic groups, though these do not appear to influence cell uptake either[25,26]. PAH.OA.10 polyplexes appear to be the best candidate to escape from the endosome and release cargo.

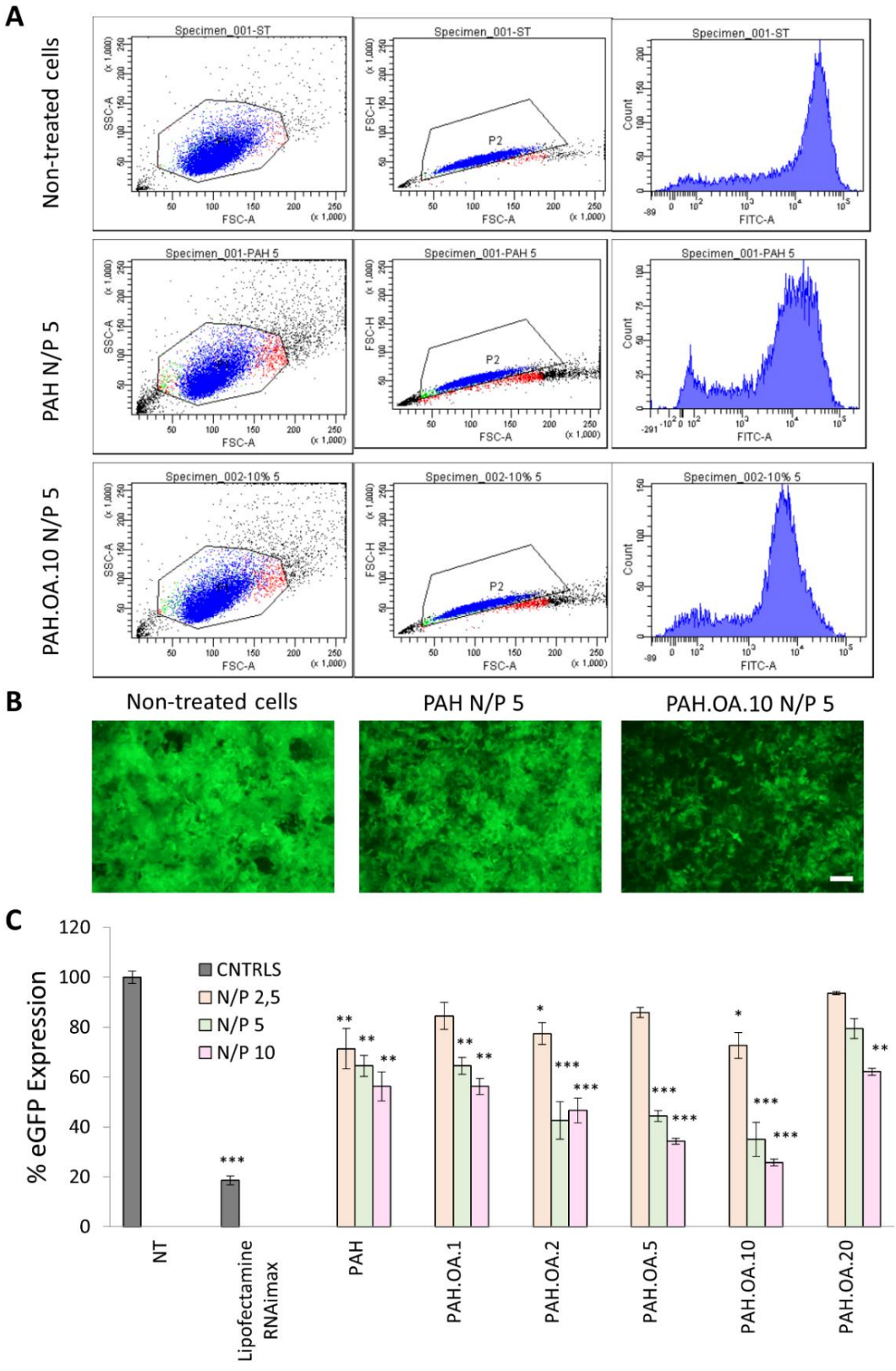

Figure 5. 9.-siRNA delivery efficiency. Expression of eGFP protein in A549-eGFP cells 96h after being treated with siRNA anti-eGFP/PAH.OA polyplexes. A) Raw data from Flow cytometry. Population of cells P1 from FSC vs SSC representing living cells, P2 from P1 in FSC-A vs FSC-H represent singlets, histogram of P2 population of FITC filter intensity. From top to bottom Non-treated cells, PAH and PAH.OA.10. B) Fluorescent micrographs of A549-eGFP cells 96h after transfection: Non-treated cells, PAH and PAH.OA.10 at N/P 5. Scale bar 50 μm. C) Percentage of eGFP expresion analysed from normalization of fluorescence intensity of non-treated cells, which represent 100%. n=3 error bars represent standard deviation. Data points marked with asterisks are statistically significant relative to Non-treated group p-value * < 0.05, ** < 0.01 ***<0.001 t-test, single tailed.

How polymers[27] and other carriers such lipid nanoparticles escape endosome is currently a topic of scientific debate. The most accepted hypothesis lies on the pKa value of the polymer or nanoparticle which should be closed to the endosomal pH, i.e. 6, when acidification starts. Thus, amino groups act as a pH buffer of incoming proton during endo-lysosomal acidification. Accumulation of protons instigates osmotic swelling and compartment disruption, an effect often referred to as the "proton sponge" effect.

5.2.4 siRNA endo-lysosomal escape

It was demonstrated that all PAH.OAs entrap siRNA and can cross the cell membrane. However, it has been observed that good siRNA delivery was only achieved with only some OA DS, actually the best transfection results were observed when polyplexes prepared with PAH.OA.10 at N/P 5 were administered.

To elucidate how those selected polyplexes can overcome endo-lysosomal compartments, CLSM studies have been carried out, labelling siRNA with the Cy5 fluorophore and lysosomes with Lysotracker™ green. Lysotracker™ consist of a fluorophore linked to a weak base that has a high selectivity for acidic organelles. Thus, lysosomes among other internal compartments will be stained. CLSM images have been performed at different time points: 2h, 24h and 48h after transfection. Lysosomes are the final destination of the endocytic pathway, where the acid hydrolases digest all molecules. If the labelled siRNA escapes from the endosome before fusing with the lysosome, the fluorescence from siRNA is not expected to co-localize with the labelled lysosomes.

Figure 5.10.-A and 5.10.-B show CLSM images of A549 cells treated with polyplexes prepared with PAH.OA10 and siRNA-Cy5 (red), as well as lysosomes with Lysotracker™ (green). In the majority of the cases, we observe co-localization, meaning that siRNA is present within the lysosomes. However, the presence of siRNA outside the lysosomes can be also observed in Figure 5.10.-B. A small leakage of siRNA molecules into the cytoplasm can be observed, although it is important to point out that most of them remain inside the lysosome.

These data are in good agreement with some studies on lipid nanoparticles (LNPs) which showed that only 1-2% of delivered siRNA manage to escape from the endosome[28] at early stages for transfection and only approximately 2000 copies of the leaked siRNA, are sufficient to promote gene knockdown[29]. Although proton sponge is the most widely accepted theory explaining nucleic acid translocation into cytoplasm, some works[28,30] have indicated that endosomes remain intact after escape occurred, meaning that there are alternative pathways that do not end up in endosome disruption. Pore hole transition or membrane disruption caused by electrostatic interactions of the polymer´s amines are another alternative explanation to cytosol translocation. In any case, the proof of siRNA endosomal release is given by the successful transfection (Figure 5.9.-C), as the oligonucleotide cannot induce gene silencing unless it reaches the cytoplasm to form a complex with mRNA.

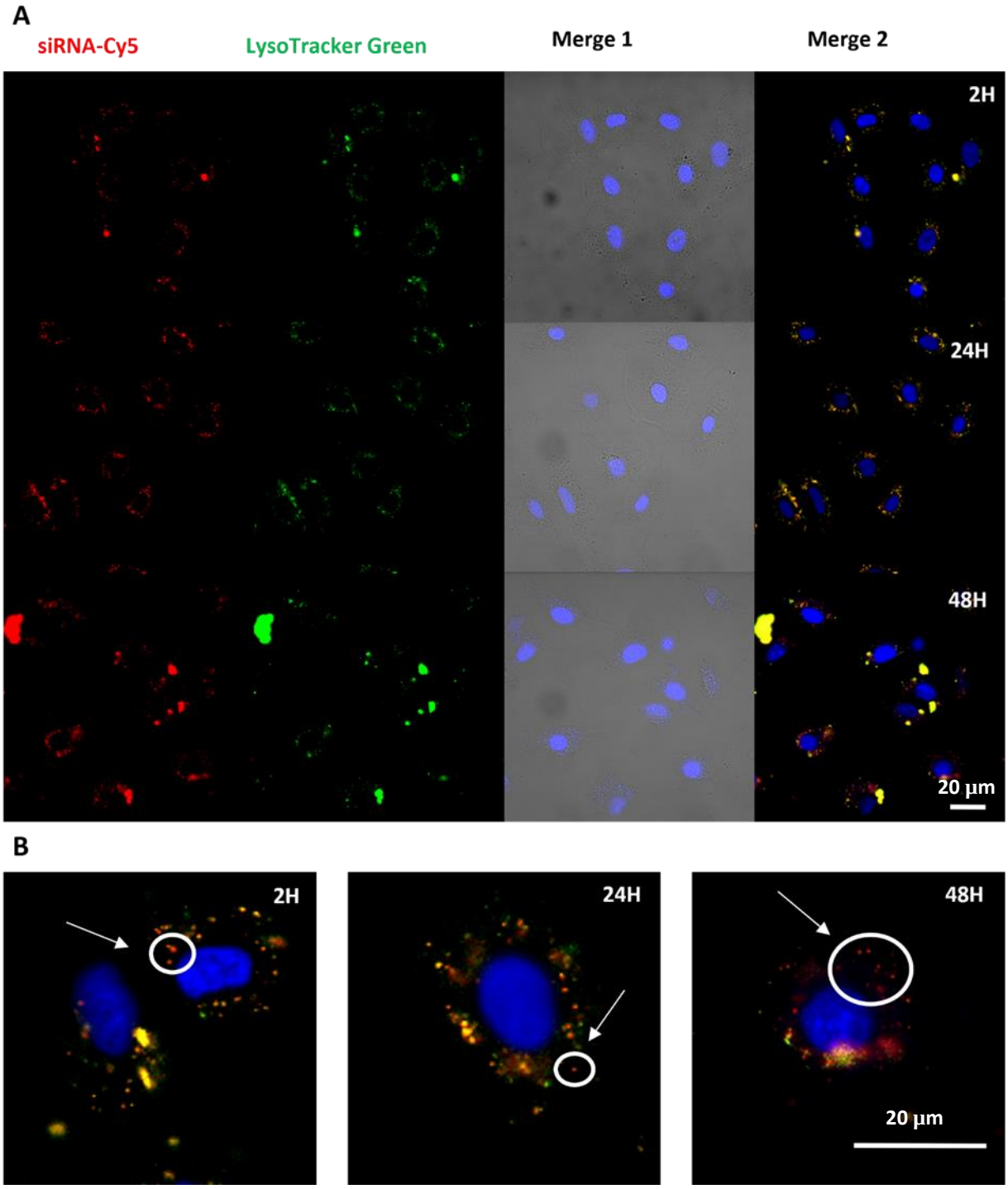

Figure 5. 10.- Confocal micrographs of A549 cells at 2, 24 and 48 hours after being transfected with polyplexes PAH.OA.10/siRNA-Cy5 N/P 5. Cells were treated afterwards with Lisotracker^{TM} Green and Hoescht 33342. A) Image are split in 4 channels: red channel for siRNA-Cy5, green channel for LisotrackerTM Green, Merge 1 with transmission light and blue channel of Hoescht 33342 and merge 2 with red channel, green channel and blue channel. Scale bar 20 µm. B) Amplified images of merge 2 channel from part A of this figure. Scale bar 20 µm. White arrows and circles reflect siRNA-Cy5 not colocalizing with lysosomes.

5.2.5 Internalization routes of PAH.OA/siRNA polyplexes

Understanding the internalization process of nanoparticles within the cells is essential for improving delivery efficiency, particularly when considering the use of polyallylamine-derived polyplexes for therapeutic purposes.

Nanoparticles can enter cells through different pathways, which are grouped into three major routes: simple diffusion of small molecules, pinocytosis, and phagocytosis. Pinocytosis includes different routes, such as micropinocytosis, clathrin-mediated endocytosis, caveolin-mediated endocytosis, receptor-mediated endocytosis, and independent endocytosis (Figure 5.11). Pinocytosis is a constitutive process that occurs in most of the cells. However phagocytosis only occurs in specialized cells, such as macrophages and typically involve the ingestion of larger particles[31].

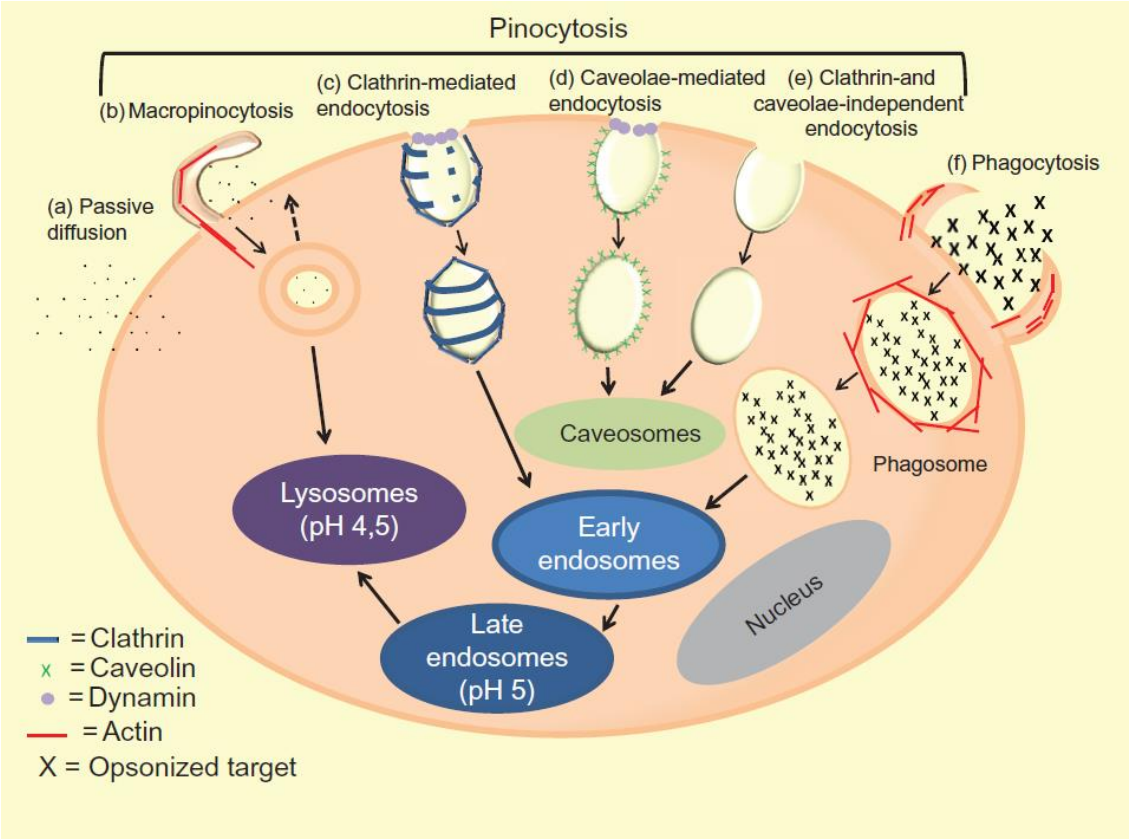

Figure 5. 11.-Scheme of pathways of cellular uptake, extracted from *Panariti et al*[31]. The image excludes most of the intracellular organelles for clarity. In this image, clathrin-mediated and receptor-mediated endocytosis share the same pathway.

The main focus of this study lies in discerning the pathways involved in the cell uptake of polyallylamine-derived polyplexes, thereby providing valuable insights into enhancing the efficacy of delivery systems. The study was mainly focused on pinocytosis routes as polyplexes are too large for simple diffusion and targeted cells do not present phagocytosis capacity.

Then, the polyplex cell uptake was investigated using the most effective vector, based on PAH.OA.10 at N/P 5, by using fluorescently labelled siRNA. To elucidate the pathway used by the selected non-

viral vector, the cells were pre-treated with specific inhibitors to selectively block different cell internalization pathways.

- Amiloride-HCl: It inhibits macropinocytosis, its mechanism is not fully understood, but it is believed that this compound can alter Na+/H+ channels. As a consequence the submembrane pH decreases and affect GPTases proteins, such as Rac1 and cdc42 involved in actin-mediated membrane lamellipodia[32].
- Amantadine-HCl: It blocks clathrin-mediated endocytosis pathway by preventing budding of clathrin-coated pits.
- Genistein: It inhibits the caveolae-mediated uptake through the blocking of Src-family tyrosine kinases. Caveolin, protein involved in the caveolae formation need to be phosphorylated for proper function, a task performed by Src-tyrosine kinases[33].
- Cytochalasin D (CytD) destroys cytoskeleton, which has a strong impact on particle transportation in cells. Specifically, CytD inhibits actin polymerization by binding to actin filaments and preventing the normal dynamic assembly and disassembly of actin filaments [34].

The following concentrations were used to pre-treat A549 cells during 2h before treatment with polyplexes[35]:

- 2 mM Amiloride HCl (macropinocytosis),
- 1 mM Amantadine-HCl (Clathrin-mediated endocytosis),
- 100 μM Genistein (Caveolin-mediated endocytosis),
- 10 μg/mL cytochalasin D (Actin-dependent pathways).

A combination of inhibitors was also used to study synergies among mechanisms. In one condition, the four inhibitors were applied and in the consecutive conditions all inhibitors were used except one, indicated in Figure 5.12.

Once the different routes were inhibited, PAH.OA.10 /siRNA-cy5 polyplexes were added to the cells, and internalization was studied by flow cytometry after 2 hours. The average of four replicates of the median fluorescence intensity of 10,000 events per condition were measured and plotted in Figure 5.12. It is noteworthy that this intensity only corresponds to living cells and singlets, which were pre-selected, and is directly proportional to the quantity of internalization.

In Figure 5.12, the grey columns depict the internalization of cells with or without inhibition of a single route, while the blue columns represent combinations of different inhibitors. Also, one of the inhibitor combinations corresponds to all four routes (Figure 5.12 comb ALL), and the remaining columns denote conditions where all but one indicated route was inhibited (Figure 5.12 Comb 1, comb 2, Comb 3 and comb 4).

Non-treated cells do not present any intensity as expected and treatment with polyplex present about 400,000 units. It can be observed that internalization is reduced when macropinocytosis and caveolae-mediated endocytosis are inhibited, with a p-value less than 0.05. On the other hand, no reduction in internalization efficiency was observed when the clathrin or the caveolae were blocked,

indicating that those 2 internalization pathways are not privileged. When all the routes considered in this study were inhibited, the lowest internalization was obtained with a significance p-value < 0.01. When all routes are inhibited except for micropinocytosis (Comb1) and caveolae (Comb 3)-mediated endocytosis, the internalization was found to be slightly lower than the one observed when all pathways were inhibited. Thus, these results of blocking single and combined internalization pathway confirmed that macropinocytosis and caveolae-mediated endocytosis are the predominant pathways for polyplex internalization. However, the relatively low internalization observed for Comb 4 when both routes, macropinocytosis and caveolae-mediated endocytosis, were inhibited revealed that the internalization process is more complex. The contribution of alternative internalization pathway, albeit less prominent, was already indicated with a significant internalization of the polyplexes observed, despite using all 4 inhibitors.

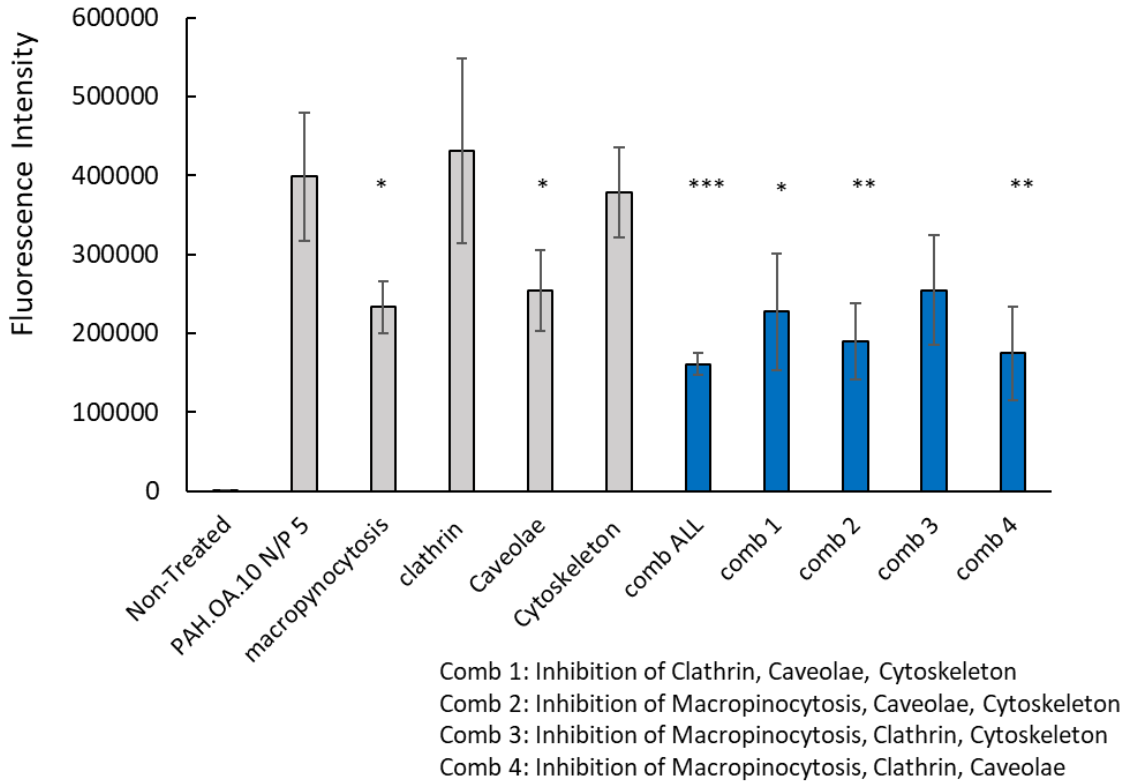

Figure 5. 12.-Fluorescence Intensity of A549 cells measured by flow cytometry, after 2h treatment with PAH.OA.10/siRNA-Cy5 polyplexes at N/P 5. Uptake pathways were inhibited by using 2 mM Amiloride HCl (macropinocytosis), 1 mM Amantadine-HCl (Clathrin-mediated endocytosis), 100 µM Genistein (Caveolin-mediated endocytosis), 10 µg/mL Cytochalasin D (Actin-dependent pathways) and the combination of them: comb ALL, Comb 1 (Inhibition of Clathrin, Caveolae, Cytoskeleton), Comb 2 (Inhibition of Macropinocytosis, Caveolae, Cytoskeleton), Comb 3 (Inhibition of Macropinocytosis, Clathrin, Cytoskeleton) and Comb 4(Inhibition of Macropinocytosis, Clathrin, Caveolae). Data points marked with asterisks are statistically significant relative to PAH.OA.10 N/P 5 p-value * < 0.05, ** < 0.01 ***<0.001 ANOVA, n=4.

According to *Panariti et al.*[31], nanoparticles with diameters above hundreds nanometres tend to enter cells primarily via macropynocitosis, while caveolin-mediated endocytosis are more likely to be the preferred pathway for smaller nanoparticles. It is possible that aggregates found by TEM and DLS depicted in Chapter 4 about 150-200 nm (Table 4.3 and Figure 4.9) are taken up by the cells using this route, and the individual polyplexes of 12 nm enter via caveolin-mediated endocytosis.

However, it is important to emphasize that these are preliminary inferences based on the available data and observed patterns so far. Further experiments are required to corroborate these hypotheses. Interestingly, PEI/siRNA polyplexes also used predominantly macropynocitosis and caveolin-mediated endocytosis[36], similarly to PAH.OA polyplexes.

The siRNA delivery efficiency could be improved by avoiding endocytosis and introducing modifications in the polyplex that enable the nanoparticle to directly fuse with the cell membrane. Such a modification would represent a strategic breakthrough in improving siRNA delivery and enhancing its therapeutic potential.

5.2.6 CD47 knockdown by PAH.OA

To further explore the potential of PAH.OAs as siRNA delivery system especially in the context of cancer therapy, CD47 gene was selected as a therapeutic target for lung cancer. As explained in the introduction, CD47 is a transmembrane protein overexpressed in cancer cells and recognized by macrophages as a "don't eat me signal[10]. Blocking the interaction between CD47 and SIRPα in macrophages will promote the phagocytosis of cancer cells as demonstrated in previous works[6,8,37,38]. Accordingly, in the subsequent parts of this study, we investigated the efficacy of PAH.OA-based delivery systems in facilitating the delivery of siRNA targeted against CD47. Specifically, we assessed the impact of such treatment on the expression levels of CD47 at the mRNA and protein stages, providing a comprehensive picture of the therapeutic potential of our proposed strategy.

Messenger RNA is the direct target of siRNA, to measure the level of CD47 mRNA after transfection, the technique of reverse transcription quantitative PCR was used (See Appendix II). A549 cells were treated with siRNA anti-CD47 using different PAH substitutes as carriers. A negative siRNA, which does not have any target described was also used as negative control. As in previous experiments, N/P 5 was chosen to keep the balance between transfection efficiency and low cytotoxicity. Levels of mRNA CD47 were quantified at 24, 48 and 72h after transfection. Delta-delta Ct method ($2^{-\Delta\Delta Ct}$) is a method of relative expression of mRNA levels against a control, which is based on the untreated cells, representing 100% of CD47 expression (See Appendix II).

The results obtained (Figure 5.13) confirmed those obtained for the GFP transfection experiments, as polyplexes prepared with PAH.OA.10 exhibited the best reduction of mRNA levels, followed by PAH.OA.5-based polyplexes. Less reduction of CD47 mRNA expression were obtained when the cells were treated with polyplexes prepared with PAH, PAH.OA.1 and PAH.OA.2, while the one prepared with PAH.OA.20 had barely any effect. As polyplexes prepared with PAH.OA.5 and PAH.OA.10 at N/P 5 were expected to be the most efficient treatment, experiments with negative siRNA (not silencing) were carried out using these two polyplex candidates. As expected, no reduction of CD47 mRNA level could be observed, confirming that the reduction of mRNA levels is due to the siRNA release and not any secondary effect from the polyplexes (Figure 5.13). Among the different time points, the highest reduction of CD47 mRNA levels was achieved after 48h while a slight recovery was observed at 72h. Interestingly, the positive control based on the transfection using Lipofectamine

RNAimax did not exhibit a significant reduction of mRNA between 24h and 48h, unlike the PAH substitutions. Such result might suggest a slower release of siRNA from the endosome using the PAH-based carrier developed in this study. Recovery of mRNA levels occurs due to the post-transcriptional nature of siRNA, since genomic gene is continuously expressed, periodic siRNA treatment would be required. As explained in the introduction chapter, repetitive treatment can be considered as an advantage to avoid irreversible genomic DNA editing.

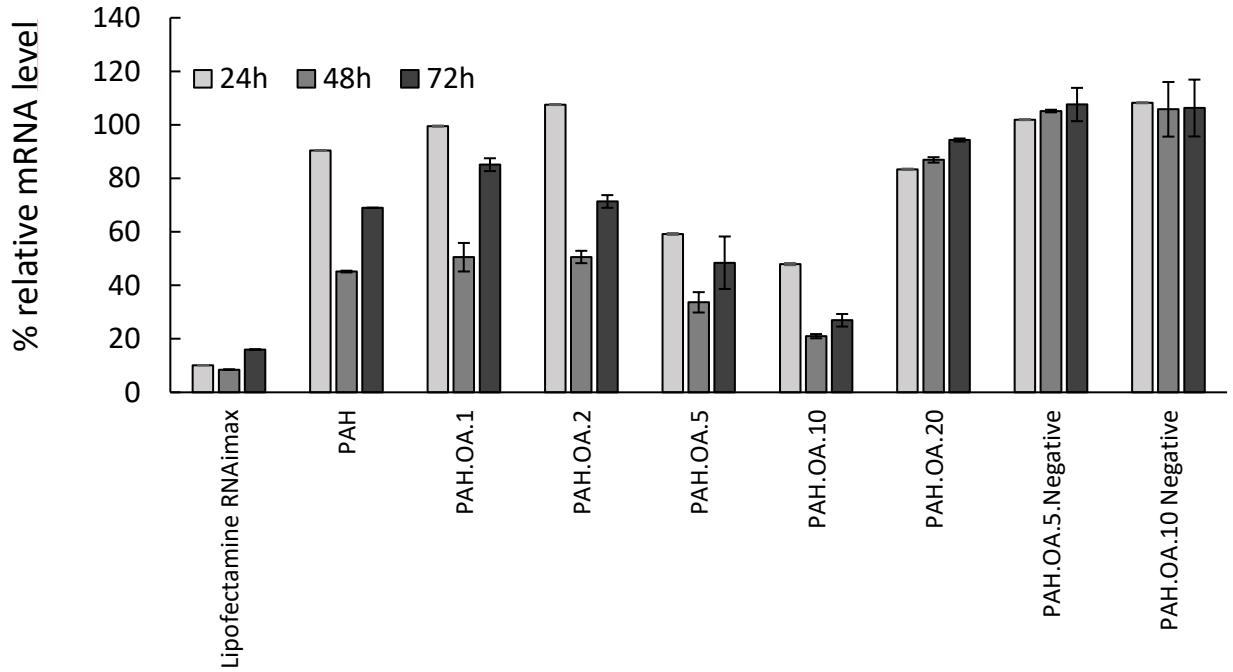

Figure 5. 13.-Level of CD47 mRNA 24h, 48h and 72h after being treated with siRNA-CD47/PAH.OA N/P 5 polyplexes. mRNA was extracted and CD47 amplified by RT-qPCR. 2-(ΔΔCq)*100 method was used to calculate the percentage of mRNA expression relative to non-treated cells.

CD47 mRNA levels are significantly reduced by PAH.OA-based polyplexes, but this result must be translated into an effective protein reduction. The protein levels of CD47 in A549 cells after siRNA treatment have been evaluated by different techniques. As there is a time delay in the transition from mRNA reduction to observable protein reduction, owing to the protein turnover rate in mammalian cells, up to every 35 hours in dividing cells[39], we extend the timeframe to assess the impact of siRNA in CD47 protein levels to 72 and 96 hours.

Immunofluorescence or immunocytochemistry (ICC/IF) is a common microscopy technique to visualize proteins based on antibody binding (See Appendix II). Method is summarized as follows: After the transfection of A549 cells with different PAH.OA/siRNA anti-CD47 N/P 5, cells were fixed and stained with mouse anti-human CD47. A secondary fluorescent rabbit anti-mouse antibody was used to fluorescently mark CD47 proteins. An isotype control of the CD47 antibody, IgG1 K, was used to confirm that no unspecific binding of the antibody occurs. siRNA negative was used as negative control to visualize any difference in CD47 expression.

Stained A549 cells were observed by CLSM 72 h after transfection, as shown in Figure 5.14. Left column represents the transfection with a negative control siRNA, middle column corresponds to the transfection with siRNA anti-CD47 and right column corresponds to siRNA CD47 transfection but with the isotype control staining. The absence of fluorescence signal showed the absence of non-specific binding of IgG1 K. On the other hand, CD47 protein is fully expressed in the cell membrane after transfection with negative control, as the staining with CD47 antibody showed expression in non-treated cells. As expected, protein expression decreased partially with the delivery of siRNA anti-CD47 by PAH, PAH.OA.1 and PAH.OA.2. However, CD47 signal mostly disappeared when PAH.OA.5 and PAH.OA.10 were used as non-viral vectors. In addition, CD47 expression remained unchanged after treatment with PAH.OA.20-based polyplexes. These data are in good agreement with the mRNA levels and with the GFP knockdown experiment. It can be confirmed that CD47 is knocked down by polyallylamine substituted polyplexes.

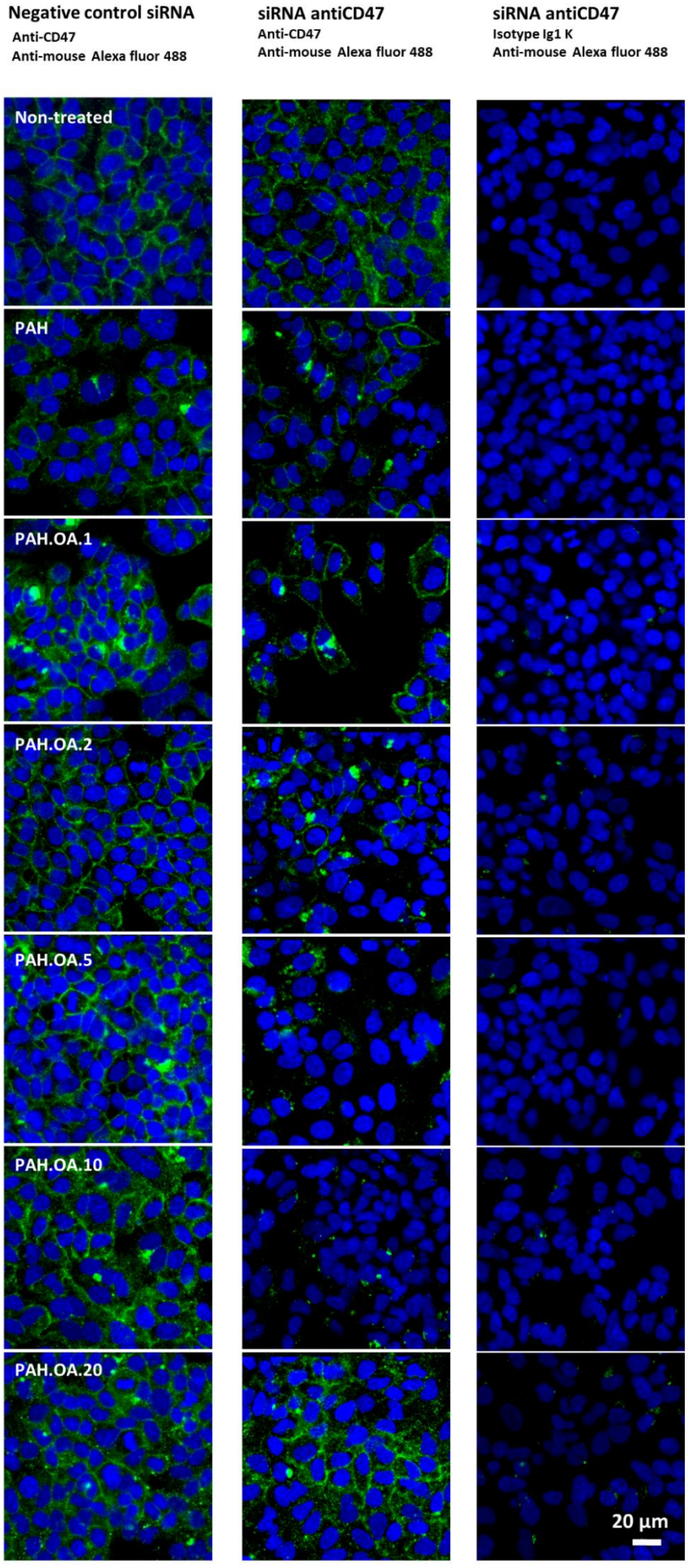

Figure 5. 14.-Inmunofluorescence of A549 cells 72h after transfection with siRNA-CD47/PAH.OA N/P 5 polyplexes. Treated and non-treated cells were fixed and stained with mouse primary anti-human CD47 antibody, isotype control IgG1 K and secondary rabbit anti-Mouse alexa fluor 488 antibody. Protein CD47 is stained in green. First column correspond to transfection with negative siRNA polyplexes. second column to siRNA anti-CD47 transfection. Third column to siRNA anti-CD47 transfection and Isotype IgG1 k staining. Scale bar 20 µm.

In addition, Western Blot was used to support data obtained in ICC/IF. Western blot is a semiquantitative technique also based on immunostaining (See Appendix II). The experiment was carried out as follows, proteins were extracted from A549 transfected cells and separated by molecular weight on a polyacrylamide gel. The proteins were then transferred to a polyvinylidene fluoride (PVDF) membrane, where immunoblotting was performed. Specific antibodies were bound to CD47 protein on the membrane and the protein was revealed using a secondary antibody labelled with horseradish peroxidase enzyme. The enzyme oxidizes luminol substrate, leading to light emission—a process known as chemiluminescence. This reaction occurs only at the spot where CD47 is located. The image of the membrane captures the chemiluminescence, revealing a band indicating the presence of CD47. The band's width can vary based on the protein quantity, which allows the partial quantification of the protein. A housekeeping protein, which is based on constitutive genes that are required for the maintenance of basic cellular function and are expressed in all cells of an organism under normal and patho-physiological condition, was used as control for condition. Therefore, it was used to validate that any change in CD47 band width was only due to the treatment.

Figure 5.15 shows Western Blot of protein CD47 after transfection with siRNA anti-CD47 polyplexes prepared with Lipofectamine RNAimax (L, as positive control), PAH (P), PAH.OA.1 (1), PAH.OA.2 (2), PAH.OA.5 (5), PAH.OA.10 (10) and PAH.OA.20 (20) at N/P 5. Cyclophilin A (CPA) was chosen as housekeeping protein because of the good separation in terms of molecular weight (18 KDa) with CD47 (47-52 KDa). Molecular weight of each protein was identified by using a protein standard ladder. CPA appeared as a single band, while CD47 presented two bands because of phosphorylation, as phosphatase inhibitor was used.

CPA expression did not change after treatment with siRNA-CD47 polyplexes. However, some polyplexes modified the expression of CD47. Non-treated cells (NT in Figure 5.15) presented wide and dark band, while the band intensity was slightly lower when polyplexes prepared with PAH, PAH.OA.1, PAH.OA.2 and PAH.OA.20 were used for treatment. Positive control, lipofectamine

RNAimax showed a fainted band, similarly to the treatment with PAH.OA.5 and PAH.OA.10, confirming the CD47 knockdown.

Again, those results are in excellent agreement with all the results previously obtained and the latest based on mRNA levels and immunofluorescence images (Figure 5.13 and 5.14).

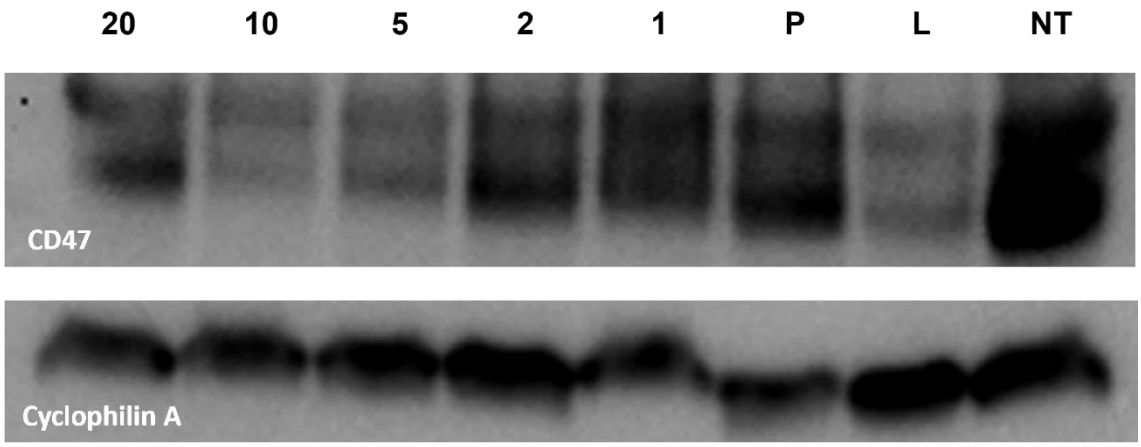

Figure 5. 15.-Western Blot of CD47 protein. Protein expression in A549 cells 72h after transfection with siRNA-CD47/PAH.OA N/P 5 polyplexes. CD47 shows two bands at ~50 and ~42 KDa and Cyclophilin A (housekeeping protein) present one band at 18 KDa. From right to left Non-treated cells (NT), Lipofectamine RNAimax/siRNA-CD47 (Lipo), PAH/siRNA-CD47 (PAH), PAH.OA.1/siRNA-CD47 1% Oleic acid (1), PAH.OA.2/siRNA-CD47 2% Oleic acid (2), PAH.OA.5/siRNA-CD47 6% Oleic acid (5), PAH.OA.10/siRNA-CD47 14% Oleic acid (10), PAH.OA.20/siRNA-CD47 >14% Oleic acid (20).

Despite the qualitative information extracted from Western Blot compared to CD47 expression, flow cytometry was used to quantify the levels of protein after staining protein with fluorescent antibodies. Fluorescence intensity of the cells is directly correlated to the quantity of CD47. Again, A549 cells were treated with siRNA anti-CD47 using polyplexes at N/P 5, and negative siRNA was delivered as well in every condition. Cells were harvested 72h after transfection and indirectly stained with kit of antibodies: mouse anti-human CD47 and Rabbit anti-mouse Alexa fluor 488. Similar to the immunofluorescence experiment, an isotype control for IgG1 k anti-CD47 was performed to discard any unspecific binding.

Figure 5.16 shows the fluorescence intensity of stained A549 either with isotype (iso) or anti-CD47 (1º) antibodies and Alexa fluor 488 secondary antibodies (2º) after different polyplex treatment.

High levels of fluorescence are achieved with anti-CD47 (> 70,000 counts) and low levels with isotype (< 7,000 counts), discarding any undesired binding.

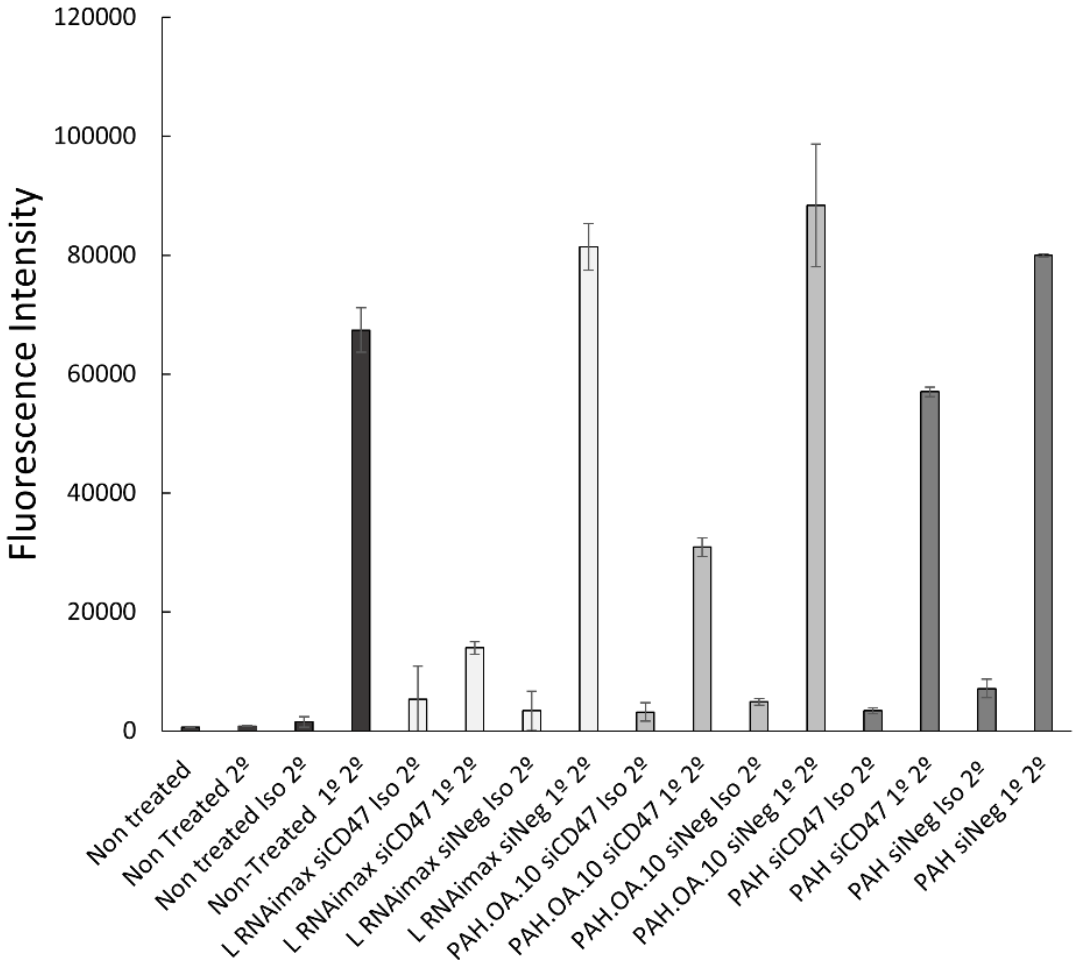

Figure 5. 16.-Flow cytometry Isotype control of CD47-stained A549 cells. Cells were transfected with siRNA anti-CD47 or negative siRNA. Cells were stained with antibodies anti-CD47 or its isotype control Ig1 K. Data represented raw fluorescence intensity mean. n=2 error bars represent standard deviation. L= Lipofectamine; siCD47= siRNA anti-CD47; siNeg= non-target-siRNA; Iso= Isotype control Ig1 k; 1º= Mouse antihuman CD47; 2º= Secondary Antibody rabbit antimouse-Alexa fluor 488;

Immunofluorescence intensity of A549 cells treated with the polyplexes developed in this study was measured by flow cytometry. Raw data were normalized and represented as a relative expression of CD47 compared to the fluorescence of CD47 treated with negative siRNA using the same polymer. Raw data of non-treated cells, Lipofectamine RNAimax, PAH.OA.10 and PAH are shown in Figure 5.16, while normalized data are shown in Figure 5.17 as percentage of CD47 expression.

Cells treated with PAH-based polyplexes expressed 60% of CD47, while PAH.OA.1 PAH.OA.2 and PAH.OA.20 resulted in 90%, 70% and 100% of CD47 expression, respectively. In any of these cases CD47 knockdown is below 50% and could not be considered as efficient. On the other hand, for the treatment with polyplexes prepared with PAH.OA.5 and PAH.OA.10 CD47 expression was reduced down to 40% and 30%, respectively. It is worth mentioning that the reduction did not achieve the one obtained with the positive control Lipofectamine RNAimax at around 25%. In any case, it is clear

that OA functionalization, in a certain DS range, increases polyallylamine delivery efficiency of siRNA.

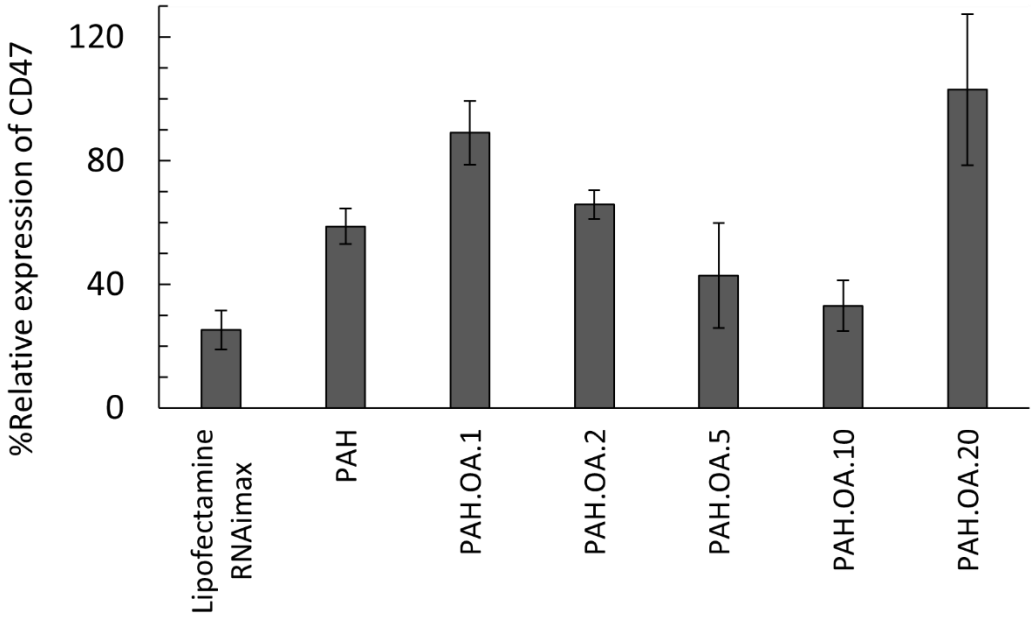

Figure 5. 17.-Flow cytometry of CD47-stained A549 cells. Data represented as relative expression of CD47 in percentage. siRNA-CD47 fluorescence values divided by siRNA negative fluorescence values of every transfection condition. n=2.

CD47 was *silenced* in mRNA and protein levels. CD47 silencing is an interesting strategy for non-small cell lung cancer (NSCLC) because blocking SIRPα/CD47 interactions with antibodies have shown to be efficient[6,37,40]. However, safety concerns arose due to the ubiquitous expression of CD47, particularly on hematopoietic cells. For example, mice that received an acute infusion of antibodies exhibited temporary anaemia or neutropenia[8]. So, a specific delivery of siRNA to the tumour should be designed to overcome this issue.

5.3 Conclusions

This chapter together with chapter 4 was evaluating the impact of OA DS on polyallylamine homopolymer on siRNA delivery. For this purpose, an increasing amount of OA was grafted to the polymer chain, at DS of 1%, 2%, 6%, 14% and >14% approximately. The previous chapter covers the chemical characterization of these new materials and the physico chemical properties of the self-assembled nanoparticles achieved when the polymers are dispersed in water. All substitutions can entrap efficiently siRNA (above 80% of 0.1 nmol) even at low N/P ratio, i.e. N/P of 2.5, between polymer and siRNA. The resulting complex between polymer and siRNA, called polyplex, was tested *in vitro* as candidate for possible oligonucleotide delivery.

In this chapter, critical barriers for siRNA delivery were investigated. Cytotoxicity studies of the polyplexes showed cell death at high N/P ratio 15, but proved to be harmless at N/P ratios 2.5 and 5. At an N/P ratio of 10, the beneficial influence of oleic acid was evident, as we observed an increase

in cell viability correlating with OA DS. This relationship was further reinforced by the absence of significant cell membrane damage in these conditions.

Interestingly, all substitutions can pass the cell membrane as it was observed in the CLSM studies, overcoming one of the obstacles encountered at cellular level. Up to 70% of the cells contained polyplexes in the cytosol, demonstrating the ability of the polyplexes to be internalized without any significant effect of OA DS. Uptake mechanism seems to be dominated by size, shape and surface charge of the nanoparticles[23], being for PAH.OA.10 polyplexes macropinocytosis and caveolae-mediated endocytosis the main pathways of internalization, although other route are surely privileged by the non-viral vectors.

The most difficult barrier encountered before the release of the siRNA is the endosome, since it could be relatively easy to enter, but not so easy to escape[27]. At this point, the presence of OA demonstrated to be beneficial, especially PAH.OA.5 and PAH.OA.10 which exhibited the best delivery efficiency. However, the highest OA DS, PAH.OA.20, did not show any transfection. In the literature, this phenomenon is explained by the pKa of cationic lipids in lipidic nanoparticles, being pKa closer to the endosome pH the most effective ones[41,42]. The value of the pKa at endosomal pH range is supported by the proton sponge hypothesis discussed in the introduction, where the endosome ends up being disrupted because of the buffering capacity of the polyplexes. Ongoing experiments are currently under progress to determine the pka of PAH.OAs polymers.

On the other hand, some works questioned the proton sponge hypothesis as no disrupted endosome was observed under microscope[28],[30] and other theories[27] are proposed like interaction of the polymers with the endosome membrane can lead to siRNA leakage. Other articles report that only a small portion of the whole siRNA transfected (1-2%) can actually escape from the endosome[28] and this amount is sufficient to trigger the *silencing* effect[29]. Thus, even if a high proportion of siRNA remains in the lysosomes after transfection with polyallylamine derivatives, small copies lead to the knockdown of eGFP proteins.

Because of the good delivery efficiency achieved by PAH.OAs polymer, especially candidate PAH.OA.10, the therapeutic treatment of the polyplexes was evaluated by targeting CD47. CD47, overexpressed in lung cancer cells, was selected in order to modulate cancer cells to be cleared by phagocytosis. This approach is not so widely explored, but resulted effective in therapies using monoclonal antibodies[6,37,40]. Hence, PAH.OAs-based polyplexes reach CD47 knockdown at mRNA and protein levels, especially for PAH.OA.10. Future work is designed to prove the phagocytosis of CD47-Knockdown-cells *in vitro* as described in other works. Finally, an *in vivo* biodistribution study of the polyplexes is planned to elucidate the circulation time and tissue extent.

5.4 Material and methods

5.4.1 Materials

A549 human lung carcinoma cell line (CCL-185), EMEM Eagle's Minimum Essential Medium (ref: 30-2003) were purchased from **ATCC**. A549 / eGFP stable cells (Blasticidin) was purchased from GeneTarget (ref: SC043-Bsd). RIPA buffer (ref:R0278), Protease Inhibitor Cocktail (Ref: P8340-5ML), Phenylmethanesulfonyl fluoride PMSF (ref: P7626-1G), Phosphatase Inhibitor Cocktail 1 (ref:P2850-1ML), TruPAGE™ TEA-Tricine SDS Running Buffer (ref: PCG3001-500ML), TruPAGE™ LDS Sample Buffer (ref: PCG3009-10ML), TruPAGE™ Transfer Buffer (ref: PCG3011-500ML), TruPAGE™ DTT Sample Reducer (ref: PCG3005-1ML), Immobilon-P Blotting Sandwich (ref: IPSN07852), MISSION® siRNA Fluorescent Universal Negative Control #1, Cyanine 5 (ref: SIC005-1NMOL) were purchase from **Sigma Aldrich**. siRNA negative control (sense 5´UUC UCC GAA CGU GUC ACG UdTdT3´ antisense 5'-ACG UGA CAC GUU CGG AGA AdTdT-3') siRNA anti-eGFP (sense 5´-CAA GCU GAC CCU GAA GUU CdTdT-3´ antisense 5´-GAA CUU CAG GGU CAG CUU GdTdT-3´) and siRNA anti-huCD47 (sense 5'-CCU CUU UGA AGA UGG AUA AdTdT-3' antisense 5'- UUA UCC AUC UUC AAA GAG GdTdT-3') were purchased by demand to **BioSpring Biotechnolgie GmbH**. Lipofectamine RNAimax (Ref: 13778030), Nuclease-free water (ref: AM9932), Opti-MEM™ Reduced Serum Medium no phenol red (ref: 11058021), Fetal bovine Serum FBS (ref:10500-064 Gibco), Trypsin-EDTA (0.25%) phenol red (ref: 25200056 Gibco), Penicillin-Streptomycin 10,000 U/mL (ref: 15140122 Gibco), Trypsin-EDTA (0.5%), no phenol red (Ref: 15400054), LIVE/DEAD™ Viability/Cytotoxicity Kit for mammalian cells(ref: L3224), Silencer™ FAM-labeled Negative Control No. 1 siRNA (ref:AM4620), Hoechst 33342 Solution (ref: 62249), ActinRed™ 555 ReadyProbes™ Reagent (Ref: R37112), CD47 Monoclonal Antibody (B6H12) eBioscience™ (Ref: 14-0479-82), Goat anti-Mouse IgG (H+L) Cross-Adsorbed Secondary Antibody, HRP (ref: G-21040), Goat anti-Mouse IgG (H+L) Cross-Adsorbed Secondary Antibody Alexa Fluor 488 (ref: A-11001), Blasticidina S HCl 10 mg/ml (ref: A1113903), were purchased from **Thermo Fisher**. Recombinant Anti-Cyclophilin A antibody EPR7511 (ref: ab126738) was purchased from **Abcam**. Atto-633-NHS ester (ref: AD 633-3) was purchased from **atto-tec GmbH**. CellTiter 96® AQueous One Solution Cell Proliferation Assay MTS (ref: G3580) was purchased from **Promega**. RNeasy Plus Mini Kit 50 (Ref: 74134) to **QIAGEN**. PrimePCR™ SYBR® Green Assay CD47 Human, PrimePCR™ SYBR® Green Assay GAPDH Human, iTaq™ Universal SYBR® Green Supermix 500 x 20 µl rxns, 5 ml (5 x 1 ml), Precision Plus Protein™ WesternC™ Blotting Standards (ref: 1610376), Clarity™ Western ECL Substrate 200 ml (ref:1705060) were purchased from **Bio-Rad**. Spectra-Por® Float-A-Lyzer® G2 3,5-% KDa 1 mL (ref: Z726060) was purchased from **Merck.** PD-10 desalting columns (ref:17085101) was purchased from **GE Healthcare**. µ-Slide 8 Well plate (ref: 80826) was purchased from **Ibidi**.

5.4.2 Methods

5.4.2.1 Cell culture

A549 human pulmonary cell line was cultured with EMEM´s Medium supplemented with 10% v/v Fetal bovine Serum FBS and 1% v/v Penicilin-Strptomicine (P/S). A549 stably expressing eGFP (A549-eGFP) were kept in EMEM´s medium 10% FBS, 1% P/S and 10 µg/mL Blasticidin.

5.4.2.2 Cytoroxicity assay: MTS and Live/dead

The cytotoxicity of polyplexes was evaluated on the A549 cell line after a 24-h exposure. Cells were seeded in either a 96-well plate for MTS or µ-Slide 8-Well plate for Live/dead, using EMEM supplemented with 10%

FBS and 1% Penicillin-Streptomycin in both cases. Once the cells were confluent (after 24h), freshly prepared polyplexes, as described in section 4.4.2.7, were added to the cell culture. Polyplexes tested included PAH, PAH.OA.1, PAH.OA.2, PAH.OA.5, PAH.OA.10, and PAH.OA.20 at four different N/P ratios: 2.5, 5, 10 and 15, with a final siRNA concentration of 200 nM per well. The medium in each well was replaced with OptiMEM serum-reduced medium, and polyplexes were added to each well in quadruplicate. The cells were then incubated for 24 hours at 37°C and 5% CO_2. Subsequently, either the MTS CellTiter 96® AQueous One Solution or Live/dead tests were conducted.

The principles of the MTS test are described in Appendix II. An equal volume of MTS solution was added to each well, matching the volume of the cells, and incubated for 2 hours at 37°C and 5% CO_2. The absorbance of the resultant Formazan product was measured at 490 nm using the Synergy HT plate reader by Biotek.

For the Live/Dead test (See principles in Appendix II), the kit components Calcein AM and Ethidium Homodimer-1 were diluted in cell medium to the recommended working concentrations of 2 µM and 4 µM, respectively. The solution was added to the wells, and the plate was incubated for 45 minutes at room temperature. Immediately afterwards, the cells were washed and observed under fluorescence microscope.

5.4.2.3 Polymer labelling with fluorophore Atto-633

Fluorophore Atto-633-NHS ester was attached to the PAH, PAH.OA.1, PAH.OA.2, PAH.OA.5, PAH.OA.10 and PAH.OA.20 following provider´s instructions with a few modifications. Labelling was performed adding 1 molecule atto-633 per 2000 monomer of polymer. Between 5-8 mg of the different polymers were used and 0,02 mg of Atto-633. Polymers were dissolved in 2 mL deionized H_2O and pH adjusted to 8. A solution of 20 µL atto-633 in dimethylformamide (DMF) was added to the polymer solution. Reaction was stirred for 2 hours protected from light. Reaction product was purified by PD-10 desalting columns and dialysis in Floatlyzer G2 2,5-5 KDa against water for 2 days. Samples were freeze-dried and analysed by ^{1}H-NMR (500 MHz D_2O) and Fluorescence Correlation spectroscopy (FCS) to verify that all the dye was attached to the polymer. Aqueous solution of labelled-polymers and free Atto-633 molecule were placed in the wells of a µ-Slide 8-Well plate and diffusion coefficient were measured using a Zeiss LSM 510 confocal laser scanning microscope.

5.4.2.4 Cell uptake studies

A549 cells were cultured in µ-Slide 8 Well ibidi plates at a density of 30,000 cells per well. After 24 hours, polymers labelled with atto-633 (PAH, PAH.OA.1, PAH.OA.2, PAH.OA.5, PAH.OA.10, PAH.OA.20) were used to form polyplexes with siRNA-6-FAM at an N/P ratio of 5, as previously described. The final siRNA concentration per well was set at 200 nM. Confluent cells were exposed to the resultant polyplexes for 24 hours for transfection. Subsequently, the cells were washed with DPBS, fixed with 4% v/v paraformaldehyde (PFA), and permeabilized with 0.5% v/v Triton-X-100, with DPBS washes between each step. Afterwards, the cell nucleus was stained with a 1:2000 dilution of Hoechst 33342 and actin with ActinRed™ 555 (two drops of stock solution as indicated by the provider). Cells prepared for imaging were preserved in DPBS. The ibidi plates were then analysed using a Zeiss LSM 510 Confocal Laser Scanning Microscope (CLSM). CLSM images were captured with 405, 488, 561, and 633 nm excitation laser lines, using a 63x objective. Z-stack experiments were also conducted and displayed as orthogonal views processed with ZEN 3.3 software and ImageJ.

Quantification of siRNA-6-FAM internalization was carried out by Flow cytometry as follows: A549 cells were seeded in a 24-well plate at a density of 60,000 cells per well. After 24 hours, polyplexes formed at N/P ratio

5 with different polymer substitutions and siRNA-6-FAM were added to the cells in OptiMEM media. siRNA kept a final siRNA concentration of 200 nM per well under all conditions. After a 24-hour incubation, the cells were washed and detached using 0.25% trypsin/EDTA without Phenol red. Trypsin activity was neutralized by adding DPBS containing 10% FBS, and the resultant cell suspension was transferred to flow cytometry tubes. A total of 10,000 events were measured on a FACS Diva Canto II flow cytometer. Data are presented as the percentage of events showing 6-FAM fluorescence, with non-treated cells set as showing 0% fluorescence.

5.4.2.5 Study of endocytic pathways

The internalization pathways of PAH.OA.10 in the A549 cell line were investigated using various inhibitors to block the main routes: Amiloride HCl for macropinocytosis, Amantadine-HCl for clathrin-mediated endocytosis, Genistein for caveolin-mediated endocytosis, and cytochalasin D for actin-dependent pathways.

The inhibitors were added to confluent A549 cell cultures in a 24-well plate to achieve the following working concentrations: 2 mM Amiloride HCl, 1 mM Amantadine-HCl, 100 µM Genistein, and 10 µg/mL cytochalasin D. A combination of these drugs was also tested, each maintaining the same final concentration per well. The combinations were: Comb All (Amiloride HCl, Amantadine-HCl, Genistein, and Cytochalasin D), Comb 1 (Amantadine-HCl, Genistein, and Cytochalasin D), Comb 2 (Amiloride HCl, Genistein, and Cytochalasin D), Comb 3 (Amiloride HCl, Amantadine-HCl, and Cytochalasin D), and Comb 4 (Amiloride HCl, Amantadine-HCl, and Genistein).

Cells were exposed to these inhibitors for 2 hour in OptiMEM serum-reduced medium, after which polyplexes of PAH.OA.10/siRNA-Cy5 at an N/P ratio of 5 were added, with a final concentration of siRNA 200 nM. After 2 hours of exposure, cells were washed with DPBS and detached using 0.25% trypsin/EDTA without phenol red and transferred to flow cytometry tubes. Then, 10,000 events were counted with a BD accuri c6 plus flow cytometer. Live cells and singlets were selected, and the median fluorescence intensity was plotted. Statistical analysis was conducted using ANOVA with a sample size (n) of 4, comparing non-inhibited cells (serving as the negative control) to their respective drug and drug combination treatments.

5.4.2.6 Delivery efficiency by flow cytometry

Delivery efficiency of siRNA inside cells was assessed by measuring the siRNA silencing of eGFP protein by flow cytometry. A549 cells stably expressing eGFP (A549-eGFP) were seeded in 24-well plates at 60,000 cells/well using EMEM 10% v/v FBS 1% v/v P/S and 10 µg/mL Blasticidin. Transfection was performed using polyplexes of PAH.OA/siRNA anti-eGFP at ratios N/P 2.5, 5 and 10, using 0.1 nmol of siRNA to achieve a final concentration of 200 nM per well. Lipofectamine RNAimax was used as positive control and complex was prepared following the protocol provided by the manufacturer, using same amount of siRNA. Cells media were substituted by OptiMEM and complexes were distributed into the well. After 24 hours incubation, cells were washed and refreshed with growth media. Cells were incubated between 72-96 hours after transfection to obtain an effective protein reduction. Once incubation finished cells were lifted with 0.25% trypsin/EDTA without phenol red. Trypsin effect was blocked with DPBS 10% FBS and the resulting cells solution was transferred to a flow cytometer´s tube. Samples were measured with a Flow Cytometer FACS diva canto II. FITC filter was applied to count eGFP expressing cells. Software BD FACS Diva was used to measure the mean fluorescence intensity of 10,000 events per condition. Data is presented as relative GFP expression normalized to the intensity of the non-treated cells, considered 100% of GFP-expression. Every condition had

3 technical replicates and experiment was conducted three times. An statistical analysis was performed using t-test single tail comparing non-treated cells as negative control to respective polyplex treatment.

5.4.2.6 mRNA quantification by RT-qPCR

A549 cells were seeded in 24-well plate at 60,000 cells/well. 4 wells per condition were used. 24 hours after, confluent cells were transfected with polyplexes in OptiMEM media. Polymers with different substitutions of oleic acid were complexed with 0.1 nmol of anti-CD47 siRNA and 0.1 nmol of negative control siRNA at ratio N/P 5, resulting in 200 nM of final siRNA concentration per well. After 24 hours cells were washed with DPBS and fresh growth media was added to the well for 48 and 72 hours. Levels of mRNA-CD47 were measured 24, 48 and 72 hours after transfection. mRNA was extracted following the instructions of QIAGEN mini kit. Briefly, after cells being washed, 350 µL of RLT buffer supplemented with β-mercaptoethanol was added to the wells. Wells were scratched with a pipette tip and solution collected in a 2 mL tube. Solution was homogenized by passing through a needle of a syringe 5 times. The homogenized lysate was transferred to gDNA eliminator spin column, centrifuged and flow-through was saved to the next step. 350 µL of ethanol was added to the solution and this was transferred to the provided RNeasy spin column. The solution was centrifuged and the flow-through discarded. Then, RNA retained in the column was washed consecutively with buffers RW1 once and RPE twice. Finally, RNA was eluted with RNAse-free water and concentration quantified with Nanodrop™ One. RNA obtained was transformed to cDNA using Reverse transcription system by Promega. RNA was diluted until having the same concentration for all conditions of 100 ng. Then a master mix of $MgCl_2$, reverse transcription buffer, dNTPs, RNAsin® ribonuclease inhibitor, Oligo(dT)15 and AMV reverse transcriptase was added to the RNA samples and set on Biometra T1 thermocycler. Samples were heated 1 hour at 42ºC. Once the retrotranscription finished samples were stored at -20ºC or directly proceeded to the next step. cDNA samples were amplified for specific gene human CD47 and the housekeeping gene human GAPDH. Bio-rad iTaq Universal SYBR green supermix was used with specific primers already designed by Bio-Rad for gene CD47 and GAPDH. Samples of every condition were put on 96-well PCR plates by triplicates, 3 replicates for target gene and 3 for housekeeping gene. Plates were introduced in Bio-Rad CFX connect Real-time PCR system. Amplification cycles were firstly 95°C denaturing, then 40 cycles of 95°C 5 seconds and 60ºC 30 seconds annealing and extension. Ct data of each sample were obtained after PCR had finished. Delta-delta Ct method ($2^{-\Delta\Delta Ct}$) was used to calculate the relative fold expression of CD47 in A549 after being transfected by siRNA anti-CD47.

5.4.2.7 Immunocytochemistry of CD47 protein

A549 cells were cultured in 8-well ibidi plates at a density of 30,000 cells per well. After 24 hours, polymers (PAH, PAH.OA.1, PAH.OA.2, PAH.OA.5, PAH.OA.10, PAH.OA.20) were used to form polyplexes with both anti-CD47 siRNA and a negative control siRNA at an N/P ratio of 5, maintaining the siRNA concentration at 200 nM per well. The cells were exposed to the polyplexes for 24 hours, after which they were washed and supplied with fresh growth media. The siRNA was then allowed to take effect for up to 72 hours. At this point, the cells were fixed with 4% v/v PFA and permeabilized with 0.5% v/v Triton-X-100. The cells were then incubated with 5% BSA in PBST (PBS with 0.1% tween 20) for 30 minutes at room temperature. Following this, the cells were incubated either with a primary antibody solution (mouse anti-CD47 antibody in a solution of PBST with 1% BSA) or only in a 1% BSA PBST solution overnight at 4°C. The next day, the wells were washed and incubated with a secondary FITC-labelled goat anti-mouse antibody for 30 minutes at room temperature. After another washing step, the cells were incubated in a solution of 2 µg/mL Hoechst 33342 at room temperature for 10 minutes. Finally, the ibidi plate was analyzed with a Zeiss LSM 510 confocal laser scanning

microscope (CLSM) using a 63x objective, and images were captured by exciting the cells with 405 and 488 nm lasers.

5.4.2.8 Western blot of CD47

The A549 cell line was cultured in 56 cm^2 Petri dishes at a density of 1,700,000 cells per dish using EMEM growth media supplemented with 10% FBS and 1% P/S. Cells were transfected with Polymer/siRNA-CD47 complexes using PAH substituted polymers (PAH, PAH.OA.1, PAH.OA.2, PAH.OA.5, PAH.OA.10, PAH.OA.20) and Lipofectamine RNAiMax as a control, all maintaining a final siRNA concentration of 200 nM per dish. After 72 hours, protein was extracted using 1 mL of RIPA buffer supplemented with 1% v/v phosphatase inhibitor cocktail 1, 1 mM PMSF, and 100 µL/mL protease inhibitor cocktail. The protein concentration in the supernatant was determined by the Bradford assay, using BSA as a standard. 90 µg of protein from each condition was mixed with TruPAGE™ LDS Sample Buffer (Laemmli buffer) and TruPAGE™ DTT Sample Reducer and incubated at 80°C for 10 minutes. Proteins were separated on a 10% bis-acrylamide SDS gel using TruPAGE™ TEA-Tricine SDS running buffer for 30 minutes (stacking phase) at 80 V and 60 minutes (resolving phase) at 120 V. After electrophoresis, proteins were transferred onto a pre-activated PVDF membrane using a wet transfer chamber filled with cold 1x TruPAGE™ Transfer Buffer. The transfer was carried out for 1 hour at a constant current of 350 mA. The membrane was then blocked with 5% milk in TBST for 1 hour at room temperature. After blocking, the membrane was incubated with primary antibodies (a 1/500 dilution of anti-CD47 in 5% milk TBST, and a 1/2000 dilution of anti-Cyclophilin A (CPA)) overnight at 4°C with stirring on a roller mixer. The next day, the membrane was washed three times with TBST before incubation with secondary antibodies (1/2000 dilution of goat-anti-mouse-HRP for CD47 and 1/2000 dilution of goat-anti-rabbit-HRP for CPA) for 1 hour at room temperature. Finally, the ECL substrate was applied to the membrane, and chemiluminescence was visualized using the iBright imaging system.

5.4.2.9 Flow cytometry evaluation of CD47 knockdown

The A549 cell line was cultured in a 24-well plate at a density of 60,000 cells per well in growth media composed of EMEM with 10% FBS and 1% P/S. After 24 hours, cells were transfected with polyplexes formed with various polymers (PAH, PAH.OA.1, PAH.OA.2, PAH.OA.5, PAH.OA.10, PAH.OA.20) and either siRNA anti-CD47 or negative control siRNA at a final concentration of 200 nM per well. Lipofectamine RNAiMax was also used as a positive control following the manufacturer's instructions. All conditions were performed in duplicate. Transfection was performed using OptiMEM media and lasted for 24 hours. Following this, cells were washed with DPBS and refreshed with growth medium. Cells were then incubated for a further 48 hours, reaching 72 hours post-transfection to allow time for the siRNA to knockdown the target protein. At this point, cells were lifted with 0.25% trypsin/EDTA and the cell suspension was transferred to a 2 mL tube. Cells were then centrifuged to form a pellet and resuspended in a blocking solution of 5% BSA in DPBS for 30 minutes at room temperature. Next, cells were washed and incubated for 30 minutes in a solution of 2% BSA with 1 µg of primary antibody against CD47 at room temperature. After washing, the secondary antibody anti-mouse-488 was added to the cells at a concentration of 10 µg/mL and incubated for 30 minutes. Subsequently, cells were transferred to flow cytometer tubes and measured with the FACS Diva Canto II. The mean FITC intensity was collected from the cytometer and the relative expression of CD47 was calculated by dividing the FITC mean of the siRNA CD47-treated cells by the FITC mean of the negative siRNA-treated cells.

5.5 References

1. Kris, M. G. *et al.* Adjuvant systemic therapy and adjuvant radiation therapy for stage I to IIIA completely resected non-small-cell lung cancers: American society of clinical oncology/cancer care Ontario clinical practice guideline update. *J. Clin. Oncol.* **35**, 2960–2974 (2017).

2. Kumar, V., Yadavilli, S. & Kannan, R. A review on RNAi therapy for NSCLC: Opportunities and challenges. *WIREs Nanomedicine and Nanobiotechnology* **13**, e1677 (2021)..

3. June, C. H., O'Connor, R. S., Kawalekar, O. U., Ghassemi, S. & Milone, M. C. C CAR T cell immunotherapy for human cancer. *Science* **359**,1361-1365 (2018).

4. Kim, H. S. *et al.* Directly reprogrammed natural killer cells for cancer immunotherapy. *Nat. Biomed. Eng.* **5**, 1360–1376 (2021).

5. Xiang, X., Wang, J., Lu, D. & Xu, X. Targeting tumor-associated macrophages to synergize tumor immunotherapy. *Signal Transduct. Target. Ther.* **6**, (2021).

6. Schürch, C. M. *et al.* Targeting CD47 in Anaplastic Thyroid Carcinoma Enhances Tumor Phagocytosis by Macrophages and Is a Promising Therapeutic Strategy. *Thyroid* **29**, 979–992 (2019).

7. Liu, R. *et al.* CD47 promotes ovarian cancer progression by inhibiting macrophage phagocytosis. *Oncotarget* **8**, 39021–39032 (2017).

8. Wang, Y. *et al.* Intravenous delivery of siRNA targeting CD47 effectively inhibits melanoma tumor growth and lung metastasis. *Mol. Ther.* **21**, 1919–1929 (2013).

9. Wu, J. *et al.* A Glutamine-Rich Carrier Efficiently Delivers Anti-CD47 siRNA Driven by a 'glutamine Trap' to Inhibit Lung Cancer Cell Growth. *Mol. Pharm.* **15**, 3032–3045 (2018).

10. Huang, C. Y., Ye, Z. H., Huang, M. Y. & Lu, J. J. Regulation of CD47 expression in cancer cells. *Transl. Oncol.* **13**, 100862 (2020).

11. Putnam, D., Gentry, C. A., Pack, D. W. & Langer, R. Polymer-based gene delivery with low cytotoxicity by a unique balance of side-chain termini. *Proc. Natl. Acad. Sci. U. S. A.* **98**, 1200–1205 (2001).

12. Paul, A., Eun, C. J. & Song, J. M. Cytotoxicity mechanism of non-viral carriers polyethylenimine and poly-l-lysine using real time high-content cellular assay. *Polymer* **55**, 5178–5188 (2014).

13. Clamme, J. P., Azoulay, J. & Mély, Y. Monitoring of the formation and dissociation of polyethylenimine/DNA complexes by two photon fluorescence correlation spectroscopy. *Biophys. J.* **84**, 1960–1968 (2003).

14. Petersen, H. *et al.* Polyethylenimine-graft-poly(ethylene glycol) copolymers: Influence of copolymer block structure on DNA complexation and biological activities as gene delivery system. *Bioconjug. Chem.* **13**, 845–854 (2002).

15. Hibbitts, A. J., Ramsey, J. M., Barlow, J., Macloughlin, R. & Cryan, S. A. In vitro and in vivo assessment of pegylated pei for anti-il-8/cxcl-1 sirna delivery to the lungs. *Nanomaterials* **10**, 1–24 (2020).

16. Ke, X. *et al.* Surface-Functionalized PEGylated Nanoparticles Deliver Messenger RNA to Pulmonary Immune Cells. *ACS Appl. Mater. Interfaces* **12**, 35835–35844 (2020).

17. Zhou, Q. *et al.* Polyplex nanovesicles of single strand oligonucleotides for efficient cytosolic delivery of biomacromolecules. *Nano Today* **39**, 101221 (2021).

18. Ye, Z. *et al.* Preliminary preclinical study of Chol-DsiRNA polyplexes formed with PLL[30]-PEG[5K] for the RNAi-based therapy of breast cancer. *Nanomedicine Nanotechnology, Biol. Med.* **33**, 102363 (2021).

19. Malhotra, M., Tomaro-Duchesneau, C., Saha, S., Kahouli, I. & Prakash, S. Development and characterization of chitosan-PEG-TAT nanoparticles for the intracellular delivery of siRNA. *Int. J. Nanomedicine* **8**, 2041–2052 (2013).

20. Liu, Z., Zhang, Z., Zhou, C. & Jiao, Y. Hydrophobic modifications of cationic polymers for gene delivery. *Prog. Polym. Sci.* **35**, 1144–1162 (2010).

21. Tian, H. *et al.* Gene transfection of hyperbranched PEI grafted by hydrophobic amino acid segment PBLG. *Biomaterials* **28**, 2899–2907 (2007).

22. Thomas, M. & Klibanov, A. M. Enhancing polyethylenimine's delivery of plasmid DNA into mammalian cells. *Proc. Natl. Acad. Sci. U. S. A.* **99**, 14640–14645 (2002).

23. Verma, A. & Stellacci, F. Effect of Surface Properties on Nanoparticle–Cell Interactions. *Small* **6**, 12–21 (2010).

24. von Gersdorff, K. *et al.* The Internalization Route Resulting in Successful Gene Expression Depends on both Cell Line and Polyethylenimine Polyplex Type. *Mol. Ther.* **14**, 745–753 (2006).

25. Neamnark, A. *et al.* Aliphatic lipid substitution on 2 kDa polyethylenimine improves plasmid delivery and transgene expression. *Mol. Pharm.* **6**, 1798–1815 (2009).

26. Aliabadi, H. M. *et al.* Impact of Lipid Substitution on Assembly and Delivery of siRNA by Cationic Polymers. *Macromol. Biosci.* **11**, 662–672 (2011).

27. Bus, T., Traeger, A. & Schubert, U. S. The great escape: How cationic polyplexes overcome the endosomal barrier. *J. Mater. Chem. B* **6**, 6904–6918 (2018).

28. Gilleron, J. *et al.* Image-based analysis of lipid nanoparticle-mediated siRNA delivery, intracellular trafficking and endosomal escape. *Nat. Biotechnol.* **31**, 638–646 (2013).

29. Wittrup, A. *et al.* Visualizing lipid-formulated siRNA release from endosomes and target gene knockdown. *Nat. Biotechnol.* **33**, 870–876 (2015).

30. Rehman, Z. U., Hoekstra, D. & Zuhorn, I. S. Mechanism of polyplex- and lipoplex-mediated delivery of nucleic acids: Real-time visualization of transient membrane destabilization without endosomal lysis. *ACS Nano* **7**, 3767–3777 (2013).

31. Panariti, A., Miserocchi, G. & Rivolta, I. The effect of nanoparticle uptake on cellular behavior: Disrupting or enabling functions? *Nanotechnol Sci Appl.* **5**, 87–100 (2012).

32. Koivusalo, M. *et al.* Amiloride inhibits macropinocytosis by lowering submembranous pH and preventing Rac1 and Cdc42 signaling. *J. Cell Biol.* **188**, 547–563 (2010).

33. Sverdlov, M., Shajahan, A. N. & Minshall, R. D. Tyrosine phosphorylation-dependence of caveolae-mediated endocytosis. *J. Cell. Mol. Med.* **11**, 1239 (2007).

34. Gottlieb, T. A., Ivanov, I. E., Adesnik, M. & Sabatini, D. D. Actin microfilaments play a critical role in endocytosis at the apical but not the basolateral surface of polarized epithelial cells. *J. Cell Biol.* **120**, 695–710 (1993).

35. Zhou, X. *et al.* Uptake of cerium oxide nanoparticles and its influence on functions of mouse leukemic monocyte macrophages. *J. Nanoparticle Res.* **17**, 1–15 (2015).

36. Lazebnik, M., Keswani, R. K. & Pack, D. W. Endocytic Transport of Polyplex and Lipoplex siRNA Vectors in HeLa Cells. *Pharm. Res.* **33**, 2999–3011 (2016).

37. Willingham, S. B. *et al.* The CD47-signal regulatory protein alpha (SIRPa) interaction is a therapeutic target for human solid tumors. *Proc. Natl. Acad. Sci. U. S. A.* **109**, 6662–6667 (2012).

38. Zhao, H. *et al.* CD47 promotes tumor invasion and metastasis in non-small cell lung cancer. *Sci. Rep.* **6**, 1–11 (2016).

39. Toyama, B. H. & Hetzer, M. W. Protein homeostasis: live long, won't prosper. *Nat. Rev. Mol. Cell Biol.* **14**, 55–61 (2013).

40. Majeti, R. *et al.* CD47 Is an Adverse Prognostic Factor and Therapeutic Antibody Target on Human Acute Myeloid Leukemia Stem Cells. *Cell* **138**, 286–299 (2009).

41. Jayaraman, M. *et al.* Maximizing the potency of siRNA lipid nanoparticles for hepatic gene silencing in vivo. *Angew. Chemie - Int. Ed.* **51**, 8529–8533 (2012).

42. Jarzębińska, A. *et al.* A Single Methylene Group in Oligoalkylamine-Based Cationic Polymers and Lipids Promotes Enhanced mRNA Delivery. *Angew. Chemie - Int. Ed.* **55**, 9591–9595 (2016).

Chapter 6:

General conclusions

and future steps

siRNA-based therapies present a tremendous potential to treat genetic disorders. However, this potential is hampered by the difficulties to deliver siRNA systemically. Some vectors have overcome those barriers and have successfully delivered siRNA into target tissue, predominantly to the liver. However, some tissues, or more interestingly tumors, are still presenting low delivery efficiency. Therefore, new vectors with high capacity of delivery are required, with polymers playing an important role, as they offer remarkable versatility for large-scale modification and production, along with excellent capacity for encapsulation of genetic material. The studies carried out throughout this thesis have focused on the development of new polymeric delivery platforms for siRNA, following two strategies. One consisted in the modification of dextran polymer with cationic groups, while the second one was based on the modification of high amino content polymer, such as polyallylamine. Following these two strategies different polymers systems were synthesized, characterized, and evaluated regarding their capacity as siRNA carriers:

- Single chain polymer nanoparticles (SCPN) of 40KDa dextran substituted with cysteamine at 21% degree of substitution (DS). **Chapter 3**
- Dextran 40KDa substituted with cysteamine 42% DS. **Chapter 3**
- Dextran 40KDa substituted with 1-(3-aminopropyl) imidazole 24% DS. **Chapter 3**
- Dextran 40KDa substituted with Spermine 30% DS. **Chapter 3**
- Dextran 40KDa substituted with Spermine-Imidazole 24-15% DS respectively. **Chapter 3**
- Dextran 40KDa substituted with Tris (2-aminoethyl)amine 20% DS. **Chapter 3**
- Dextran 40KDa substituted with 3,3'-(piperazine-1,4-diyl)bis(propan-1-amine) 21% DS. **Chapter 3**
- Dextran 20KDa substituted with cysteamine 17% DS. **Chapter 3**
- Dextran 6KDa substituted with cysteamine 17% DS. **Chapter 3**
- Polyallylamine(17KDa)-Oleic acid with 1% estimated DS. **Chapter 4**
- Polyallylamine(17KDa)-Oleic acid with 2% estimated DS. **Chapter 4**
- Polyallylamine(17KDa)-Oleic acid with 6% estimated DS. **Chapter 4**
- Polyallylamine(17KDa)-Oleic acid with 14% estimated DS. **Chapter 4**
- Polyallylamine(17KDa)-Oleic acid with >14% estimated DS. **Chapter 4**

In **Chapter 3**, delivery platforms based on dextran were synthesized by introducing amino groups (positively charged) to trigger electrostatic interactions with nucleic acids (negatively charged). A high incorporation of amines was targeted, as literature suggests that amines, not only allow encapsulation of oligonucleotides, but also help for the endosomal escape. The synthetic route consisted in modifying the backbone of dextran with methacrylate group, by a transesterification between glycidyl methacrylate with the hydroxyl group of the glucose units, that would allow a subsequent reaction with the thiol groups of the cysteamine, via Thio-Michael addition, to obtain dextran with amine groups. Dextran was successfully functionalized with amine group, but substitution of only 42% and 21% of cysteamine were achieved for the dextran polymer and the SCPN, respectively. Since cysteamine substitution provides only one primary amine, the number of amine groups per chain was very limited by the amount of methacrylate groups grafted. The resulting vectors SCPN-NH_2 and DXT-NH_2 exhibited very poor transfection efficiency, which was attributed to the low number of amine groups, inherent to the functionalization procedure followed.

In addition, the evaluation of the transfection performances of the polyplexes prepared with cationic SCPN was discontinued due to the absence of siRNA inside the cell after internalization assay, probably because of the low stability of the complex with siRNA. However, additional experiments should be carried out to investigate the low stability of the polyplexes obtained with SCPN-NH_2.

On the other hand, additional modifications of the dextran polymer were investigated to increase the number of amines per dextran chains. Different molecules, which display three to four amines of different types (including primary, secondary, and tertiary amines), were covalently linked to the polymer, such as 1-(3-aminopropyl) imidazole, Spermine, Tris (2-aminoethyl) amine, and 3,3'-(piperazine-1,4-diyl) bis(propan-1-amine). However, due to the absence of a thiol group in those molecules to proceed with the Michael Addition, a new strategy using the Traut reagent was selected to introduce this functional group via one of the primary amine. The reaction, performed at pH 8, occurred successfully. However, hydrolysis of the ester group was observed, limiting the degree of substitutions, as well as the reproducibility of the reaction. Although polymers achieved performed better as non-viral vector for siRNA than the cysteamine-substituted dextran, none of these modified cationic dextrans could achieve a transfection efficiency above 50%.

Other attempt to obtain dextran with higher DS of amine group, by preparing dextran with higher amount of methacrylate group, resulted insufficient as DS of 57% with no satisfactory transfection efficiency.

Also, the effect of the dextran molecular weight was studied, as high molecular weights could trigger a strong interaction between the genetic material and the polymer, impeding its release inside the cells. Again, the functionalization route resulted in low DS, which was attributed to the inherent hydrolysis of the ester during the cysteamine functionalization, and the polyplexes did not offer any transfection.

The dextran polymer systems achieved along this thesis, albeit with good encapsulation efficiency, is clearly far to be an efficient non-viral vector for siRNA, as they do not promote release inside the cell. Actually, the chemical route followed was not the most efficient to incorporate amino groups, as ester hydrolysis was found, both in the Michael addition of the cysteamine and in the Traut´s reactions of the other amine-containing molecules. A different strategy to covalently attach amines to the dextran and achieve high density of cationic charges could involve the opening of the glucose ring by oxidation and then reducing it by forming secondary amine bonds, which is a more stable bond than the ester. Based on this strategy, other carriers based on dextran can be tested, i.e. nanogels of dextran using spermine as cross-linker, or any other amino molecule, as well as a single-chain nanoparticles using a polyamine-based polymer.

A completely different approach consisted in using polymers that display amines in each monomer units. In **Chapters 4** and **5**, Polyallylamine (PAH), a polymer with one primary amine per repeating unit, was selected. The Soft Matter Laboratory had gained experience working with PAH and found encouraging results for the encapsulation and liberation efficiency of siRNA. However, the transfection efficiency using this polymer did not exceed 50%, and some degree of cytotoxicity was also observed. To improve the transfection efficiency of polyallylamine and reduce its cytotoxicity, aliphatic chains were incorporated to the polymer backbone, as inspired by the successful results

obtained with lipid nanoparticles for gene delivery. Specifically, 5 different amounts of oleic acid were covalently linked to polyallylamine to study the impact of the degree of functionalization on the delivery performances of siRNA. However, one major issue encountered during the chemical characterization of these compounds was their limited solubility in different solvents, which proved to be challenging to quantify the exact degree of substitution of PAH with oleic acid. Clearly, FTIR, Elemental Analysis, and TGA demonstrated the successful functionalization of PAH with an increasing amount of aliphatic chains. On the other hand, only an estimation of the degree of substitution was obtained by ^{1}H-NMR in D_2O due to the lack of solubility of the oleic acid and their self-assembly via hydrophobic interactions in aqueous media. More interestingly, the oleic acid-functionalized PAH could encapsulate siRNA with an efficiency greater than 90%, as measured by Quant-IT Ribogreen. Internalization studies, by confocal laser microscope, showed that more than 70% of A549 cells treated with any of the polyplexes prepared PAH, functionalized or not, penetrate the cell membrane. More importantly, only the polyplexes prepared with PAH.OA with a targeted DS of 5 and 10% could release efficiently the siRNA from the endosome, with silencing effect of 60% and 70% achieved, respectively. Those modified PAH showed levels of protein reduction similar to the gold standard based on Lipofectamine RNAimax, a commercial vector based on lipids.

Clearly, the incorporation of oleic acid, in a specific range, improves PAH performances as a vector for siRNA. It is worth mentioning that the same results were obtained when the therapeutic anti-CD47 siRNA was used on A549 cell line, with a clear silencing of CD47 gene expression.

The translation of potential therapies using polyallylamine derivative vectors into clinical practice may encounter some barriers, which require preliminary evaluation. First, during the characterization process, the solubility issues of the modified PAH made difficult the determination of the exact degree of substitution by ^{1}H-NMR. An optimal solvent or mixture of solvents must be identified to determine the exact amount of oleic acid attached, as quality control of the material. Current efforts are under progress to develop analytical methods of the polymeric material for its future translation.

On the other hand, the reason for the improvement in silencing efficacy has not been clearly established yet. The literature suggests a relationship between the delivery efficiency and the pKa of the amines, which should be similar to the endosomal pH (6.2-6.4) to provide a higher buffering capacity and promote endosomal disruption (Proton Sponge theory). Therefore, it would be interesting to determine the pKa of the polyallylamine derivatives and determine its relationship with the delivery efficiency. So far, pKa determination of PAH derivatives have not been successful, as the titration curve for this polymer did not follow the sigmoid curve used to calculate the pKa.

In contrast, some studies question the proton sponge theory, and it is possible that siRNA is released, thanks to the interaction of the aliphatic chains with the membrane lipids of the endosome. On such point, an interesting study would be to examine the relationship between the hydrophobic character of grafted polymers and the efficiency of siRNA release. For instance, one could compare the performance of a molecule with the same length as oleic acid but without its hydrophobic properties. If the delivery efficiency of siRNA remains similar even without the hydrophobic properties, it could suggest that the enhanced siRNA release may not be due to the hydrophobic interaction per se, but due to a reduction in the interaction between polyallylamine (PAH) and siRNA, facilitated by the presence of oleic acid. This reduced interaction between PAH

and siRNA could promote a more effective siRNA release. This investigation would provide valuable insights into the nuances of siRNA delivery and could lead to more refined strategies for designing and optimizing polymer-based delivery systems.

The polyplexes have been tested for silencing CD47 in a pulmonary cancer cell line. As discussed in **Chapter 5**, CD47 is a gene involved in the recognition of macrophages. Thus, an obvious follow-up experiments would consist in testing in vitro that CD47-knockout cancer cells become susceptible to macrophage engulfment, opening a potential pathway to the body own immune system to combat cancerous cells.

Polyplexes should be evaluated in terms of hemocompatibility and protein corona, because of its positive surface charge. It is known that lipid nanoparticles (LNPs) based vectors present protein corona effect that helps, in this case, the internalization into hepatocytes. In other cases, protein adsorption promotes aggregates formation and affect the stability of the vector in vivo, which significantly reduce cell uptake. The current strategy to improve plasma stability would be grafting neutral polymers such as poly(ethylene glycol) (PEG) oligopolymers. However, such functionalization might also affect the transfection performances of the resulting polyplexes.

More importantly, *in vivo* biodistribution and *in vivo* efficacy studies will have to be carried out, as the translation between *in vitro* transfection and animal testing is not trivial. Therefore, tissue accumulation of siRNA must be evaluated, while mRNA and protein levels of the targeted gene must be quantified. Thanks to the structure of polyallylamine, targeting molecules, such as peptide or polysaccharides, can be easily incorporated to promote accumulation of the vectors to the area to treat.

Furthermore, to enhance the polyplexes solubility and biocompatibility, one alternative strategy would be to use PAH.OAs in a lipid nanoparticles formulation to replace the expensive, and usually patent protected, ionizable lipids. This approach can potentially transform the formulation into lipopolyplex structures, presenting a more finely tuned vehicle for gene delivery.

Regarding the administration route, delivering these polyplexes directly to the lungs via an aerosol method could bypass systemic delivery entirely. This localized delivery strategy might be particularly advantageous if systemic delivery results in insufficient accumulation of the polyplexes in the lungs.

Polyallylamine-based polyplexes offer a versatile platform for delivering different therapeutic siRNAs, greatly broadening their potential applications in treatment strategies. However, a notable challenge to overcome is the potential inability of some target tissues to be effectively transfected by these polymeric carriers. Therefore, the suitability of different tissues for transfection with these polyplexes must be extensively investigated. To address this, *in vitro* screening of different cell lines and even primary cells will have to be undertaken. This will help in identifying the range of tissues receptive to transfection by these polyplexes, thereby highlighting potential areas for their application.

The convergence of lipids and polyamines in forming polyplexes has indeed resulted in a promising synergy for the delivery of siRNA. This promising partnership has opened a new avenue for exploring the potential of lipid-polyamine polyplexes in gene therapy. Notably, the physicochemical

properties of these polyplexes, such as the length and degree of unsaturation of the aliphatic chains, even the chemical route of linkage, can significantly impact their efficacy. Therefore, future research should focus on studying these parameters in detail to optimize the transfection efficiency of these polymers. Through systematic analysis and adjustment of these properties, these polyplexes can potentially enhance their performances to deliver siRNA, further expanding the toolbox for precision gene therapy.

The emergence of mRNA-based therapeutics and innovative genetic tools, such as the CRISPR/Cas9 system, requires the development and use of vectors for their efficient delivery. In this context, PAH.OAs, explored in this thesis, could be evaluated as potential delivery vehicles for these biologically active molecules. It is critical to recognize that the characteristics of these molecules-including, but not limited to, molecular length and surface charge-differ substantially from those of siRNA. Consequently, delivery systems suitable for siRNA may not be optimal for mRNA or plasmid DNA, and vice et versa.

APPENDICES

Appendix I

Table A.1 of RNAi-based-therapeutic drugs currently in clinical trials or already approved by FDA.

Therapeutic name	Condition(s)	Modification chemistry	Delivery system	Target(s)	Sponsor	Phase
ONPATTRO® (patisiran,ALN-TTR02)	TTR-mediated amyloidosis	2′-OMe, 2′-F	LNP (DLin-MC3-DMA)	TTR	Alnylam Pharmaceuticals	Approved, 3
GIVLAARI™ (givosiran,ALN-AS1)	Acute hepatic porphyrias	PS, 2′-OMe, 2′-F	GalNAc–siRNA conjugate	ALAS1	Alnylam Pharmaceuticals	Approved, 3
OXLUMO® (Lumasiran,ALN-GO1)	Primary hyperoxaluria type 1	PS, 2′-OMe, 2′-F	GalNAc–siRNA conjugate	HAO1	Alnylam Pharmaceuticals	Approved, 3
AMVUTTRA™ (Vutrisiran, ALNTTRSC02)	Amyloidosis	PS, 2′-OMe, 2′-F	GalNAc–siRNA conjugate	TTR	Alnylam Pharmaceuticals	Approved, 3
Leqvio®(Inclisiran,ALN-PCSsc)	Hypercholesterolemia	PS, 2′-OMe, 2′-F	GalNAc–siRNA conjugate	PCSK9	Alnylam Pharmaceuticals	Approved, 3
Fitusiran (ALN-AT3SC)	Hemophilia	PS, 2′-OMe, 2′-F	GalNAc–siRNA conjugate	AT	Alnylam Pharmaceuticals	3
Cemdisiran (ALN-CC5)	Complement-mediated diseases	PS, 2′-OMe, 2′-F	GalNAc–siRNA conjugate	C5	Alnylam Pharmaceuticals	3
Belcesiran (ALN-AAT02)	Alpha-1 liver disease	PS, 2′-OMe, 2′-F	GalNAc–siRNA conjugate	AAT	Alnylam Pharmaceuticals	2

Therapeutic name	Condition(s)	Modification chemistry	Delivery system	Target(s)	Sponsor	Phase
ALN-HBV02 (VIR-2218)	Hepatitis B virus Infection	PS, 2′-OMe, 2′-F,GNA	GalNAc–siRNA conjugate	HBV gene	Alnylam Pharmaceuticals	2
ALN-APP	Alzheimer´s disease; cerebral amyloid angiopathy	*undisclosed*	C16-alkyl-chain-siRNA conjugate	APP	Alnylam Pharmaceuticals	1
ALN-HSD	Nonalcoholic Steatohepatitis	*undisclosed*	GalNAc–siRNA conjugate	HSD17B13	Alnylam Pharmaceuticals	1
ALN-XDH	Gout	*undisclosed*	*undisclosed*	XDH	Alnylam Pharmaceuticals	1
AB-729	Hepatitis B	Undisclosed	GalNAc–siRNA	HBV gene	Arbutus Biopharma corporation	2
ARO-AAT	Alpha-1 antitrypsin deficiency	PS, 2′-OMe, 2′-F,Inverted base	GalNAc–siRNA conjugate	AAT	Arrowhead Pharmaceuticals	2
ARO-HBV (JNJ-3989)	Hepatitis B	undisclosed	GalNAc–siRNA conjugate	HBV gene	Arrowhead Pharmaceuticals partnered with Jansen	2
ARO-APOC3	Hypertriglyceridemia	PS, 2′-OMe, 2′-F,inverted base	GalNAc–siRNA conjugate	ApoC3	Arrowhead Pharmaceuticals	3
ARO-ANG3	dyslipidemia	PS, 2′-OMe, 2′-F,inverted base	GalNAc–siRNA conjugate	ANGPTL3	Arrowhead Pharmaceuticals	2
ARO-HSD (JNJ-75220795)	Nonalcoholic Steatohepatitis	Undisclosed	GalNAc–siRNA conjugate	PNPLA3	Arrowhead Pharmaceuticals partnered with Jansen	1
ARO-C3	Complement Mediated Disease	Undisclosed	GalNAc–siRNA conjugate	C3	Arrowhead Pharmaceuticals	1
ND-L02-s0201 (BMS-986263)	Idiopathic pulmonary fibrosis	Undisclosed	LNP, vitamin A	HSP47	Bristol-Myers Squibb partnered with Nitto Denko Corporation	2

APPENDICES

Therapeutic name	Condition(s)	Modification chemistry	Delivery system	Target(s)	Sponsor	Phase
RG6346(DCR-HBVS)	Hepatitis B	Undisclosed	GalNAc–siRNA conjugate	HBV gene	Dicerna Pharmaceuticals partnered with Roche	2
DCR-AUD	Alcohol use disorders	Undisclosed	GalNAc–siRNA conjugate	ALDH2	Dicerna Pharmaceuticals, Inc.	2
BMT101	Hypertrophic scar	Undisclosed	cp-asiRNA	CTGF	Hugel	2
SXL01	Advanced cancers	Undisclosed	NA	AR	Institut Claudius Regaud	1
ARO-HBV (JNJ-3989)	Hepatitis B	undisclosed	GalNAc–siRNA conjugate	HBV gene	Arrowhead Pharmaceuticals partnered with Jansen	2
ARO-APOC3	Hypertriglyceridemia	PS, 2'-OMe, 2'-F,inverted base	GalNAc–siRNA conjugate	ApoC3	Arrowhead Pharmaceuticals	3
ARO-ANG3	dyslipidemia	PS, 2'-OMe, 2'-F,inverted base	GalNAc–siRNA conjugate	ANGPTL3	Arrowhead Pharmaceuticals	2
ARO-HSD (JNJ-75220795)	Nonalcoholic Steatohepatitis	Undisclosed	GalNAc–siRNA conjugate	PNPLA3	Arrowhead Pharmaceuticals partnered with Jansen	1
ARO-C3	Complement Mediated Disease	Undisclosed	GalNAc–siRNA conjugate	C3	Arrowhead Pharmaceuticals	1
AMG 890	Cardiovascular disease	Undisclosed	GalNAc–siRNA conjugate	Lp(a)	Arrowhead Pharmaceuticals partnered with Amgen	2
Nedosiran (DCR-PHXC)	Primary hyperoxaluria	Undisclosed	GalNAc–siRNA conjugate	LDHA	Dicerna Pharmaceuticals	3

Therapeutic name	Condition(s)	Modification chemistry	Delivery system	Target(s)	Sponsor	Phase
DCR-AUD	Alcohol use disorders	Undisclosed	GalNAc–siRNA conjugate	ALDH2	Dicerna Pharmaceuticals, Inc.	2
BMT101	Hypertrophic scar	Undisclosed	cp-asiRNA	CTGF	Hugel	2
Mesenchymal stromal cell-derived exosomes with siG12D-KRAS	Pancreatic cancer	Unknown	Exosome	Kras G12D Mutation	M.D. Anderson Cancer Center	1
siRNA-EphA2-DOPC	Advanced cancers	Undisclosed	Liposome	EphA2	M.D. Anderson Cancer Center	1
Cobomarsen (MRG-106)	Blood cancers	LNA (antimiR)	NA	MicroRNA-155	Viridian (miRagen Therapeutics)	2, discontinued
Remlarsen (MRG-201)	Pathologic fibrosis	2′-OMe, 2′-F, mismatch, PS, Chol (microRNA-29b mimic)	NA	CTGF	Viridian (miRagen Therapeutics)	2, discontinued
MRG-110 (S95010)	Ischemic conditions	LNA (antimiR)	NA	MicroRNA-92	Viridian (miRagen Therapeutics)	1, discontinued
NU-0129	Gliosarcoma	Undisclosed	Gold nanoparticle	BCL2L12	Northwestern University	1
OLX101A	Hypertrophic scar	2′-OMe, PS	cp-asiRNA platform (cholesterol-siRNA conjugate)	CTGF	Olix Pharmaceuticals	2
OLX301A	Age-related macular degeneration	Undisclosed	cp-asiRNA	CTGF	Olix Pharmaceuticals	Preclinical
QPI-1007	Nonarteritic anterior ischemic optic neuropathy	2′-OMe	None	Caspase-2	Quark Pharmaceuticals	3, discontinued

APPENDICES

Therapeutic name	Condition(s)	Modification chemistry	Delivery system	Target(s)	Sponsor	Phase
PSCT19 (MiHA-loaded PD-L-silenced DC caccination)	Hematological malignancies	Undisclosed	Ex vivo transfection	PD-L1/L2	Radboud University	1/2
RXI-109 (sd-rxRNA)	Hypertrophic scar	Undisclosed	None	CTGF	RXi Pharmaceuticals	2
SLN360	Cardiovascular disease	Undisclosed	GalNAc–siRNA conjugate	Lp(a)	Silence Therapeutics	1
SLN226	Alcohol use disorders	Undisclosed	GalNAc–siRNA conjugate	ALDH2	Silence Therapeutics	1, discontinued
Atu027	Pancreatic ductal carcinoma,advanced solid tumors	2′-OMe	AtuPlex, liposomal	PKN3	Silence Therapeutics	1/2, discontinued
SLN124	Nontransfusion-dependent thalassemia low-risk myelodysplastic syndrome	Undisclosed	GalNAc–siRNA conjugate	TMPRSS6	Silence Therapeutics	1
siG12D-LODER	Pancreatic ductal adenocarcinoma,pancreatic cancer	Undisclosed	Polymeric matrix	KRAS G12D	Silenseed Ltd	2
si-PT-LODER	Prostate cancer	Undisclosed	Polymeric matrix (LODER polymer)	HSP90	Silenseed Ltd	Preclinical
STP705 (cotsiranib)	solid tumors and Hypertrophic scar	Undisclosed	HKP, polypeptide nanoparticle	TGF-β1 and Cox-2	Sirnaomics	2
STP707	Bowen's disease cutaneous squamous cell carcinoma in situ	Undisclosed	HKP, polypeptide nanoparticle	TGF-β1 and Cox-2	Sirnaomics	1
RBD1016	Hepatitis B	Undisclosed	GalNAc–siRNA conjugate	HBV gene	Suzhou Ribo Life Science Co., Ltd	Preclinical
RB-HLP002	Hyperlipidemia	Undisclosed	GalNAc–siRNA conjugate	undisclosed	Suzhou Ribo Life Science Co., Ltd	Preclinical
Bamosiran (SYL040012)	Ocular hypertension, glaucoma	Undisclosed	None	ADRB2	Sylentis, S.A	2, discontinued

Therapeutic name	Condition(s)	Modification chemistry	Delivery system	Target(s)	Sponsor	Phase
SYL1801	Choroidal neovascularization (CNV)	Undisclosed	None	NRARP	Sylentis, S.A.	2
APN401 (siRNA transfected PBMCs)	Solid tumors that are metastatic or cannot be removed by surgery	Undisclosed	Ex vivo siRNA electroporated PBMCs	Cbl-b/DC	Wake Forest University Health Sciences	1
SXL01	Advanced cancers	Undisclosed	NA	AR	Institut Claudius Regaud	1

Appendix II

The biomaterials synthesized during this thesis were characterized using the following techniques. The principles and fundamentals of these techniques are described in this appendix.

Nuclear magnetic resonance spectroscopy

Nuclear magnetic resonance (NMR) spectroscopy is arguably the most powerful and broadly applicable technique for structure determination available to organic chemists. Indeed, the structure of a compound can often be determined using NMR spectroscopy alone, although in practice, structural determination is generally accomplished through a combination of techniques that includes NMR and IR spectroscopy and mass spectrometry[1].

All nuclei of atoms of matter consisting of an odd number of protons and neutrons possess a quantum mechanical property called nuclear spin. the nuclear spin can be considered as a rotational motion that generates a magnetic field around the nucleus called magnetic moment, which is polarized. When an external magnetic field is applied to the atom this magnetic moment is aligned with the external magnetic field or against it. This is called the α (with) spin state or β (against) spin state. If the nuclei subjected to a magnetic field are stimulated with the appropriate frequency of radio waves, the atoms absorb energy and pass from the spin α state to the spin β state and are said to be in resonance with the magnetic field. When the magnetic field ceases, the nuclei return to their normal state and release the absorbed energy (Figure A.1). This energy generates an electrical impulse in a receiver coil. The receiver coil records a complex signal, called a free induction decay (FID), which is a combination of all the electrical impulses generated by each type of proton. The FID is then converted into a spectrum via a mathematical function called Fourier transform.

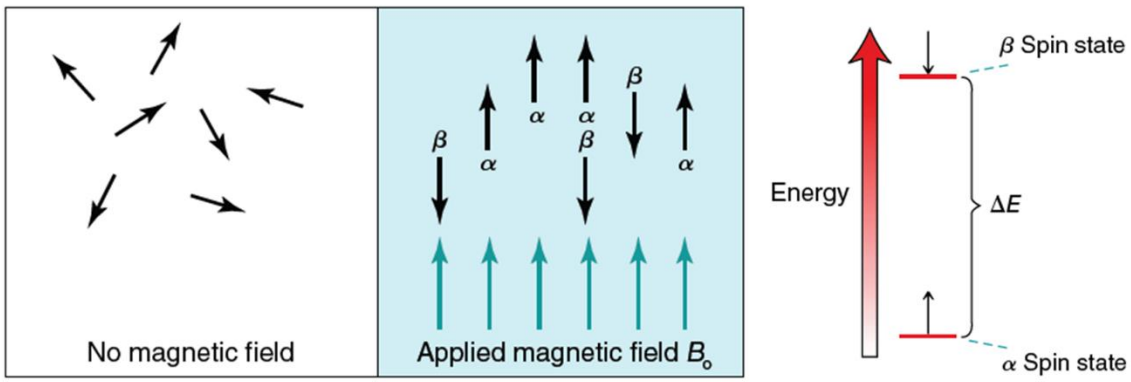

Figure A. 1.-The orientation of the magnetic moments of protons in the absence of an external magnetic field or the presence of an external magnetic field (alignment). Atoms can pass from a β spin state to a α spin state after the absorption of energy from appropriate radio wave frequency[1].

At a particular magnetic field strength, we might expect all nuclei to absorb the same frequency of radio waves radiation. Luckily, this is not the case, as nuclei are surrounded by electrons. In the presence of an external magnetic field, the electron density circulates, which produces a local (induced) magnetic field that opposes the external magnetic field. When electron density circulates

around a proton, this is now subjected to two magnetic fields—the strong, external magnetic field and the weak induced magnetic field established by the circulating electron density. The proton therefore experiences a net magnetic field strength that is slightly smaller than the external magnetic field. The proton is said to be shielded by the electrons. Not all protons occupy identical electronic environments. Some protons are surrounded by more electron density and are more shielded, while other protons are surrounded by less electron density and are less shielded, or deshielded. As a result, protons in different electronic environments will exhibit a different energy gap between the α and β spin states and will therefore absorb different frequencies of radio waves radiation. This allows us to probe the electronic environment of each atom in a molecule. Nucleus of Atoms with even protons and neutrons do not have nuclear spin and cannot be analyzed by NMR. Commonly atoms studied are ^{1}H, ^{13}C, ^{15}N, ^{19}F, ^{31}P, which possess nuclear spin. In the case of this thesis only ^{1}H has been analyzed. The molecular structure can be determined by ^{1}H-NMR spectrum. Different Hydrogen protons or only protons in a molecule or polymer with different electronic environment will absorb radio waves radiation in different frequency. Each frequency is represented in the spectrum as a peak with different location, called its chemical shift δ. Chemical shift δ is the difference of the observed signal and the signal of reference compound tetramethylsilane (TMS). TMS produces a signal at a lower frequency than most organic compounds. The chemical shift instead of being given in Hertz, is given parts per million (ppm). Chemical shift in ppm is calculated from the difference (in hertz) between the resonance frequency of the proton being observed and that of tetramethylsilane (TMS) divided by the operating frequency of the spectrometer multiplied by 10^{6}. Most organic compounds signals will fall in a range between 0 and 12 ppm. All spectra performed during this thesis are ^{1}H conducted by Bruker 500 MHz.

Fourier transform infrared spectroscopy

The principle of the infrared (IR) spectroscopy resides in that chemical bonds of a molecules get excited when are exposed to IR radiation. Bonds acquire vibrational excitation, *stretching* between atoms, like a spring or *bending* in different ways (Figure A.2.-A). Each type of chemical bond will absorb energy of infrared radiation at characteristic frequency. Thus, allows identify different chemical bonds in a same compound. The compound is simply irradiated with all frequencies of IR spectrum and then frequencies of absorption are detected. In an IR spectrometer, a sample is irradiated with frequencies of IR radiation, and the frequencies that pass through (that are not absorbed by the sample) are detected. A plot is then constructed showing which wavelenght were absorbed by the sample. The most used type of spectrometer, called a Fourier transform (FT-IR) spectrometer, irradiates the sample with all frequencies simultaneously and then utilizes a mathematical operation called a Fourier transform to determine which wavelength are absorbed by the sample. The plot of FTIR is typically reported in % of transmittance and wavenumber. The wavenumber is simply the frequency of light absorbed by the compound divided by the constant of speed of light and values range from 4000 to 400 cm^{-1} (right to left). % Transmittance is calculated from intensity of light transmitted (passed through the object) divided by intensity of light emitted. The signals of IR spectrums are called absorption bands and point down (See Figure A.2.-B). IR spectra can be divided into two main regions. The diagnostic region (>1500 cm^{-1}) generally has fewer peaks and provides the clearest information. This region contains all signals that arise from

double bonds, triple bonds, and simple bonds. The fingerprint region (<1500 cm^{-1}) contains signals resulting from the vibrational excitation of most single bonds (stretching and bending). This region generally contains many signals and is more difficult to analyze. This region is called the fingerprint region because each compound has a unique pattern of signals in this region, pretty similar to the unique Fingerprint of each person.

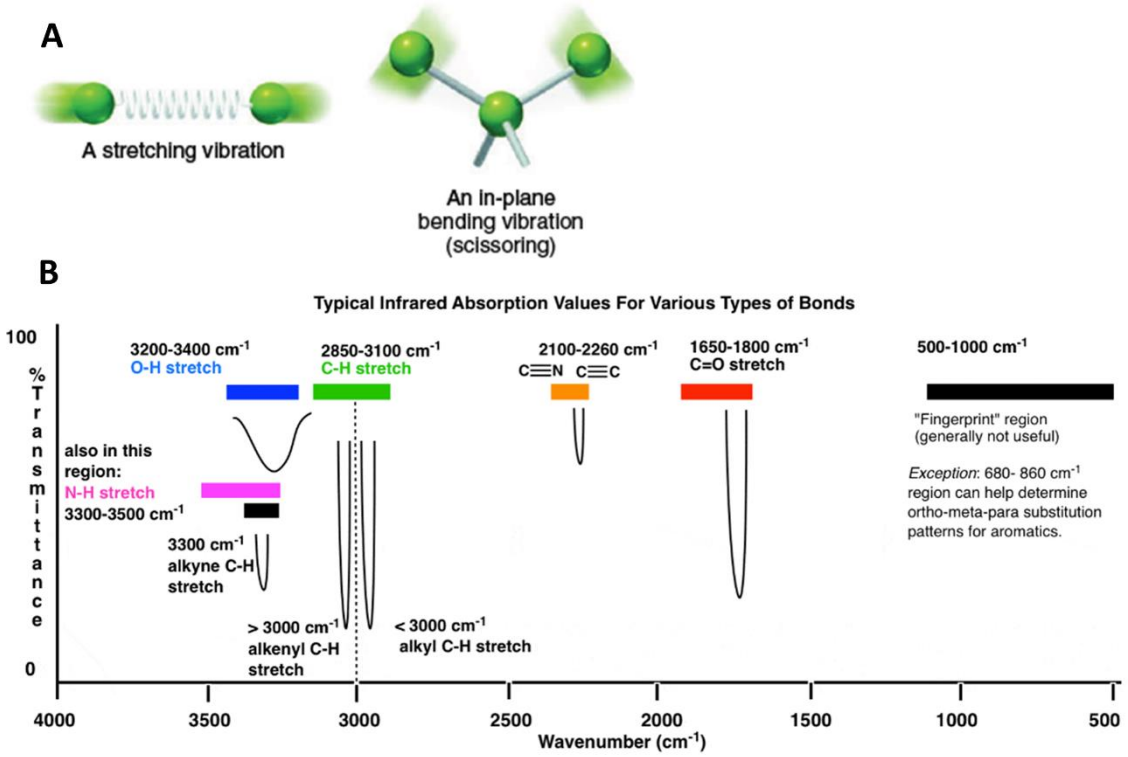

Figure A. 2.-A) Different kinds of vibrational excitation of the bonds in a molecule. bonds store vibrational energy several ways: *stretching*, like the way a spring stretches, and *bending* in different number of ways, such as *scissoring*[1]. B) FTIR spectrum, with the diagnostic region above 1500 cm^{-1} and the fingerprint region below 1500 cm^{-1}. Highlighted areas, where typically appears various types of bonds[2].

FTIR spectra obtained during this thesis were carried out using complement attenuated total reflection (ATR) that enables samples to be examined directly in the solid or liquid state without further preparation.

Elemental analysis

The elemental analysis of organic elements is a technique that determines qualitatively and quantitatively the elements of carbon, hydrogen, nitrogen, sulfur, and oxygen within an organic sample. The device used is called elemental analyzer or CHNSO analyzer and is capable of handling a wide variety of sample types, including solids, liquids, volatile and viscous samples, in the fields of pharmaceuticals, polymers, chemicals, environment, food and energy. The basic operating principle is based on the burning of the sample at high temperature (≥1100^{O}C). The gaseous sample is sent to the chromatography column with an inert gas (helium, He) used as the carrier. Here, the gaseous sample is combusted with oxygen (O_2) gas and passed through the oxidation zone followed by oxidation with suitable catalysts to fully perform the quantitative combustion process. After the

process, C, H, N, S elements are converted to CO_2, H_2O, N_2 and SO_2 gases, separated by gas chromatography and sent to the thermal conductivity detector (TCD). This detector uses heated metal filament to sense small changes in thermal conductivity of the carrier gas. Thermal conductivity of the carrier gas only gives an essentially constant signal. The presence of vapors of the different components of the mixture in carrier gas brings about changes in the thermal conductivity proportional to their amount in the stream (Figure A.3).

The determination of Oxygen in the organic sample is special. The sample is pyrolyzed by hydrogen-helium (H_2-He) gas mixture. All oxygen-containing products formed because of combustion are converted to carbon monoxide and detected by gas chromatography thermal conductivity (Figure A.3). Results reported by the device show a weight percentage of elements in the compound[3].

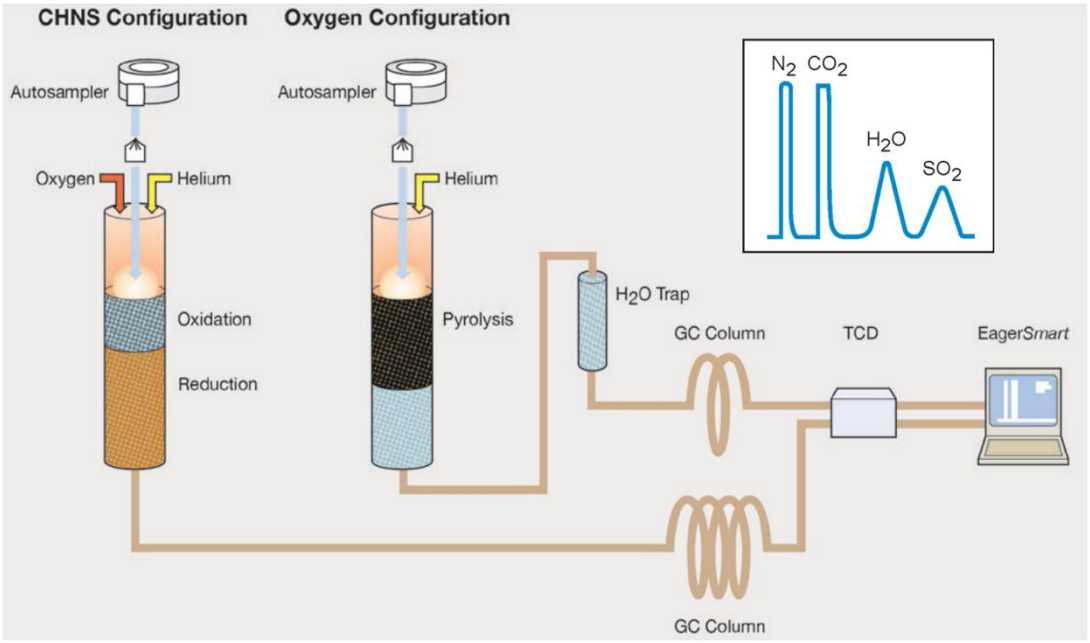

Figure A. 3.-Elemental Analyzer with a CHNS/O configuration[4].

In this thesis elemental analyzer was used for further characterization of polyallylamine oleic acid derivatives. Samples were analyzed with Euro EA CHNSO analyzer.

Thin layer chromatography

Thin layer chromatography (TLC) is a commonly used type of chromatography with a polar stationary phase based on silica gel. The mobile phase is a solvent or a mixture of solvents, which will separate the compounds depending on their polarity. Samples are placed onto the silica near one end of the plate. Then, silica plates are placed vertically inside a close chamber with the edge nearest the applied spot immersed in the mobile phase. The solvent rises through the stationary phase by capillarity. As the solvent ascends the plate, the compounds in the sample separate because of their equilibria between the mobile and stationary phases. The more a compound binds to the stationary phase, the more slowly it moves on the TLC plate. In silica plates, nonpolar compound travel up fast and polar compound move slowly. Once mobile phase arrived at 1 cm from

the top of the plate, this is taken out of the chamber and dried. Separated components can be visualized immediately because their color or must be stained with an appropriate reagent[5,6] (See Figure A.4).

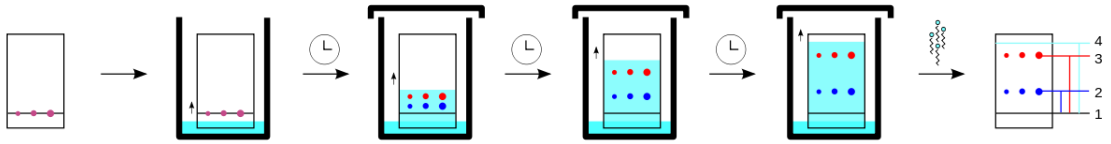

Figure A. 4.-TLC Procedure. Samples are deposited onto the silica plate, which is subsequently placed within the chromatography chamber containing the mobile phase. The mobile phase migrates via capillary action, facilitating the separation of distinct compounds. Image sourced from a web page.[7]

In this thesis TLC was used to determine if the elimination of oleic acid, thus the purification of PAH.OA, was successful. In that case, mobile phase based on a mixture of hexane:ethyl acetate:acetic acid in a 80:19:1 proportion was used. Stationary phase was a silica gel 60 from Merck 105554, while $KMnO_4$ staining was used.

Thermogravimetry analysis

Thermogravimetric analysis (TGA) is an analytical technique used to determine a material's thermal stability and its fraction of volatile components by monitoring the weight change that occurs as a sample is heated at a constant rate (Figure A.5). The measurement is normally carried out in air or in an inert atmosphere, such as helium, argon or nitrogen and the weight is recorded as a function of temperature[8]. Temperature ranges for commercial TGAs are typically ambient to 1000 ° C. Polymers generally exhibit mass loss, which may be categorized as volatile components such as absorbed moisture, residual solvents, or low - molecular - mass additives or oligomers. The most frequent and classical use of TGA involves the pyrolysis of a polymer at a constant heating rate that typically falls within 5 – 20 ° C/min. In general, the degradation mechanisms of polymers are free - radical processes initiated by bond dissociation at the temperature of pyrolysis. The specific pathway followed is related to the bond strengths and structure of the polymer. These mechanisms are generally grouped into three categories: random scission, unzipping to monomer, and side group elimination[9]. Thermogravimetric analysis can provide valuable information, often quantitative, on the composition of polymeric materials. If a multicomponent material contains low - molecular - mass compounds, polymeric material, and inorganic additives, the three groups can be separated by temperature. It is typically used to quantify the amount of polymer coating in inorganic nanoparticles[10].

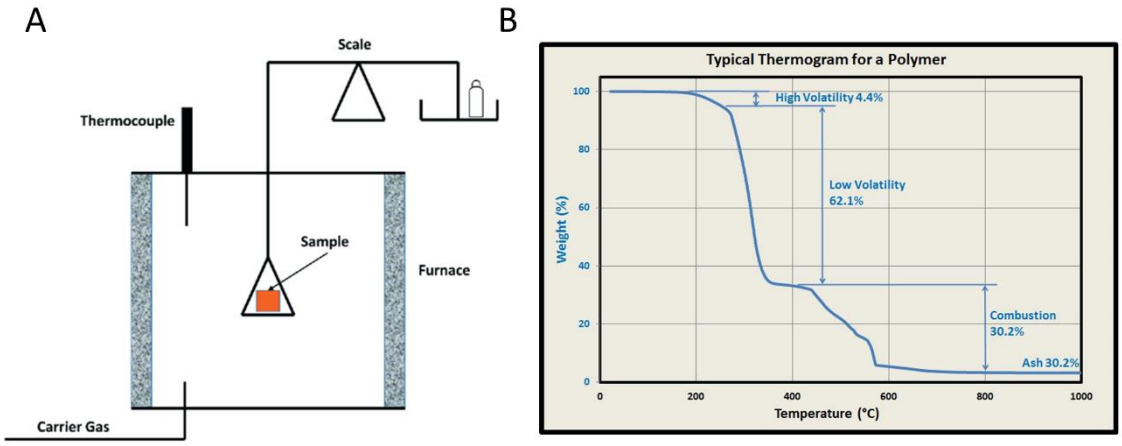

Figure A. 5.-A) Schematic representation of thermogravimetric method, consisting of a sample inside the pan, hanging from the scale inside a furnace[11]. B) Typical thermogavimetric curve of a polymer[12].

In this work TGA was attempted to quantify the amount of oleic acid grafted as temperatures of decomposition appeared to look different.

Dynamic light scattering

Dynamic light scattering (DLS) is a powerful technique for probing soft matter particles mainly at the sub-micron region. Dynamic Light Scattering (also known as PCS - Photon Correlation Spectroscopy) measures Brownian motions and relates this to the size of the particles[13]. It does this by illuminating the particles with a laser and analyzing the intensity fluctuations in the scattered light. Particles suspended in a liquid are never stationary. The particles are constantly moving due to Brownian motions, which are the movement of particles due to the random collision with the molecules of the liquid that surrounds the particle. An important feature of Brownian motion for DLS is that small particles move quickly, and large particles move more slowly. A laser pass through a suspension of particles, when the light hits a particle, it is deflected from its path and ends up in a detector positioned at a certain angle to the laser beam(Figure A.6). The intensity of scattered light is registered, and information is passed through a digital correlator. As particles are moving this intensity will vary during a period of time.

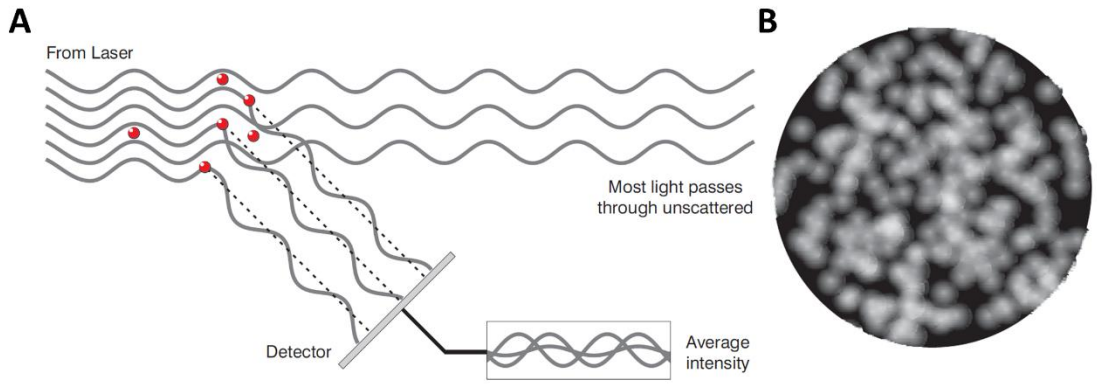

Figure A. 6.-A laser beam is transmitted through a colloidal solution containing dispersed particles. Upon interaction with the particles, the laser light scatters at specific angles, where a strategically placed detector captures the scattered

light[13]. **B)** Consequently, the particles' scattered light creates a speckle pattern on the detector screen, comprising bright and dark regions. This pattern undergoes temporal changes as the particles continuously move within the solution[13].

A signal in time point t will be very similar to signal t+б̄t in short period of time, both signals are going to be strongly correlated. If we then compared the original signal a little further ahead in time (t+2б̄t), there would still be a relatively good comparison between the two signals, but it will not be as good as at t+б̄t. The correlation is therefore reducing with time. Much later in time correlation between two signals will be so low, or no correlation at all, 0. smaller particles will have fast decays in the correlation function from 1 to 0, bigger particles slower (Figure A.7).

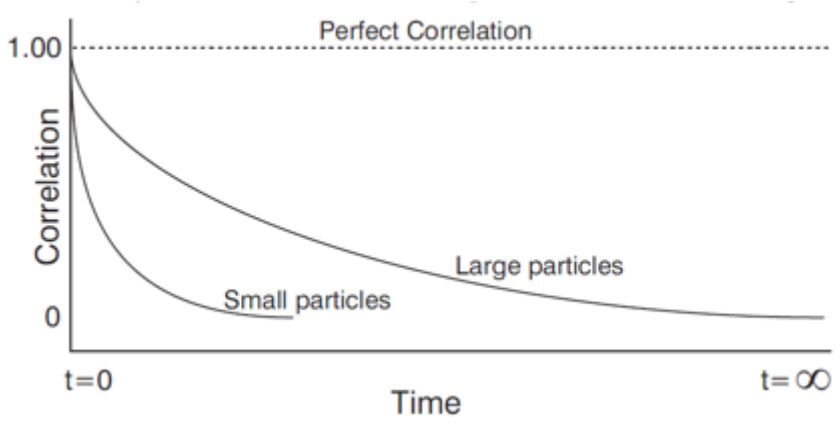

Figure A. 7.-Correlation function of scattered light in a period of time. Rate of decay of small particles is faster than it is for large particles[13].

From these decays is extracted the translational diffusion coefficient *D*. Then Stokes-Einstein equation is used to extract the hydrodynamic radius of the particles.

$$D = \frac{K_B \, \mathrm{T}}{6\pi\eta R_H}$$

Where D is the diffusion coefficient of the particle,

K_B is the Boltzmann constant (1.380649×10^{-23} J/K),

T is the absolute temperature (in Kelvin),

η is the dynamic viscosity of the fluid,

R_H is the hydrodynamic radius of the spherical particle.

In this study, the device used is Zetasizer nano ZS is provided with software, which represents data obtained from autocorrelation into size distribution graph. The X axis shows a distribution of size classes, while the Y axis shows the relative intensity of the scattered light. It also permits to see the degree of polydispersity in a solution. From 0-1, <0.1 solution is considered monodisperse, polydispersity over 0.5, it is unwise to rely on the Z-average mean.

Aqueous electrophoresis

The development of a net charge at the particle surface affects the distribution of ions in the surrounding interfacial region, resulting in an increased concentration of counter ions close to the surface. Thus, an electrical double layer exists around each particle. An inner region, called the Stern layer, where the ions are strongly bound and an outer region where they are less firmly attached. Outer boundary of this layer is called the surface of hydrodynamic shear or slipping plane (Figure A.8). When a particle moves (e.g. Brownian motions), ions within these layers move with it, but any ions beyond slipping plane do not travel with the particle. The potential that exists at this slipping plane is known as the Zeta potential. The magnitude of the zeta potential gives an indication of the surface charge of a nanoparticle, solid-liquid colloid system.

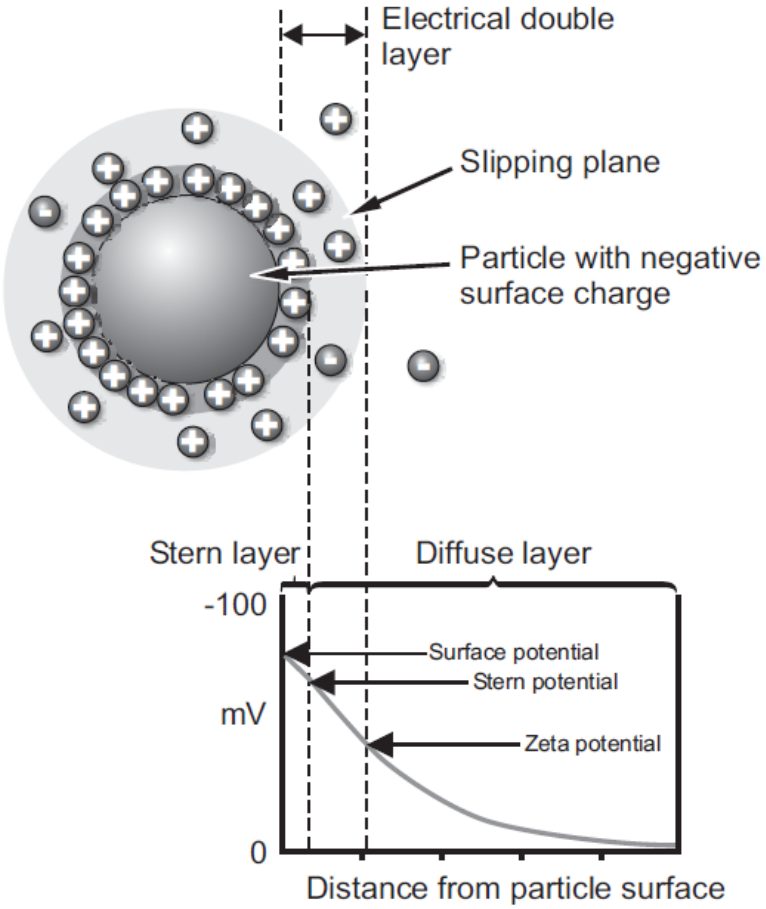

Figure A. 8.-Schematic representation of the Z-potential in particles in a colloidal suspension. The zeta potential represents the electrostatic potential at the interface between the outermost layer of counterions and the surrounding medium[13].

The measurement of Zeta-potential is achieved based on the principle of electrophoresis. An important consequence of the existence of electrical charges on the surface of particles is that they will exhibit certain effects under the influence of an applied electric field. One of these effects is electrophoresis, where charged particles suspended in the electrolyte are attracted towards the electrode of opposite charge. Viscous forces acting on the particles tend to oppose this movement. When equilibrium is reached between these two opposing forces, the particles move with constant

velocity. The velocity of a particle in an electric field is commonly referred to as its electrophoretic mobility. Zeta-potential can be calculated from electrophoretic mobility using Henry equation:

$$U_E = \frac{2\,\mathrm{Ɛ}\,z\,f(Ka)}{3\,\eta}$$

Where U_E is Electrophoretic mobility

Ɛ=Dielectric Constant

Z=zeta-potential

F(Ka)=Henry´s function

η=viscosity

In aqueous media with low ion strength F(Ka) is resolved by using Smoluchowski approximation. Electrophoretic mobility is the data directly measured and then Zeta-potential is obtained by Smoluchowski approximation. Electrophoretic mobility is measured by using folded capillary cell with electrodes at either end. A potential is applied, and particles move towards the electrode of opposite charge, their velocity is measured and expressed in unit field strength as their mobility. The technique used to measure this velocity is laser doppler velocimetry (LDV). Similar to DLS, a laser pass through the cell and record scattered light by the particles, fluctuation rate in the intensity of scatter light is proportional to particle velocity (Figure A.9). The Potential applied in the chamber will move the particle at certain velocity to the opposite pole. This particle velocity is turned into Zeta-potential.

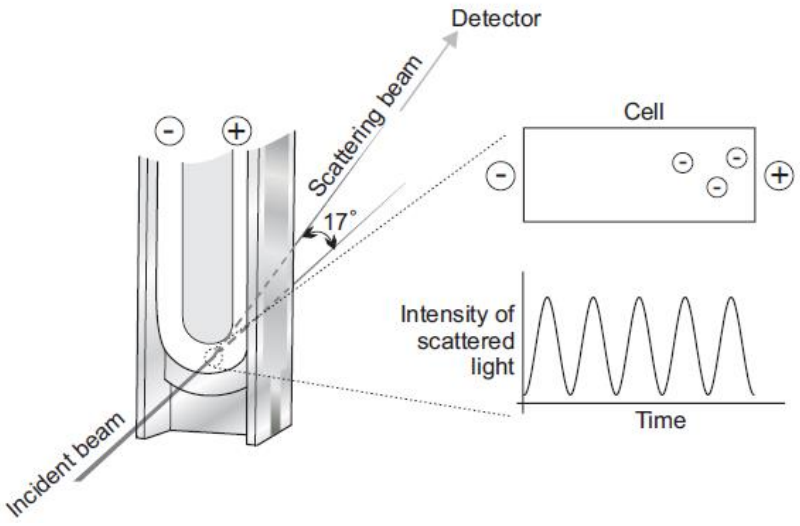

Figure A. 9.-In the laser Doppler velocimetry the light scattered at an angle of 17° is combined with the reference beam. This produces a fluctuating intensity signal where the rate of fluctuation is proportional to the speed of the particles. A digital signal processor is used to extract the characteristic frequencies in the scattered light[13].

In this thesis Zetasizer nano ZS has been used for measurements of zeta-potential. A special technique has been applied called Diffusion barrier technique (DBT) to measure small quantities of sample[14]. High volume >700 µL of sample is needed for a zeta-potential measurement and at high concentrated sample. The amount of siRNA required for this purpose is too high, therefore DBT was followed to reduce 700 µL to 50 µL of sample (Figure A.10).

Figure A. 10.-A. Cell entirely filled with blue dextran in 10 mM NaCl. B. Cell filled with 10 mM NaCl and loaded with 50 µl blue dextran for the diffusion barrier[14].

The diffusion barrier technique is a method for reliably measuring the electrophoretic mobility of proteins and small particles by minimizing the impact of the measurement process. Contact of the particles with the electrodes required for the application of the electric field is known to damage proteins and can cause them to denature and aggregate. It is often erroneously thought that it is the electric field itself of a few volts per centimeter that causes the sample aggregation. The diffusion barrier technique separates the sample molecules from the electrodes, so the effect on the particle caused by the measurement is dramatically reduced. The diffusion barrier technique manages this by introducing a small plug of sample e.g. 20 µL, separated from the electrodes by the same buffer that the nanoparticle is dissolved in. The physical distance between the sample and the electrodes means that the sample is protected from damage by contact with the electrodes. Since the protection is afforded simply by the distance of the sample from the electrodes, the sample is protected for as long as it takes for it to diffuse to the electrodes, which makes measurement of the sample much more reliable, as the mobility of only the soluble native nanoparticle is measured.

Transmission electron microscopy

Electron microscopy (EM) has been used to observe shape and size of the polyplexes obtained in this thesis.

The principle of electron microscopy resides in the use of electrons instead of photons to magnify an object. In microscopy two terms are important, magnification and resolution or resolving power. Magnification is the ability to make small object seem larger. Resolution is the level of detail

obtained from this enlarged image after magnification, defined as the ability to distinguish the distance of two points very close to each other, that can be perceived as just one in low resolution power. Magnification and resolution of an electron microscope is higher than traditional optical microscope, thus EM is widely used in nanomedicine for the observation of nano scale particles.

In light microscopes magnification is obtained from a set of lenses, where light cross through them and diffract the light amplifying the object. In electron microscope, an electron beam is generated and passes along vacuum chamber. Different copper coils are placed inside the chamber and act as electromagnetic lenses. Once electrons pass through electromagnetic field its direction is diffracted convergently or divergently like optical lenses and make the amplification of the object.

Resolution in terms of Rayleigh criterion is defined by:

$$\delta = \frac{0.61\lambda}{\mu \sin \beta}$$

Where λ is the wavelength of the radiation

μ is the refractive index of the viewing medium

β is the semiangle of collection of the magnifying lens.

The resolution of a microscope depends on the wavelength of the radiation and the numerical aperture (NA) of the set of lenses, which is also known as μ sin β. Most of the optical microscopes have a NA of 1. Refractive index (μ) in air =1 and the highest semiangle possible is lower than 90º, which sin 90 =1. In some inmersion microscopes oil is used to increase the refractive index, which can provide NA ~1.4. So, optical microscopes are limited to the wavelength of light. Green light 500 nm and (Inmersion oil NA 1.4) has a resolving power of 0.2 μm approximately[15].

$$\delta = \frac{0.61\ (500)}{1.4} = 217.85\ nm$$

One way to beat the diffraction limit of light is to use an illumination source with a shorter wavelength than photons, such as electrons. The wavelength of electrons is much smaller than that of photon. Thus, the resolution of an electron microscope is higher than 0.2 μm making perfect for the study of nanoparticles often smaller than the light microscope resolution.

The wavelength of which an electron propagates is related to its energy, discovered by Louis de Broglie. So, approximately 100 KeV of energy represent 0,004 nm of wavelength. However, resolution is limited to 0.1 nm because objective lenses are not perfect.

Electrons are negatively charged particles and are repelled by electrons surrounding the nucleus of atoms. This interaction causes propagating electrons to scatter. Thus, contrast can be generated by electron-dense materials in the path of the electron beam. There are two factors affecting scattering in transmission electron microscopy: sample thickness and the atomic number of the contrasting

agent. The penetration depth of electrons depends on the section thickness of the specimen. By applying a high-voltage driving force, electrons will penetrate through material sections with very little scattering. Typically, ~100-150 nm is the thickest sample that can be observed using a 100 keV accelerating voltage. The generation of contrast depends on the atomic number of atoms. Atoms with high atomic number possess more electrons around their nucleus, and thus more incident electrons will be scattered (Figure A.11).

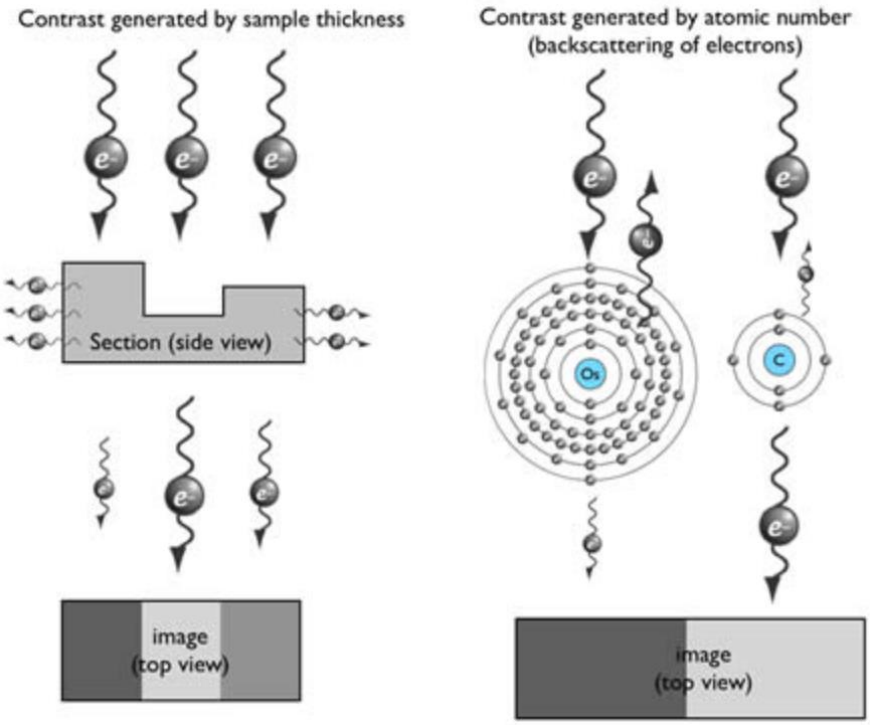

Figure A. 11.-Image contrast generated by electrons transmission microscopy depends on sample thickness and atomic number of the sample[16].

Unfortunately, polymers are organic samples made mostly by carbon, hydrogen, nitrogen and oxygen, atoms with similar atomic numbers. Typically staining with heavy metals is required to gain contrast in the sample[17], as it was done in this thesis.

Diluted samples are deposited in copper grids cover by a carbon film. Nanoparticles deposited on this carbon film have similar atomic number, thus low contrast between the sample and the background is achieved. Particles deposited are stained with heavy metal salts and then washed. Some stain residue remains surrounding the edges of nanoparticles allowing the shape to observed. The opposite is the positive staining where heavy metal salts are absorbed by the particles itself turning them into dark over light background. There are different type of heavy metal salts, that will be used depending on the nature of the sample, hydrophobicity and charge repulsion, to achieve a negative or positive staining[18,19] (Figure A.12).

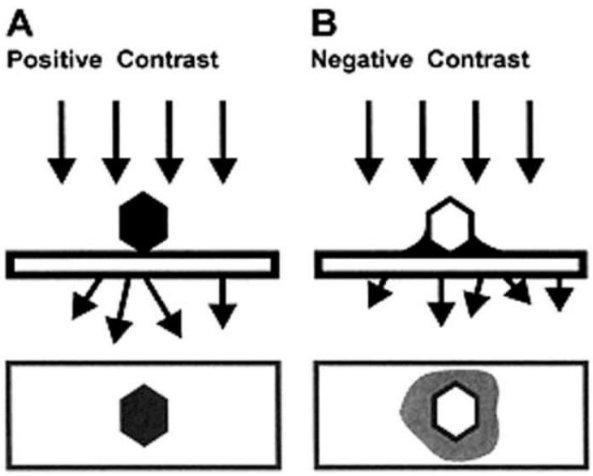

Figure A. 12.-Scheme of positive and negative staining of organic nanoparticles for Transmission electron microscopy[18].

Gel retardation assay

The gel retardation assay is a method used to investigate interactions between nucleic acids (e.g., DNA or RNA) and various molecules, including proteins, peptides, and polymers. In the context of siRNA polyplexes, this assay is employed to evaluate the complexation efficiency and stability of siRNA-polymer complexes, crucial for effective gene silencing. The assay consists of two steps: polyplex formation and agarose gel electrophoresis. To form the polyplexes, solutions of siRNA and polymer are mixed at different polymer/siRNA ratios, also referred to as N/P ratio (moles of protonable amines in the polymer and moles of phosphate in the oligonucleotide). Higher encapsulation efficiency is expected at higher N/P ratios. After polyplex formation, agarose gel electrophoresis is performed.

Agarose gel electrophoresis is a widely-used molecular biology technique for separating and identifying nucleic acids. The method involves applying an electric field, causing molecules to migrate through a gel matrix based on size, charge, and structure. Nucleic acids, negatively charged at neutral pH, migrate towards the positive electrode under an electric field. These molecules are embedded within an agarose gel, a natural polysaccharide derived from algae that forms fibers in aqueous media. The fibers create a network of channels with diameters ranging from 50 nm to 200 nm, depending on agarose concentration. Smaller molecules travel more rapidly through the agarose, resulting in molecular weight-based separation. Nucleic acids are separated based on length, and migration distances are often compared to samples containing molecules of known sizes (molecular weight standards or "ladders") for approximate sizing (Figure A.13).

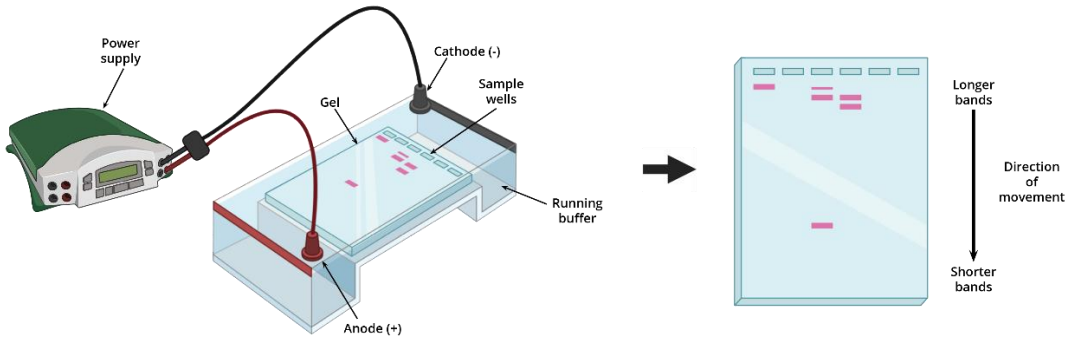

Figure A. 13.-A typical electrophoresis setup in a molecular biology laboratory. The setup consists of a chamber containing a precast agarose gel submerged in an electrophoresis running buffer, usually Tris-acetate-EDTA (TAE) or Tris-borate-EDTA (TBE) buffer. The electrophoresis chamber features a negative (cathode) and positive (anode) electrode, attracting positive molecules and ions. Following the run, the gel is stained with EtBr or an alternative nucleic acid stain, revealing DNA/RNA bands. Illustration made with Biorender.

After a typical 20-40 minute run, molecules are well separated, and the gel is stained to visualize nucleic acid bands. Historically, Ethidium Bromide (EtBr) was used to stain nucleic acids, as it binds to nucleotide strands and fluoresces under UV light. However, EtBr mutagenic and carcinogenic properties pose health risks and require careful handling. Safer alternatives, such as SYBR Safe and GelRed, have been developed by various companies, offering similar binding principles with reduced health hazards.

In a gel retardation assay, the nucleic acid, in this case siRNA will suffer a retard during the run because of its interaction with polymer. The complex will acquire higher molecular weight and will run slower, sometimes, complexes cannot even move from the loading well. The samples are compared to the control of free siRNA, which have run until certain position in the gel. Polymers that cannot complex siRNA will show a band at same height than the control, sometimes can be identified part of the oligonucleotide complexed in the well and part that has not been encapsulated at the same height than the control (Figure A.14). This assays allows to identified the binding strength of polymers and it can be quantified the encapsulation if a standard with knowing concentrations is used. However, for proper quantification other methods are preferred.

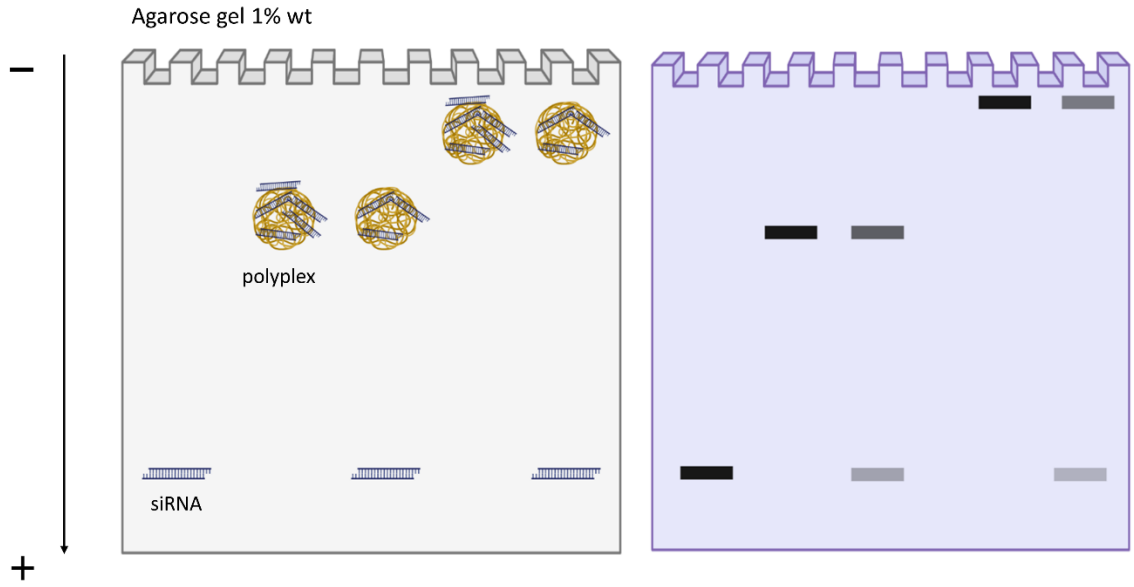

Figure A. 14.-Illustration of a gel retardation assay with an siRNA polymer/polyplex. The image presents several potential results. A free siRNA control is incorporated to visualize its electrophoretic migration. The polymer could completely encapsulate the siRNA, resulting in a single band on the gel. If the polymer is too large for the pore size, it will not be able to pass through the gel and the band will be visible in the loading well. In contrast, if the polyplex is small enough, it will migrate through the gel but at a slower rate than free siRNA, resulting in a band at a shorter distance from the wells. In cases of incomplete siRNA encapsulation, two bands will appear on the gel, although they will be less intense than those of free siRNA. Illustration made with Biorender.

Quant-IT Ribogreen for encapsulation efficiency test

Quant-iT™ RiboGreen® RNA reagent is an ultra-sensitive fluorescent nucleic acid stain for quantitating RNA in solution provided by Invitrogen. It is a molecule not disclosed by Invitrogen that binds to RNA chain when it is free in solution, but it cannot bind when it is attached or encapsulated to nanoparticles. Ribogreen bound to RNA is excited at maximum 500 nm of wavelength and emits at maximum of 525 nm. Fluorescence intensity measured is correlated to RNA concentration in solution. It is sensitive up to 1 ng/mL and resolve many problems encountered in traditional UV absorbance at 260 nm technique and it is applied in many molecular biology procedures. In this work it was used to determine the encapsulation efficiency of siRNA by the polyplexes. siRNA encapsulated by polyallylamine modified polymers is mixed with Quant-iT™, the possible siRNA free in solution not attached to the nanoparticle will give fluorescence emission measured by fluorometer. Then, these data are normalized to fluorescence given by polyplexes treated with a solution Heparine/Triton-X-100, which will release the amount of siRNA encapsulated. The encapsulation efficiency was then calculated following this formula:

$$Encapsulation\ efficiency(100\%) = 100 - (\frac{(U_{Sample} - U_{Blank})}{(T_{sample} - U_{Blank})} * 100)$$

Where U_{sample} represents samples untreated with Heparin/Triton-X-100 solution

T_{sample} represents polyplexes treated with Heparin/Triton-X-100

Blank represent buffer with Quant-IT™ without RNA.

This method allows the amount of siRNA encapsulated by polyplexes to be quantified in a accurating manner.

Cytotoxicity measured by metabolic activity and fluorophores

Nanoparticles may cause undesired toxicity to the cells. There is different type of assays to evaluate cytotoxicity. One the most recognized and well established is to test the metabolic activity of the cells after treatment with nanoparticles and the membrane healthiness.

Metabolic activity is measured by MTS using the CellTiter 96® AQueous One Solution Cell Proliferation Assay from Promega. MTS [3-(4,5-dimethylthiazol-2-yl)-5-(3-carboxymethoxyphenyl)-2-(4-sulfophenyl)-2H-tetrazolium, inner salt is a novel tetrazolium compound derived from classic version MTT. The MTS tetrazolium compound (Owen's reagent) is bioreduced by cells into a colored formazan product that is soluble in tissue culture medium (Figure A.15). This conversion is presumably accomplished by NADPH or NADH produced by dehydrogenase enzymes in metabolically active cells. The quantity of formazan product as measured by absorbance at 490 nm is directly proportional to the number of living cells in culture. Because the MTS formazan product is soluble in tissue culture medium, the CellTiter 96®AQueous One Solution Assay requires fewer steps than procedures that use tetrazolium compounds such as MTT or INT. Absorbance of cells treated with polyplexes are measured in the spectrophotometer. Data obtained are normalized to non-treated cells as hundred percent of viability. Different concentrations of dextran-based carriers or polyallylamine derived polymers were tested and percentage of viability of different compound was expressed as cytotoxicity.

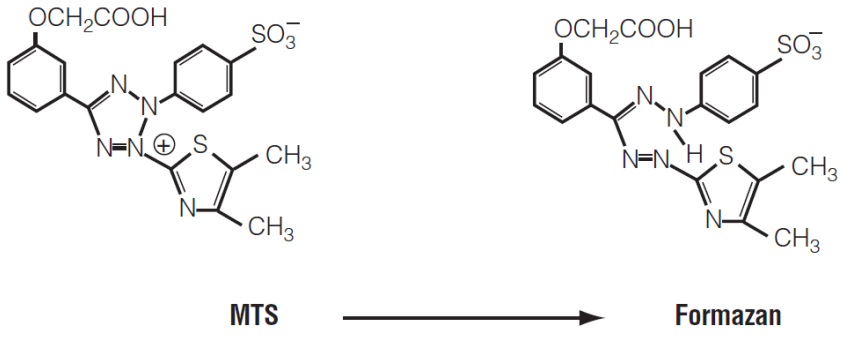

Figure A. 15.-Structures of MTS tetrazolium and its formazan product[20].

Another well-established protocol is the LIVE/DEAD® Viability/Cytotoxicity Assay by Invitrogen. a two-color fluorescence cell viability assay that is based on the simultaneous determination of live and dead cells with two probes that measure recognized parameters of cell viability—intracellular esterase activity and plasma membrane integrity. Molecular Probes has found that calcein AM and ethidium homodimer (EthD-1) are optimal dyes for this application. Live cells are distinguished by the presence of ubiquitous intracellular esterase activity, determined by the enzymatic conversion of the virtually nonfluorescent cell-permeant calcein AM to the intensely fluorescent calcein. The

polyanionic dye calcein is well retained within live cells, producing an intense uniform green fluorescence in live cells (ex/em ~495 nm/~515 nm). EthD-1 enters cells with damaged membranes and undergoes a 40-fold enhancement of fluorescence upon binding to nucleic acids, thereby producing a bright red fluorescence in dead cells (ex/em ~495 nm/~635 nm). EthD-1 is excluded by the intact plasma membrane of live cells. The determination of cell viability depends on these physical and biochemical properties of cells. Background fluorescence levels are inherently low with this assay technique because the dyes are virtually non-fluorescent before interacting with cells. Cells were observed under fluorescence microscope and images were taken. Integrity of membrane and esterase activity were visually determined (Figure A.16).

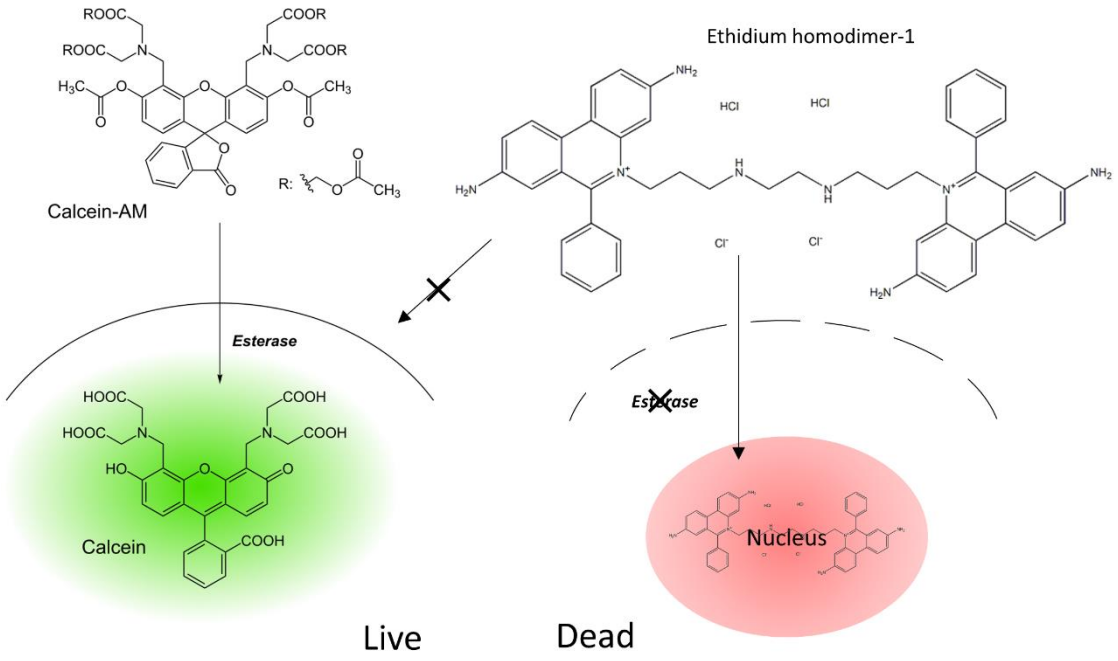

Figure A. 16.-Live/Dead assay determine membrane integrity based on two compounds: calcein AM and Ethidium homodimer-1. Calcein AM enter the cell by passive diffusion and is converted to fluorescent calcein by esterases present in the cytoplasm. Intact membrane does not allow the entrance of ethidium homodimer-1 (EthD-1), but it does damaged membranes, where EthD-1 strongly binds to nucleic acid and emitting fluorescence.

Using both methods will cover the cytotoxic events that can occur because of nanoparticle exposure. MTS data is given as quantitative results and LIVE/DEAD as qualitative data. Both results were considered to select the best candidate.

Fluorescence correlation spectroscopy

Fluorescence correlation spectroscopy (FCS) as a technique was developed in the early 1970s as a "miniaturization" of dynamic light scattering. The novelty of FCS lay in the analysis of minute intensity fluctuations in the fluorescence emission caused by spontaneous deviations of the sample molecules, instead of using average intensity of the fluorescence emission like other fluorescence-based techniques[21]. These fluctuations of intensity are due to Brownian motions of fluorophore or nanoparticle attached to the fluorophore. FCS is performed in Confocal Scanning laser microscope (Figure A.17.-A).

Tiny fluctuations in the fluorescence signal from excited molecules can be correlated with a delayed copy of itself, which is known as autocorrelation. Fluorescence autocorrelation measures the fluorescence intensity at different time points. One of the common criteria that can be measured using FCS is the diffusion rate of the fluorescent molecules in and out of the observation volume. Once the fluorescent molecular enters the area, fluctuations in fluorescence intensity can be observed. By converting fluorescence fluctuations to an autocorrelation function, the diffusion coefficient and concentration can be extracted. Diffusion of a molecule depends on its size. large particles will have small diffusion coefficient. High fluorescence intensity is due to high concentration of fluorophore in the sample[22] (Figure A.17.-B).

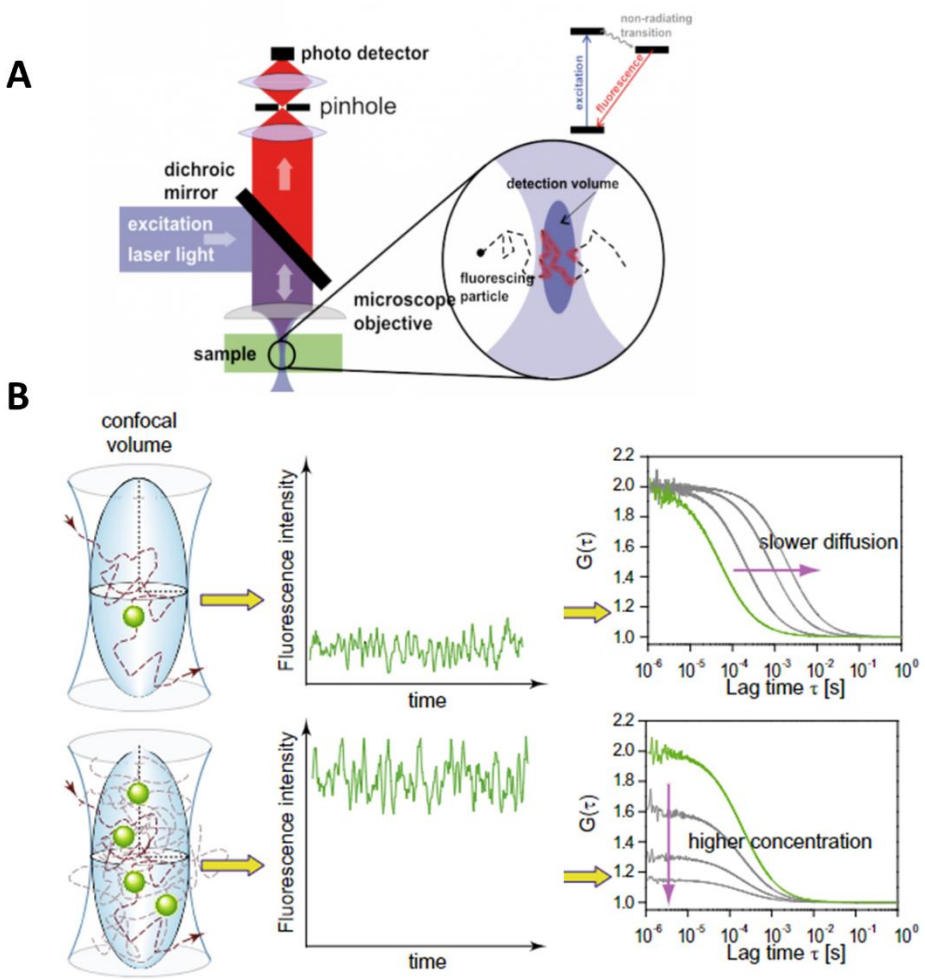

Figure A. 17.-A) FCS system in a confocal laser scanning microscope. B) Illustration of principles of confocal FCS. FCS analyze fluctuations of fluorescence intensity collected from a small observation volume. Any process that changes the fluorescence intensity can thus be observed; however, the most common process measured is the diffusive movement of fluorescently labelled molecules in and out of the observation volume. Considering the diffusion only, the fluctuations contain information on the average transition time of the molecules through the observation volume, i.e. their diffusion coefficient, and the number of particles present, i.e. their concentration. This information can then be directly obtained from the autocorrelation function G(τ) of the fluctuating intensity. The diffusion coefficient is inversely proportional to the width of the G(τ) and the concentration is inversely proportional to the G(τ) amplitude[22].

Uptake by confocal laser scanning microscopy

Confocal laser scanning microscopy (CLSM) is an optical imaging technique with increased resolution and depth selectivity. The primary functions of a confocal microscope are to produce a point source of light and reject out-of-focus light, which provides the ability to image deep into tissues with high resolution, and optical sectioning for 3D reconstructions of imaged samples. The basic principle of confocal microscopy is that the illumination and detection optics are focused on the same diffraction-limited spot, which is moved over the sample to build the complete image on the detector. While the entire field of view is illuminated during confocal imaging, anything outside the focal plane contributes little to the image, lessening the haze observed in standard light microscopy with thick and highly scattering samples, and providing optical sectioning[23] (Figure A.18).

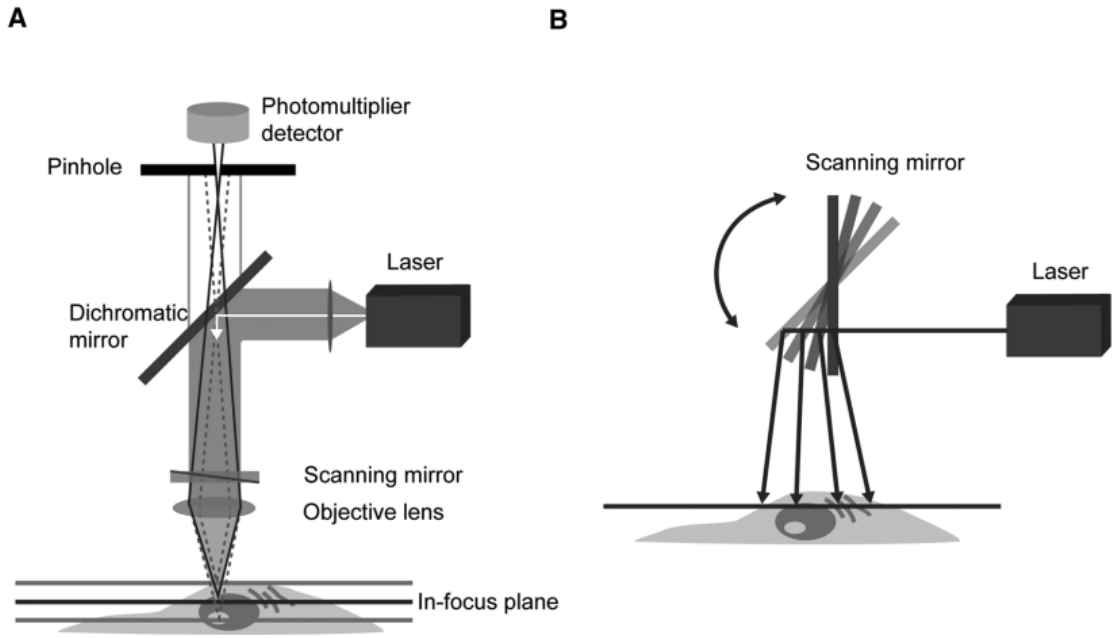

Figure A. 18.-Components of a confocal microscope. **A)** Light from a laser source is passed through collimating optics to a variable dichromatic mirror and reflected to the objective lens, which focuses the beam on a point in the sample. Scanning mirrors sweep the excitation beam over the sample point-by-point to build the image. Emitted fluorescence passes back through the objective lens and the dichromatic mirror and is detected by the photomultiplier detector. A pinhole placed in the conjugate image plane to the focal point in the sample serves to reject out-of-focus light, which is not picked up by the detector. Varying the size of the pinhole changes the amount of light collected and the optical section thickness. **B)** A schematic of the scanning mirrors employed by confocal microscopes to sweep the excitation light across the sample[23].

All images were taken with Zeiss LSM 510. This microscope is equipped with different laser at different wavelengths, 405, 488, 561 and 633 nm were the most used during the work of this thesis. For the study of polyplexes uptake different fluorophores were carefully selected to mark polymers, siRNA and parts of the cell, nucleus and actin cytoskeleton at the same time

Hoechst 33342 is fluorophore used to label the nucleus of the cell. It can penetrate the nucleus and bind to DNA. It has its maxim peak emission at 545 nm, corresponding to blue light. ActinRed™ 555 is a high-affinity F-actin probe (phalloidin) conjugated to the red-orange fluorescent dye tetramethylrhodamine (TRITC). it is excited by 561 laser and has maximum emission peak at 565

nm, corresponding to the orange-red range of visible light. siRNA were purchased with indicated fluorophore 6-FAM, 6-carboxyfluorescein, which gets excited by 488 laser and it has maximum emission peak at 520 nm. Polymers were labeled in the in the laboratory with different fluorophore, depending on the chemical nature of the polymer. Dextran-based SCPN and dextran polymer were marked with Rhodamine B, fluorophore excited by 561 laser and maximum emission at 568 nm, orange light. Polyallylamine based carriers were labeled with Atto633, fluorophore with maximal absorption at 630 nm and maximal emission at 651 nm, corresponding to red light. Nanoparticles are considered internalized inside the cell if they colocalize with Actin and are near the nucleus because every fluorescent are at the same focal plane. Another interesting approach to determine the cell uptake of nanoparticles by confocal microscopy is rendering a 3D image of the cell. It is called Z-stacked and is the result of horizontal sample slices. The sample is scanned in the x-y plane at a known depth to produce an optical slice. Then, the process is continued whilst changing the z-axial focus each time by moving the sample stage. Once the image is reconstructed in 3D it is expressed as an orthogonal view, wherein slice of the 3D image is sectioned by cross sections. This cross section displays an image in the X-Z plane or Y-Z plane, permitting the localization of the nanoparticle in the Z-axis.

Uptake and delivery efficiency by flow cytometry

Flow cytometry is a sophisticated instrument measuring multiple physical characteristics of a single cell such as size and granularity simultaneously as the cell flows in suspension through a measuring device. Its performance depends on the light scattering features of the cells under investigation, which may be derived from dyes or monoclonal antibodies targeting either extracellular molecules located on the surface or intracellular molecules inside the cell. This approach makes flow cytometry a powerful tool for detailed analysis of complex populations in a short period of time[24]. The main components of flow cytometer are fluidics, optics (excitation and collection), an electronic network (detectors) and a computer. The fluidics is responsible for directing liquid containing particles to the focused light source. The excitation optic focuses the light source on the cells/particles while collection optics transmits the light scatter or fluorescent light to an electronic network. The electronic network detects the signal and converts the signals to a digital data that is proportional to light intensity and the computer analyze the data (Figure A.19).

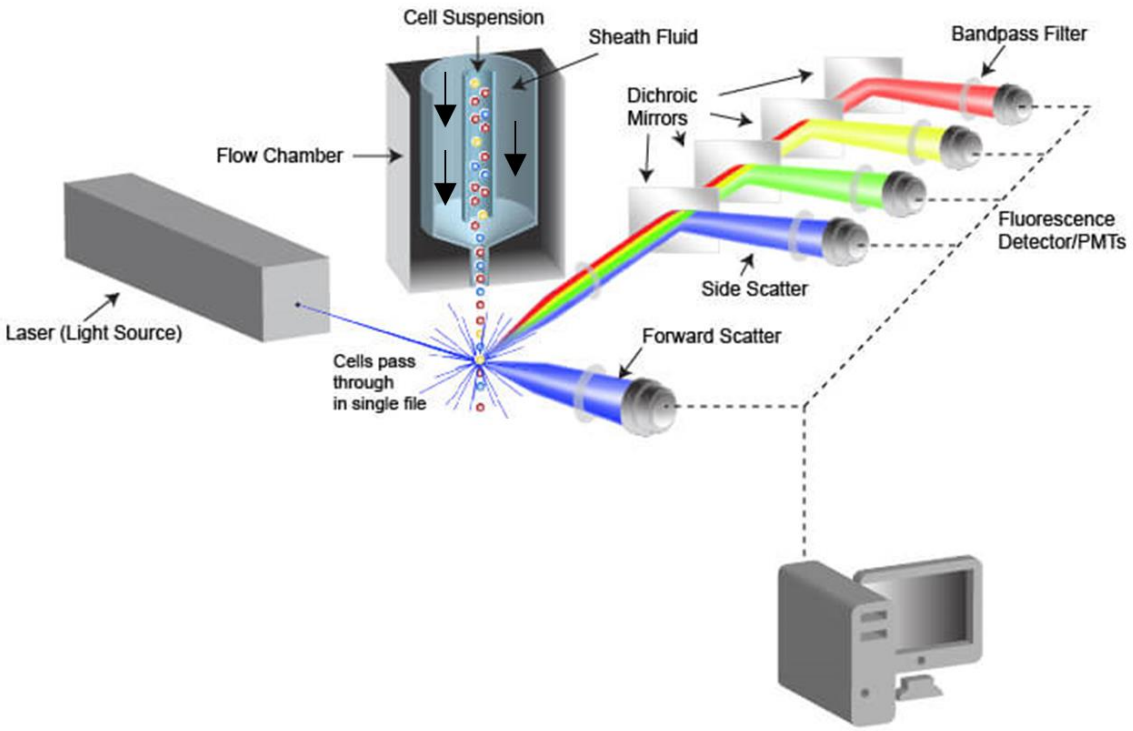

Figure A. 19.-Configuration of a flow cytometer. The fluidic system in a flow cytometer ensures a uniform stream of single cells for accurate analysis by employing hydrodynamic focusing formed by sheath fluid, and adjustable flow rates. The optical system, which includes laser illumination sources, filters, and collection optics, quantifies both scattered light (forward and side scatter) and fluorescent emissions from cells or other objects. The gathered data is collected by photodiodes or photomultiplier tubes (PMTs), which convert photons into numerical values for further display and analysis[25].

Photons produced by laser strike the cells passing through the fluidic system, light is deflected around the edges of the cells. Two types of light scatter occur named as forward scatter (FSC) and side scatters (SSC). FSC light is a result of diffraction collected along the same axis as the laser beam. FCS is proportional to cell-surface area or size. On the other hand, SSC light is a measurement of mostly refracted and reflected light, which is collected at approximately 90 degrees to the laser beam. SSC is proportional to cell granularity or internal complexity as important as the fluorescent light derived from fluorescent-labeled antibodies or dyes, which are reflected at the same angle as SSC (Figure A.20). Software displays this information as a dot plot, which represent every single cell passing through the fluidics. According to size and complexity, different populations of cells can be distinguished in the plot and analyzed. Different subgroups of populations can be selected according to fluorescence after staining specific protein characteristic of a cell type.

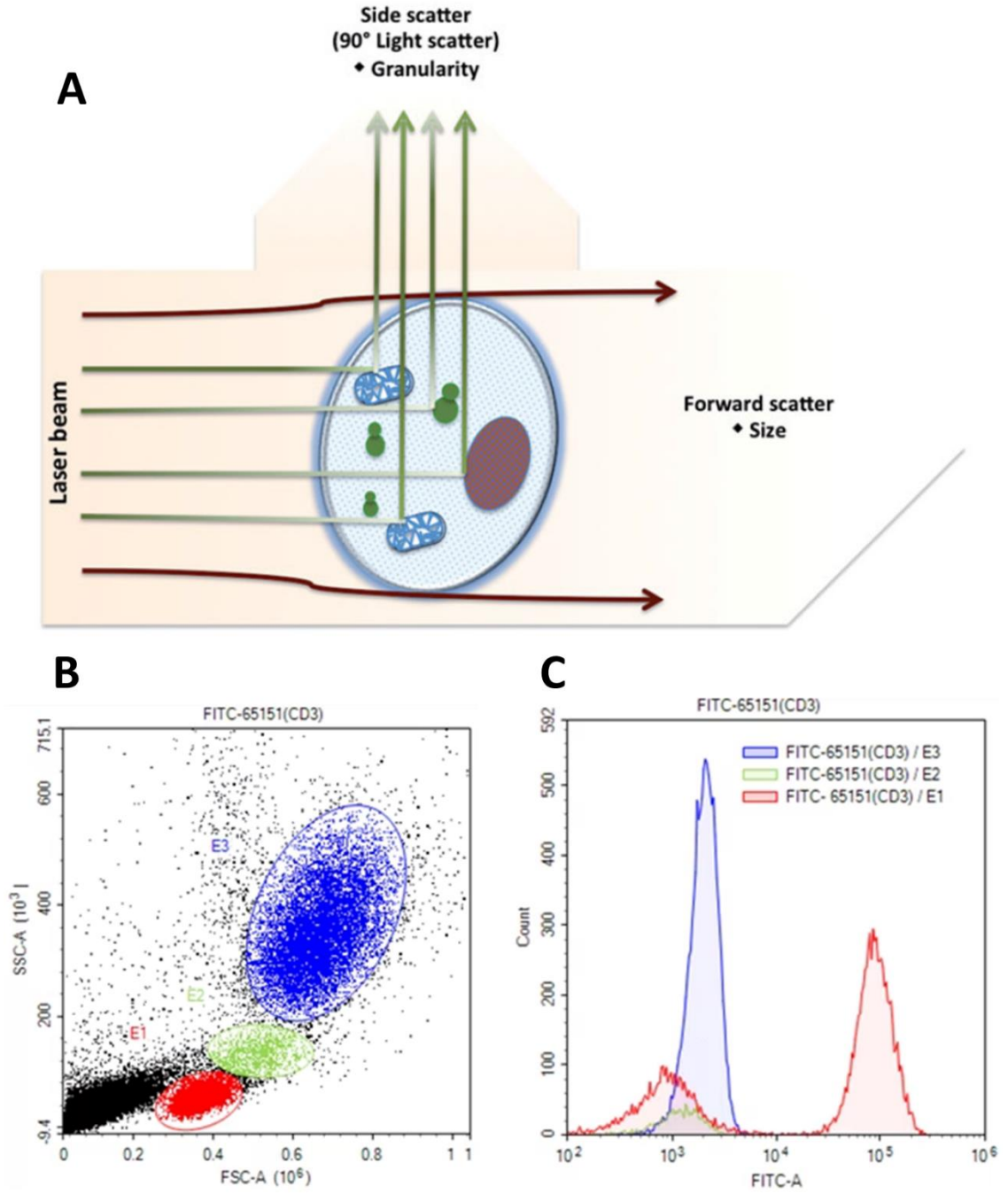

Figure A. 20.-A) Representative image of forward and side scattering of light after hitting cells in the flow cytometry. FSC is proportional to size while SSC is proportional to cell granularity or internal complexity[24]. B) Example of typical dot plot generated by FSC and SSC data, where different population of cells (E1, E2 and E3) are displayed according to their size and complexity. C) Example of typical histogram generated by fluorescence emitted by the cells. In this case fluorophore fluorescein isothiocyanate (FITC) present high intensity for the population E1, but very low for E2 and E3[26].

In the present work, flow cytometry has been used mainly for quantifying uptake of nanoparticles by cells and quantifying the siRNA delivery efficiency.

A549 cells were treated with different compounds, dextran based and polyallylamine based carriers loaded with 6-FAM siRNA. Transfected cells contain green fluorescence derived from 6-FAM. Percentage of populations with fluorophore of the total number of cells passed by the cytometer is used to quantify the internalization efficiency.

Flow cytometry was employed to assess siRNA delivery efficiency using a unique cell line: A549 stably expressing enhanced green fluorescent protein (eGFP). This approach obviated the need for fluorophore staining, as siRNA targeting eGFP was utilized. When siRNA successfully silences eGFP expression, the mean fluorescence intensity of the cell population decreased. Such decrease in the mean fluorescence of A549-eGFP cells after polyplex treatment indicates efficient cytosolic release by the delivery system. Consequently, an ideal candidate will exhibit reduced fluorescence intensity in A549-eGFP cells. Mean fluorescence is compared to non-treated cells and cells treated with negative siRNA that lack a target. Data normalization is performed relative to non-treated cells, which represent 100% eGFP expression. To assess siRNA integrity, a positive control Lipofectamine RNAimax supplied by Invitrogen® is used, which reduces expression to 20%.

This experiment represents a quick method for screening different carriers of different nature. As if siRNA works, it means that every different barrier for delivery is overcome. Different candidates have been passed through flow cytometry to quantify the protein knockdown achieved by the carriers. The best candidates were corroborated by other experimental techniques.

Western blot

Western blot is a protein detection technique based on molecular weight separation and staining with antibodies. It is divided into three procedures. The term Western blotting was coined to retain the 'geographic' naming tradition initiated by E.M. Southern[27], who first used the method to detect DNA. So, Southern is used to DNA, Northern to RNA and Western to protein blotting.

In the first step proteins are separated by electrophoresis in a polyacrylamide gel (PAGE), typically denatured by sodium dodecyl sulfate (SDS). In the next step proteins are transferred to an adsorbent membrane made of nitrocellulose or polyvinylidene difluoride (PVDF). Final step is the treatment of the membrane with specific antibodies targeting the desired protein (Figure A.21).

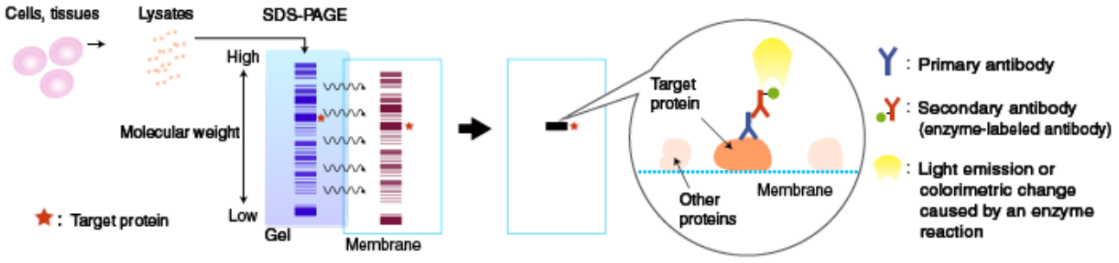

Figure A. 21.-Scheme of steps in Western blotting procedure: extraction of proteins, separation by molecular weight in a denaturing polyacrylamide gel (SDS-PAGE) by electrophoresis, protein transferring to a membrane and inmunoblotting [28].

Before proceeding with the western blot proteins are obtained from culture cells after treatment with polyplexes. Cultured A549 cells are scratched using radio inmuno Precipitation Assay (RIPA) lysis buffer and incubated in the mix with proteases, phosphatases, and phosphorylases inhibitors. Proteins are purified from the rest of cells components by centrifugation. The concentrations of

obtained protein solution was determined by Bradford test using bovine serum albumin (BSA) standard.

First step in the western blot is the PAGE-SDS protein separation by molecular weight. Polyacrylamide gels are made of a mix of acrylamide and bis-acrylamide, ammonium persulfate (APS) and tetramethylethylenediamine (TEMED) are added to initiate the polymerization. The resulting network has pores through which analytes can move. The smaller the pore size, the smaller the proteins that will be able to pass through. The ratio of bisacrylamide to acrylamide impact the pore size. Proteins are denaturalized by incubating at 80^{o}C 10 minutes, dithiothreitol (DTT) and SDS, secondary and tertiary structures disappear, and protein are linearized. Heat disrupts hydrogen bonds and DTT sulfide-bridges. SDS will attach to positive residues of the linear protein, and cover it, so the whole protein will have a negative charge that will migrate to cathode and will be separated only by its molecular weight. Electrophoresis gel has two parts, the stacking and resolving. The role of stacking section is to allow sample loading and guide proteins to enter at the same time in the resolving section. For this purpose, the percentage of acrylamide is 4%, which forms large pores. The role of resolving section is to separate the proteins by molecular weight, depending on the weight of the target protein the percentage of acrylamide will vary, typically between 7-12%. The voltage used and run time will vary depending on the percentage resolving gel being used, analyte size and whether an SDS or native analysis is being run. Here, the gel was run at 80 V for 30 minutes to facilitate protein stacking, followed by running at 120 V for 60 minutes to achieve protein resolution.

The next step is to transfer the proteins separated to a solid membrane to make the proteins accessible to antibody detection. The main method for transferring proteins is called electroblotting, which uses an electric field oriented perpendicular to the surface of the gel, to pull proteins out of the gel and move into the membrane. A membrane made of PVDF is preactivated, meaning it is treated to enhance its binding capacity for proteins. This preactivated membrane is then positioned facing the gel. Both the membrane and gel are stacked together, with filter papers placed on either side, creating a sandwich-like structure (Figure A.22). This assembly is inserted into a cassette to be immersed in a special transfer buffer. The transfer buffer is typically based on a Tris-glycine buffer system, which helps maintain the appropriate pH and ionic strength for efficient protein transfer. Additionally, the transfer buffer includes methanol and SDS to facilitate the transfer process. Methanol enhances protein transfer efficiency, while SDS helps denature the proteins and keep them soluble during transfer. There are three types of transfers, wet, semi-dry and dry, which differ from each other by the amount of buffer used. In wet transfer the stacked cassette is fully submerged in the buffer, usually ice-cold. Transfers are typically carried out under cold temperatures to dissipate the heat produced during the running of 60 min under 100 Volts and 250-300 mA. Once transfer has finished an optional middle step is to stain the proteins with Ponceau S solution to visualize the bands on the membrane and check the running was carried out successfully.

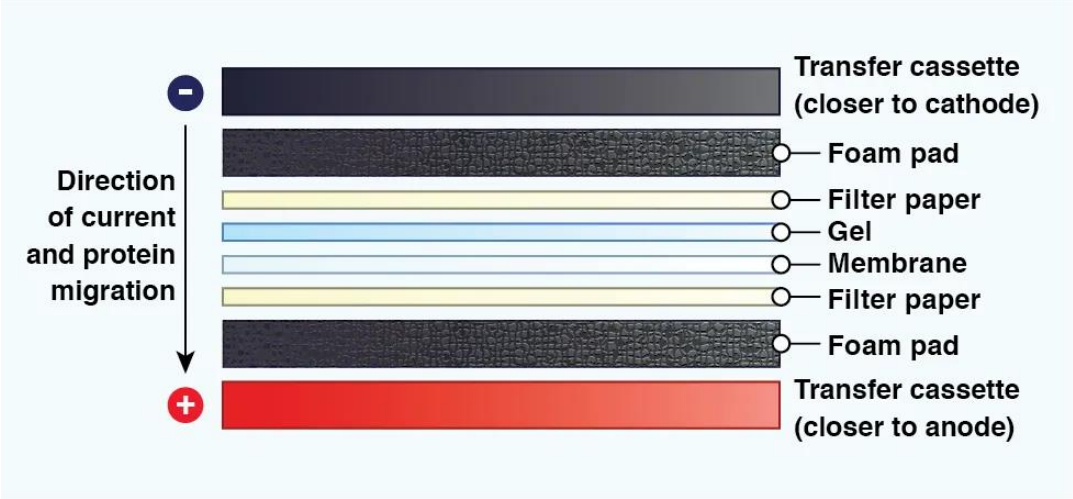

Figure A. 22.-Scheme of the transfer cassette for wet electroblotting, where proteins are transferred from the gel to the membrane. Several layers of filter papers and a foam pad are stacked above and below the gel-membrane assembly all embedded in transfer buffer. Extracted from web page[29].

The final step is to incubate the membrane with antibodies of the desired protein. First, the membrane is blocked with proteins to prevent antibodies to bind to non-specific spots. The blocking solutions typically used is BSA at 5% or non-fat milk. Then the primary antibody is incubated overnight at 4ºC under agitation. The antibody will bind to the protein attached on the membrane. Afterwards, a secondary antibody is used to reveal the band of the protein. Revealing step can be carried out by different methods, colorimetric, chemiluminescent and fluorescence. The secondary antibody will be conjugated to an enzyme or fluorophore and has to be specific against the specie of the primary antibody (Figure A.23). The most typical method to reveal and the one used in this work is by chemiluminescence and capture the luminescence by CCD camera. In this case the secondary antibody is conjugated to horseradish peroxidase (HRP). HRP catalyze the oxidation of luminol to 3-aminophthalate. This product is in an excited state, which decay to lower energy state by releasing photons of light at 425 nm (Figure A.24). As enzyme are attached to antibody, light is only produced in the area of the protein. Bands observed in the image taken by the camara are thick or thin depending on the amount of protein, allowing this method to be semi-quantitative to compare protein knockdown.

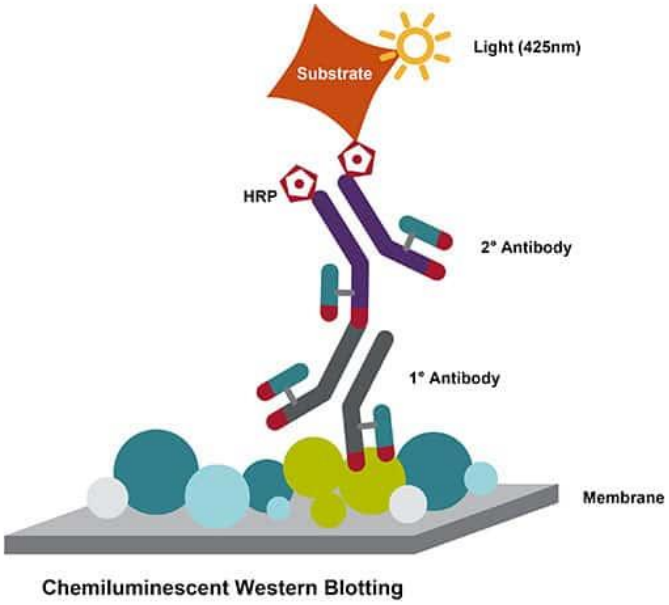

Figure A. 23.-Antibody incubation of proteins attached to PVDF membrane. First antibody recognizes protein epitope and secondary antibody attaches to the primary antibody. The secondary antibody is carrying the enzyme horseradish, which can oxidize a substrate, which can emit light. Illustration extracted from web page[30].

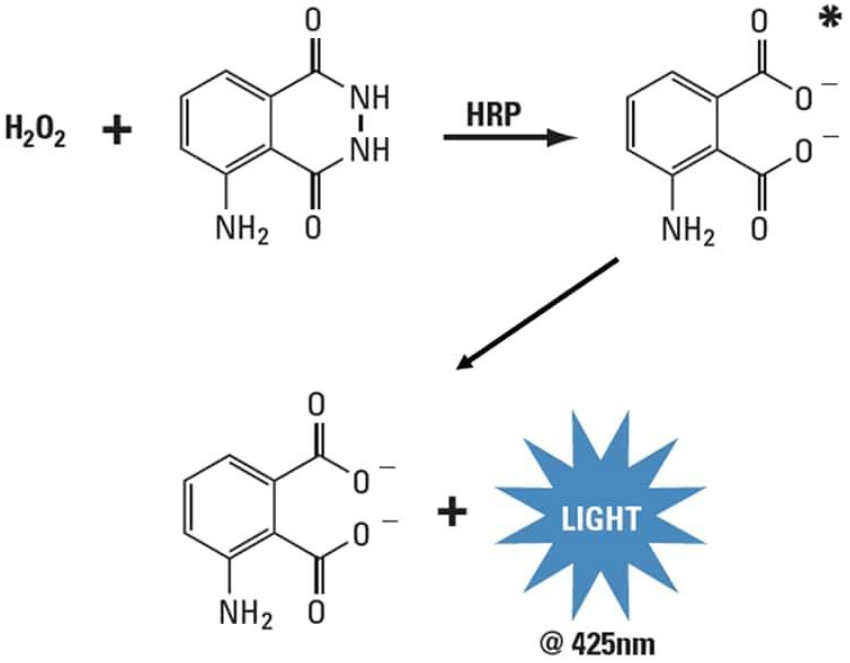

Figure A. 24.-Horseradish peroxidase (HRP) oxidizes luminol to 3-aminophthalate. In this process emission of light is produced, phenomenon known as chemiluminescence. Illustration extracted from web page[30].

In this thesis Western Blot has been used to detect CD47 in A549 cells after the treatment of polyplexes with siRNA anti CD47. Although it can be used as semi-quantitative method, in this case have been used only qualitativeobservation was considered.

Reverse transcription quantitative polymerase chain reaction

Quantification of mRNA expression is possible thank to reverse transcription quantitative polymerase chain reaction (RT-qPCR). RT-qPCR is currently the most sensitive technique available for mRNA detection and quantification. It can accurately quantify genes present at only a few hundred copies per sample and has become the method of choice for the examination of gene expression. The technique consists of two parts: synthesis of cDNA from RNA by reverse transcription, and amplification of a specific cDNA by polymerase chain reaction (PCR).

RNA starting material is mRNA, because the objective is to quantify the reduction of transcripts after siRNA treatment. mRNA is extracted from A549 treated cells together with RNA and DNA. Usually, genomic DNA is eliminated by DNAses or using special retention membranes. Selection of mRNA from the rest of RNA is done by using oligo deoxyribose thymine (oligo-dT) that will anneal with poly adenosine tail only found in mRNA. cDNA will be synthesized from this RNA using a reverse transcriptase and deoxynucleotides. The cDNA will serve as template for the quantitative PCR.

A quantitative or real time PCR is a PCR where products are detected as the reaction proceeds, qPCR has a much wider dynamic range of analysis than conventional, end-point PCR; from a single copy to around 10^{11} copies are detectable within a single run. Quantitative real-time PCR and subsequent amplicon detection is carried out in a closed-tube format which eliminates the need for post-PCR manipulation, such as gel electrophoresis and significantly reduces the risk of cross contamination. A fluorescent reporter dye is used as an indirect measure of the amount of nucleic acid present during each amplification cycle. The increase in fluorescent signal is directly proportional to the quantity of exponentially accumulating PCR product (Figure A.25). There is different type of reporter molecules, dsDNA binding dyes, dyes conjugated to primers and dyes conjugated to oligonucleotides[31].

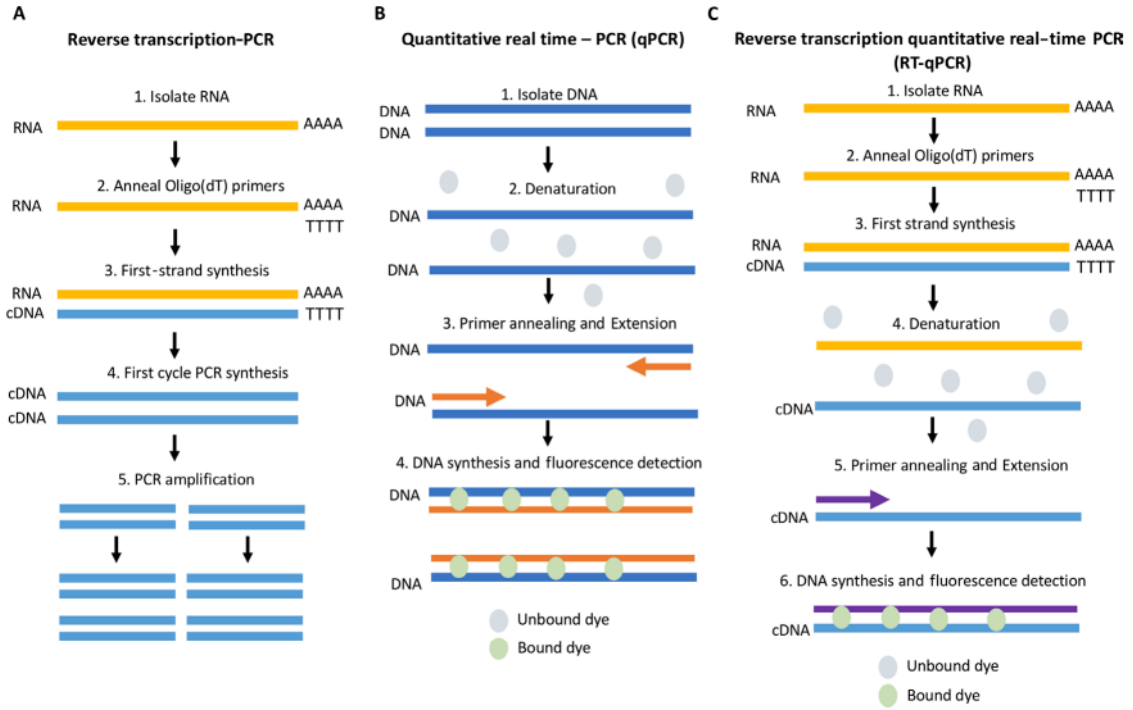

Figure A. 25.-Schematic comparing RT-PCR, qPCR and RT-qPCR. (A) RT-PCR workflow. RNA is isolated and cDNA is generated via reverse transcription (RT); PCR is then carried out to amplify areas of interest. (B) qPCR schematic. DNA is isolated and amplified; amplification is quantitated using a probe which fluoresces upon intercalation with double-stranded DNA. (C) RTqPCR procedure. RNA is isolated and cDNA generated before commencing a qPCR procedure[32].

dsDNA binding dyes is the simplest form of detection chemistry. Most common dye used and the one used in this work is SYBR® green. When free in solution or with only single-stranded DNA (ssDNA) present, SYBR Green I dye emits light at low signal intensity. As the PCR progresses and the quantity of dsDNA increases, more dye binds to the amplicons and hence, the signal intensity increases(Figure A.26). One key parameter in qPCR and in every PCR is the selection of primers. Primers must be designed to anneal to gen of interest for amplification. A pair of primers for both bands 5´→3´and 3´→5´. As it is cDNA, only exons must be considered as introns will be discarded during the mRNA maturation. General criteria should be followed to have a good annealing i.e., %GC content, length of nucleotides, avoid secondary structures and dimerization. Commercial houses have already designed primers for multiple genes and already tested that allows to skip this process. Other components in the mix are deoxynucleotides (dNTPs) buffer, magnesium necessary for enzyme activity and polymerase. Polymerase used is named Taq Polymerase and comes from thermophilic eubacteria *Thermus aquaticus*, Taq. It is thermo resistance and its optimal temperature activity is 75-80ºC. It has been modified with antibody-blocked or chemically blocked ('hot start') to prevent enzyme activity until the high-temperature, denaturation has been achieved. Typical repeated cycles in qPCR consist of two steps. Denaturation and second step of Annealing and Extension that repeat for 40 cycles. During denaturation, the reaction temperature is increased to 95°C for 10 sec to melt all dsDNA. Annealing and Extension, the temperature is lowered to 60°C for 30 sec to promote primer binding to the template and subsequent elongation occurs due to sufficient activity of the DNA polymerase at this temperature. Primer extension is most efficient at 72 °C because this is the optimal temperature for processivity of most DNA polymerases. At 72 °C, polymerization occurs at a rate of approximately 100 bases per second. However, there is still

processivity at lower temperatures that is sufficient to amplify shorter templates. qPCR amplicons are typically shorter (<200 bases) than conventional PCR products as amplified gene is not necessary to be used afterwards.

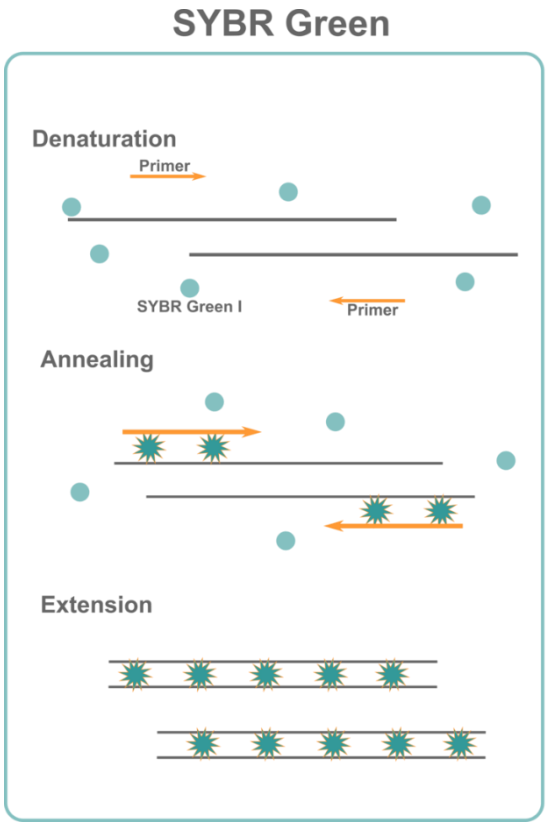

Figure A. 26.-Scheme of a cycle of qPCR with the steps denaturation, annealing and extension using SYBR green as DNA binding dye. Illustration extracted from web page[33].

The change in fluorescence over the course of the reaction is measured by a real-time PCR thermal cycler. Dedicated real-time PCR instruments combine temperature cycling with an optical unit. The optical unit provides light at a suitable wavelength to excite the fluorophore and detects the resulting emission. Many modern instruments have an affixed display screen or nearby computer monitor, which allows the reaction to be tracked as it progresses. RT-qPCR could be carried out in one step or two step. In two steps reactions occur sequentially in separated tubes, first the reverse transcription and then the qPCR. In one-step both reactions occur in one tube, the experimental setup is simplified and there is a lower chance of contamination because there is no requirement for further handling of the sample. Same buffer for both enzymes, oligo-dT primers and gene-specific primers and DNA dye are mixed together (Figure A.27).

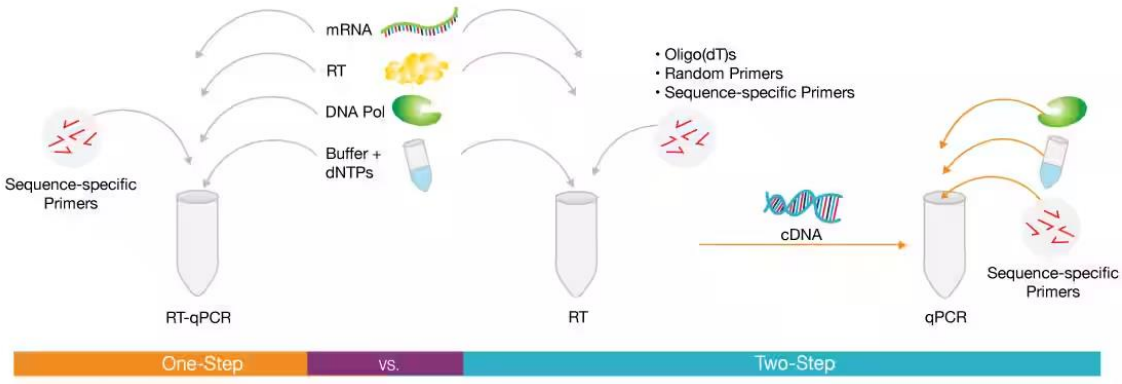

Figure A. 27.-Scheme of RT-qPCR in One-step versus in Two-steps. Illustration extracted from web page[34].

The amount of product yielded by a qPCR approximates a sigmoidal curve when it is plotted as a function of reaction cycle completed (X axis) to fluorescence intensity (Y axis). A ground phase or background fluorescence is observed at low cycles, then an exponential phase starts following by a linear phase. Finally, a plateau phase is reached since no new products are synthesized. Cycle Threshold C_T, also called Cycle quantification C_q is defined as the number of cycles required to exceed background levels of fluorescence. A threshold is set within the exponential phase and above the background fluorescence of the amplification curve. The number of fractional cycles required to eclipse this threshold provides a correlate to the initial amount of template. Thus, Ct is the unit used to quantify the amount of gene expression. C_T levels are inversely proportional to the amount of target nucleic acid in the sample, i.e., C_T 15 represents great amount of gene expression, C_T 25 represents lower amount (Figure A.28).

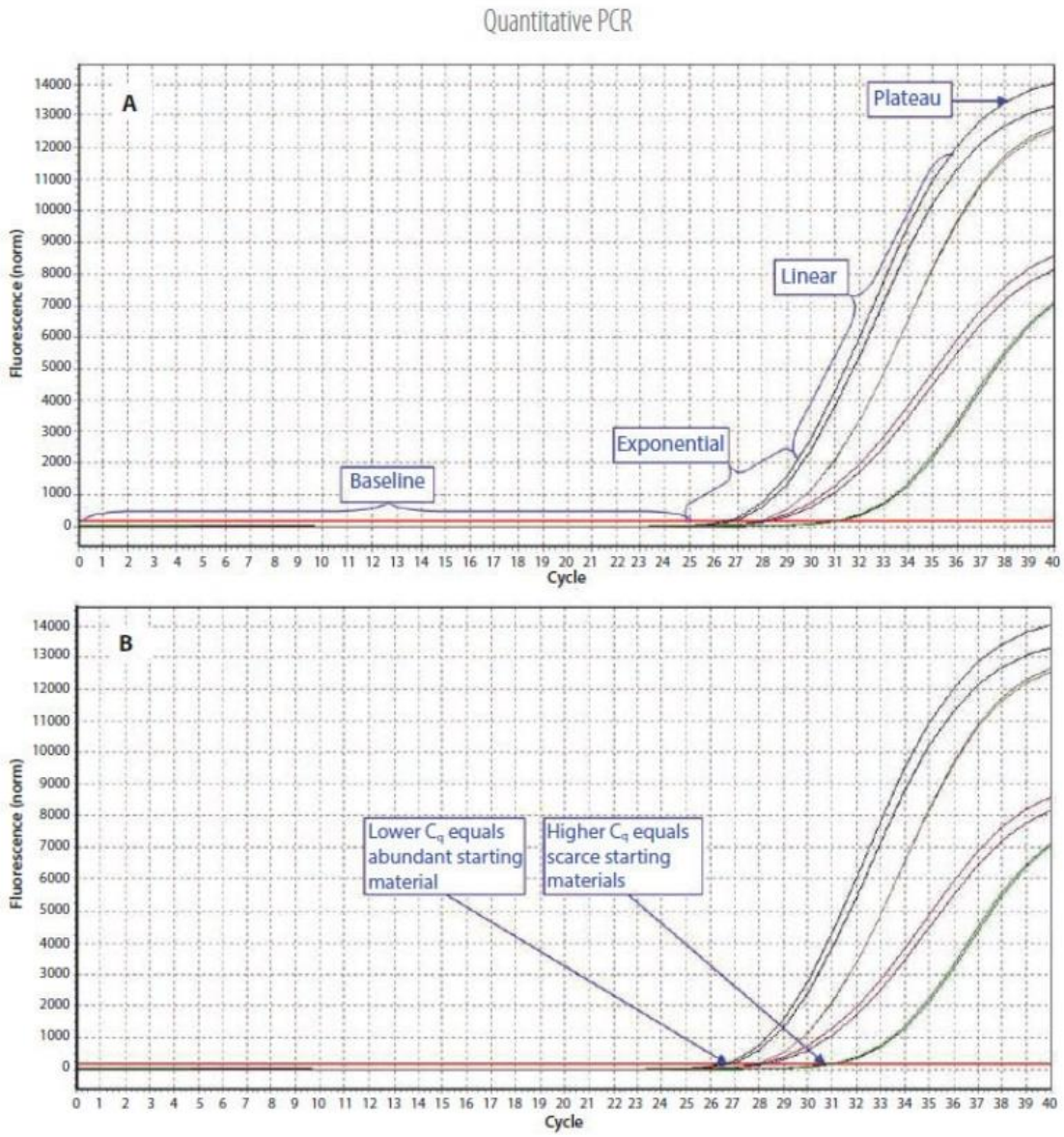

Figure A. 28.-Example qPCR Assay Data. **A)** The different phases of the reaction. Baseline: The initial concentration of template is low; therefore, the fluorescence intensity is too low to be detected and only the background signal is evident. Exponential: After the target yield has reached the detection threshold, shown as the red threshold line, the course of the reaction can be followed through the exponential phase. Linear: As the concentration of template increases the available DNA polymerase concentration reduces and the reaction rate decreases. Plateau: The reaction is at the maximum yield. **B)** Individual reactions are characterized by the cycle at which fluorescence first rises above the threshold, which is referred to as the Quantification Cycle (Cq). If the starting material is abundant, amplification is observed in earlier cycles and the Cq is lower. If the starting material is scarce, amplification is observed in later cycles and the Cq is higher. This correlation between fluorescence, Cq and amount of amplified product enables quantification of the template over a wide dynamic range[31].

There are two general approaches to conducting RT-qPCR experiments. The first, known as absolute quantification, is based on calibration to a standard curve generated from a known external source that enables one to express data in terms of transcripts per biological unit (e.g., copies/µg of tissue). The second, known as relative quantification, describes expression in arbitrary units that are based on comparisons to a calibrator sample or a series of calibrator samples (e.g., RNA isolated from control or unmanipulated sources). Because the relative quantification approach makes fewer assumptions, is less labor intensive, and is sufficient for most applications, it is the method most

frequently used in basic research and is thus the method used to quantify the gene expression of cells treated with siRNA delivered by the vectors developed in this work. A housekeeping gene is used as reference of specificity of siRNA to a target. Housekeeping genes are recognized as cellular maintenance genes which regulate basic and ubiquitous cellular functions, and therefore are valid candidates to act as internal controls or reference for gene expression.

In relative quantification data are normalized by delta-delta-Ct method ($2^{-\Delta\Delta CT}$) to give results as fold change or percentage of gene expression relative to non-treated samples. The method was devised by Kenneth Livak and Thomas Schmittgen[35] and it is used as follows:

$$\Delta Ct = Ct(gene\ of\ interest) - Ct(housekeeping\ gene)$$

Where Ct (housekeeping) is the cycle when the housekeeping gene is starting to be amplified and Ct (target gene) is the cycle set for the beginning of target gene amplification.

After the subtraction of housekeeping expression, the samples are normalized to the control, which are the untreated samples. The value of the untreated sample is subtracted from all samples.

$$\Delta\Delta Ct = \Delta Ct(treated\ sample) - \Delta Ct(Untreated\ sample)$$

Where ΔCt (untreated sample) is the difference between housekeeping gene and target gene in a sample that was not treated with siRNA, its targeted gene values are at basal levels. ΔCt (treated sample), is the difference of housekeeping and targeted gen of sample treated with siRNA. If siRNA has taken effect, the Ct value of gene of interest should be increased respect to untreated targeted gene.

Finally, to work out the fold gene expression after the treatment 2 of the power of negative ΔΔCt is calculated.

$$2^{-\Delta\Delta Ct}$$

Untreated sample has value 1 and samples depend on the effect of siRNA. Values can be expressed as percentage by multiplying by 100.

In this work changes in the CD47 gene expression after treatment of siRNA against CD47 have been calculated by RT-qPCR using the $2^{-\Delta\Delta Ct}$ method of relative quantification. Results are expressed in percentage where non-treated cells represent 100% of CD47 expression.

Immunostaining and protein quantification by flow cytometry

Immunofluorescence (IF) is a powerful approach for getting insight into cellular structures and processes using microscopy. Specific proteins can be assessed for their expression and location, making immunofluorescence indispensable for scientists to solve many cell biological questions. An immunofluorescence experiment is based on the following principal steps: Specific antibodies bind to the protein of interest and fluorescent dyes coupled to these immune complexes allow the

protein of interest to be visualized using microscopy. Immunofluorescence could be direct or indirect. In direct immunofluorescence, the primary antibody is directly coupled to a fluorophore (also called fluorochrome), allowing for easy handling and quick visualization. In indirect immunofluorescence, a secondary fluorophore-coupled antibody, which specifically binds to the primary antibody, is used to visualize the structure of interest.

This method has been used to detect CD47 cell-membrane protein in A549 without and with treatment of siRNA anti-CD47. The typical workflow of immunostaining has been followed which present the major steps: cells culture, treatment, fixation, staining and imaging (Figure A.29).

After the treatment with siRNA and proper incubation of 72h to let siRNA to knockdown levels of CD47 protein the immunostaining has been done. Cells are fixated with 4% of paraformaldehyde after incubation 10 min at room temperature. Paraformaldehyde causes covalent cross-links between molecules, effectively gluing them together into an insoluble meshwork that alters the mechanical properties of the cell surface. Fixation preserves cells for long-term periods allowing to carry out the experiment in several days. Living cells could be also stained, but images must be taken in a few hours after the antibody treatment. After fixation, it is very important to wash the sample 3x for 5 minutes in a washing solution, (e.g., PBS) to remove the fixation solution completely. If desired protein to detect is intracellular, cells need to be permeabilized to make possible the entrance of antibodies. Permeabilization requires incubation in a detergent, for example Triton X-100 or Tween-20 in a PBS solution. In the case of this study CD47 is a transmembrane protein, which antigen is shown outwards. Thus, permeabilization was not required.

Staining step includes blocking non-specific antigens to minimize intra- or extracellular background signals. The sample is incubated in (1) the serum of the host, in which the secondary antibody was made, (2) bovine serum albumin (BSA), or (3) milk. Typical blocking times are from 30 minutes up to one hour. BSA was the option chosen for the blocking step. Then it was proceeded to the primary antibody incubation. The selection of the primary antibody and its incubation conditions is the most critical step of an immunofluorescence staining protocol. A suitable primary antibody must have a high specificity for the antigen of interest. Another highly relevant property of the primary antibody is its originating host, as it determines the secondary antibody. CD47 antihuman made in mouse primary antibody was purchased from Thermo Fisher and was incubated overnight at 4^{o}C. After incubation with the primary antibody, the samples were washed 3x for 5 minutes in a Dulbecco's Phosphate Buffered Saline (DPBS) to avoid background fluorescence. In standard immunofluorescence assays, the secondary antibody is conjugated to a fluorophore, which emits light when excited at a defined wavelength. The secondary antibody Goat antimouse specifically binds to the mouse primary antibodies. It was incubated 30 minutes at room temperature and washed in PBS 3x for 5 minutes in order to avoid background fluorescence. Secondary antibody has attached FITC, which excites at 490 nm and emits at 525 nm at maximum peak. Whole experiment is performed in 8-well plate optically prepared to be observed under confocal microscope.

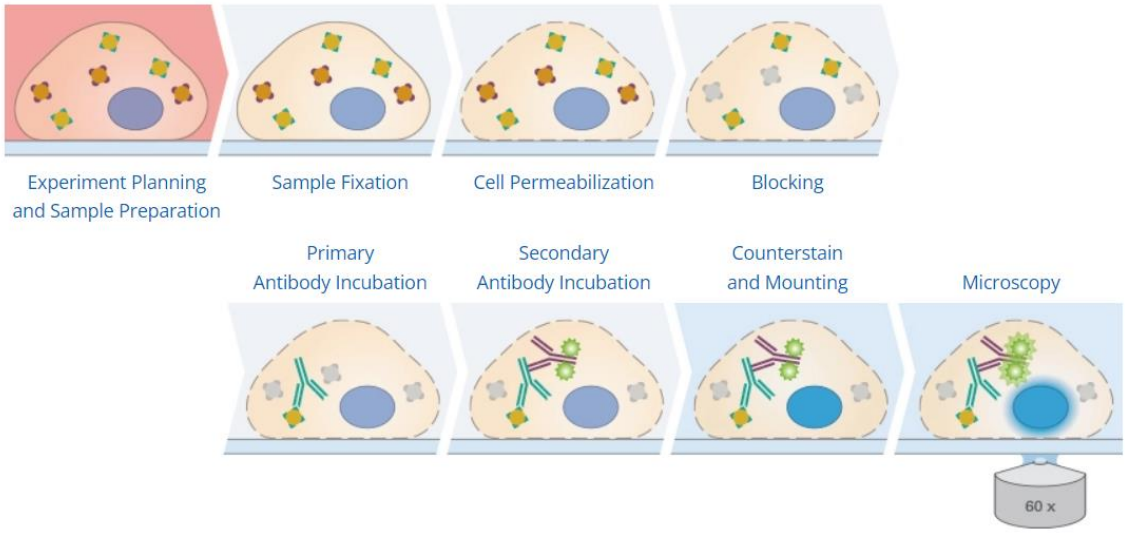

Figure A. 29.-Scheme of Immunofluorescence workflow[36].

Antibodies were also used to stain living cells for CD47 quantification by flow cytometry. Flow cytometry principles were described above. Proteins of interest can be quantified by flow cytometry since fluorescence intensity can be correlated to protein amount. For this purpose, primary antibody specificity is a key in the process as well as unspecific secondary antibody binding. As for immunostaining there is the direct or indirect method. The direct method avoids handling much the sample and allows to skip centrifugation step in which quantity is lost. On the other hand, an indirect method achieves more fluorescence intensity. In this case Fixation is avoided and staining was made directly to living cells. Cells were detached by trypsin and antibody incubation was made in cell suspension.

Appendix III

Calculation of the degree of substitution (DS) of different moieties substituted in the dextran polymers described in chapter 3.

Degree of substitution of Dextran-methacrylate, DXT-MA

To calculate the DS, first the proton value of every moiety must be obtained, in this case free glucose and methacrylate-glucose. Proton value of free glucose is obtained by subtracting the proton value of the methacrylate-glucose and divide it by 6 protons, according to the following formula:

$$Int_{Glcfree} = \frac{Int_{Glc} - 5(Int_{GlcMA})}{6H}$$ **equation 3.2.1.1**

$Int_{Glcfree}$ corresponds to the integrated value of the protons from unsubstituted glucose moieties.

Int_{GlcMA} corresponds to the integrated value of the protons from substituted glucose with methacrylate moieties.

Int_{Glc} corresponds to the integrated value of the protons of total glucoses obtained in the peak 3.3-4.2 ppm.

To solve the equation, the proton integral of the MA moiety observed at 5.7 ppm was assigned with a value of 1, as it corresponds to only one proton. Then, the integral of 3.3-4.2 ppm peaks displays 12.21 (Figure 3.4) corresponding to substituted and unsubstituted moieties of glucose. The value of 5 protons corresponding to MA-substituted glucose units is subtracted from the 3.3-4.2 integral to determine the number of protons of the unsubstituted glucose units. Finally, this value is divided by the 6 protons to obtain the number of unsubstituted glucose, as shown in equation 3.2.1.1:

$$Int_{Glcfree} = \frac{12.21 - 5(1)}{6H} = \frac{7.21}{6} = 1.2$$

Once obtained the proton value of substituted and unsubstituted glucose, at 1:1.2 GlcMA:Glcfree ratio. The DS, as percentage, is obtained using the following formula:

$$DS = \frac{Int_{GlcMA}}{Int_{GlcMA} + Int_{Glcfree}} * 100$$ **equation 3.2.1.2**

Taking the example considered here:

$$DS\% = \frac{1}{1 + 1.2} * 100 = \frac{1}{2.2} * 100 = 45\%$$

The DS of the obtained DXT-MA was 45%.

Degree of substitution of 3,6-dioxa-1,8-octane-dithiol DODT, also known as degree of cross-linking DC, SCPN

To determine the degree of crosslinking (DC) similar method as the one applied to determine DS of DXT-MA was used using ^{1}H NMR. However, in this case the crosslinker moiety must be considered and a modification of the equation 3.2.1.1 was required to remove the 9 protons corresponding to the crosslinker ($Int_{GlcDODT}$) from the integral of the 3.3-4.3 ppm region, while 5 protons correspond to the glucose units substituted with the methacrylate group:

$$Int_{Glcfree} = \frac{Int_{Glc} - 5(Int_{GlcMA}) - 9(Int_{GlcDODT})}{6H}$$ **equation 3.2.1.3**

The peak at 6.1 ppm corresponding to one of the protons of the alkene group was integrated by 1. Then the value of the peak at 1.8 ppm corresponding to the CH_3 of the methacrylate group acquired the value of 3, corresponding to its 3 protons. The signals of the hydrogen of DODT linker 2.9-2.56 ppm (d) and 1.2 ppm (c) obtained integrals value of 4 and 2.18, respectively, while the hydrogens of the glucose unit located at 3.3-4.3 ppm acquired a value of 30.50. Signal 2.9-2.56 ppm corresponding only to crosslinker is known to have 5 protons. So, this integral value is divided by number of protons (4.00 / 5H =0.8) to achieve the value of linker protons ($Int_{GlcDODT}$). Then equation 3.2.1.3 would be as follows:

$$Int_{Glcfree} = \frac{30.50 - 5 * (1) - 9 * (0.8)}{6H} = \frac{18.3}{6} = 3.05$$

DS was then calculated same procedure described above. Equation 3.2.1.2 was modified to include the moiety of crosslinker:

$$DS\% = \frac{Int_{GlcMA/DODT/free}}{Int_{GlcMA} + Int_{Glcfree} + Int_{GlcDODT}} * 100$$ **equation 3.2.1.4**

$$Glc_{MA}\ DS = \frac{1}{1 + 3.05 + 0.8} * 100 = \frac{1}{4.85} * 100 = 21\%$$

$$Glc_{DODT}\ DS, DC = \frac{0.8}{1 + 3.05 + 0.8} * 100 = \frac{0.8}{4.85} * 100 = 16\%$$

$$Glc_{free}\ DS = \frac{3.05}{1 + 3.05 + 0.8} * 100 = \frac{3.05}{4.85} * 100 = 63\%$$

So, DC is 16%, 21% is the DS for Glucoses substituted with methacrylate and 63% DS for free glucose. The sum of linker and methacrylate suppose a 37% of substitution in total. That is a 8% less than previous reaction of DXT-MA 45%. A 22.5% of linker substitution was expected because of stoichiometry 1:0.5 MA:DODT, however 16% is achieved. That occurred because during cross-linking reaction pH is adjusted to 9.5, which have induced hydrolysis in the ester of methacrylate.

Degree of substitution of cysteamine in SCPN and DXT-MA, SCPN-NH_2 and DXT-NH_2

DXT-SCPN-MA and DXT-MA were functionalized with cysteamine by Michael addition and new material was characterized by ^{1}H-NMR (See chapter 3). The DS of cysteamine was calculated using a modification of equation 3.2.1.1, introducing the cysteamine moiety Int_{GlcNH2}:

$$Int_{Glcfree} = \frac{Int_{Glc} - 5(Int_{GlcMA}) - 9(Int_{GlcDODT}) - 5(Int_{GlcNH_2})}{6H}$$ **equation 3.2.2.1**

As the H of all glucose units have similar chemical shift, the amount of substituted unit must be calculated by subtracting the unsubstituted saccharide to the whole integral. The DS of the different moieties were calculated from the proton values using the following formula:

$$DS\% = \frac{Int_{GlcMA/DODT/free/NH_2}}{Int_{GlcMA} + Int_{Glcfree} + Int_{GlcDODT} + Int_{GlcNH_2}} * 100$$ **equation 3.2.2.2**

In DXT-NH_2, peak 3.2 ppm was integrated by 2 as it corresponds to the 2 protons of the CH_2 next to the primary amine group. Protons of the glucose units (3.3-4.3 ppm) integrated for 13.37 and the proton of the methyl group at 1.3 ppm integrated 3. No crosslinker was added and no unreacted methacrylate moieties remained in the polymer (see chapter 3, Figure 3.9), so the proton integral value of unaltered glucose units was obtained using 3.2.2.1 formula:

$$Int_{Glcfree} = \frac{13.37 - 5(0) - 9(0) - 5(1)}{6H} = \frac{8.37}{6} = 1.39$$

As DXT-NH_2 has not been intracross-linked, the integral of the protons of DODT cross-linker is 0:

$$Glc\ free\ DS\% = \frac{1.39}{0 + 1.39 + 0 + 1} * 100 = \frac{1.39}{2.39} * 100 = 58\%$$

$$Glc\ NH2\ DS\% = \frac{1}{0 + 1.39 + 0 + 1} * 100 = \frac{1}{2.39} * 100 = 42\%$$

In summary, DXT-NH_2 is composed of 42% of glucose units functionalized with cysteamine, which is in a good agreement with the original DS of DXT-MA at 45% of methacrylate groups. Thus, theoretically the 3% difference between both DS could be attributed to the hydrolysis of ester group formed to obtain DXT-MA. However, this could be also considered as part of the NMR resolution usually estimated at 5%.

In SCPN-NH_2, peak 3.2 ppm was integrated by 2 and used as reference assignment. Then the proton values at 1.3 ppm, 2.56-2.9 ppm and 3.3-4.3 ppm signals acquired values of 5.37, 9.41 and 30.62, respectively. The value of the DODT protons was found by subtracting the value of the cysteamine protons from the methyl signal, common for both moieties: (5.37-3(1H) =2.37)). Then this value is divided by the number of protons in the methyl group (2.37/3H=0.79). The integral value of unaltered glucose protons was obtained by the consecutive subtractions of Glucose-DODT and Glucose-cysteamine protons:

$$Int_{Glcfree} = \frac{30.62 - 5(0) - 9(0.79) - 5(1)}{6H} = \frac{18.51}{6} = 3.085$$

Once all proton values were assigned, the DS of the glucose substitutions was achieved:

$$Glc\ NH2\ DS\% = \frac{1}{0 + 3.085 + 0.79 + 1} * 100 = \frac{1}{4.875} * 100 = 21\%$$

$$Glc\ DODT\ DS, DC\% = \frac{0.79}{0 + 3.085 + 0.79 + 1} * 100 = \frac{0.79}{4.875} * 100 = 16\%$$

$$Glc\ free\ DS\% = \frac{3.085}{0 + 3.085 + 0.79 + 1} * 100 = \frac{3.085}{4.875} * 100 = 63\%$$

In summary, SCPN-NH_2 exhibited a DS for cysteamine of 21% with DC of 16%, which correspond to the initial amount of MA and DODT groups. Thus, hydrolysis did not occur during the reaction.

Degree of substitution of 1-(3-aminopropyl)imidazole in DXT-MA, DXT-imidazole

DXT-MA was substituted with 1-(3-aminopropyl)imidazole mediated by Traut reagent. The new polymer was analyzed by ^{1}H-NMR (See chapter 3). The DS of imidazole substitution in the glucose was obtained from the integral values. Imidazole and methacrylate proton values can be elucidated directly from the spectrum. The free glucose proton proportion is extracted using a derived formula from 3.2.1.1:

$$Int_{free\ Glc} = \frac{Int_{Glc} - 5(Int_{NH2}) - 5(Int_{met})}{6H}$$ **equation 3.2.8.1**

Int_{Glc} represents proton integral value of glucose moiety, free and substituted with imidazole and methacrylate.

Int_{NH2} represents integral value of amino molecule protons, in this case imidazole.

Int_{met} represents integration value of methacrylate protons

The substituted glucose units present 5 protons in common with free glucoses in the 3.45-4.1 ppm region. Integrals of these protons must be subtracted to obtain the proton value of the free glucose. The 7.17 ppm peak corresponding to the imidazole is easily recognized and is known to represent 1 proton. Therefore, it is integrated by 1 and consequently 6.22 ppm and 3.45-4.1 ppm signals obtained 0.78 and 23.20 values respectively. From integral of 3.45-4.1 ppm the imidazole and methacrylate proton values are subtracted. Since the glucose molecule has 6 protons, the value obtained is divided by 6. The above formula 3.2.8.1 would be as follows:

$$Int_{free\ Glc} = \frac{23.20 - 5(1) - 5(0.78)}{6H} = \frac{14.3}{6} = 2.38$$

The proportions of unaltered glucose, imidazole protons and methacrylate protons are 2.38:1:0.78 respectively. To obtain a percentage of degree substitution, a derived formula from 3.2.1.2 is applied:

$$\%_{Free\ Glc/NH2/met} = \frac{Int_{Free\ Glc/NH2/met}}{Int_{free\ glc}+Int_{NH2}+Int_{met}} * 100$$ **equation 3.2.8.2**

Degree of glucose substituted by imidazole group:

$$\%_{Imida} = \frac{1}{2.38+1+0.78} * 100 = \frac{1}{4.16} * 100 = 24\%$$

Degree of glucose substituted by non-quenched methacrylate:

$$\%_{met} = \frac{0.78}{2.38+1+0.78} * 100 = \frac{0.78}{4.16} * 100 = 19\%$$

Percentage of free glucose:

$$\%_{Free\ Glc} = \frac{2.38}{2.38+1+0.78} * 100 = \frac{2.38}{4.16} * 100 = 57\%$$

24% degree of substitution of imidazole group, meaning that 24% of repeating units are substituted with imidazole. 24% of 222 repeating units are 53 units of imidazole per polymer chain. 19% of glucoses have non-reacted methacrylate groups and 57% are unaltered glucose units.

Degree of substitution of spermine in DXT-MA, DXT-spermine

DXT-MA was substituted with spermine mediated by Traut reagent. The new polymer was analyzed by ^{1}H-NMR (See chapter 3). The DS of spermine substitution in the glucose was obtained from the integral values, 1.29 ppm peak was integrated by 3 and the resulting integral value of 3.45-4.1 ppm was 19.07. Since methyl group has 3 protons, value of spermine protons is 1. The formula 3.2.8.1 was applied to calculate the proton proportions of the different moieties:

$$Int_{free\ Glc} = \frac{19.07 - 5(1) - 5(0)}{6H} = \frac{14.07}{6} = 2.35$$

The ratio between unaltered glucose and glucose-spermine was 2.35:1. The degree of substitution of spermine in the polymer chain was calculated using formula 3.2.8.2:

$$\%_{spermine} = \frac{1}{2.35+1} * 100 = \frac{1}{3.35} * 100 = 30\%$$

$$\%_{Free\ Glc} = \frac{2.38}{2.35+1} * 100 = \frac{1}{4.16} * 100 = 70\%$$

Dextran-metacrylate was substituted with a 30% of spermine. As it has been started from 54% of MA, a 24% loss of methacrylates is found. Probably hydrolysis of the ester occurred due to the pH 8.

Degree of substitution of Tris (2-aminoethyl)amine in DXT-MA, DXT-TAEA

DXT-MA was substituted with Tris (2-aminoethyl)amine mediated by Traut reagent. The new polymer was analyzed by ^{1}H-NMR (See chapter 3). The DS of TAEA substitution in the glucose was obtained from the integral values, methyl peak 1.29 ppm was integrated by 3 as TAEA proton value. 3.45-4.1 ppm region of glucose resulted in 28.24 integral value. Ratio of unsubstituted and substituted glucose was calculated using equation 3.2.8.1:

$$Int_{free\ Glc} = \frac{28.24 - 5(1) - 5(0)}{6H} = \frac{23.24}{6} = 3.87$$

3.87 unaltered glucoses to 1 substituted glucoses. The percentage of substitutions were calculated as follows (equation 3.2.8.2):

$$\%_{TAEA} = \frac{1}{3.87+1} * 100 = \frac{1}{4.87} * 100 = 20\%$$

$$\%_{Free\ Glc} = \frac{3.87}{3.87+1} * 100 = \frac{3.87}{4.87} * 100 = 80\%$$

Dextran-MA has been substituted with 20% of Tris (2-aminoethyl)amine and a 34% of hydrolysis occurred.

Degree of substitution of 3,3'-(piperazine-1,4-diyl)bis(propan-1-amine) in DXT-MA, DXT-piperazine

DXT-MA was substituted with 3,3'-(piperazine-1,4-diyl)bis(propan-1-amine) mediated by Traut reagent. The new polymer was analyzed by ^{1}H-NMR(See chapter 3). The DS of piperazine substitution in the glucose was obtained from the integral values, methyl peak at 1.29 ppm was integrated by 3 as piperazine proton value. The glucose region 3.45-4.1 ppm show 27.76 of integral value. The following calculations was performed (equation 3.2.8.1 and 3.2.8.2):

$$Int_{free\ Glc} = \frac{27.76 - 5(1) - 5(0)}{6H} = \frac{22.76}{6} = 3.79$$

$$\%_{piperazine} = \frac{1}{3.79+1} * 100 = \frac{1}{4.79} * 100 = 21\%$$

$$\%_{Free\ Glc} = \frac{3.79}{3.79+1} * 100 = \frac{3.79}{4.79} * 100 = 79\%$$

Dextran-MA has been substituted with 21% of piperazine and a 33% of hydrolysis occurred.

Degree of substitution of 1-(3-aminopropyl)imidazole and spermine in DXT-MA, DXT-imidazole-spermine

DXT-imidazole with unreacted MA moieties was substituted with spermine mediated by Traut reagent. The new polymer was analyzed by ^{1}H-NMR (See chapter 3). The DS of imidazole and spermine substitution in the glucose was obtained from the integral values, reference peak 7.07 ppm of imidazole group was integrated by 1. To differentiate between imidazole or spermine moiety, value of methyl group (1.29 ppm) was used. Proton value of spermine was subtracted from the methyl integral, which was 4.88. 4.88 -3(1) =1.88/3H= 0.63. Knowing that, the ratio of the different proton values was calculated same as equation 3.2.8.1, considering the spermine value:

$$Int_{free\ Glc} = \frac{23.25 - 5(1) - 5(0.63) - 5(0.27)}{6H} = \frac{13.75}{6} = 2.3$$

Ratio of unaltered glucose units and glucose units substituted with imidazole, spermine and unreacted methacrylate was 2.3:1:0.63:0.27 respectively. The degree of substitution of every moiety was calculated by equation 3.2.8.2:

$$\%_{Imida} = \frac{1}{2.3+1+0.63+0.27} * 100 = \frac{1}{4.2} * 100 = 24\%$$

$$\%_{met} = \frac{0.27}{2.3+1+0.63+0.27} * 100 = \frac{0.27}{4.2} * 100 = 6\%$$

$$\%_{spermine} = \frac{0.63}{2.3+1+0.63+0.27} * 100 = \frac{0.63}{4.2} * 100 = 15\%$$

$$\%_{Free\ Glc} = \frac{2.3}{2.3+1+0.63+0.27} * 100 = \frac{2.3}{4.2} * 100 = 55\%$$

Dextran has been substituted with 24%DS of imidazole and 15% DS os spermine. 6% of methacrylate are still reactive and free glucose represents 55% of the polymer. Hydrolisis of 10% has occurred.

Degree of substitution of cysteamine in DXT-6KDa-MA, 6-DXT-cysteamine

DXT-MA of 6 KDa dextran was firstly synthesized and analyzed by ^{1}H-NMR (See chapter 3) and then, subsequently reacted with cysteamine by Michael addition. To calculate the degree of substitution of glucose with methacrylate moieties same equations 3.2.1.1 and 3.2.1.2 as for 40 KDa polymer were applied. 5.78 ppm signal was used as methacrylate proton value and was integrated by 1. The protons of glucose ring reached 15.19 integral value. Equations go as follows:

$$Int_{free\ Glc} = \frac{15.19 - 5(1)}{6H} = \frac{10.19}{6} = 1.69$$

$$\%_{met} = \frac{1}{1.69 + 1} * 100 = \frac{1}{2.69} * 100 = 37\%$$

The DS of cysteamine in 6KDa DXT-Cysteamine was calculated. Peak 3.11 ppm belonging only to cysteamine was integrated by 2 and used as reference. Glucose ring proton integral achieved 34.98 value. The formulas 3.2.2.1 and 3.2.2.2 were applied:

$$Int_{free\ Glc} = \frac{34.98 - 5(1)}{6H} = \frac{29.98}{6} = 5$$

$$\%_{cysteamine} = \frac{1}{5 + 1} * 100 = \frac{1}{6} * 100 = 17\%$$

The 6 KDa polymer achieved 17% DS of cysteamine. A 20% of hydrolysis from DXT-MA occured.

Degree of substitution of cysteamine in DXT-20KDa-MA, 20-DXT-cysteamine

DXT-MA of 20 KDa dextran was firstly synthesized and analyzed by ^{1}H-NMR (See chapter 3) and then, subsequently reacted with cysteamine by Michael addition. To calculate the degree of substitution of glucose with methacrylate moieties same equations 3.2.1.1 and 3.2.1.2 as for 40 KDa polymer were applied. 5.78 ppm peak was integrated by 1 and 3.4-4.1 ppm achieved 12.94 proton value. The proton ratio and degree of substitution were obtained with equations 3.2.1.1 and 3.2.1.2:

$$Int_{free\ Glc} = \frac{12.94 - 5(1)}{6H} = \frac{7.94}{6} = 1.32$$

$$\%_{met} = \frac{1}{1.32 + 1} * 100 = \frac{1}{2.32} * 100 = 43\%$$

The DS of cysteamine in 20 KDa DXT-Cysteamine was calculated. The peak 3.2 ppm corresponding to cysteamine was integrated by 2 and used to the proton ratio calcualtion. 3.4-4.1 ppm obtained 33.52 proton value. As unreacted methacrylates were also present (See Chapter 3), its value (0.52/3H=0.17) has been also taken into account for the subtractation from free glucoses, 3.2.2.1:

$$Int_{free\ Glc} = \frac{33.52 - 5(1) - 5(0.17)}{6H} = \frac{27.67}{6} = 4.611$$

4.611 unaltered glucoses per 1 substituted with cysteamine and 0.17 glucoses with methacrylate groups. Then, the degree of substitution was calculated, 3.2.2.2:

$$\%_{cysteamine} = \frac{1}{4.611 + 1 + 0.17} * 100 = \frac{1}{5.781} * 100 = 17\%$$

$$\%_{met} = \frac{0.17}{4.611 + 1 + 0.17} * 100 = \frac{0.17}{5.781} * 100 = 3\%$$

$$\%_{Free\ Glc} = \frac{4.611}{4.611 + 1 + 0.17} * 100 = \frac{4.611}{5.781} * 100 = 80\%$$

20 KDa dextran achieved 17% cysteamine of degree substitution, 3% is unreacted methacrylate and 80% are unaltered glucoses.

Degree of substitution of cysteamine in DXT-40KDa-MA >50% DS, 40-DXT-cysteamine 57% DS

A 40 KDa dextran was substituted with x2 glycidyl methacrylate following same conditions of reaction (Se chapter 3). The resulting product was not soluble in water and DMSO-d6 was not appropriated to analyze the peaks as residual solvent interfere in the integral values. Thus, the reaction with cysteamine was continued and the new material now soluble in water was analyzed by ^{1}H-NMR. The spectrum is very similar to other 40KDa Dextran-cysteamine. The peak at 3.23 ppm was integrated by 2 and taken as a reference. The integral of the protons of the glucose ring obtained a value of 9.51. the equation 3.2.2.1 and 3.2.2.2 were used to obtain the cysteamine degree of substitution:

$$Int_{free\ Glc} = \frac{9.51 - 5(1)}{6H} = \frac{4.51}{6} = 0.75$$

$$\%_{cysteamine} = \frac{1}{0.75 + 1} * 100 = \frac{1}{1.75} * 100 = 57\%$$

a cysteamine conversion of 57% was obtain.

APPENDICES

Appendix IV

Calculation of the degree of substitution (DS) of oleic acid in polyallylamine backbone described in chapter 4.

As in the case of the dextran-modified polymers in Chapter 3, to obtain the degree of substitution, the proton value of each moiety must first be obtained. The proton value is the value of the integral of one hydrogen proton in a moiety. The proton value of the unsubstituted polyallylamine ($PAH_{free\ H}$) is aimed to be determined. This value is obtained from the integration of peak 3.0 ppm. However, this peak corresponds to substituted (CH_2-NH-C=O) and unsubstituted (-CH_2-NH_2) monomers, which have the value of 2 protons each. The peak 0.9 ppm is used as reference and integrated by 3, because a methyl group contains 3 hydrogen atoms. The resulting integral value of peak 3.0 ppm is subtracted by the value of oleyl proton (Ol_H), already obtained from peak 0.9 ppm. The following formula has been established:

$$PAH_{free} = \frac{PAH_{total} - 2\ (Ol_H)}{2} \quad \textbf{equation 4.2.2.1}$$

PAH_{free} corresponds to the proton value of unsubstituted monomers among the polyallylamine chain.

PAHtotal corresponds to the proton value of unsubstituted and substituted monomers.

Ol_H corresponds to the proton value of substituted monomers, which is the same as oleyl moiety.

Once every proton value is known, the degree of substitution is calculated by dividing the proton value of oleic acid (Ol_H) by the sum of the proton value of oleic acid (Ol_H) and the proton value of the unsubstituted polyallylamine (PAH_H). As indicated in the following formula:

$$\%DS = \frac{Ol_H}{Ol_H + PAH_{free\ H}}\ x\ 100 \quad \textbf{equation 4.2.2.2}$$

Degree of substitution of PAH.OA.1

The degree of substitution of PAH.OA.1 would be as follow: after integrating the signal at 0.9 ppm for its corresponding 3 protons, the integration at 3.0 ppm is 180.31, proton value (Ol_H) is 1.

$$PAH_{free\ H} = \frac{180.31 - 2\ (1)}{2} = 89.155$$

$$\%DS = \frac{1}{1 + 89.155}\ x\ 100 = \frac{1}{90.155}\ x\ 100 = 0.01109\ x\ 100 = 1.11\%$$

PAH.OA.1 present 1.11% Degree of substitution, i.e, approximately 1% of the monomers are substituted with oleic acid.

Degree of substitution of PAH.OA.2

The degree of substitution of PAH.OA.2 would be as follow: after integrating the signal at 0.9 ppm for its corresponding 3 protons, the integral at 3.0 ppm is 102.16, proton value (OI_H) is 1.

$$PAH_{free\ H} = \frac{102.16 - 2\ (1)}{2} = 50.08$$

$$\%DS = \frac{1}{1 + 50.08} x\ 100 = \frac{1}{51.08}\ x\ 100 = \ 0.01957\ x\ 100 = 1.957\%$$

PAH.OA.2 present 1.96% Degree of substitution, i.e, approximately 2% of the monomers are substituted with oleic acid.

Degree of substitution of PAH.OA.5

The degree of substitution of PAH.OA.5 would be as follow: after integrating the signal at 0.9 ppm for its corresponding 3 protons, the integration at 3.0 ppm is 34.37, proton value (OI_H) is 1.

$$PAH_{free\ H} = \frac{34.37 - 2\ (1)}{2} = 16.185$$

$$\%DS = \frac{1}{1 + 16.185} x\ 100 = \frac{1}{17.185}\ x\ 100 = \ 0.0581\ x\ 100 = 5.81\%$$

PAH.OA.5 present 5.81% Degree of substitution, i.e, aproxiamtely 6% of the monomers are substituted with oleic acid.

Degree of substitution of PAH.OA.10

The degree of substitution of PAH.OA.10 would be as follow: after integrating the signal at 0.9 ppm for its corresponding 3 protons, the integration at 3.0 ppm is 14.33, proton value (OI_H) is 1.

$$PAH_{free\ H} = \frac{14.33 - 2\ (1)}{2} = 6.165$$

$$\%DS = \frac{1}{1 + 6.165} x\ 100 = \frac{1}{7.165}\ x\ 100 = \ 0.1395\ x\ 100 = 13.95\%$$

PAH.OA.10 present 13.95% Degree of substitution, i.e, approximately 14% of the monomers are substituted with oleic acid.

Degree of substitution of PAH.OA.20

The PAH.OA.20 derivative presents a unique challenge due to its turbid nature and poor solubility, resulting in ^{1}H-NMR spectra characterized by a high level of background noise. Consequently, the

integration of the peaks is unlikely to yield accurate values for this sample. Therefore, the DS for PAH.OA.20 is represented as an approximation, with a value of greater than 14%.

Appendix References

1. Klein, D. *Organic Chemistry*. (John Wiley and Sons, Inc., 2021).

2. Ashenhurst, J. Infrared Spectroscopy: A Quick Primer On Interpreting Spectra. *October 31st, 2022* https://www.masterorganicchemistry.com/2016/11/23/quick_analysis_of_ir_spectra/.

3. Thompson, M. CHNS Elemental Analyzers. *Anal. Methods Comm. AMCTB No 29, R. Soc. Chem.* (2008).

4. Krotz, L. & Giazzi, G. Elemental Analysis: CHNS/O determination of marine samples. 1–6 (2018).

5. Chemistry Hall. Thin Layer Chromatography: A Complete Guide to TLC. *2020* https://chemistryhall.com/thin-layer-chromatography/.

6. Mohrig, J. R., Alberg, D. G., Hofmeister, G. E. & Schatz, P. F. *Laboratory Techniques in Organic Chemistry*. *Chemical & Engineering News Archive* vol. 54 (1976).

7. Quantockgoblin. Thin-layer chromatography. https://en.wikipedia.org/wiki/Thin-layer_chromatography (2008).

8. Rajisha, K. R., Deepa, B., Pothan, L. A. & Thomas, S. Thermomechanical and spectroscopic characterization of natural fibre composites. in *Interface Engineering of Natural Fibre Composites for Maximum Performance* 241–274 (Woodhead Publishing, 2011). doi:10.1533/9780857092281.2.241.

9. Prime, R. B., Bair, H. E., Vyazovkin, S., Gallagher, P. K. & Riga, A. Thermogravimetric Analysis (TGA). in *Thermal Analysis of Polymers: Fundamentals and Applications* 241–317 (John Wiley & Sons, Ltd, 2008). doi:10.1002/9780470423837.ch3.

10. Gabbott, P. *Principles and Applications of Thermal Analysis*. *Principles and Applications of Thermal Analysis* (Blackwell Publishing Ltd, 2008). doi:10.1002/9780470697702.

11. De Blasio, C. *Fundamentals of Biofuels Engineering and Technology*. *Springer* (2019).

12. LPD Lab Services. TGA Plots Mass Loss Interpretation and ODT. https://www.lpdlabservices.co.uk/analytical_techniques/chemical_analysis/tga_interpret.php (2022).

13. Instruments, M. *Zetasizer Nano User Manual*. *Malvern Instruments Ltd. Malvern* vol. 0485 https://www.malvernpanalytical.com/es/learn/knowledge-center/user-manuals/man0485en (2013).

14. Malvern Instruments Ltd. *The Diffusion Barrier Technique , Practical Aspects and Data interpretation*. (2012).

15. Evennett, P. J. & Hammond, C. Microscopy - Overview. in *Encyclopedia of Analytical Science: Second Edition* 32–41 (Elsevier Inc., 2004). doi:10.1016/B0-12-369397-7/00376-9.

16. The University of Utah. Electron Microscopy Tutorial. https://advanced-

microscopy.utah.edu/education/electron-micro/ (2011).

17. Williams, D. B. & Carter, C. B. Transmission electron microscopy: A textbook for materials science. *Transm. Electron Microsc. A Textb. Mater. Sci.* 1–760 (2009) doi:10.1007/978-0-387-76501-3/COVER.

18. Hazelton, P. R. & Gelderblom, H. R. Electron Microscopy for Rapid Diagnosis of Emerging Infectious Agents. *Emerg. Infect. Dis.* **9**, 294 (2003).

19. Scarff, C. A., Fuller, M. J. G., Thompson, R. F. & Iadaza, M. G. Variations on negative stain electron microscopy methods: Tools for tackling challenging systems. *J. Vis. Exp.* **2018**, e57199 (2018).

20. Promega Corporation. *CellTiter 96 ® AQueous One Solution Cell Proliferation Assay*. *Www.Promega.Com/Protocols/* www.promega.com/protocols/ (2012).

21. Bacia, K., Haustein, E. & Schwille, P. Fluorescence correlation spectroscopy: Principles and applications. *Cold Spring Harb. Protoc.* **2014**, 709–725 (2014).

22. Macháň, R. & Wohland, T. Recent applications of fluorescence correlation spectroscopy in live systems. *FEBS Lett.* **588**, 3571–3584 (2014).

23. Elliott, A. D. Confocal Microscopy: Principles and Modern Practices. *Curr. Protoc. Cytom.* **92**, (2020).

24. Adan, A., Alizada, G., Kiraz, Y., Baran, Y. & Nalbant, A. Flow cytometry: basic principles and applications. *Critical Reviews in Biotechnology* **37**, 163–176 (2017).

25. Cell Signaling Technology. Overview of Flow Cytometry. https://www.cellsignal.com/applications/flow-cytometry/flow-cytometry-overview (2023).

26. Proteintech. Popular antibodies for flow cytometry. https://www.ptglab.com/support/flow-cytometry-protocol/popular-antibodies-for-flow-cytometry/ (2023).

27. Southern, E. M. Detection of specific sequences among DNA fragments separated by gel electrophoresis. *J. Mol. Biol.* **98**, 503–517 (1975).

28. Corporation, M. international. The principle and method of Western blotting (WB). https://www.mblintl.com/resources/scientific-resources/fundamentals-for-planning-research/the-principle-and-method-of-western-blotting-wb/#:~:text=In Western blotting (WB)%2C,the gel are electrophoretically transferred.

29. Stewart, R. Western Blotting. https://www.antibodies.com/es/western-blotting.

30. Scientific, T. F. Chemiluminescent Western Blotting. https://www.thermofisher.com/es/en/home/life-science/protein-biology/protein-biology-learning-center/protein-biology-resource-library/pierce-protein-methods/chemiluminescent-western-blotting.html.

31. Sigma, M. Quantitative PCR Basics. https://www.sigmaaldrich.com/ES/en/technical-documents/technical-article/genomics/qpcr/quantitative-pcr.

32. Adams, G. A beginner's guide to RT-PCR, qPCR and RT-qPCR. *Biochem. (Lond).* **42**, 48–53 (2020).

33. Mészáros, É. qPCR: How SYBR® Green and TaqMan® real-time PCR assays work. *11. May 2022* https://www.integra-biosciences.com/japan/en/blog/article/qpcr-how-sybrr-green-and-taqmanr-real-time-pcr-assays-work.

34. Scientific, T. F. Basic Principles of RT-qPCR. https://www.thermofisher.com/es/es/home/brands/thermo-scientific/molecular-biology/molecular-biology-learning-center/molecular-biology-resource-library/spotlight-articles/basic-principles-rt-qpcr.html.

35. Livak, K. J. & Schmittgen, T. D. Analysis of Relative Gene Expression Data Using Real-Time Quantitative PCR and the 2−ΔΔCT Method. *Methods* **25**, 402–408 (2001).

36. Ibidi. Immunofluorescence Staining: A Typical Workflow. https://ibidi.com/content/365-immunofluorescence-staining-a-typical-workflow.

APPENDICES

In the relentless pursuit of advancing gene therapy, this comprehensive study takes a deeper look into the world of polymer-based nanoparticles and their potential in siRNA delivery. The initial efforts were focused on dextran-derived single-chain polymeric nanoparticles, provided a platform but demonstrated limited success in intracellular siRNA delivery.

Aware of the limitations, the research took a turn and introduced a pioneering strategy that combined the proven properties of polyallylamine (PAH) with the natural benefits of oleic acid. Once developed and refined, these new synthetic polymers did more than present an alternative: they rivaled the transfection efficacy of leading commercial solutions.. The study examined the effect of different degrees of oleic acid substitution in the PAH polymer and how they influence the performance of the resulting vector. The most notable achievement was the silencing of CD47, a protein associated with the ability of tumor cells to evade the immune system, especially in non-small cell lung cancer.

The results of this research have exciting implications for the future of gene therapy and RNAi-based treatments. As knowledge from this research expands, its implications could extend beyond the treatment of lung cancer, possibly offering avenues to address other medical challenges and charting a future in which gene therapies can be more personalized, effective and accessible.

cidetec
MEMBER OF BASQUE RESEARCH & TECHNOLOGY ALLIANCE

CIC biomaGUNE
MEMBER OF BASQUE RESEARCH & TECHNOLOGY ALLIANCE

eman ta zabal zazu
Universidad del País Vasco
Euskal Herriko Unibertsitatea